Satbayev University

TOLEUTAY GAUKHAR

Physico-chemical, complexation, and catalytic properties of linear and crosslinked polyampholytes

6D072100 - Chemical technology of organic substances

A thesis submitted for the scientific degree of
Doctor of Philosophy (Ph.D.)

Scientific supervisors

Dr. Chem. Sci., Professor,
Kudaibergenov S.E.
Satbayev University

Ph.D., Professor
Galaev I.Yu.
DSM Biotechnology Center,
The Netherlands

The Republic of Kazakhstan
Almaty, 2019

CONTENT

NORMATIVE REFERENCES

In this dissertation, references are made to the following standards:

GOST 7.32-2001. Report on research work. Structure and design rules.

GOST 7.1-2003. Bibliographic record. Bibliographic description. General requirements and compilation rules.

GOST 4517-87 Reagents. Methods for the preparation of auxiliary reagents and solutions used in the analysis.

GOST 23932-90 E. laboratory glassware and equipment.

GOST 25336-82. Laboratory glassware and equipment. Types, basic parameters, and sizes.

GOST 29252-91. Laboratory glassware. Burettes. Part 1. General requirements.

GOST 1770-74. Measuring laboratory glassware. Cylinders, beakers, flasks, test tubes. General specifications.

GOST 2922-91. Laboratory glassware. Graduated pipettes.

GOST 9147-80. Porcelain laboratory glassware and equipment. Technical conditions

GOST 20292-74. Volumetric flasks with a capacity of 100, 200, 500, 1000 ml. Technical conditions

GOST 12.1.008-76. Occupational safety standards system. Biosafety. General requirements. Technical conditions.

LIST OF ABBREVIATIONS

The following designations and abbreviations were used in the given dissertation:

AMPS –	2-Acrylamido-2-methyl propane sulfonic acid sodium salt
APTAC –	3-acrylamidopropyl)trimethylammonium chloride
APS –	Ammonium persulfate
CTMAC –	Cetyltrimethylammonium chloride
C_0	Total monomer concentration
C_M	Monomer concentration
DDBSNa –	Dodecylbenzenesulfonate
DMAEM –	2-(Dimethylamino)ethyl methacrylate
DMA –	N,N-Dimethylacrylamide
DSC –	Differential scanning calorimetry
DLS	Dynamic light scattering device
E_a –	Activation energy
FRP –	Free radical polymerization
GPC –	Gel permeation chromatography
NMR-spectroscopy –	Nuclear magnetic resonance spectroscopy
FTIR-spectroscopy –	Fourier Transform Infrared spectroscopy
MAA –	Methacrylic acid
MB –	Methylene blue
MO –	Methyl orange
MBAA –	N,N′-Methylenebis(acrylamide)
ODA–	N-octadecyl acrylate
PA –	Polyampholytes
PSD –	Pore size distribution
QPA –	Quenched polyampholytes
QPaH –	Quenched polyampholyte hydrogels
SDS –	Sodium dodecyl sulfate
TMEDA –	N,N,N′,N′-Tetramethylethylenediamine
TOF –	Turnover frequency
TON –	Turnover number
TGA –	Thermal gravimetric analysis
UV-Vis spectroscopy–	Ultra violet visible spectroscopy
X_{AMPS}	Content of AMPS in molar ratio
λ –	Wavelength

INTRODUCTION

Assessment of the current state of the scientific or scientific-technological problems to be solved. According to a survey of the applicable literature, the strongly charged or so called "quenched" polyampholytes are a less studied subject in comparison with annealed polyampholytes [1, 2]. The present study focuses on the synthesis of linear and crosslinked polyampholytes based on 2-acrylamido-2-methyl-1-propanesulfonic acid sodium salt-*co*-(3-acrylamidopropyl)trimethylammonium chloride (AMPS-*co*-APTAC). Further study was done on the structure and morphology, physico-chemical and physico-mechanical properties of quenched polyampholytes. The complexation ability of strongly charged polyampholytes with respect to surfactants and dyes is shown. The mechanical and self-healing ability of polyampholyte hydrogels was improved by the addition of a hydrophilic monomer, N,N-dimethylacrylamide (DMA), and a hydrophobic monomer, N-octadecyl acrylate (ODA). Gold nanoparticles were immobilized within the matrix of amphoteric cryogels, and the catalytic properties of cryogel-immobilized gold nanoparticles in hydrogenated nitroaromatic compounds were examined.

Basis and initial data. Strongly-charged polyampholytes of linear and crosslinked structures based on anionic and cationic monomers undergo conformational and volume-phase transitions and show stimuli-sensitive behavior in response to temperature, ionic strength, and the thermodynamic quality of solvent. The isoelectric effect of polyampholytes has been proposed for application in purification of waste water, as well as separation and purification of proteins. Further, macroporous amphoteric cryogels could be utilized as flow-through catalytic reactors.

The general methodology for conducting research included synthetic, physico-chemical, and catalytic components. The methods utilized include: free radical polymerization, UV-polymerization, cryopolymerization, gravimetry, volumetry, ultraviolet, visible and infrared spectroscopy, scanning electron microscopy, differential scanning calorimetry and thermogravimetry, viscometric method, gel-permeable chromatography, electrophoresis and dynamic laser light scattering, as well as compression, tensile and rheological tests.

Justification of the need for research on the topic. This research is important in furthering the understanding of synthetic polyampholytes. At the International level, the results of the work may be interesting for specialists engaged in both the theory and application of polyampholytes. The results obtained can considerably expand knowledge of synthetic and naturally-occurring polyampholytes in terms of modeling the behavior of proteins and nucleic acids, enzymatic catalysis, molecular recognition, and self-assembling, among other areas [1, 3, 4].

From a practical point of view, the antipolyelectrolyte effect can be used for water desalination and in polymer flooding technology, which is used in increasing oil recovery in reservoirs.

The fundamental findings of strongly charged polyampholytes may be used for solving of the following practical tasks:

1)   application of strongly charged polyampholytes as thickeners in saline media for polymer flooding technology;

2)   desalination of saline water;

3)   purification of wastewater from metal ions, organic dyes, and surfactants;

4)   separation and purification of proteins and development of drug delivery systems;

5)   development of thermostable, active, and selective molecularly-imprinted catalytic systems.

Strong, tough and highly stretchable physically-crosslinked hydrogels and chemically-crosslinked polyampholyte hydrogels can be used in biotechnology and medicine. Further, polymapholyte cryogels can be used as flow-through catalytic reactors [1, 10, 11].

Information about the planned scientific and technical level of development. In spite of the considerable success of scientists in the synthesis and characterization of polyampholytes [5-10], in literature the information on strongly charged polyampholytes is still marginal, except for older publications. As distinct from weakly charged (or annealed) polyampholytes consisting of ionizable acidic and basic monomers, in which the net charge and the charge distribution along the chain are controlled mainly by changing the pH of the solution, the strongly charged (or quenched) polyampholytes represent fully charged macromolecules prepared from the charged cationic and anionic monomers retaining, in contrast to annealed polyampholytes, their respective charges over a wide pH range. In the case of strongly charged polyampholytes, the electrostatic attraction between oppositely charged monomers at the isoelectric state is so strong and effective that collapse (or precipitation) of the macromolecular chains can occur. Aqueous solutions of strongly charged polyampholytes behave unusually in saline media, and at the isoelectric point can cause the so-called antipolyelectrolyte effect, thus causing swelling instead of shrinking, and the isoelectric effect, forcing out previously complexed, or adsorbed, high- and low-molecular weight ions, such as metal ions, dye molecules, surfactants, and proteins. Publications on complexation of strongly charged polyampholytes with respect to metal ions, dye molecules, surfactants, proteins and enzymes have appeared sporadically. The study of three-dimensional structures of strongly charged amphoteric gels is absent, except for recent publications, such as that by a group of Japanese scientists [1].

Conclusions of the patent research. Analysis of the research and patent literature showed that charged polymers have attracted much attention both theoretically and experimentally due to their unique properties and technological importance [11]. They are the most important class of macromolecules due to their wide range of industrial applications [12]. These types of polymers range from naturally occurring biopolymers such as proteins and polynucleotides to synthetic viscosity modifiers and soaps. Therefore, polyampholytes are attractive for tissue engineering, cryopreservation, and drug delivery. This work involved synthesis of strongly charged polyampholytes of linear and crosslinked structures, study of their physico-chemical and physico-mechanical properties, and demonstration of the

potential application in various areas, such as biomaterials, nanocatalysts and drug delivery system, among others.

Information about the metrological provision of research. The Institute of Polymer Materials and Technologies has certified, metrologically-verified methods for carrying out scientific and applied research in the field of functional polymers, in order to determine their structure, composition and properties. The certified precision equipment that was utilized included: Nano-Z590 Malvern Zetasizer (UK), Eclipse LV150N polarization microscope (Nikon, Japan), Bruker Avance III 500 spectrometer, Carry 660 (Agilent, USA) DSC 131 EVO Setaram and TGA «Labsys EVO» Setaram (France), SEM (Jeol JSM-6490LA, Japan), and texture analyser TA.XT plus, Stable Micro Systems, (UK). The viscosity of aqueous solutions of polyampholytes was measured using a Ubbelohde viscometer at room temperature 25±0.1 °C (capillary length of 90 mm, capillary diameter of 0.86 mm, the range of viscosity measurement is based on the National 40 Standard GOST 10028–81).

The relevance of the research topic. From a scientific point of view, the qualities of linear and crosslinked amphoteric macromolecules are interesting, including their ability to adopt globular, coil, helix and stretched conformations, and to demonstrate coil-globule, helix-coil phase transitions, and sol-gel, collapsed-expanded volume changes depending on the pH, temperature, ionic strength of the solution, thermodynamic quality of solvents, and so forth. Synthetic polyampholytes constantly attract the attention of theorists and researchers because the hierarchy of amphoteric macromolecules can repeat, more or less, the structural organization of proteins. That is why the study of polyampholytes falls within several disciplines, including polymer chemistry and physics, molecular biology, colloid chemistry, and catalysis.

Complexation of polyampholytes with polyelectrolytes, surfactants, transition metal ions, and organic ions is important in understanding the problems of the complementarity of macromolecules and molecular recognition.

Hydrophobically modified polyampholytes containing hydrophobic moieties at the side chain or in the polymer backbone can self-assemble into micelles, vesicles, and lamellar aggregates, among others. There are applications in several areas, including immobilization of metal catalysts, enhanced oil recovery (as pour point depressants and wax inhibitors), cryopreservation of living cells, and delivery of drugs, genes and proteins. Water-swollen cross-linked polyampholytes, i.e. polyampholyte (PA) hydrogels, also exhibit unique features, such as their sensitivity to pH and salt concentration variations, low toxicity, good biocompatibility, and similarity to many biological structures. Therefore, they have a variety of applications including antibacterial, anti-fouling, and in the production of saline-resistant materials. For instance, PA cryogels exhibit stimuli-responsive behavior and catalytic properties when metal nanoparticles are immobilized within the cryogel network.

The novelty of the dissertation topic. Polyampholytes are macromolecules that contain both acidic (anionic) and basic (cationic) monomers in the macromolecular chain[1]. Proteins containing amino acid residues also belong to polyampholytes [13]. Conditionally, synthetic polyampholytes can be divided into three classes: annealed, quenched (or "fully-charged") and betainic (or zwitterionic).

Annealed polyampholytes consist of acid-base monomers that are ionized depending on pH, whereas quenched polyampholytes containing strongly charged cationic and anionic monomers retain their respective charges independently of pH. Betainic polyampholytes are macromolecules containing identical numbers of acid-base (or fully charged anionic-cationic) species in the same monomer units[1, 2, 11, 13, 14]. The macromolecules that exist via compensation of the cationic-anionic monomer pairs without counterions are also zwitterionic polymers. The behavior of polyampholytes in solution is controlled by either attractive or repulsive interactions between the positively and negatively charged groups. If the overall charge of polyampholyte is positive or negative, the electrostatic forces between monomers become repulsive, and the polymer chain extends and adopts a necklace-like conformation in dilute solution. If polyampholytes contain equal numbers of positively and negatively charged groups they collapse due to attractive forces between opposite charges. In a particular case, called the isoelectric point (IEP), the overall charge of polyampholytes tends to be zero.

For the first time, charge-balanced and charge-imbalanced quenched polyampholytes of linear and crosslinked structures based on anionic monomer – 2-acrylamide-2-methylpropane-1-sulfonic acid sodium salt (AMPS) and cationic monomer – (3-acrylamidopropyl) trimethylammonium chloride (APTAC) have been synthesized. They were analyzed using H^1 NMR, FTIR, GPC, DLS, DSC, viscometry, swelling-deswelling experiments, and mechanical tests.

Charge-balanced and charge-imbalanced quenched polyampholytes (QPAs) were found to exist in core-shell state and exhibit antagonism in aqueous-salt solution. Addition of low-molecular-weight salts tends to shrink the shell, polyelectrolyte, region and to swell the core, polyampholyte, region. Such antagonism between polyelectrolyte and polyampholyte effects can take place at relatively high ionic strengths.

The complexation of charge unbalanced linear and crosslinked polyampholytes was studied in aqueous solution with respect to ionic dyes and surfactants. Complexation of QPAs was found to occur with the anionic surfactant, sodium dodecylbenzenesulfonate (SDBS) and the cationic surfactant, cetyltrimethyl ammonium chloride (CTMAC), and is accompanied by changes in turbidity, zeta-potential and average hydrodynamic diameter of colloid particles, while complexation of AMPS-APTAC hydrogels with SDBS and CTMAC is accompanied by gradual shrinking of samples due to binding of anionic and cationic surfactants with excessive anionic and cationic groups of hydrogels.

For the first time, hydrophobically modified quenched polyampholyte hydrogels were prepared via micellar polymerization of cationic and anionic monomers in the presence of the hydrophobic monomer ODA. Hydrogels containing 60-90% water sustain a high tensile strength (up to 202 kPa) and exhibit a high stretchability (up to 1239%), demonstrating much better mechanical properties in comparison with corresponding non-swolen ones. Cut-and-heal tests revealed that non-swolen hydrogels exhibit a healing efficiency of 90±10% of their original Young's modulus.

Macroporous amphoteric cryogels of annealed and quenched types were initially prepared, then gold nanoparticles were immobilized inside of the porous structure. Afterwards, the system was used as an effective flow-through catalytic reactor for hydrogenation of nitroaromatic compounds into corresponding aminoaromatic derivatives, with high conversion and low activation energy.

Relationship of the present research with other work. The research was carried out in the framework of grant project № AP05131003 of the Ministry of Education and Science of the Republic Kazakhstan: "Fundamental Problems of Strongly Charged Polyampholytes at the Isoelectric Point" (2018-2020).

The purpose and tasks of the research. The research work was aimed at synthesizing strongly charged linear polyampholytes, hydrogels and cryogels, and to study their physico-chemical, physico-mechanical, complexation and catalytic properties.

Main tasks of the research:

−	synthesis of strongly charged polyampholytes of linear and crosslinked structure and study of their physico-chemical properties;

−	study of the hydrodynamic, conformational, and volume-phase properties of polyampholytes in mediums of varying pH and ionic strength, and in mixtures of water-organic solvents;

−	study of the complexation properties of polyampholytes with respect to dye molecules and surfactants;

−	Synthesis of highly stretchable polyampholyte hydrogels by adding DMA monomer, and study of the the mechanical properties;

−	synthesis of hydrophobically modified polyampholyte hydrogels by micellar polymerization, and study of mechanical properties and self-healing efficiency;

− immobilization of gold nanoparticles in the amphoteric cryogel matrix, and study of the catalytic properties of cryogel-immobilized gold nanoparticles as a flow-through type catalytic reactor.

Objects of the research. Polymers of linear and crosslinked structures based on APTAC, AMPS, MAA, DMAEMA, DMA, ODA monomers.

Main provisions to be defended:

1)	Quenched linear polyampholytes, chemically and physically crosslinked quenched polyampholyte hydrogels and cryogels based on anionic and cationic monomers (AMPS and APTAC) were synthesized and obtained

2)	The composition, structure, molecular weights, polydispersity, conformation, swelling, shrinking, volume-phase behavior, rheology, morphology, mechanical properties and thermostability of quenched polyampholytes of linear and crosslinked structure were studied by various physico-chemical and physico-mechanical methods.

3)	The complexation of linear and crosslinked quenched polyampholytes with respect to ionic surfactants and dyes were studied;

4)   Tough and highly stretchable, chemically and physically crosslinked polyampholytes, containing hydrophilic and hydrophobic monomers and possessing self-healing properties were obtained;

5)   Flow-through catalytic reactors based on macroporous amphoteric cryogels with immobilized gold nanoparticles was developed.

The personal contribution of the author. Consists of the collection, analysis, and summarization of the available literature on polyampholytes, performing experiments, and interpreting and discussing the results.

Approbation of work and publications. The results of the work can be found in 18 publications: 3 publications in journals included in the Scopus database, 2 publications approved by the Committee for Control in the Field of Education and Science of the Republic of Kazakhstan, 12 abstracts at International and National Symposia and Conferences, and 1 innovation patent of the Republic of Kazakhstan.

Dissertation structure. The dissertation includes a review of applicable literature, an explantion of methodology, a discussion of the results, a conclusion, and a list of available sources. The total volume is __ pages, including __figures, __ tables, and a bibliography of __ titles.

1 STATE OF THE ART OF POLYAMPHOLYTES

1.1 Current state of polyampholytes

Charged polymers have attracted much attention both theoretically and experimentally due to their unique properties and technological importance [11, 15-71]. They are the most important class of macromolecules due to their wide range of industrial applications [12]. These types of polymers range from naturally occurring biopolymers such as proteins and polynucleotides to synthetic viscosity modifiers and soaps. Ion containing polymers can be classified into two major categories, namely, polyelectrolytes and polyzwitterions. Polyelectrolytes contain either anionic or cationic functional groups along the polymer chain, while polyzwitterions contain both anionic and cationic groups. Common polyelectrolytes include polyacrylic and polymethacrylic acids and their salts, sulfonated polystyrene, and other strong polymeric acids and bases [72].

The intra - primarily governs the aqueous solution properties such as viscosity and hydrodynamic volume of polyelectrolytes and polyzwitterions- and intermolecular electrostatic interactions that occur among the cations and anions in aqueous media. In dilute, salt-free aqueous solutions, the coulombic repulsions between like charges along a polyelectrolyte chain lead to an expansion in the hydrodynamic volume of the polyelectrolyte coil; however, the addition of electrolytes like sodium chloride (NaCl) results in coulombic shielding and a decrease in hydrodynamic volume and thus solution viscosity. This solution behavior is termed the polyelectrolyte effect [72]. For polyzwitterions, the charges may be located either on the pendent side chains of different monomer units, or in the case of some polyesters, polyphosphazene, and polybetaines, one or both of the charges may be located along the polymer backbone.[11] The distinction between zwitterionic polyampholytes and polybetaines is not always clear from the literature. The term polyzwitterion includes all polymers that possess both cationic and anionic groups. Polyampholytes refers to those polymers that specifically possess charged groups on different monomer units, while polybetaines refer to those polymers with anionic and cationic groups on the same monomer unit. In contrast to polyelectrolytes, structure-property relationships of polyampholytes are governed by coulombic attractions between anionic and cationic polymer units [72].

The coulombic interactions between positively and negatively charged repeat units of polyampholytes reduce hydrodynamic volume, as a result of which the polymer adopts a collapsed or globular conformation in dilute, salt-free aqueous media [72]. In some cases, the electrostatic interactions are so strong that the polymer may become insoluble. On adding simple electrolytes like NaCl to a polyampholyte solution in the dilute regime, the hydrodynamic volume of the polymer coil increases due to the screening of the intramolecular charge-charge attractions, allowing the transition from a globule to a random coil conformation. Such a solution behavior is known as the anti-polyelectrolyte effect and is evidenced by increased polymer hydrodynamic volume and solution viscosity.

In addition to interactions with small molecule electrolytes, other factors such as charge density and distribution, charge balance, monomer sequence distribution

(random, alternating, and block), and the nature of the ionizable groups along the polymer backbone plays an important role in determining polymer conformation and rheological behavior of polyzwitterions in aqueous solution [72]. For polyampholytes, the magnitude of the globule-to-coil transition, the extent of polymer solubility, and the hydrodynamic volume are typically governed by the charge density of the system. Larger concentrations of electrolytes are needed to elicit coil expansion as charge density is increased; however, the magnitude of hydrodynamic volume increase observed is greater with an increased number of zwitterionic interactions. As the degree of charge imbalance [73-75] on a polyampholyte chain increases, the polymer tends to behave in a manner that is more characteristic of a conventional polyelectrolyte.

Typically, polymers that have random incorporation of charged species exhibit more profound antipolyelectrolyte behavior than polyampholytes with alternating incorporation of anionic and cationic groups. This is due to long-range electrostatic interactions in the random moieties versus the alternating ones, which are governed by short-range interactions. The solution properties of polyampholytes also depend on the chemical nature of the charged groups [72]. Polyampholytes bearing strong acids or salt-like functionalities such as sulfonic acids and quaternary ammonium ions are generally insensitive to changes in solution pH; thus, the charge balance and charge density are determined solely by the relative incorporation of the anionic and cationic monomers. However, in polyampholytes containing weak acid/base functionalities such as carboxylic acid and primary, secondary, or tertiary amine groups, the charge density and charge balance of the polymer are determined by the relative incorporation of the ionizable monomers. An example is that of a polyampholyte containing equimolar amounts of a carboxylic acid and quaternary ammonium functional groups. At low pH, this polymer behaves as a cationic polyelectrolyte due to an overall net charge that is a result of virtually no ionization of the acidic groups.

As the solution pH is raised, these groups are ionized, eventually establishing a charge balance, at which point the polymer exhibits polyampholyte behavior. For polyampholytes in which the amphoteric repeat units (for example, in monomers containing carboxylic acid units) are present more than permanently charged repeat units, polyampholyte behavior is observed at the isoelectric point (IEP). The isoelectric point (IEP) is defined as the pH at which the number of cationic and anionic groups are equal. As the solution behavior is adjusted from the IEP, polyelectrolyte behavior is observed due to the increase in the net charge [72]. The first study of synthetic polyampholytes was reported by Alfrey, Morawetz, Fitgerald, and Fuoss in their 1950 article "Synthetic Electrical Analog of Proteins" .

Polyampholytes are interesting for several reasons, not the least of which is the fact that they are synthetic analogs of naturally occurring biological molecules such as proteins, and find applications in areas such a lithographic film, formulation of emulsions and drug reduction. Polyampholytes can be grouped into four subclasses, based on their responses to changes in pH, as shown in figure 1.1 First; the polyampholyte may contain both anionic and cationic species that may be neutralized (1.1a). Secondly, the anionic group may be neutralized, but the cationic groups are

insensitive to pH changes, for example, quaternary alkylammonium groups (1.1b). Thirdly, the cationic species may be neutralized, with the anionic groups showing no response to pH changes, for example, sulfonate groups – which called like highly charged polyampholytes- (1.1c), and finally both the anionic and cationic species may be insensitive to changes in the pH of the solution throughout the useful range (1.1d).
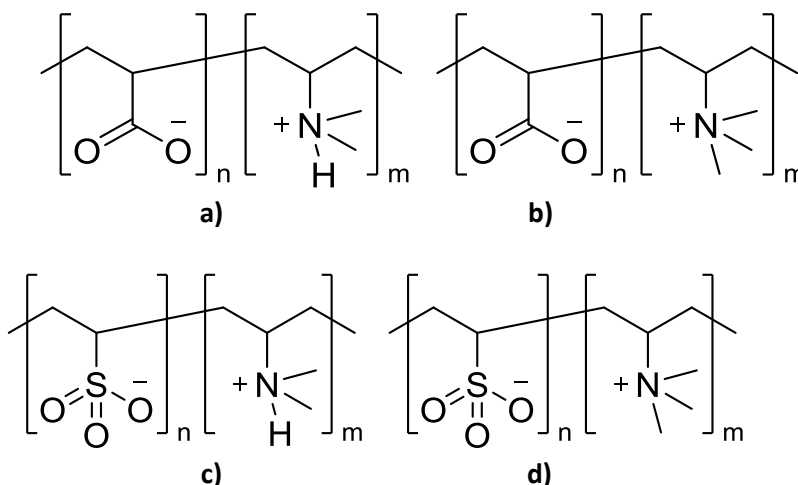
(1.1a). The anionic group may be neutralized, but the cationic groups are insensitive to pH changes (1.1b). The cationic species may be neutralized, with the anionic groups are insensitive to pH changes (1.1c). Both the anionic and cationic species may be insensitive to changes in the pH of the solution (1.1 d).The polyampholyte may contain both anionic and cationic species that may be neutralized
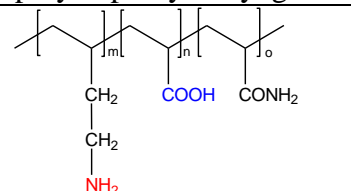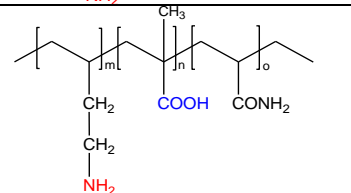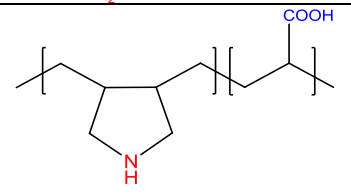
Figure 1.1 – Representative structures of the four subclasses of polyampholytes

More reports on the synthesis of polyampholytes first published in the 1950s. These polyampholytes synthesized via conventional free radical polymerization. Some examples include methacrylic acid-stat-2(dimethylamino)ethyl methacrylate copolymers, synthesized by Ehrlich and Doty, acrylic acid-stat-2-vinyl pyridine copolymers, synthesized by Alfrey and Morawetz, and acrylic acid-stat-2-(dimethylamino)ethyl methacrylate copolymers reported by Alfrey and Pinner Since then, numerous researchers have reported on the synthesis and properties of a variety of statistical polyampholytes

These were block copolymers of 2-vinyl pyridine and trimethylsilyl methacrylate (TMSMA). Poly(TMSMA) was readily hydrolyzed to poly(methacrylic acid) using a water/methanol mixture. Subsequently, Varoqui and co-workers synthesized AB diblock polyampholytes from styrene sulfonate and 2-vinyl pyridine. Later, Morishima and co-workers reported the synthesis of block copolymers of TMSMA and p-N,N-dimethylaminostyrene [76]. Creutz and co-workers have developed the synthesis of block copolymers of methacrylic acid with co-monomers like dimethylaminoalkyl methacrylates [77]. These were synthesized by anionic polymerization using tert-butyl methacrylate (tBMA) as the protected precursor to
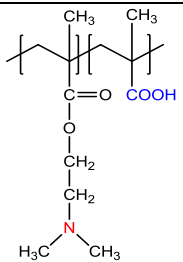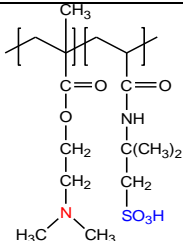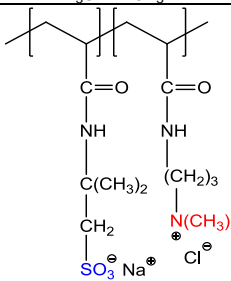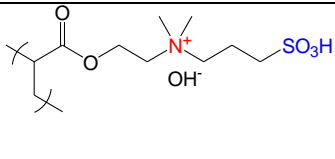
poly (methacrylic acid) groups. Until recently, classical anionic polymerization was the most attractive route to the synthesis of block polyampholytes. Patrickios and co-workers, in 1994, reported on the synthesis of diblock, triblock, and statistical methacrylic polyampholytes by employing group transfer polymerization (GTP) [78, 79]. Similar to anionic polymerization, monomers with labile protons, namely methacrylic acid, could not be directly polymerized, and protected acid monomers were required. Patrickios and co-workers selected TMSMA and 2-tetrahydropyranyl methacrylate (THPMA) as protected methacrylic acid (MAA) monomers. TMSMA was chosen because it is commercial and can easily be converted to MAA, and THPMA can be converted to MAA under very mild acidic conditions. They copolymerized the protected monomers with 2- (dimethylamino)ethyl methacrylate (DMAEMA), and in the synthesis of the triblock copolymers, methyl methacrylate (MMA) was introduced as the third hydrophobic comonomer. Subsequently, Lowe, Billingham, and Armes synthesized AB diblock copolymers of DMAEMA with MAA using THPMA as a protected precursor [80]. The recent developments in controlled free radical polymerization techniques, such as nitroxide-mediated polymerization (NMP) [81], atom-transfer radical polymerization (ATRP) [82], and reversible addition-fragmentation chain transfer (RAFT) [83] polymerization, allow for direct synthesis of many polyampholytic block copolymers without the need for protecting group chemistry. McCormick and co-workers have prepared AB diblock copolymers of DMAEMA with acrylic acid (AA) via RAFT. They also accomplished the polymerization of sodium acrylate directly in aqueous solution via RAFT as well as the anionic acrylamido monomers, 2-acrylamido-2-methyl propane sulfonic acid (AMPS) and 3-acrylamido-3-methylbutanoic acid (AMBA). Some typical examples of polyampholytes are shown in table 1.1.

Table 1.1 - Typical examples of structures of polyampholytes.

Chemical structure polyampholyte cryogels*	Name, Acronym	Ref.
	allylamine-*co*-acrylic acid-*co*-acrylamide, P(AA-*co*-AAc-*co*-AAm)	[84]
	allylamine-*co*-methacrylic acid-*co*-acrylamide, P(AA-*co*-MAA-*co*-AAm)	[85]
	diallylamine-*co*-acrylic acid, P(DAA-*co*-AAc)	[86]

Continuation of Table 1.1

	N,N-dimethylaminoethylmethacrylate-*co*-methacrylic acid, P(DMAEM-*co*-MAA)	
	N,N-dimethylaminoethylmethacrylate-*co*-2-acrylamido-2-methyl-1-propanesulfonic acid P(DMAEM-*co*-AMPS)	[87]
	2-acrylamido-2-methyl-1-propanesulfonic acid sodium salt-*co*-(3acrylamidopropyl)trimethylammonium chloride, P(AMPS-*co*-APTAC)	[88]
	Poly[2-(methacryloyloxy)ethyl]dimethyl-(3-sulfopropyl)ammonium hydroxide, Poly (PMODMSPA)	[85]
[*]Primary, secondary, tertiary amine and quaternary ammonium groups of polyampholytes are in red, carboxylic and sulfonic groups are in blue		

1.1.1 Annealed polyampholytes

Annealed polyampholytes are copolymers consisting of weak acid/weak base, strong acid/weak base (or else weak acid/strong base), and strong acid/strong base monomers in which the net charge and the charge distribution along the chain are monitored mainly by changing pH of the solution. Typically annealed polyampholytes consisting of the weak acid and weak base groups are copolymers of acrylic (or methacrylic) acid and vinyl pyridines, which were first synthesized in the 1950s by Alfrey and Katchalsky as have written before [89, 90]. While copolymers of vinyl- or styrene sulfonic acid and N-substituted allylamine derivatives belong to strong acid/strong base polyampholytes. Usually, radical copolymerization of acidic and basic monomers results in statistical copolymers due to the difference in reactivity of monomers. A classic example is that of the copolymerization of 2-vinyl pyridine (a weak base) and methacrylic acid (weak acid), which leads to the formation of statistical copolymers. A significant influence of salt and hydrogen bonds form between acidic and basic monomers on the kinetics and mechanism of radical copolymerization has thoroughly been discussed by Kabanov et al. [91].

Most of the early studies concerned annealed polyampholytes because of their analogy with biological molecules, and until recently [92, 93].

1.1.2 Zwitterionic polyampholytes

Polymeric betaines or zwitterionic polyampholytes are polyampholytes whose oppositely charged groups remote one from another are displaced on one pendant substituents [80]. When the positive and negative charges are replaced on one pendant group and form inner salt without counterions they are classified as ampholytic ionomers. The synthetic strategy of polyampholytes with betaine structure has been outlined in detail in pioneering works of Salamone et al. . Polymeric betaines [94] can be synthesized directly by polymerization of betaine monomers or modification of functional polymers [95, 96] studied the kinetic features of the radical polymerization of the betaine type monomers. The rate of polymerization Rp was found to be proportional to the square root of the initiator and monomer concentration, which is in good agreement with the general peculiarities of radical polymerization. The enhancement of the polymerization process in the presence of salt is accounted for the diminishing of electrostatic repulsion between the reacting monomers. There are several types of polymers with betaine structure: poly-carboxy betaines, polysulfobetaines, and polyphosphobetaines. poly(N-ethyleneglycine) (1), poly[(N-3-sulfopropyl)-N-methacryloyloxyethyl-N,N-dimethylammonium betaine] (2) and poly(2-methacryloyloxyethylphosphorylcholine) (3) are typical examples of this kind of zwitterionic polyampholytes.

The structural similarity of the latter to natural phospholipids is very useful to model the cell membranes investigated the morphology of giant uni-lamellar phosphatidylcholine vesicles in solutions of varying pH-gradient across the membrane and found that raising the pH in the exterior of the vesicles induces budding.

McCormick et al. [97] described the synthesis of a series of copolymers of acrylamide (AA) and with a novel carboxy betaine monomers_ The novel carboxy betaine monomers, 4-(2-acrylamido-2-methylpropyldimethylammonio)butanoate (AMPDAB) and 6-(2-acrylamido-2 methylpropyldimethylammonio) hexanoate(AMPDAH) involve the quaternization of the monomeric tertiary amine by the reaction with ethyl 4-brombutyrate and 6-bromhexenoate. Free radical polymerization of vinylbenzyl chloride or block copolymerization of vinylbenzyl chloride and styrene resulted in reactive polymers with narrow molecular weight distribution and hydrophilic/hydrophobic balance [98, 99]. The further modification of polymer precursors leads to corresponding amphiphilic polycarboxybetaines containing a hydrophobic styrene block. Kaladas et. al. [100] described the synthesis of a series of zwitterionic copolymers based on the copolymerization of N,N-diallyl-N,N-dimethylammonium chloride (DADMAC) (or N,N-diallyl-N-methylamine (DAMA with 3-(N,N-diallyl-N-methylammonio)propane sulfonate (DAMAPS) (or 4-(N,N-diallyl-N-methyl ammonio)butanoate (DAMAB). A series of polycarboxybetaines and polysulfobetaines with varying distances between the positively and negatively charged groups were synthesized [101]. The synthesis of

poly(ampholyte-electrolytes) via hydrolysis of the poly(N,N-diallyl quaternary ammonium salts), which were prepared from the nonzwitterionic monomer, has been described by authors [102]. The specific features of these polymers are that they exhibit both polyelectrolyte and polyampholyte character simultaneously.

By adding AA to a solution of polyiminoethylene or polyiminohexamethylene both, a protonation and a Michael addition reaction take place simultaneously. Carboxyethylation reaction proceeding in pure chloroform yields a poly ampholyte with more than 90% zwitterion structure. Ethyl ester of 3-amino-2-butenoic acid existing in enamino and imino tautomeric forms has been involved in the copolymerization process with unsaturated carboxylic acids. The reactivity of ethyl ester of 3-amino-2-butenoic acid is very low due to the formation of intramolecular hydrogen bonds that stabilize 1t-conjugated bonds.

1.1.3 Fully charged " quenched" polyampholytes.

A typical example of quenched polyampholyte is a copolymer of 2-acrylamido-2-methylpropanesulfonate (NaAMPS) and 2-acrylamido-2-methylpropoyldimethylammonium chloride (AMPDAC) (figure 1.2) Salamone et al. first synthesized cationic-anionic monomer pairs either by neutralization reaction or by precipitation of charged monomer counterions as silver salt. For instance, the stoichiometric mixture of 2-methacryloyloxyethyltrimethylammonium iodide (METMAI) and a silver salt of 2-methcaryloyloxyethanesulfonate (AgMES) gives AgI as precipitation and METMA-MES as ion-pair monomers in solution (figure 1.3). The polymerization of such ion pairs produces equimolar quenched polyampholyte without inorganic counterions. Quenched polyampholytes prepared in solution tend to be alternative because of the strong electrostatic attractive forces acting between the oppositely charged monomers. Whereas microemulsion polymerization due to differences in copolymerization mechanism in microenvironment leads to almost random quenched polyampholytes. A series of polyampholytes of sodium-2-acrylamido-2- methylpropanesulfonate (NaAMPS) and 2-(methacryloyloxy)ethyl trimethylammonium chloride (MADQUAT) has been synthesized by free-radical polymerization in aqueous solution and microemulsions [103, 104]. The microstructure of NaAMPS-MADQUAT copolymers prepared in microemulsion and inhomogeneous aqueous solution with and without neutral salt was compared, taking into account their reactivity ratios.
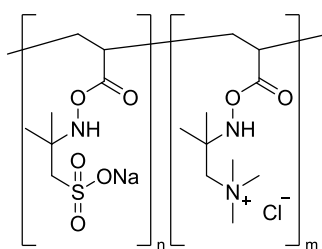

Figure 1.2 - Structure of quenched polyampholytes based on 2-acrylamido-2-methylpropanesulfonate (NaAMPS) and 2-acrylamido-2-methylpropoyldimethylammonium chloride (AMPDAC) [1]
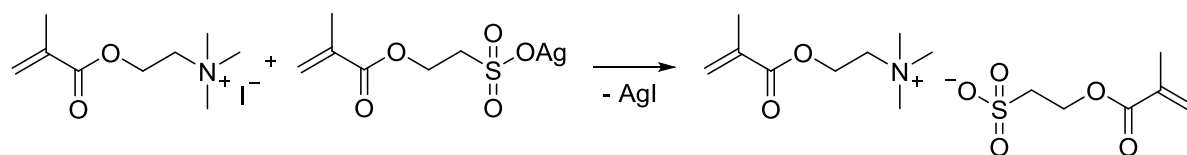
Figure 1.3 - Structure of 2-methacryloyloxyethyltrimethylammonium iodide (METMAI) and a silver salt of 2-methcaryloyloxyethanesulfonate (AgMES) gives AgI as precipitation [1]

McCormick et al. [105] synthesized a series of low- and high-charge-density ampholytic copolymers of AMPS and AMPDAC and thoroughly studied their solution properties. In studied systems, the sulfonate and quaternary ammonium groups are pH insensitive, and the composition of copolymers exclusively determines the charge balance of these terpolymers. Low-charge-density polyampholytes were derived from the polymerization of cationic and anionic monomers with acrylamide or N-isopropyl acrylamide [106]. For terpolymers, the relationships between the radius of gyration and molecular weight (R_g – M) and between the intrinsic viscosity and molecular weight ($[\eta]$ – M) were found. Charge-balanced terpolymers exhibited antipolyelectrolyte behavior at the isoelectric point (IEP) pH 6.5 ± 0.2 while unbalanced terpolymers exhibited typical polyelectrolyte character. The dilute solution behavior of the terpolymers is in good agreement with the theoretical predictions of authors [107].

In general, fully charged polyampholytes prepared in solution from charged cationic and anionic monomers tend alternation, as a result of the strong electrostatic attractive [108]forces acting between the opposite charges [109, 110]. However, microemulsion polymerization leads to almost random polyampholytes, that is, to copolymers more homogeneous in composition than those prepared in solution. This result was accounted for by the marked differences in mechanism and microenvironment between the two processes.

Polyampholyte hydrogels based on cationic (quaternized N,N-dimethylaminoethylmetharylate, 2-methacrylamido-2-propyl trimethyl ammonium chloride) and anionic (2-acrylamido-2-methyl propane sulfonic acid, the sodium salt of styrene sulfonic acid) monomers represent a new class of tough and viscoelastic materials that can be tuned to change multiple mechanical properties over wide ranges. These polyampholyte hydrogels exhibit excellent biocompatibility and anti-biofouling properties, and due to excellent mechanical properties in physiological solutions, they have high potential as structural biomaterials in medicine.

Quenched polyampholytes can also be classified as semi-quenched when one of the monomer units bears permanent charge, while another contains ionizable acidic or basic group. Typical examples of self-quenched polyampholytes are copolymers of N,N'-dimethyl-N,N'-diallyl ammonium chloride (DMDAAC) with acrylic acid (AA)] and maleic acid or alkyl (aryl) derivatives of maleamic acids, sodium styrene sulfonate (SSS)-4-vinyl pyridine (4VP) [77, 111], etc. Such self-quenched polyampholytes are pH-responsive and adopt globular or collapsed confirmation at the IEP when the cationic and anionic charges are fully compensated,

and the whole macromolecules are quasineutral. According to the literature survey, the quenched polyampholytes are less considered in comparison with annealed polyampholytes and polymeric betaines [4].

1.2 Studies of polyampholyte solutions

The conductivity, viscosity, and coil size of weakly hydrophobic polyampholytes have minima at the isoelectric pH are basic findings for dilute polyampholyte solutions [112]. Due to the collapse of the polymer coil because of intramolecular electrostatic attractions between cationic and anionic repeat units [109]. Hydrophobic polyampholytes [113, 114] precipitate close to the isoelectric pH. The addition of salt to a nearly charge-balanced polyampholyte increases the viscosity and coil-size [115]. For polyampholytes with a large net charge, the viscosity and coil-size decrease as salt are added. In this case, the polyampholyte behaves as a polyelectrolyte [74]. The viscosity and coil-size in pure water display a strong minimum as a function of copolymer composition, where positive and negative charges are balanced. Katchalsky and Miller studied the influence of oppositely charged groups on dissociation, and they found that increasing the acid content of their copolymers, caused a larger fraction of the basic monomers to dissociate at a given pH [11]. As expected, the addition of salt screens the electrostatic interactions and thus reduces the inductive influence of neighboring groups. McCormick and co-workers have confirmed many of the classical findings for dilute polyampholyte solutions, as described above [105, 116, 117].

Modern theories of polyampholytes also expect this behavior, as salt first screens the charge repulsion on large scales that extends the chain, and only at higher salt concentration the charge attraction, which compresses the polyampholyte locally, is screened, causing the chain to swell [118]. Candau and co-workers explored the composition distribution of randomly prepared polyampholytes in detail [103, 119]. This paper reports the study of a low charge density terpolymer prepared using microemulsion polymerization by incorporating acrylamide (AM) as a neutral water-soluble monomer, along with sodium 2-(acrylamido)-2- methyl propane sulfonic acid (NaAMPS) and [2-(methacryloyloxy)ethyl]-trimethylammonium chloride (MADQUAT) as the charged monomers. In a medium of high salt content, the electrostatic interactions are screened out, and all the chains are soluble. Below a critical salt content, attractive electrostatic interactions are dominant, and the chains with a zero or small net charge precipitate due to the polyampholyte effect. The supernatant contains highly swollen oppositely charged polyampholyte molecules. The polymer concentration in the supernatant decreases with decreasing salt content, with increased swelling of chains [118]. Thus, salt can, in some cases, provide a means of fractionation, in which the neutral chains precipitate. Theory of Polyampholyte Solutions The properties of polyampholyte chains in solutions depends not only on the fractions of positively and negatively charged monomers, but also on the distribution of charged monomers along the polymer backbone [2]. Theoretical models as well as computer simulations of charge-balanced polyampholytes usually consider ensemble average properties. This corresponds to

averaging over all possible charge sequences along the polymer backbone with fixed fractions of charged groups and charge asymmetry.

Consequently, the properties of the whole ensemble of chains are often represented by the properties of the most probable member, which may not always be valid. It is for this reason that model random polyampholytes having a random distribution of compositions are needed to test the theory of polyampholyte solutions. Random polymerization reactions produce synthetic polyampholytes. Such samples contain chains with different fractions of positively and negatively charged groups. The balance of four factors determines the overall size and shape of polyampholytes in dilute salt-free solutions: (1) the fraction of positive and negative charges on the chain, (2) the charge sequence, (3) the degree of polymerization, and (4) the ratio of the Bjerrum length to the monomer size. The Bjerrum length is the distance at which the electrostatic interaction energy between two elementary charges is equal to the thermal energy in a medium of a given dielectric constant. As the polyampholyte chain, approaches charge balance, its collapse into a globule due to intrachain electrostatic attractions. In polyampholytes with a net charge, the globule elongates and forms a charge-balanced necklace. For synthetic polyampholytes prepared by copolymerization reactions, one only has control over the composition of the initial monomeric mixture. Even for symmetric mixture with equal concentrations of positive and negative monomers, the individual polymer molecules produced will have an excess of positively charged groups or negatively charged groups, or be neutral. The width of the charge asymmetry distribution is determined by the propagation reaction rate constants between monomers that could favor alternating, random, or blocky charge sequences. The charge sequence of a polyampholyte chain consisting of weakly acidic or basic groups can be adjusted by either changing the pH of the aqueous solution or by imposing an external electrostatic potential, for example, by placing chains near charged surfaces. Such polyampholytes are called annealed polyampholytes [2, 112, 120, 121].

A qualitative study of the properties of polyampholyte solutions was reported by Katchalsky and co-workers [122]. The effect of net charge on the shape of a polyampholyte chain was studied independently by Kantor, Gutin, and Dobrynin [93, 123, 124]. They found that excess charge deforms the polyampholyte chain into an elongated globule, whereas fluctuation-induced attraction collapses the chain into a globule. However, the interplay of globule surface energy and repulsion of the net unbalanced charge elongates the globule. Applications of Polyampholytes, although polyampholytes have not been extensively used in commercial applications, their unusual solution properties present unique opportunities for formulation in the presence of electrolytes. These include areas such as personal care, enhanced oil recovery, and flocculation. Water-soluble and water-swelling polyampholytes could be used in the desalination of water, sewage treatment, flocculation, and coagulation, drilling fluids, and enhanced oil recovery. The ability of polyampholytes to swell and be effective viscosity enhancers in high salinity media plays a crucial role in enhanced oil recovery (EOR) processes. In the recovery of oil from oil-bearing reservoirs, an important component is the formulation of drilling muds. A conventional water-based drilling mud formulation includes water, clay such as

bentonite, lignosulfonate, a weighting agent such as $BaSO_4$, and a caustic material such as sodium hydroxide to adjust the pH between 10 and 10.5. Amphoteric terpolymers have been found to act as viscosity control additives for water-based drilling muds. They are chemically and thermally stable in high ionic strength environments. The solution viscosity remains essentially invariant to temperature changes. Terpolymers composed of acrylamide, metal styrene sulfonate, and methacrylamidopropyltrimethylammonium chloride show improved drag reduction in water, while efficient drag reduction in a variety of organic solutions was exhibited by terpolymers of styrene, metal styrene sulfonate, and 4-vinyl pyridine.Protein-polyelectrolyte complexes have found application for protein separation and enzyme immobilization. The interaction of proteins with DNA is central to the control of gene expression and nucleic acid metabolism. One method for protein separation by water-soluble polyampholytes that have random sequences is based on a selective complexation of a polyampholyte with a protein that has a net complementary charge. A prerequisite of the process is that the latter interaction is stronger than that between other proteins in the same solution. Thus, only one of the proteins will form a complex with the polyampholyte and phase separate, while the other proteins remain in the supernatant phase. The resultant protein/polyampholyte assembly can be removed from the system and redissolved at a different pH. The phenomenon of adsorption of polyampholytes on a charged surface has great potential because many biological and technological processes are closely connected with the adsorption phenomenon [1, 125].

1.3 Interaction of polyampholytes with surfactants, dyes, and behavior in water-organic mixtures

Many recent studies concern the interaction of ionic surfactants or micelles [126] with homopolyelectrolytes [127, 128] or anionic surfactants and the natural polyampholytes, such as gelatin, collagen, and lysozyme [87, 129, 130].

Similar to the interaction of individual polyanions and polycations with surfactants, cationic detergents form cooperative complexes with acidic groups of polyampholytes, and anionic ones - with their basic group. Interaction of statistical copolymer of 1,2, S-trimethyl-4-vinylethynylpiperidinol-4, and acrylic acid (TMVEP-AA) and the regular copolymer of styrene and N,N-dimethylaminopropylmonoamide of maleic acid (St-DMAPMAMA) with sodium dodecyl sulfate (SDS) and cetyltrimethylammonium chloride (CTMACl) has been studied in water and water-methanol solutions. The addition of detergents leads to the considerable variation of pH, electroconductivity, turbidity, and viscosity of the system. This is connected with the formation of compact particles stabilized by hydrophobic contacts of the long alkyl chain of surfactants. These particles are preserved in solution with the help of noncomplexing components of copolymers. The increasing of the reduced viscosity for the system [St-DMAPMAMA] / [SDS] can be explained by additional adsorption of surfactant molecules to the complex particles, which lead to recharge of the macromolecules. The conformational transition from the compact structure of complex particles to expanded one is observed for the water-methanol mixture. These results are interpreted as follows: up

to a methanol content in the mixture of 60 vol.%, the compact conformation of the complex is stabilized by hydrophobic interactions of the nonpolar part of the surfactant. In the mixture from 60 to 80 vol.%, the complex particles are cooperatively destroyed due to preferentially solvation of the hydrophobic parts of the complex by methanol and hydrophilic ones by water [1, 131, 132].

1.4 Polyampholyte hydrogels

1.4.1 General knowledge of quenched polyampholyte hydrogels

PA hydrogels are usually prepared by free-radical copolymerization of cationic and anionic monomers in the presence of a chemical cross-linker [23, 133]. However, such chemically cross-linked PA hydrogels exhibit poor mechanical properties such as a low modulus and tensile strength limiting their load-bearing applications. Gong et al. synthesized high-strength charge-balanced physical PA hydrogels via random copolymerization [127, 134] of cationic and anionic ionic monomers at a high concentration. Formation of ionic bonds of various strengths due to the random distribution of charges along the polymer chains provided the formation of both permanent (strong) and sacrificial (weak) ionic bonds creating an effective energy dissipation that prevents crack propagation [53, 135].

PA hydrogels also exhibit unique features such as their sensitivity against pH and salt concentration variations, low toxicity, good biocompatibility [32, 136], and similarity to many biological systems [24, 137] and hence, they have a variety of applications including antibacterial, anti-fouling, and saline-resistant materials [138, 139].

By selecting the functional groups, polyampholytes have an isoelectric point (IEP). IEP happens at pH when the whole polyampholyte is charged neutrally. Furthermore, the IEP is the state where the polyampholyte will have the most compact conformation due to electrostatic attractions between balanced, opposite charged functional groups. As the pH increases or decreases from the IEP, the polyampholytes total charge shifts beyond neutral, creating electrostatic repulsive forces between similar areas, increasing and expanding polyampholyte. Similarly, once salt ions occur, ions disrupt electrostatic interactions between oppositely charged subunit regions. It allows the polyampholyte to swell as shown in figure 1.4. The degree of pH or salt swelling depends on polymer structure and architecture [11, 140].
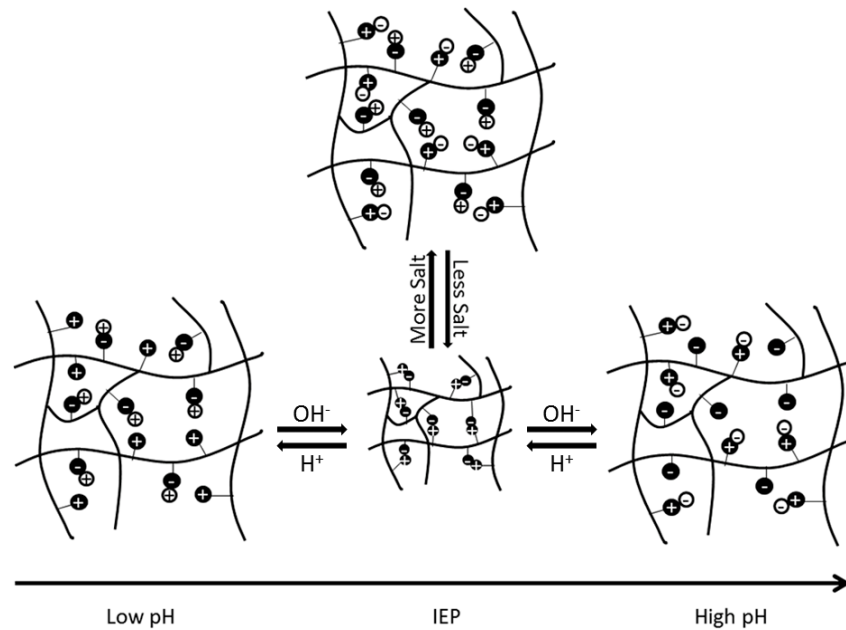
Figure 1.4 - Schematic representation of the impact that changes in pH and salt concentrations have on electrostatic interactions within a polyampholyte hydrogel [140].

The important general characteristic of neutral polyampholyte polymers is their inherent non-fouling properties. Previously, it has been widely shown and examined that this native resistance to non-specific protein adsorption stems from the development of a heavy hydration layer due to interactions between the normal dipole distribution in water and the charged regions of the underlying polyampholyte substratum. This is important because this non-fouling property is assumed to contribute to a reduced response to foreign bodies in the in vivo environment, as seen with similar zwitterionic systems [140-145].

1.4.2 Mechanical properties of quenched polyampholyte hydrogels

Polyampholyte systems composition-dependent tunability also provides a unique method to efficiently regulating biomaterials mechanical properties. An implanted biomaterial mimic needs to facilitate better tissue regeneration and integration, the tissue's native properties being supplanted [43, 146]. There is, of course, tremendous variance in tissue mechanical properties, as properties vary from soft and flexible (skin) to solid, with the ability to absorb impact forces (bone). Even high water content.

Based on polymer matrix, these sacrificial bonds can be covalent bonds, hydrogen bonds, ionic bonds, or hydrophobic interactions. Multiple approaches can also be incorporated into the base matrix, including double network gels, ionically linked gels, metal ion gelation, and composite gels [53]. The resulting hydrogels from all these methods show great mechanical strength, heat dissipation, and dispersion to slow down cracking and crack distribution [147]. The use of a double network hydrogel consisting of poly(2-acrylamido-2-methyl propane sulfonic acid) and

poly(acrylamide) was shown to increase compressive fracture pressure from 0.4–0.8 to 17.2 MPa [140, 148].

Nonetheless, with polyampholyte, double-network hydrogels exhibiting permanent deformation attempts started to use other bond forms that could be reversible and self-healing. Electrostatic interactions and hydrophobic interactions allowed some work. Mechanical properties are highly pH-dependent as the interactions that bind the system together may be weak or strong depending on the monomer charged state. The substance also swells and drops with pH changes [111, 149]. One research paper added partially quaternized poly (4-vinylpyridine) to an elastic hydrogel, introducing electrostatic, hydrophobic, and hydrogen-bonding interactions to dissipate energy better. It resulted in a 44-1000 J / m^2 rise in fracture power [140, 150].

For polyampholytes, it is normal to use electrostatic interactions as a secondary sacrificial bond to toughen materials through the use of opposite-charged functional groups spread throughout the process. Strong electrostatic interactions serve as permanent crosslinks and weaker interactions split and restart reversibly [23]. These bonds can also occur via inter and intra-chain interactions. Polyampholytes and polyion-complex hydrogels (PIC) all contain opposite charged functional groups and have the ability to be rough, self-healing. PICs arise from opposite electrostatic interactions.

Gong et al. prepared high-toughness polyampholyte hydrogels using free-radical copolymerization of opposite-charged ionic monomers at a high concentration around the zero net charge point [146, 148]. It has been shown that random charges contribute to several ionic bonds with a wide distribution of strengths. Although strong bonds function as permanent cross-links, weak bonds acting as reversible sacrificial bonds easily break under low stress and thus dissipate energy to prevent crack spread [151]. Although the hydrogels exhibit high mechanical strength, they do not display typical swelling characteristics of polyampholyte hydrogels due to their low water contents, e.g., 52–61 wt.%, and the presence of strong electrolyte functional groups.

Polyampholytes form the toughest hydrogels near-zero net charge, while PIC systems can form tough gels in weakly off-balanced compositions. PICs are generally stronger than polyampholytes when they have the same monomer compositions, as PIC hydrogels are smaller than polyampholytes [127, 140].

Similar techniques were also used to improve the ionic bonding mechanical properties of hydrogels. In one example, the removal of co-ions before gelation facilitated improved ionic bond-forming [148]. In another research, Cui et al. designed a pre-stretching system where hydrogels are prepared and extended. This stretching helps to bind chains parallel to each other, as opposed to the original random alignment when the chains are opposite, tighter ionic bonds, which in effect strengthens the polyampholyte hydrogel overall [134]. Fang et al. explored a similar approach to attain a tough and stretchable hydrogel by altering the structure of the material [140]. Beginning with a protein-based hydrogel, they pressured globular domain unfolding. The resulting collapse and aggregation of the unfolded material

make for physical intertwining and electrostatic interactions. The resultant hydrogels have a low swelling ratio, high stretchability, and durability unique properties [140].

Byette et al. got inspiration from the methods used to bind wet surfaces to toughen polyampholyte materials. Mussels use byssus, a protein-based material, to obtain solid surfaces. Byssus has a self-healing ability paired with strength partially because metal ions form sacrificial bonds with amino acid subunits. Byette et al. developed and treated the byssus protein hydrolysate with Ca^{2+} or Fe^{3+}. Fe^{3+} films showed the biggest increase in strength and toughness. Huang et al. used a similar method, forming a semi-interpenetrating polymer network of carboxymethyl chitosan (CMCH), acrylamide, and maleic acid with carboxylic–Fe3+ interactions acting as ionic sacrificial bonds. Through increasing maleic acid ratio and Fe^{3+} concentration, the strongest hydrogels showed 1.44 MPa tensile stress. Additionally, CMCH provided antibacterial properties against gram-positive Staphylococcus aureus and gram-negative Escherichia coli [140, 152].

1.4.3 Application of polyampholytes in tissue engineering, cryopreservation, and drug delivery.

Besides of tunable, sensitive, and non-fouling properties, polyampholyte also have a high moisture-holding capability that is generally associated with biocompatibility.

Jian described advances in the application of polyampholyte hydrogels for bioengineering, and Matsumura developed a nanocomposite hydrogel using COOH–PLL and synthetic clay laponite XLG, which shows promise as a tissue engineering scaffold due to its controlled release profiles, good mechanical properties, and cell adhesion capability [153]. Such gels are cytocompatible and had flexible properties. Furthermore, hydrogel formulation regulated cell adhesion. When the polymer chains are covalently cross-linked with PEG-NHS, certain laponite surfaces were covered, reducing cell adhesion. Conversely, when only mechanically crosslinked hydrogels PEG-NHS (polyethylene glycol- N-hydroxy succinimide) existed, there was more visible laponite surface area, leading to increased cell binding [140].

Another important element of tissue engineering is deep-term scenario cell survival. This is usually done using cryopreservation in liquid nitrogen cell freezer. Usually, before freezing, a cryoprotective agent (CPA) is applied to a cell solution to deter cell death. One of the most widely used CPAs is dimethyl sulfoxide (DMSO), but it is extremely cytotoxic and must be removed quickly after thawing. DMSO also mediated the division of many cell types. The need for a modern, more reliable CPA has motivated work into using polyampholytes for cryopreservation.

Matsumura et al. showed the use of COOH-PLL(carboxylated ε-poly-l-lysine) as a modern CPA for human bone bone-derived mesenchymal stem cells (hBMSCs) [140, 154].

Depending on the promising COOH-PLL tests, other polyampholytes were also examined as CPAs. Such experiments were both to extend the CPA formulation scope and to better understand how polyampholytes protect the cell membrane during freezing. For one example, 2-(dimethylamino) ethyl methacrylate (DMAEMA) and methacrylic acid (MAA) are copolymerized for different ratios of monomers [155].

Besides, N-butyl methacrylate (Bu-MA) and N-octyl methacrylate (Oc-MA) hydrophobic groups were inserted into the polymer backbone at 2–10% of the total monomer number. The range of polyampholyte polymers was checked, and the subsequent freezing occurred at a total solution polymer concentration of 10%, with 5% consisting of Bu-MA or Oc-MA. Through testing this range of polyampholyte compounds, cryoprotective properties are strongly correlated with hydrophobicity. Often suited for closely related zwitterionic polymers 3-(3-acrylamidoproply)dimethylammonio)-propane-1-sulfonate and 2-(2-methacryloyloxy))-dimethylamino acetate [156]. The zwitterionic species cryoprotective capabilities were compared to poly(MAA-DMAEMA), not exhibiting comparable cell viability, giving more insight into the preservation process. Through these experiments, it was concluded that the cryoprotective property is the result of strong interactions between the polyampholyte CPA and the cell membrane, strongly accompanied by minimal hydrophobic interactions [140, 155, 156].

Kudaibergenov et al. also used several guest molecules to characterize N,N-dimethylaminoethyl methacrylate and methacrylic acid with a N,N-methylenebisacrylamide crosslinker [87]. The guest species tested included methylene blue, methyl orange, sodium dodecylbenzene sulfonate (SDBS), and lysozyme. pH 9.5 adsorbed lysozyme and methylene blue, and pH 7.5 adsorbed SDBS and methyl orange Similar to the work by Barcellona et al., and Kudaibergenov et al. [131, 157] electrostatic forces drove the binding interactions between the cryogel and the guest molecules. Nonetheless, at pH 7.1 of the IEP, amphoteric cryogel allowed 93–98% of the adsorbed species to be released. Barcellona's findings are also backed by simulation-based research that suggests that electrostatic interactions play a major role in mediating drug release from polyampholyte systems [140, 158].

Mishra et al. used poly 3-[(methacryoylamino)propyl trimethylammonium chloride-co-methacrylic acid](PMAPTAC-MAAc) copolymers with various monomer concentrations and charged indomethacin (IND) [159]. IND is a semi-steroidal non-inflammatory drug used to treat rheumatoid arthritis, ankylosing spondylitis, and osteoarthritis. Hydrogel design played a major role in IND continuous release, and PMAPTACMMAc-5 lead to the highest percentage of IND release. This equation extracted 75% of entrapped IND within eight hours and 82% after 12 hours. Certain formulations showed release levels ranging from ~44% to 77% after 12 h. The release was primarily diffusion-based, following non-Fickian release kinetics. Though diffusion is often successful for drug delivery, a controlled release approach will provide more targeted delivery. Salicylic acid has been used as a model drug in a polyampholyte consisting of casein and poly(N-isopropyl acrylamide), and temperature, pH, and crosslinker density influenced the development [160]. This prompted Cao et al. to assume that this delivery vehicle is perfect for oral drug delivery. Finally, Sankar et al. showed the pH-sensitive release of promethazine hydrochloride from hydrogels including carbon nanotubes [161]. Such nanotubes are integrated into the hydrogel as a method to improve this delivery system's mechanical properties without compromising drug delivery capabilities [140].

Researchers have started integrating polyampholytes into multi-component structures to improve performance or provide additional benefits. For example, Wang et al. tested a polyampholyte hydrogel-based pyromellitic diester diacid chloride (PDDC) release system combined with diethylenetriamine (DETA) and triazine combinations [162]. This polyampholyte system showed a pH-dependent release capability that overcame previous problems with terephthaloyl chloride (TC) encapsulants instead of PDDC. The latest microcapsule formulation demonstrated high load strength and consistent, controlled release at pH = 7.4. It also demonstrated increased release at both pH5 and pH10. The release properties were also tunable by adjusting the DETA-triazine ratio, demonstrating the potential for tunable release speed applications to optimize this microcapsule formulation [140].

Others have also incorporated polyampholyte polymers into their drug delivery vehicles to add pH-responsive release characteristics. For example, Schulze et al. [163-166] saw potential in lamellar liquid crystalline systems, but the structure did not react to environmental stimuli such as pH. By inserting the polyampholyte poly (N,N′-diallyl-N,N′-dimethyl-almaleamic carboxylate) into a lamellar liquid crystalline network of sodium dodecyl sulfate, decanol, and water, it was found that release from the new structure could be controlled by varying pH or temperature. This suggests a new structural structure for drug delivery systems [163]. In another example, paracetamol, an analgesic drug, was extracted from a matrix of laponite, polyacrylamide and poly (3-acrylamidopropyl) trimethylammonium chloride. Drug release was tested based on environmental changes in pH and ionic strength and electrical field activity. Without an electrical field, paracetamol was released at pH 1.1, but with the addition of an electrical field continued product release at other pH values [167]. Eventually, Ali et al. produced a novel polymer containing alendronic acid residues that display pH-sensitive responses suggested as a drug delivery mechanism [140, 168].

Asayama et al. have integrated a polyampholyte polymer, carboxymethyl poly (1-vinyl imidazole) (CM-PVIm) an existing system. CM-PVIm was used to bind complexes of poly(ethylenimine)/DNA (PEI / DNA) to eliminate anti-specific protein adsorption to this delivery platform. Results showed this coating did not significantly decrease gene transfection or cell viability. Therefore The authors found that CM-PVIm is an effective coating for better circulation of gene therapy agents [169]. The use of applying polyampholytes to drug delivery vehicles is based on their good holding power. Polyampholyte acrylic latexes are integrated into product tablet coatings to minimize the amount of water lost during tablet drying [170]. In refining this method, Ladika et al. focused on finding a polymer solution of comparable viscosity to the industry standard but a much higher solid density. Today's standard tablet coatings vary from 4–10 wt.%. The proportion of solids and new polyampholyte acrylic latexes was 37–39 wt.% of solids. Three latex forms are explored: soft acid / strong base latexes, strong acid / weak base latexes, and anionic and cationic hybrids. Latex formulations for all three varieties are established with viscosities similar to current coating solutions, higher solid structure, and pH-tunable to enable selective delivery of active pharmaceutical ingredients [140].

1.5 Polyampholyte cryogels in catalysis

Polyampholyte cryogels can consist of a primary, secondary and tertiary amine, quaternary ammonium groups, on the one side, and carboxylic, sulfonic, or sulfonate moieties, and acrylamide monomers, on the other [26]. Such polyampholyte cryogels can be defined as «annealed» polyampholyte cryogels in addition to «quenched» polyampholyte cryogels, consisting of fully charged amphoteric cryogels prepared from temporarily charged cationic and anionic monomers. Whether cryogels contain the same amount of pH-dependent acid-base or pH-independent anionic-cationic groups in the same monomer units, they can be called "betaine" or «zwitterionic» cryogels. Low-and high-charge-density polyampholyte cryogels. Low-charge polyampholyte cryogels can be derived from cationic and anionic monomers with nonionic species such as acrylamide [17-19] or N-isopropylacrylamide [20].

One of the key attributes of any polyampholyte is ionization constants for acid-base groups (pKa or pKb) and isoelectric point (IEP) values in which the whole macromolecule is quasi-neutral. Figure 1.6 shows the composition, continuous ionization of allylamine groups and isoelectric pH of allylamine-co-acrylic acid-co-acrylamide P(AA-*co*-AAc-*co*-AAm) cryogels crosslinked by N,N-methylene bisacrylamide (MBAA) [18,19] .Amphoteric cryogels differ each other by the content of acid-base and AAm monomers and abbreviated as ACG-550, ACG-442, ACG-334, ACG-226, and ACG-118.

m: n: o (mol/mol/mol)
50:50:0   (ACG-550)
40:40:20 (ACG-442)
30:30:40 (ACG-334)
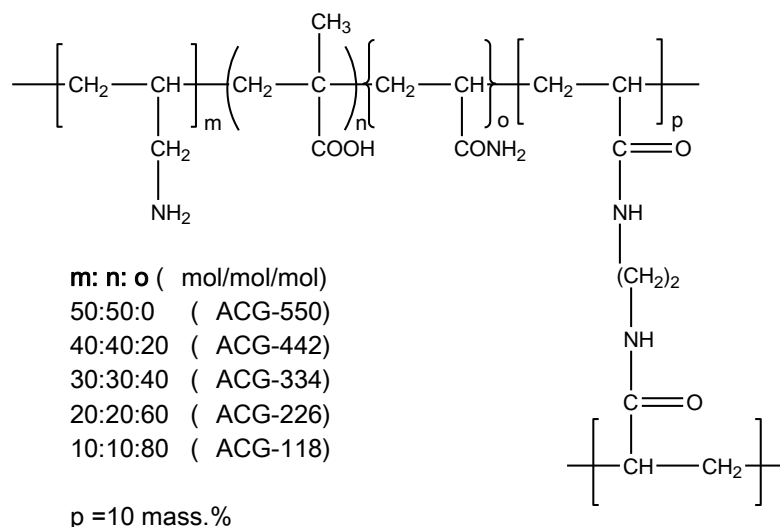20:20:60 (ACG-226)
10:10:80 (ACG-118)

p =10 mass.%

Figure 1.6 - Structural units of amphoteric cryogels derived from AA, MAA and AAm crosslinked by MBAA [171]

Cryogel catalysts are attractive materials due to inherent features: macroporous structures, customizable hydrophilicity and hydrophobicity, and the versatile catalytic unit selection and mix. Remobilization of polymer-metal complexes, metal nanoparticles, and biomolecules in the polymer matrix promises to model the catalytic structures [172] that enhance the reactions of decomposition, hydrogenation, oxidation [173], isomerization, etc. Such polymers will continually or discontinuously alter conformation and morphology-based on environmental factors.

This, in effect, allows the structure and properties of immobilized to be incorporated into the polymer matrix, thereby regulating and controlling their architecture and catalytic behavior.

In various chemical reactions, all polyampholyte cryogel and cryogel-immobilized metal nanoparticles possess unusual catalytic properties. Cryogels main advantage in catalysis is their macroporous structure, which can provide both metal nanoparticles and unhindered liquid flux within cryogels. Superporous cryogels of poly(2-hydroxyethylmethacrylate) and poly(3-sulfopropylmethacrylate), poly(acrylic acid), poly(4-vinyl pyridine), poly(2-acrylamide-2-methyl-1-propane sulfonic acid), poly[2-(methacrylate)ethyl]dimethyl(3-sulfopropyl)ammonium hydroxide and its metal nanoparticles composites (Co, Ni, Cu, and Fe) were used in the redox reaction of NaBH4 and hydrogenation of $NaBH_4$. Substrate reduction is easily controlled by calculating peak absorption at 414 nm, 400 nm, and 380 nm for 2-NP, 4-NP, and 4-NA, respectively [171].

Modified polyacrylamide-based amphoteric cryogels were tested as catalytically active substances in transesterification of glyceryl oleate. The highest conversion of glyceride was equal to 88.4%, and the yield of methyl oleate is about 64.% [171].
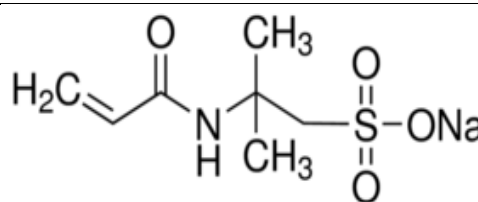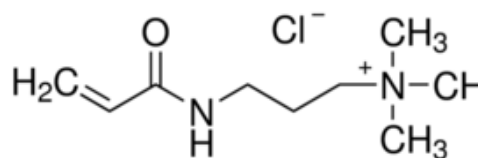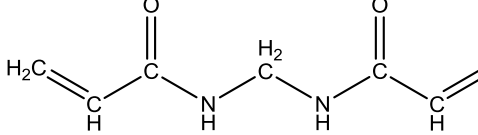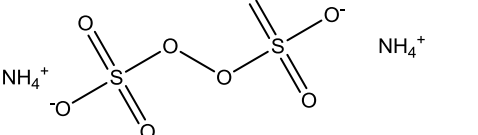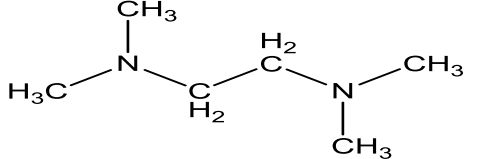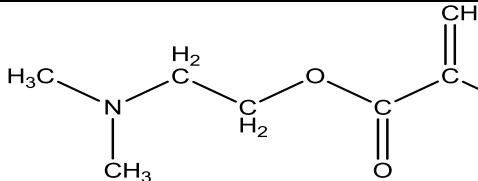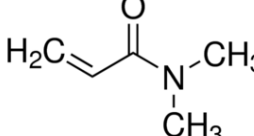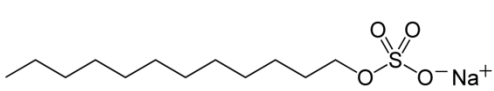
The catalytic reduction of 4-NP by $NaBH_4$ and oxidation of D, L-dithiothreitol (DTT) by hydrogen peroxide in the presence of AuNPs supported on cryogel matrix of P(DMAEM-*co*-MAA) was evaluated and the kinetic parameters, turnover number (TON), turnover frequency (TOF) and activation energy of hydrogenation of 4-NP have been calculated [172].

Therefore, cryogels based on catalysts (DMAEM-*co*-MAA)/AuNPs exhibit high catalytic activity and conversion in 4-NP reduction and DTT oxidation, as well as can function as a catalytic 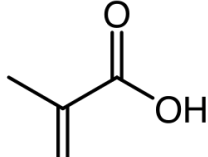flow-through reactor as well as provide cascade-type reaction without inhibition of intermediary products. The main advantage of the macroporous structure is a large catalyst-substrate contact region, reusability, and ease of material isolation from the reaction medium [87, 171].

2 EXPERIMENTAL PART
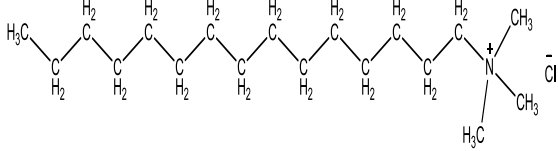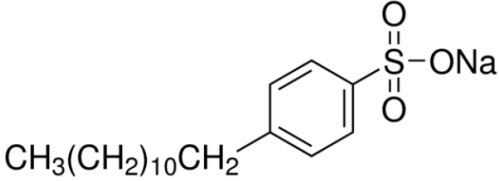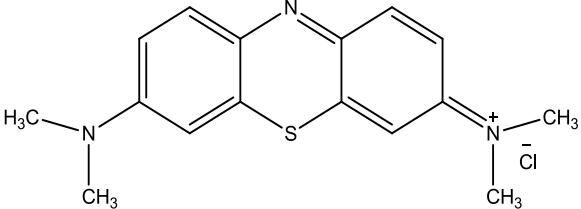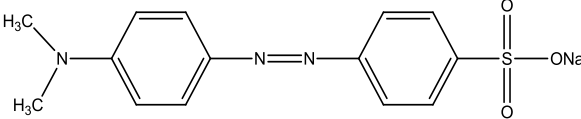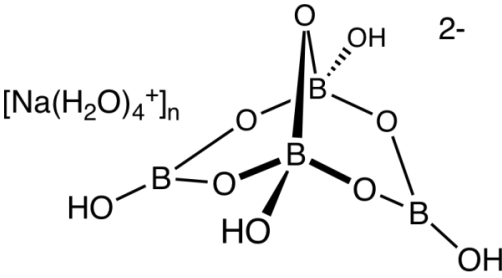
2.1 Objects of the research

Table 2.1- Objects of the research

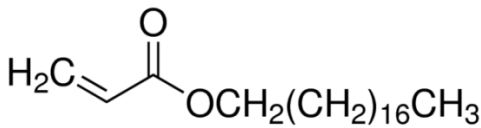| Name, Abbreviation	Chemical structure
2-Acrylamido-2-methyl propane sulfonic acid sodium salt (AMPS, 50 wt.% in water), Mr = 229.23 g/mol from "Sigma-Aldrich", was used without further purification.	
3-acrylamidopropyl) trimethylammonium chloride (APTAC, 75 wt.% in water), Mr = 206.71 g/mol ,"Sigma-Aldrich", was used without further purification.	
N,N′-Methylenebis(acrylamide), Mr = 154.17 g/mol, "Sigma-Aldrich", was used without further purification.	
Ammonium persulfate (APS), Mr = 228.2 g/mol, made by Changzhou Qi Di Chemical Co. (China), was used without further purification.	
N,N′,N′N′-Tetramethylethylenediamine (TMEDA), Mr=116.2 g/mol, "Sigma-Aldrich", was used without further purification.	
Methacrylic acid (MAA), Mr = 86.09 g/mol, "Sigma-Aldrich" was used without further purification.	
2-(Dimethylamino)ethyl methacrylate-(DMAEMA), Mr = 157.21 g/mol, "Sigma-Aldrich", was used without further purification	
N,N-Dimethylacrylamide (DMA)- Mr = 99.13 g/mol, "Sigma-Aldrich", was used without further purification.	
Sodium dodecyl sulfate (SDS), Mr = 288.38 g/mol, "Sigma-Aldrich", was used without further purification.	

Continuation of Table 2.1

Octadecyl acrylate (ODA), Mr = 324.54 g/mol, "Sigma-Aldrich", was used without further purification.	H_2C = ... $OCH_2(CH_2)_{16}CH_3$
Cetyltrimethylammonium chloride solution (CTMACl), Mr = 305.97 g/mol, 25 wt.% in H_2O (Aldrich), AppliChem GmbH, was used without additional purification	H_3C—...—$N^+(CH_3)_3$ Cl^-
Dodecylbenzenesulfonate (DDBSNa), Mr = 348.48 g/mol, "Sigma-Aldrich", was used without further purification	$CH_3(CH_2)_{10}CH_2$—...—$S(=O)_2$—ONa
Methylene blue, Mr = 319.85 g/mol, of "Reachim", was used without further purification	
Methyl orange, Mr = 327.33 g/mol, of the company "Reachim" brand, was used without further purification	
Potassium chloride – KCl, Mr = 74.55 g/mol, "Reachim", was used without further purification	
Sodium hydroxide – NaOH 0.1 M Prepared from fixanal (the contents of fixanal were quantitatively transferred into a 1000 mL volumetric flask, and the volume was made up to the mark with water)	
Sodium chloride – NaCl Mr = 58.44g/mol, "Reachim" brand, clean, was used without further purification	
Sodium tetraborate decahydrate— $Na_2B_4O_7 \cdot 10H_2O$, 0.05 M. 19.07 g of the substance was dissolved in water, and the volume was adjusted to the mark in a 1000 mL volumetric flask	$[Na(H_2O)_4^+]_n$ ... $^{2-}$

Continuation of Table 2.1

Disodium Phosphate (DSP) – Na_2HPO_4 $Mr = 141.96$ g/mol 0.2 M. 28.392 g of the substance was dissolved in water, and the volume of the solution was adjusted to the mark in a 1000 mL volumetric flask	O ‖ HO–P–ONa | OH
Ethanol (90% aqueous solution), "Format", was used without further purification	H H H | | / H—C—C—O | | H H
Acetone, "Format", was used without further purification	O ‖ H₃C CH₃

2.2 METHODS OF THE RESEARCH

2.2.1 Synthetic protocol of strongly charged linear and crosslinked polyampholytes

2.2.1.1 Synthesis of linear polyampholytes

Linear polymers were prepared using solution polymerization of AMPS and APTAC in the presence of APS as an initiator at 60°C. Initial monomer concentration was fixed at 5 wt.% with respect to the solution mass. (figure 2.2.1, table 2.2.1).

In order to prepare AMPS50 linear polyampholytes, APTAC (4.12 g) and AMPS (4.49 g) were mixed at room temperature and stirred for 15 min to form a homogeneous solution. After the addition of APS (0.05 mg) and stirring for 1–2 min, nitrogen was bubbled 30 min to eliminate oxygen from the reaction mixture. The solution then was transferred into cylindrical vessels of a volume of about 10 mL, and set in a thermostatically-controlled environment of 60°C. The reaction mixtures were kept at this temperature for 5 h. After preparation, unreacted monomers were removed through a dialysis membrane in a 5 L distilled water tank followed by lyophilization[174-180].
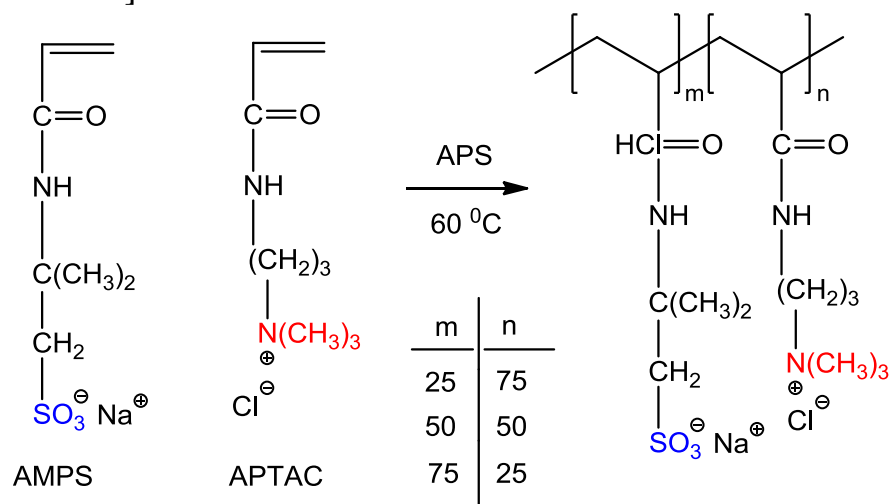
Figure 2.2.1 - Schematic illustration of polymerization of AMPS-APTAC copolymers

Table 2.2.1 - The feed composition of linear polyampholytes

Code	AMPS / g	APTAC / g	APS / mg
AMPS 75	15.30	3.04	0.08
AMPS 50	10.52	6.01	0.05
AMPS 25	5.38	9.80	0.08

2.2.1.2 Synthesis of polyampholyte hydrogels

Hydrogels were prepared at 60°C in aqueous solutions of various AMPS concentrations C_{AMPS} between 25 and 75 mol.% in the presence of MBAA as a cross-linker. Initial monomer concentration was fixed at 5 wt.%, while the cross-linking agent was 20 mol.% with respect to monomers (table 2.2.2).

In order to prepare H-AMPS50 polyampholyte hydrogels, APTAC (0.28 g) and AMPS (0.46 g) monomers and crosslinking agent MBAA (0.06 g) were mixed at room temperature and stirred for 15 min to form a homogeneous solution. After the addition of APS (30 mg) and stirring for 1–2 min, nitrogen gas was bubbled through the homogeneous solution for 30 min to eliminate oxygen from the reaction mixture. Then, the solution was transferred into cylindrical vessels of a volume of about 10 mL, and set in a thermostatically-controlled environment of 60°C. The reaction mixtures were kept at this temperature for 24 h. After preparation, unreacted monomers were removed using a beaker and poured into distilled water to remove unreacted components until fully washing [174-180].

Table 2.2.2 - The feed composition of the hydrogels

Code	AMPS / g	APTAC / g	MBAA/ g	APS / g
H-AMPS25	0.24	0.43	0.06	0.03
H-AMPS50	0.46	0.28	0.06	0.03
H-AMPS75	0.68	0.14	0.06	0.03

The polymerization protocol and scheme of APMPS-APTAC hydrogels are shown in figures 2.2.2 and 2.2.3, respectively.

Figure 2.2.2 – A schematic illustration of polymerization of AMPS-APTAC hydrogels

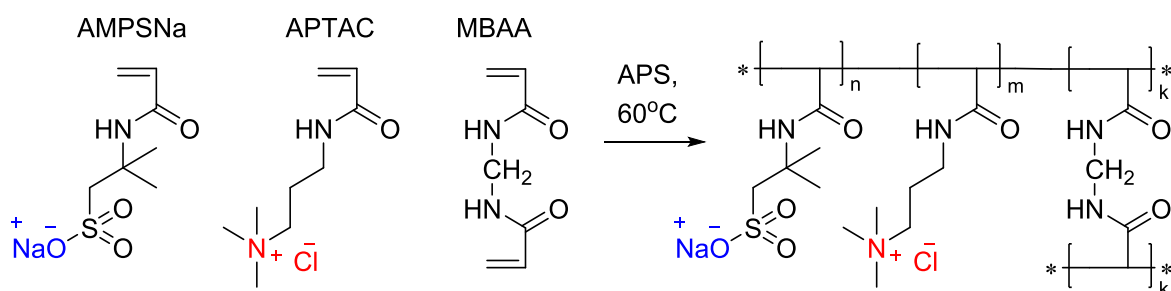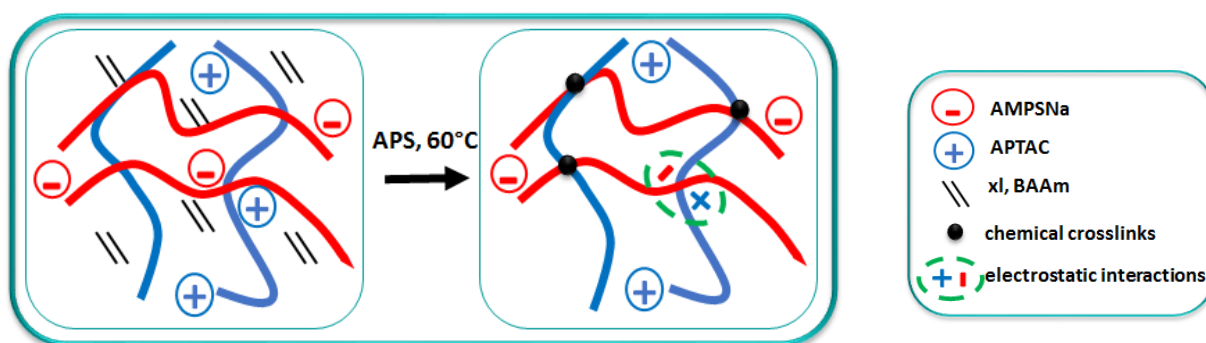Figure 2.2.3 – A schematic illustration showing the intermolecular electrostatic interactions between ionized APTAC and AMPS segments, and chemical crosslinks of polyampholyte hydrogels

2.2.1.3 Synthesis of polyampholyte hydrogels using N,N-Dimethylacrylamide (DMA).

AMPS-50H composition was fixed as a reference, and total monomer concentration was increased from 5 to 30 wt.% ($C_M = 1.35$ M), whereas the chemical-crosslinker was varied between 20-0.1 mol% with respect to total monomer concentration. Also, DMA was added to the comonomer mixture to increase stretchability. The volume of DMA in the feed composition was changed between 5 and 20 mol% (table 2.2.3). The above-mentioned synthesis procedure was followed for the preparation of hydrogels at $C_0 = 30$ wt.%, MBAA = 0.5, and DMA mol.% = 20, in the presence of 10 mM APS initiator. AMPS (2.364 g), APTAC (0.948 g) and DMA (0.169 g) were mixed and dissolved in 1.5 mL distilled water at room temperature to form a homogeneous solution. After the addition of MBAA (5.3 mg), nitrogen gas was bubbled through the homogeneous solution for 30 min to eliminate oxygen from the reaction mixtre. Taking into account total monomer concentration, APS (10 mM) was added, and the solution was transferred into plastic syringes of 1 mL volume. Polymerization lasted for 24 h at 60°C.

Synthesis parameters $x_{AMPS} = 0.5$ and $C_M = 1.35$ M are included in table 2.3.3, showing hydrogels with the highest limit of initial monomer concentration and minimal chemical crosslinker, in order to make stretchable material with additional DMA monomer .

Table 2.2.3 - Synthesis parameters: AMPS $x_{AMPS} = 0.5$ and $C_M = 1.35$ M

Series	MBAA / mol%	DMA / mol%	APS / mM
A	5-0.1	-	10
B	0.5	5-20	10

2.2.1.4 Synthesis of hydrophobically modified polyampholyte hydrogels

Two sets of hydrogels were prepared by free-radical copolymerization of AMPS and APTAC using UV light in the presence of a 2-oxoglutaric acid initiator (0.25 mol.%, with respect to the monomers). In the first set, the reactions were carried out in a mixture of equimolar AMPS and APTAC monomers via micellar copolymerization in the presence of the hydrophobic monomer C18A. Both the amount of C18A in the monomer mixture and the total monomer concentration C_o were varied between 1 – 25 mol.%, and 1.0 – 2.5 M, respectively. An aqueous solution of SDS in 0.5 M NaCl was used as the micellar solution due to the significant solubilization of the resulting worm-like SDS micelles. SDS concentration was 7 and 14 w/v% for C18A contents below and above 10 mol.%, respectively. In order to prepare hydrophobically modified hydrogels with 20 mol.% C18A at $C_o = 1.0$ M, C18A (0.65 g) was first dissolved in 4 mL 0.5 M NaCl solution containing 1.4 g SDS at 35 °C for 2 h to form a homogeneous solution. The aqueous solutions of 50 wt.% AMPS (2.29 g) and 75 wt.% APTAC (1.38 g) were then added to the micellar solution of C18A and stirred for 30 min. After the addition of 2-oxoglutaric acid (4 mg), the solution was transferred into plastic syringes of 4.6 mm in diameter to

conduct the polymerization reactions at 23 ± 2 °C using UV light at $\lambda = 360$ nm for 24 h (tables 2.2.4 and 2.2.5). A schematic showing the structure (a) of physically-crosslinked polyampholyte hydrogels before (b) and after (c) gelation of the monomers via the micellar polymerization technique are shown in figure 2.2.4. The feed composition of the hydrogels and synthesis parameters of the composition of hydrophobically-modified hydrogels are shown in tables 2.2.4-2.2.5.
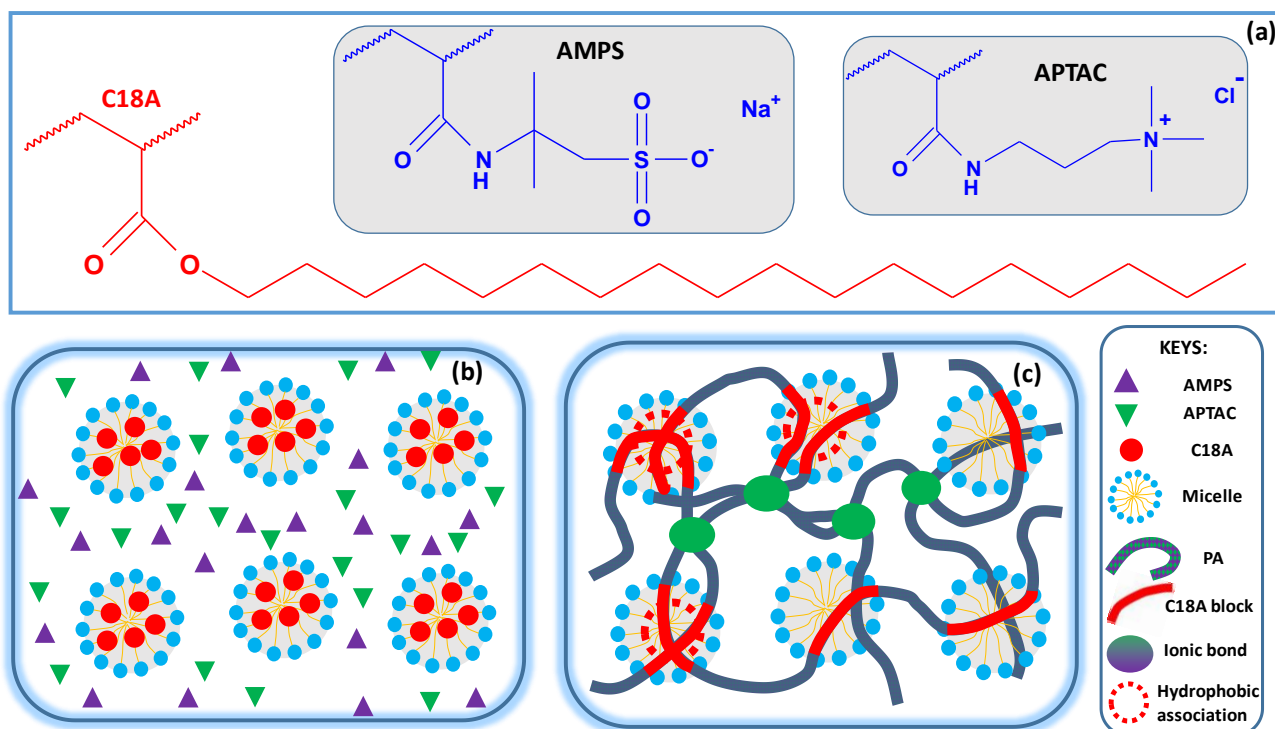
Figure 2.2.4 - (a): Structure of 2-acrylamido-2-methyl-1-propanesulfonic acid sodium salt (AMPS), (3-acrylamidopropyl)trimethylammonium chloride (APTAC), and n-octadecyl acrylate (C18A) repeat units of physically-crosslinked polyampholyte hydrogels. (b, c): Scheme showing before (b) and after gelation of the monomers via micellar polymerization method (c)

Table 2.2.4 - The feed composition of the hydrogels. Initiator mass was fixed as 0.25 mol.% with respect to the total monomer concentratration

ODA, mol.%	AMPS /g	APTAC /g	ODA /g	SDS / g	NaCl /g	Distilled water / g
1	2.292	1.378	0.320	0.700	0.2925	5.302
2	2.292	1.378	0.065	0.700	0.2925	5.274
5	2.292	1.378	0.1625	0.700	0.2925	5.175
7	2.292	1.378	0.227	0.700	0.2925	5.107
10	2.292	1.378	0.325	1.400	0.2925	4.313
15	2.292	1.378	0.488	1.400	0.2925	4.149
20	2.292	1.378	0.650	1.400	0.2925	3.987
25	2.292	1.378	0.813	1.400	0.2925	3.824

Table 2.2.5 - Synthesis parameters of the composition of hydrophobically-modified hydrogels

Series	X_{AMPS}	C_M / M	MBAA/ mol.%	C18A/ mol.%[*]
A	(varied, 0 – 1)	1	1.25	-
B	0.5	1	-	(varied, 1 – 25)
C	0.5	varied 1 - 2.7	-	-
D	0.5	varied 1 -2.7	-	2
[*] Respect to total monomers				

2.2.1.5 Synthesis of polyampholyte cryogels.

Cryogels were synthesized at -12°C in aqueous solutions of various AMPS concentrations C_{AMPS} between 25 and 75 mol.% in the presence of the MBAA cross-linker and TEMED (0.25 v/v%) as a catalyst. The initial monomer concentration was fixed at 5 wt.%, while the cross-linking agent was set at 10 mol.% with respect to the monomers (table 2.2.5).

In order to prepare AMPS50 polyampholyte cryogels, APTAC (0.5912 g) and AMPS (0.982 g) were mixed at room temperature and stirred for 15 min to form a homogeneous solution. Then the solution was cooled to 0°C and TEMED was added. The reaction mixture was then purged with nitrogen for 10 min. After the addition of APS (11 mg) and stirring for 1–2 min, nitrogen gas was bubbled through the homogeneous solution for 30 min to eliminate oxygen. The solution was then transferred into cylindrical vessels of a volume of about 10 mL, and set in a thermostatically-controlled environment of -12°C. The reaction mixtures were kept at this temperature for 48 hours. After preparation, unreacted monomers were removed from the vessels, placed in a 200 mL beaker and poured into distilled water to remove unreacted components. The synthesis of cryogels using DMAEMA-MAA, with a molar ratio 50:50 mol.% and MBAA 2.5 mol.% with respect to total monomer concentration, was performed by an identical method (table 2.2.6).

Table 2.2.5 - The feed composition of AMPS-APTAC cryogels (total 10 g)

Code	AMPS / g	APTAC / g	MBAA / g	Initiator / g
AMPS25	0.50	0.91	0.07	0.01
AMPS50	0.98	0.59	0.07	0.01
AMPS 75	1.44	0.29	0.06	0.01

Table 2.2.6 - The feed composition of DMAEMA-MAA cryogels (total 10 g)

Code	DMAEMA / g	MAA / g	MBAA / g	Initiator / g
DMAEMA-MAA	0.626	0.343	0.031	0.01

2.2.2 Characterization and identification of AMPS-APTAC copolymers

2.2.2.1 FTIR spectroscopy

A sample of the APTAC-AMPS copolymers were ground in an agate mortar to a powder state, then a 2 mg sample of the powder was measured out and transferred to a Cary 660 FTIR IR spectrophotometer (Agilent Technologies, USA) using a single-bounce diamond attenuated total reflectance (ATR) accessory equipped with a liquid nitrogen-cooled mercury-cadmium-telluride detector, and the spectrum of the sample was recorded. Because the samples of linear polymers already had a powder-like texture, they were studied without preliminary sample preparation on the FTIR IR spectrophotometer, and the spectrums of the samples were also recorded.

2.2.2.2 H^1 NMR spectroscopy

^{1}H NMR spectra of the copolymers dissolved in D_2O (10 mg/mL) were recorded at room temperature on a Bruker 400 MHz Fourier NMR spectrometer using tetramethylsilane as an internal standard. The peaks between d = 1.8–2.0 ppm are assigned to methyl groups of amide, while the peaks between 3.4 and 3.6 ppm characterize the methyl groups of the AMPS. The ionic segment content of the copolymers was determined from the area ratio of meta-protons to methyl proton peaks in ^{1}H NMR spectra of AMPS-APTAC linear polymers in D_2O.

2.2.2.3 Gel-permeable chromatography (GPC)

The average molecular weights (M_w and M_n) of aqueous solutions of AMPS-APTAC were measured by gel permeation chromatography (GPC) using a Viscotek (Malvern) chromatograph equipped with 270 dual detectors (Malvern) and VE 3580 RI detector (Malvern). Two 6000M columns (Malvern) were used, and the flow rate of DMF in mobile phase was 0.7 mL/min. Polystyrene standard samples (PolyCAL™, Malvern) were used to plot the calibration curve. The injection volume of the sample was equal to 100 μL.

2.2.2.4 Differential scanning calorimetry (DSC) and thermogravimetric analysis (TGA)

10 mg of AMPS-APTAC copolymer powder was placed in a cuvette, and the sample was analyzed using a DSC 131 device (Setaram, France). For TGA analysis, a 10 mg sample was placed in a cuvette and tested using Labsys Evo equipment (Setaram, France).

2.2.2.5 Scanning electron microscopy (SEM)

The morphology of cryogels was studied using a scanning electron microscope, JSM-6390 LV (JEOL, Japan).

2.2.3 Mechanical and rheological properties of AMPS-APTAC copolymers

2.2.3.1 Rheological measurements

The measurements were conducted on a Bohlin Gemini 150 rheometer system (Malvern Instruments, UK) equipped with a Peltier device for temperature control. Hydrogel samples were prepared and placed between rheometer plates at 60°C to

monitor gelation. The frequency sweep tests were carried out over a frequency range of 0.1 to 100 rad.s^{-1}, with the gels, following preparation, placed between the cone and plates (diameter, 40 mm) of the instrument, and then set at a constant distance of 150 μm. The frequency-sweep tests were carried out at a strain amplitude of $\gamma o = 0.01$ and temperature of 25 °C.

2.2.3.2 Mechanical testings

Uniaxial compression and elongation tests were performed at 24 ± 2°C on a Zwick Roell Z0.5 TH test machine using a 500 N load cell. Load and displacement data were collected using cylindrical hydrogel samples of 4.6 mm in diameter. For uniaxial compression measurements, the hydrogel samples were compressed at a strain rate of 1 min^{-1}. Before the test, an initial compressive contact of 0.05 N was applied to ensure complete contact between the gel and the plates. For uniaxial elongation measurements, the initial sample length between the jaws was set at a strain rate of 10 ± 1 mm and 1 min^{-1}, respectively. The stress was measured at nominal σ_{nom} and true values σ_{true} ($=\lambda \ \sigma_{nom}$), which are the forces per cross-sectional area of the undeformed and deformed specimens, respectively, with the strain represented as λ, the deformation ratio (deformed length/initial length). The strain ε is also defined as the change in the length of the gel specimen relative to its initial length, i.e., $\varepsilon = \lambda - 1$ or $\varepsilon = 1 - \lambda$, for elongation and compression, respectively. The Young's modulus E was calculated from the slope of the nominal stress-strain curves between 5 and 15% deformation. The compressive strength σ_f was calculated from the maxima in true stress-strain curves [37]. Cyclic tensile experiments were conducted at a strain rate of 5 min^{-1} to a maximum strain ε_{max}, followed by immediate retraction to zero displacement and a waiting time of 1 min and 2 min, respectively, until the next cycle (figure 2.2.5).

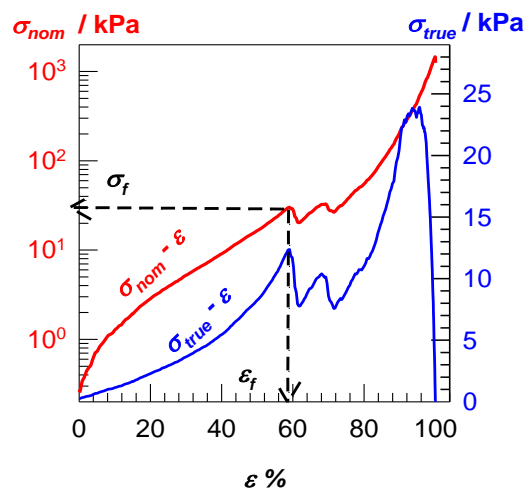Figure 2.2.5 - Typical stress-strain curves of AMPS 50 hydrogel samples under compression where the nominal stress σ_{nom} (red curve) and true stress σ_{true} (blue curve) are plotted against the compressive strain ε. Dashed lines represent calculations of the fracture stress σ_f and fracture strain ε_f from the maximum in the $\sigma_{true}-\varepsilon$ curve

2.2.4 Conformational properties of linear quenched polyampholytes

2.2.4.1 Solution properties of quenched linear polyampholytes

The isoelectric point and zeta potential of linear polyampholytes were determined using the dynamic laser light scattering (DLS) technique on a Malvern Zetasizer (UK) at 25°C. Distilled water and solutions of potassium chloride with 0.05, 0.1, 0.5, 0.75, and 1.0 mol/L concentrations were used as solvents. The concentrations of the APTAC-AMPS solutions were varied from 0.3 to 0.1.

Concentration dependence of the reduced viscosity of AMPS-APTAC in solutions of different ionic strengths (μ) is expressed as mol/L of KCl.

The intrinsic and reduced viscosities of linear polymers were determined by viscometry on a water thermostat at a temperature at 25± 0.1°C with the help of a Ubbelohde viscometer. Distilled water and solutions of potassium chloride concentrations with 0.05, 0.1, 0.5, 0.75 and 1.0 mol/L were used as solvents.

The intrinsic viscosity is determined by the formula:

$$[\eta] = \lim_{C \to i} \frac{\eta_{red}}{C} \tag{2.2.1}$$

where is the η_r–reduced viscosity;
C – concentration of polymer.
Inherent viscosity η_{inh} is determined by the formula:

$$\eta_{inh} = \frac{\ln \eta_r}{C} \tag{2.2.2}$$

where is the η_r – reduced viscosity;
The reduced viscosity was calculated by the formula:

$$\eta_r = \frac{\eta_{sp}}{C} \tag{2.2.3}$$

where is the η_{sp} is specific viscosity
The specific viscosity of the polymer is determined by the formula:

$$\eta_{average} = \frac{t_{average} - t_0}{t_0} \tag{2.2.4}$$

where is the $t_{average}$ − the average value of expiration of the dilute polymer solution;

t_0 − expiry time for solvent.

2.2.4.2 Complexation of quenched linear polyampholytes with surfactants and dyes

The polyampholyte-surfactant and, dye complexes were studied by the turbidimetric method. Optical characteristics were studied using a Specord 210 plus UV spectrophotometer (Germany) at room temperature in quartz glass cells at a wavelength of 340 nm.

The preparation protocol of solutions and molar ratio of interacting components are described in tables 2.2.7 and 2.2.8.

The complexation schematic of APTAC-AMPS with surfactants and dyes is shown in figures 2.2.7 , 2.2.8.

Table 2.2.7 - Ratio calculation of AMPS-APTAC – surfactants solution

APTAC-AMPS solution			CTMACl, SDBS solution		
Ratio	V, mL	C=const, mol/L	Ratio	V, mL	C, mol/L
9	5		1	5	$1.11*10^{-4}$
8	5		2	5	$2.50*10^{-4}$
7	5		3	5	$4.29*10^{-4}$
6	5	$1.00*10^{-3}$	4	5	$6.67*10^{-4}$
5	5		5	5	$1.00*10^{-3}$
4	5		6	5	$1.50*10^{-3}$
3	5		7	5	$2.30*10^{-3}$
2	5		8	5	$4.00*10^{-3}$
1	5		9	5	$9.00*10^{-3}$

Table 2.2.8 - Ratio calculation of AMPS-APTAC – dye solutions

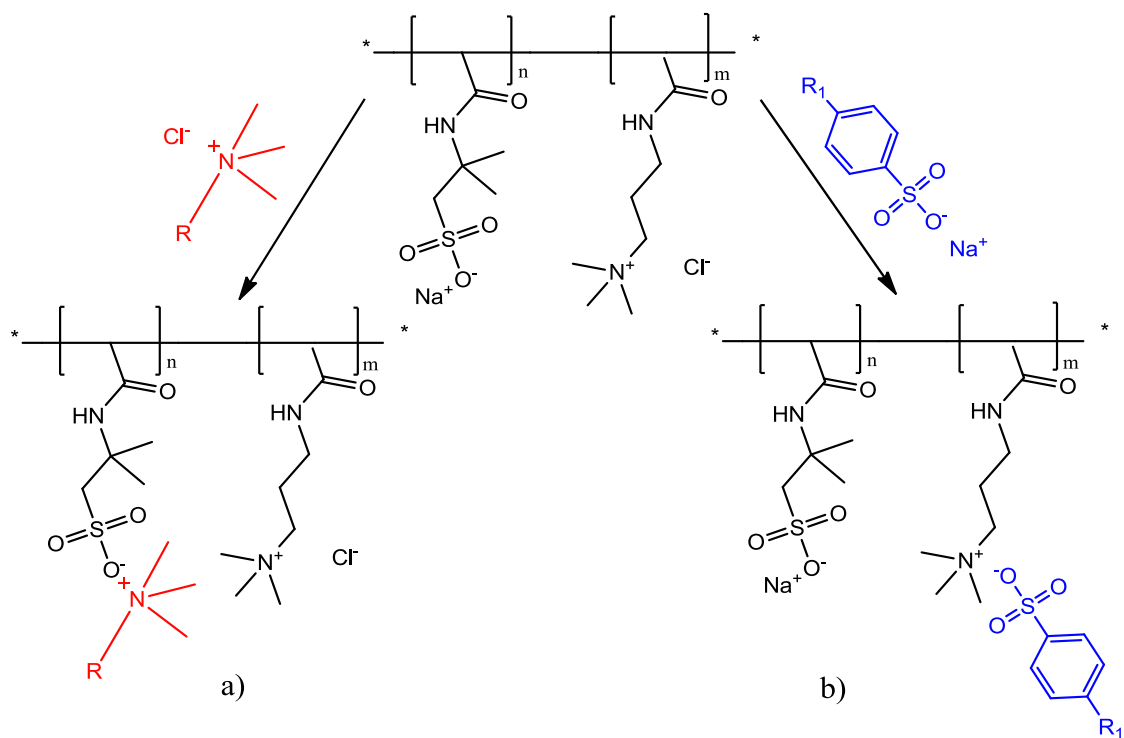| APTAC-AMPS solution			MB, MO solution		
Ratio	V, mL	C, mol/L	Ratio	V, mL	C=const, mol/L
1	5	$9.00*10^{-4}$	9	5	
2	5	$4.00*10^{-4}$	8	5	
3	5	$2.33*10^{-4}$	7	5	$1.00*10^{-4}$
4	5	$1.50*10^{-4}$	6	5	
5	5	$1.00*10^{-4}$	5	5	
6	5	$6.67*10^{-5}$	4	5	
7	5	$4.29*10^{-5}$	3	5	
8	5	$2.50*10^{-5}$	2	5	
9	5	$1.11*10^{-5}$	1	5	

Figure 2.2.8 - Complexation schematic based on [APTAC]:[AMPS] with surfactants: a) CTMACl, where R is C16H33, and b) SDBS, where R1 is C12H25
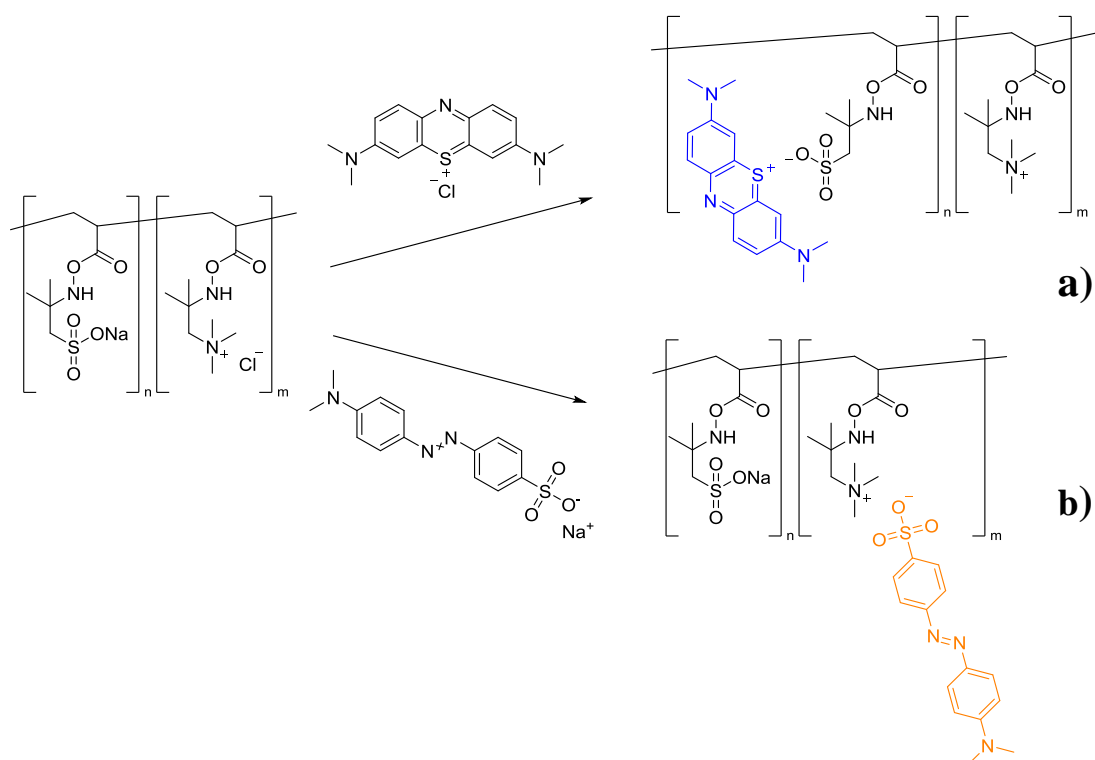

Figure 2.2.9 - Complexation schematic based on [APTAC]:[AMPS] with dyes: a) MB and b) MO

2.2.5 Swelling kinetics and complexation properties of quenched polyampholyte hydrogels.

2.2.5.1 Swelling kinetics of (QPaH) hydrogels in aqueous and aqueous-salt solutions

Hydrogels taken out of the syringes after a reaction time of 24 h were cut into small pieces of about 1 cm in length, which were immersed in water. After reaching an equilibrium degree of swelling, which was monitored by recording the mass and the diameter of the gel, the specimens were taken out of the water and freeze-dried (Christ Alpha 2-4 LDplus). The fraction of the monomers converted into a water-insoluble polymer, that is, the gel fraction W_g was calculated as:

$$W_g = \frac{m_{dry}}{C_0 \times m_0} \qquad (2.2.5)$$

where m_{dry} and m_0 are the weights of the gel specimens in dried and as-prepared states, respectively;

C_0 - is the monomer concentration (w/w) in the initial reaction solution.

The relative weight (m_{rel}) and volume (v_{rel}) swelling ratios in comparison to the initial states were determined as:

$$m_{rel} = \frac{m_{swl}}{m_0} \qquad (2.2.6)$$

where k is the swelling rate constant, n is a characteristic exponent indicating the amount of penetrant (water) in the transport mechanism, t is absorption time, M_t is the mass of water absorbed at time t, M_∞ is the mass of water absorbed at infinite time t_∞ .

$$V_{rel} = \left(\frac{d_{swl}}{d_0}\right)^3 \qquad (2.2.7)$$

where d_0 and d_{swl} are the diameters of the specimens in initial and swollen states, respectively, while m_{swl} is the weight of the specimens in the swollen state.

Water content (W) of swollen hydrogels was calculated as,

$$W\ \% \ = 10^2 \left(1 - \frac{m_{dry}}{m_s}\right) \qquad (2.2.8)$$

for initial : $W\ \% = 10^2(1 - w_M),$

for swollen: $W\ \% = \ 10^2\left(1 - \frac{m_{dry}}{m_s}\right).$

where m_{dry}, m_o, and m_s are the masses of hydrogels in dry, initial, and equilibrium swollen states, respectively, w_M is the mass fraction of the monomers in the reaction solution without SDS and NaCl. The water content of the initial hydrogels was calculated from the composition of the reaction solutions.

The swelling rate was expressed as:

$$kt^n = M_t/M_\infty \qquad (2.2.9)$$

The values of k and n were calculated from the slopes and intersect of the plots of $\ln(M_t/M_\infty)$ vs. $\ln t$.

The equilibrium degree of swelling was calculated from the formula:

$$\alpha = \frac{m_{swelled} - m_0}{m_0} \qquad (2.2.10)$$

where $m_{swelled}$ – is the mass of the swollen hydrogel; m_0 – is the mass of the original hydrogel; α – degree of swelling (g/g).

2.2.5.2 Uptake and release of dye molecules and surfactants from AMPS-APTAC hydrogels

In the evaluation, in order to assess the absorption characteristics of AMPS-APTAC hydrogels, anionic and cationic dyes (MB, MO) and surfactants (DDBSNa, CTMAC) were utilized. Fixed hydrogel samples were put into the aqueous solutions of MB, MO, DDBSNa, CTMAC with a concentration of $1*10^{-3}$ mol/L. The binding kinetics and the amount of absorbed and desorbed dyes were determined spectrophotometrically from calibration graphs of absorbance (or disturbance) versus concentration at = 611 (or 662) nm for MB, λ= 464 nm for MO, for DDBSNa and CTMAC λ = 280 nm .

The release of dye molecules from the hydrogel matrix was performed in a medium of 0.5 M KCl.

2.2.5.3 Healing efficiency of quenched polyampholyte hydrogels

To quantify the healing efficiency of the hydrogels, cut-and-heal tests were performed on cylindrical gel samples of 4.6 mm in diameter and 1 cm in length. At a stable temperature of 50±3°C quantify the healing efficiency of the hydrogels, cut-and-heal tests were performed on cylindrical gel samples of 4.6 mm in diameter and 1 cm in length between 1 and 24 h. Healing efficiency was estimated from the ratios of Young's modulus and fracture stress of the healed samples to those of the virgin ones.

2.2.6 Physico-chemical, mechanical, and catalytic properties of polyampholyte cryogels

2.2.6.1 Post - preparation procedure of polyampholyte cryogels

The washed and swollen cryogels were transferred to Petri dishes and cut into pieces of about 1 cm in length. The cryogels were then firstly dried in the air and then in a vacuum drying oven at room temperature in order achieve a constant weight. After the samples were dried, all the samples were weighed to determine the mass fraction of the yield, and the resulting samples were then used for further studies.

2.2.6.2 Immobilization of gold nanoparticles into cryogel matrix using 1) DMAEMA-MA and 2) APTAC-AMPS, and study of the catalytic properties of cryogel-immobilized gold nanoparticles

Solution of 2 ml of $HAuCl_4$ with a concentration of 100 mg/L was mixed with 18 mL of water and boiled. After 30 min of heating, the colorless cryogel sample turned into a raspberry-red color. To obtain and verify that the colorization of the cryogel was connected to the plasmonic spectra of the AuNPs, the sample was stabilized by 1) poly(DMAEM-*co*-MAA) or 2) poly(AMPS-*co*-APTAC). The maximum adsorption peak at 530 nm confirms the formation of gold nanoparticles stabilized by 1) poly(DMAEM-*co*-MAA) or 2) poly(AMPS-*co*-APTAC).

2.2.6.3 *P*-nitrobenzoic acid (*p*-NBA) as a flow-through type catalytic reactor for hydrogenation

$NaBH_4$ was used to evaluate the catalytic activity of AuNPs in a cryogel matrix with respect to reduction p-NBA. Hydrogenation of *p*-NBA was carried out in the flow-through catalytic reactor shown in figure 2.2.10, which is comprised of a glass tube with an inner diameter of 6-7 mm and height of 100 mm, which is filled with dry cryogel pieces that have a diameter of 5 mm and a height of 10 mm. The bottom part of the glass tube is closed by a Shott filter, ending in a valve. At first, 10 or 15 mL of deionized water is passed through the cryogel sample. Due to the quick swelling of the cryogel, a tight seal develops between the inner wall of the glass tube and the swollen sample.
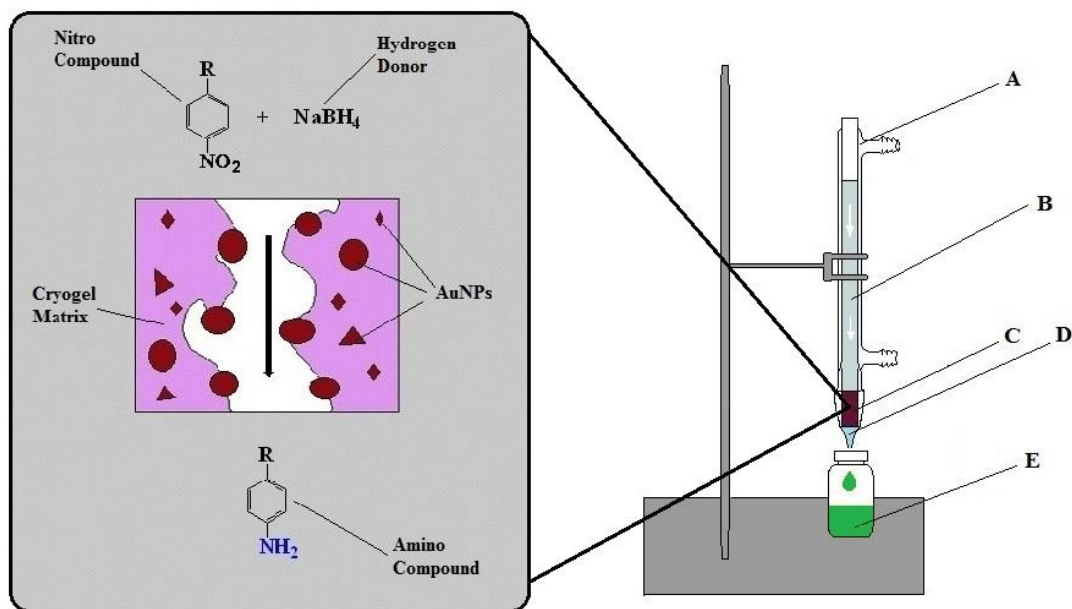

Figure 2.2.10 - Schematic representation of the flow-through catalytic reactor for the catalytic reduction of *p*-NBA using a cryogel-AuNPs catalyst. A-thermostatically-controlled glass reactor, B-aqueous solution of initial nitro compound, C- cryogels sample/AuNPs catalyst, D- Schott filter, E- aqueous solution of amino product

In the case of *p*-NBA hydrogenation, a 10 mL aqueous solution composed of 1 mL $5*10^{-4}$ mol/L *p*-NBA, 1 mL $1*10^{-1}$ mol/L $NaBH_4$ and 8 mL of deionized water was pumped through the cryogel sample containing AuNPs as described above. The concentrations of *p*-ABA and *p*-NBA were determined at 266 and 274 nm, respectively on Specord 210 plus UV spectrophotometer (Germany). After passing the solution through the cryogel matrix additional times, further reduction of Au^{3+} takes place, leading to further accumulation of gold nanoparticles in the macropores.

3 RESULTS AND DISCUSSION

3.1. Identification and characterization of AMPS-APTAC copolymers

The prepared linear copolymers were dissolved in distilled water, dialyzed with deionized water and freeze-dried. ^{1}H NMR spectra of AMPS-75, AMPS-50 and AMPS-25 in D_2O are shown in figures 3.1.1-3.1.3.

The identification of the AMPS:APTAC structure using ^{1}H NMR spectroscopy [9] established that the resonance bands observed at 3.0–3.8 ppm strongly overlap, suppressing the peaks of the vinyl groups in the monomers. However, the proton NMR spectroscopy spectra obtained can be used to establish the feed and copolymer composition of AMPS:APTAC from the integrated proton intensities of the CH_3 groups of the structural units of each comonomer (figures 3.1.1-3.1.3, table 3.1.1).

Following determination of the equimolar ratio of AMPS:APTAC, one proton unit of APTAC has been shown to correspond to the 9H protons of 3 methyl groups in the region of 3.03 ppm (figure 3.1.1).

Moreover, one structural unit of AMPS corresponds to the 6H protons of 2 methyl groups, resonating in the region of 1.36 ppm (figure 3.1.1, table 3.3.1). Accordingly, the copolymer composition of AMPS:APTAC at a molar ratio of 50:50 is equal to [AMPS]:[APTAC] = ([H] AMPS / 6)/([H] APTAC / 9) = (6/6)/(9.19 / 9) = 1:1.02 = 0.98:1.
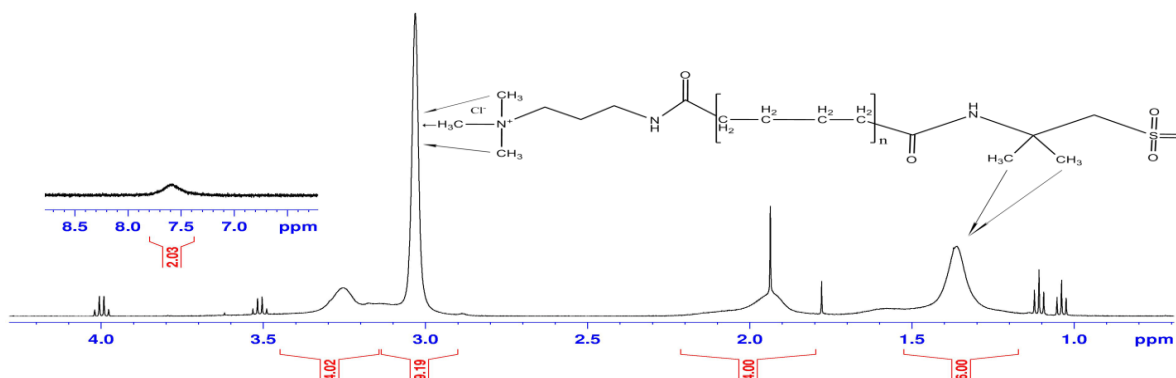
Figure 3.1.1 - ^{1}H NMR spectum of a polyampholyte composition: [AMPS]:[APTAC] = 50:50 mol.% in D_2O

The following experimental ratio was found with regards to the 9H protons of 3 methyl groups of one structural unit of AMPS, whose resonance signal is located at 3.14 ppm and the 6H protons of 2 methyl groups of one structural unit of AMPS, which manifests itself at 1.47 ppm of AMPS:APTAC composition: 75:25 mol.% (figure 3.1.2, table 3.1.1): [AMPS]:[APTAC] = ([H] AMPS/6)/([H] APTAC/9) = (17.65/6)/(9.0/9) = 2.942:1.
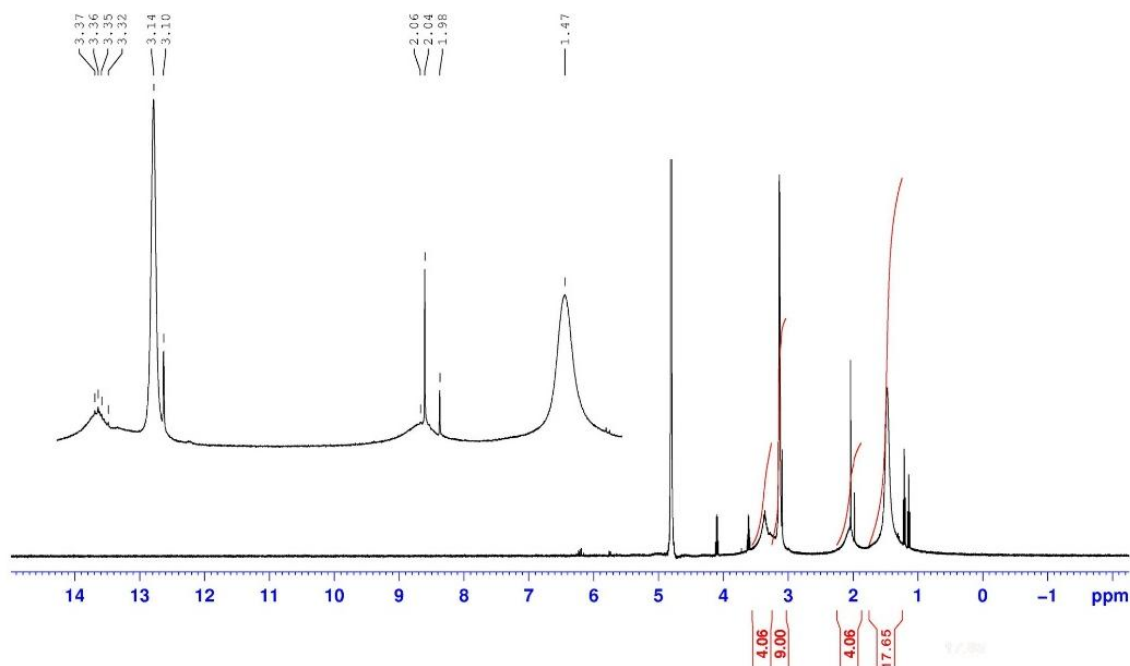
Figure 3.1.2 - ^{1}H NMR spectrum of a polyampholyte composition: [AMPS]:[APTAC] = 75:25 mol.% in D$_2$O

The chemical shift of 9H protons of 3 methyl groups of one APTAC structural unit is 3.21 ppm (APTAC 75 mol.%), one AMPS structural unit where 6H protons of 2 methyl groups reside at 1.54 ppm (AMPS:APTAC-25:75 mol.%, respectively) (figure 3.1.3, table 3.1.1). The experimentally calculated composition of APTAC for AMPS is equal to [AMPS]:[APTAC=([H] AMPS/6)/([H] APTAC/9)=(6.12/6)/(27.0/9) = 1.03:3.
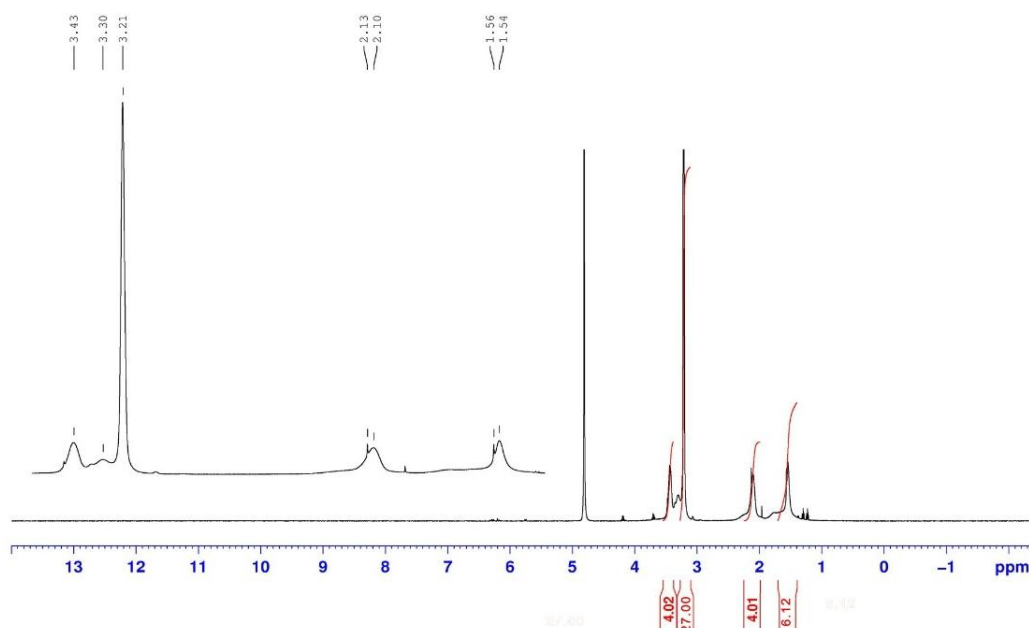
Figure 3.1.3 - ^{1}H NMR spectrum of a polyampholyte composition: [AMPS]:[APTAC] = 25:75 mol.% in D$_2$O

Table 3.1.1 - Theoretical and experimentally calculated the molar composition of AMPS-APTAC copolymers

No. samples	Theoretically prescribed	Experimentally found from ^{1}H NMR spectra
1	[75]:[25]	[74.4]:[25.6]
2	[25]:[75]	[25.4]:[74.6]
3	[50]:[50]	[50.5]:[49.5]

FTIR spectrum of AMPS-50 (figure 3.1.4), together with the identification of characteristic bands of functional groups of AMPS-25 and AMPS-75, are presented in figure 3.1.5 and table 3.1.2.

Figure 3.1.4 - FTIR spectrum of AMPS-50
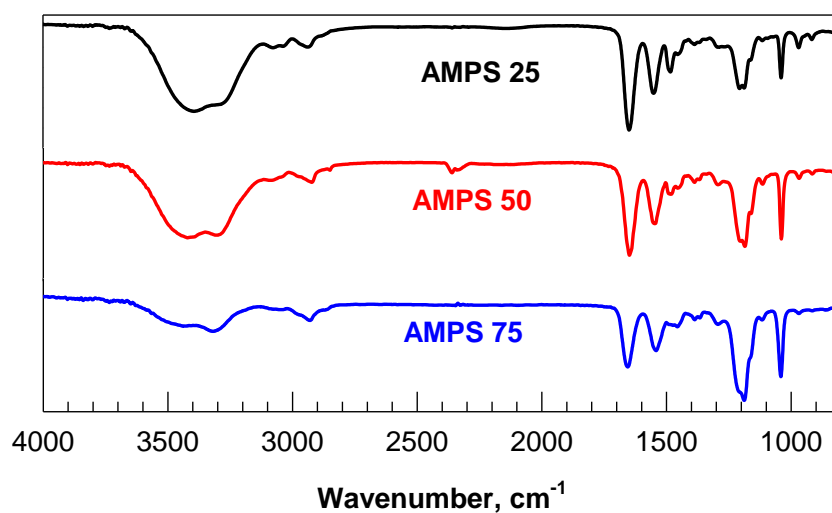
Figure 3.1.5 - FTIR spectra of polyampholyte hydrogels. The mole fraction of AMPS in the comonomer feed for spectra 25:75, 50:50, and 75:25 mol.%, respectively

Table 3.1.2 - Identification of FTIR spectra of AMPS-25, AMPS-50, and AMPS-75

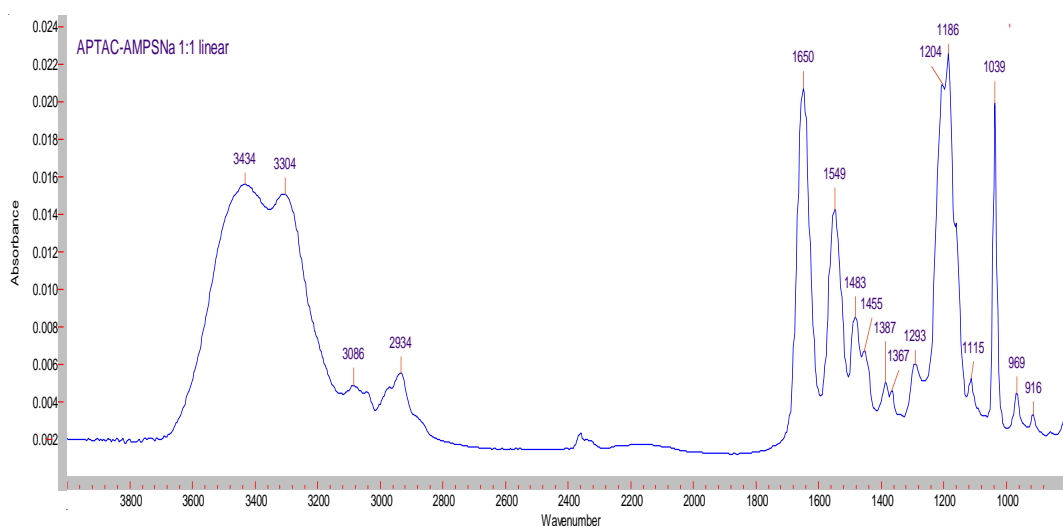| Functional groups	$\nu(NH)$	$\nu(CH)$	$\nu(CONH)$ Amide I,	$\nu(CONH)$ Amide II,	$\delta(CH)$	$\nu(S=O)$
Band assignments, cm^{-1}	3434, 3304	2934	1650	1548	1186, 1204	1039

Thus, both ^{1}H NMR and FTIR spectra confirm the compositional closeness of copolymers to that of the monomer feed, indicating the formation of homogeneous AMPS-APTAC copolymers in the course of radical polymerization. The conversion of AMPS-APTAC copolymers observed in ^{1}H NMR spectra exceeded 80%.

Gel permeation chromatography results for AMPS-75 and AMPS-50 are shown in figures 3.1.5 and 3.1.6.

Figure 3.1.5 - Gel chromatogram of the AMPS-75 sample

Figure 3.1.6 - Gel chromatogram of AMPS-50 sample

The weight-average molecular weight (M_w), the number-average molecular weight (M_n), and z-average molecular weight (M_z) together with a polydispersity

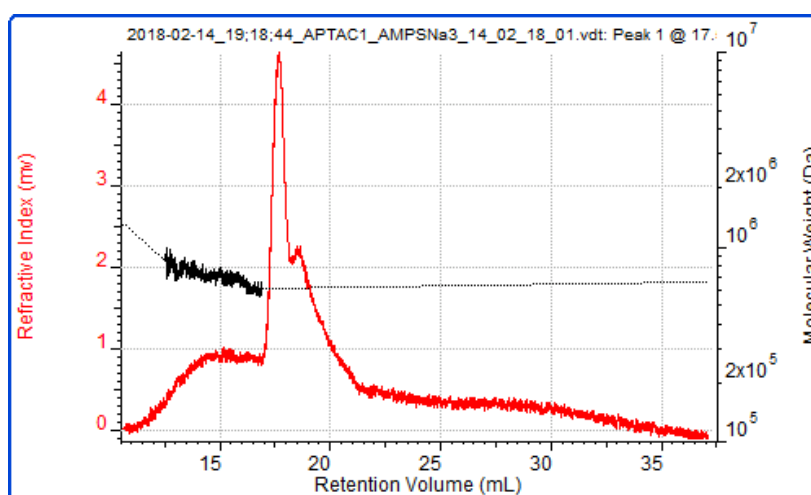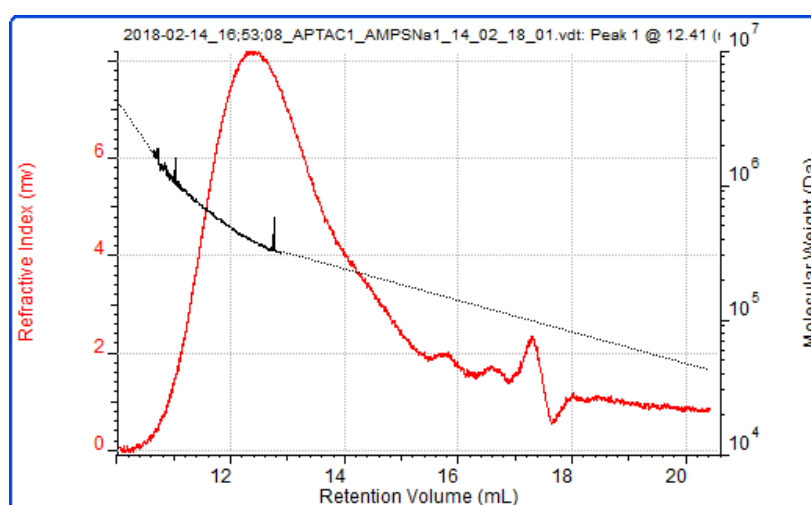index (PDI) of AMPS-APTAC copolymers according to GPC measurements are summarized in table 3.1.3.

Table 3.1.3 - Weight-average molecular weight (M_w), number-average molecular weight (M_n) and z-x average molecular weight (M_z), also polydispersity index (M_w/M_n) of AMPS 50 and 75 polyampholytes, respectively

Abbreviation	$M_w \cdot 10^5$	$M_n \cdot 10^5$	$M_z \cdot 10^5$	M_w/M_n
AMPS-75	6.40	6.37	6.50	1.01
AMPS-50	3.31	2.01	5.11	1.65

The molecular weight distribution of AMPS-75 is rather narrow (M_w/M_n = 1.01) compared to AMPS-50 (M_w/M_n = 1.65). This indicates the regular structure of polyampholytes.

An important characteristic of polyampholytes is their thermal stability in various temperatures. The results of thermal studies of APTAC-AMPS copolymers in various ratios are presented in figure 3.1.7. In all samples, the temperature of the onset of mass loss is in the range 121.98-143.73°C. All samples of polyampholytes are characterized by a stepwise change in mass with increasing temperature.

Initial weight reduction of copolymers is observed within the temperature range of 65-120°C, and is associated with moisture loss. In the temperature range of 310-325°C, thermal decomposition of the copolymers is observed, accompanied by a sharp decrease in mass (curves 1-3, figure 3.1.7). TGA data are in good agreement with DSC analysis. The DSC curve of all polyampholyte samples exhibited an exothermic effect, revealed in the temperature range of 310-325°C. The first exothermic effect, occurring at maximum at 310°C, could be attributable to the decomposition of the carbonyl groups of APTAC and AMPS. The second exothermic effect, occurring at a maximum of 325 °C, is characterized by oxidation of C–C bonds in APTAC and AMPS molecules (curves 1a – 3a, figure 3.1.7).
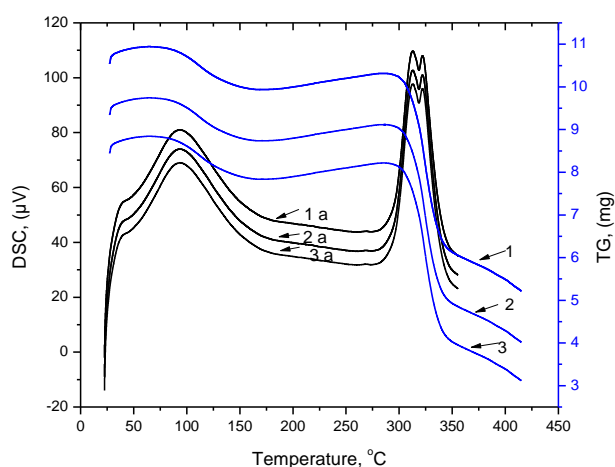

Figure 3.1.7 - TGA and DSC curves of polyampholytes based on AMPS-APTAC composition: 1 – AMPS 50; 2 – AMPS 75; 3 – AMPS 25 mol.%, respectively

CONCLUSION TO CHAPTER 3.1

Highly charged linear and crosslinked polyampholytes based on the AMPS anionic monomer and APTAC cationic monomer were synthesized using free radical polymerization.

NMR and FTIR spectroscopy were used to analyze the structure and composition of highly charged polyampholytes of linear and crosslinked copolymers. The composition of the prepared copolymers were shown to coincide with the composition of the initial monomer mixture. The results are in good agreement with theoretical expectations and prior literature. The copolymer composition of AMPS:APTAC at a molar ratio of 50:50 is equal to [AMPS]:[APTAC] -50.5:49.5, and the copolymer composition of AMPS:APTAC at a molar ratio of 75:25 and 25:75 are equal to [AMPS]:[APTAC] -74.4:25.6 and 25.4:74.6 respectively.

Gel permeation chromatography (GPC) determined the weight average and the average molecular weights, as well as the molecular weight distribution of the samples. The average number (M_n) and weight average (M_w) molecular weights of polyampholytes determined by GPC are in the range of $(2-6.4)*10^5$ and $(3.3-6.4)*10^5$ Daltons. Due to polydispersity, highly charged linear polyampholytes have a narrow molecular weight distribution, with M_w/M_n equal to 1.01-1.65.

3.2. Solution properties and complexation of linear quenched polyampholytes

3.2.1 Solution properties of linear quenched AMPS-APTAC polyampholytes

Concentration dependence of the reduced viscosity of polyampholytes, AMPS-75 (1) and AMPS-25 (2), in distilled water is shown in figure 3.2.1. As seen in the figure, the reduction in reduced viscosity upon dilution of the polyampholytes based on AMPS-ATAC, in ratios 25:75 and 75:25 mol.% in distilled water, means that the polyampholyte initially behaves in solution as an uncharged polymer.

This appears to be due to oppositely charged molecules prevailing over the mutual repulsion of like-charged groups, folding the polymer into a coil. As the solution of polyampholyte AMPS-25 becomes more dilute, reduced viscosity increases.

This is caused by so-called polyelectrolyte swelling, i.e. an increase in the electrostatic repulsion of the positively charged chain links prevailing in APTAC, leading to an increase in the macromolecular coil. Polyelectrolyte swelling is weakly expressed in the polyampholyte AMPS-75, where the negatively charged units of AMPS mainly predominate.
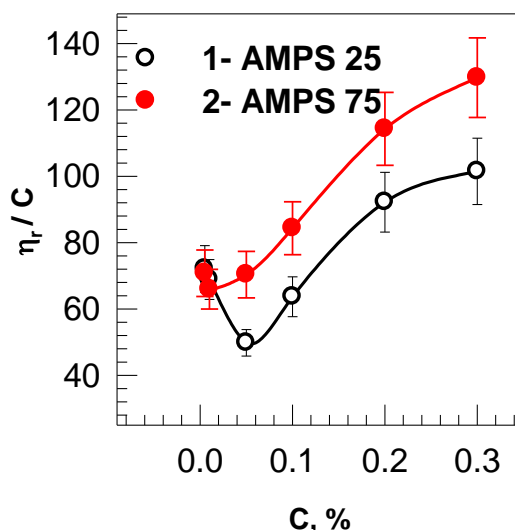
Figure 3.2.1 - Concentration dependence of the reduced viscosity of polyampholytes AMPS-75 and AMPS-25 in distilled water

The average hydrodynamic dimensions of the AMPS-75 and AMPS-25 macromolecules, measured in distilled water, are shown in figure 3.2.2. The average hydrodynamic sizes of the AMPS-75 and AMPS-25 macromolecules tend to increase with dilution. This is especially pronounced for AMPS-75, the average hydrodynamic size of which reaches 2100 nm at a concentration of [AMPS-75] = 0.05%.

Concentration dependence of the reduced viscosity of AMPS-APTAC at different ionic strengths of the solution (μ), expressed as mol/L of KCl, is shown in figures 3.2.4 -3.2.7.
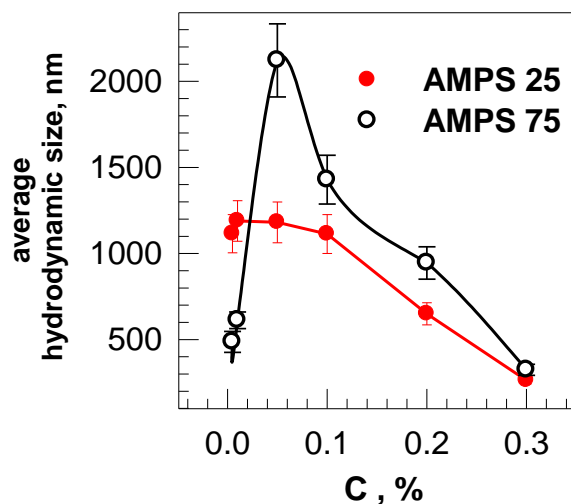
Figure 3.2.2 - Concentration dependence of the average hydrodynamic dimensions of polyampholytes AMPS-75 (1) and AMPS-25 (2) in distilled water
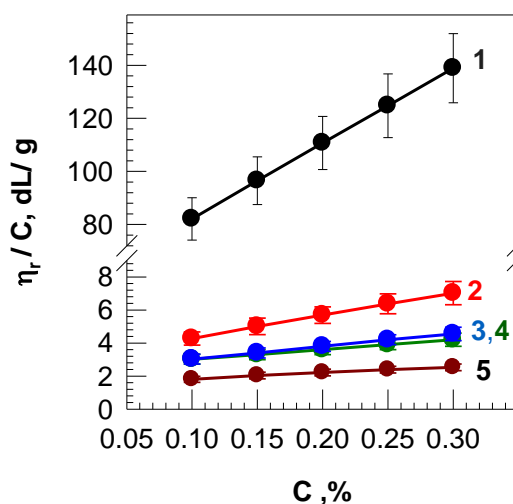
Figure 3.2.4 - Concentration dependence of the reduced viscosity of AMPS-25 at $\mu = 0$ (1), 0.1 (2), 0.5 (3), 0.75 (4) and 1.0 mol/L (5) of KCl
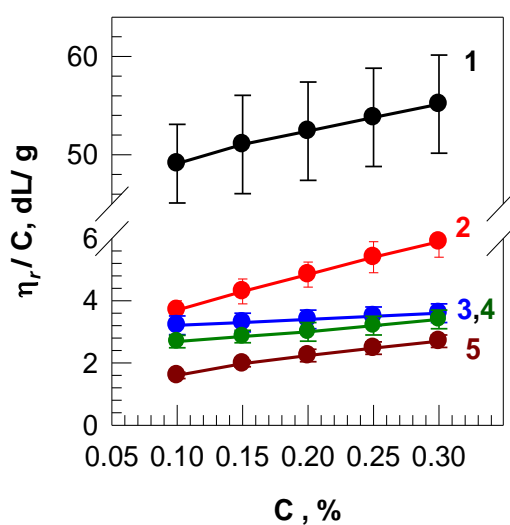
Figure 3.2.5 - Concentration dependence of the reduced viscosity of AMPS-75 at $\mu = 0$ (1), 0.1 (2), 0.5 (3), 0.75 (4) and 1.0 mol/L (5) of KCl
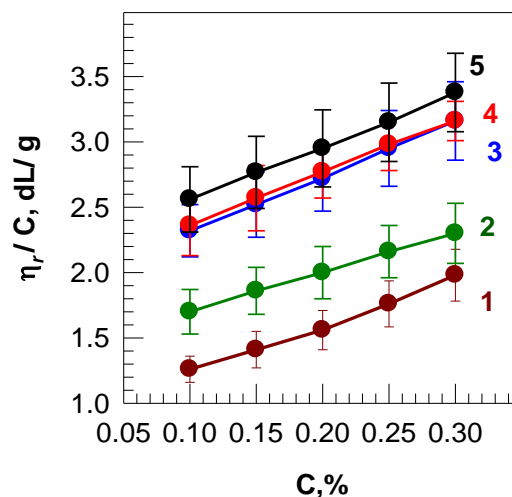
Figure 3.2.6 - Concentration dependence of the reduced viscosity of AMPS-50 at μ = 0.05 (1), 0.1 (2), 0.75 (3), 1.0 (4) and 0.5 mol/L (5) of KCl
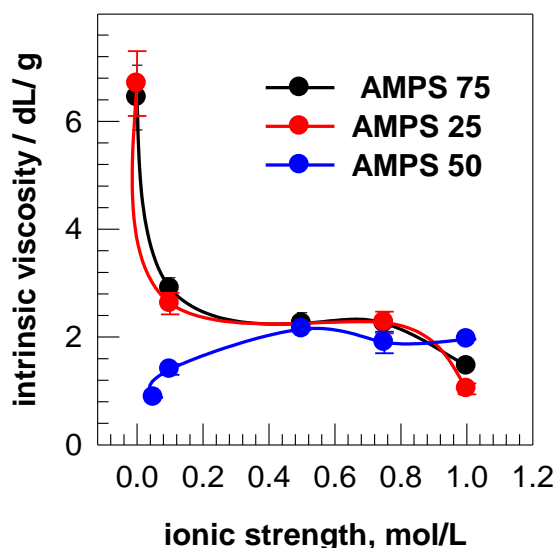
Figure 3.2.7 - Dependence of the intrinsic viscosity of AMPS-APTAC copolymers on the ionic strength of the solution based on KCl content

The unbalanced AMPS-APTAC polyampholytes, to which belong AMPS-25 and AMPS-75, can be considered a combination of the polyampholyte and polyelectrolyte effects, because the charge imbalance causes an increase in the net charge of the macromolecules. In such a case, the conformational state of AMPS-25 and AMPS-75 in aqueous solution can be said to have a core and shell structure. The core part contains an equal amount of positive (25 mol.%) and negative (25 mol.%) charges, which are mutually compensated and belong to the polyampholyte region. The shell part contains an excess of either positive or negative charges, is responsible for water solubility, and provides the macromolecules with a polyelectrolyte character. Because the core part of AMPS-50 is comprised of an equal number of positive and negative charges, making it a balanced polyampholyte, and has no

excess positive or negative charges in the shell, it forms a fine suspension in water, but is soluble in a salt solution. Surprisingly, in pure water, AMPS-25 and AMPS-75 do not exhibit a polyelectrolyte effect, in spite of the excess of positive (Z = +50 mV) and negative (Z = -40 mV) charges. The concentration dependence of the reduced viscosity has a linear character (figures 3.2.4 and 3.2.5). The decrease in the reduced viscosity upon dilution is probably connected with the domination of the polyampholyte effect over the polyelectrolyte effect. Intramolecular salt bonds (50 mol.%), formed between 25 mol.% positive and 25 mol.% negative charges (polyampholyte effect), provide electrostatic repulsion of similar charges (polyelectrolyte effect) in macromolecular chains. In other words, due to the counteraction of the polyampholyte and polyelectrolyte effects, the conformation of the macromolecules remains unchanged (or only slightly changed) upon dilution, despite the excess of positive or negative charges. As seen in figures 3.2.4 and 3.2.5, the reduced viscosity of AMPS-25 and AMPS-75 decreases with increasing ionic strength.

In contrast, the reduced viscosity of AMPS-50 increases upon the addition of KCl, demonstrating antipolyelectrolyte behavior (figures 3.2.5 and 3.2.6). Because AMPS-25 and AMPS-75 contain an excess of positive and negative charges and have a polyelectrolyte character, the addition of low-molecular-weight salts shields the electrostatic repulsions. In turn, the addition of low-molecular-weight salts to AMPS-50 shields the electrostatic attraction between the opposite charges in macro chains, which results in an increase in reduced viscosity. In the case of AMPS-25 and AMPS-75, the simultaneous realization of both polyelectrolyte and polyampholyte behavior is expected. Screening of similarly charged monomers by low-molecular-weight salts tends to shrink the shell (polyelectrolyte part), while the low-molecular-weight salts that surround the oppositely charged monomers tend to swell the core (polyampholyte part). Such antagonism between the polyelectrolyte and polyampholyte effects may not cause a dramatic decrease in the intrinsic viscosity upon increasing the ionic strength.

3.2.2 Behavior of linear polyampholytes AMPS-APTAC at the isoelectric point (IEP)

In pure water, the isoelectric points (IEP) of AMPS-APTAC copolymers corresponding to zero net charges (quasi-electroneutral) of macromolecules are around of pH 6.1 ± 0.1 (figure 3.2.8). At IEP, the average hydrodynamic size of quenched polyampholytes is minimal due to the strong electrostatic attraction of oppositely charged monomers. Increasing the average hydrodynamic size of amphoteric macromolecules from both sides of IEP is interpreted in terms of expanding the macromolecular chains due to strong electrostatic repulsion of anionic or cationic groups, respectively [16-18].
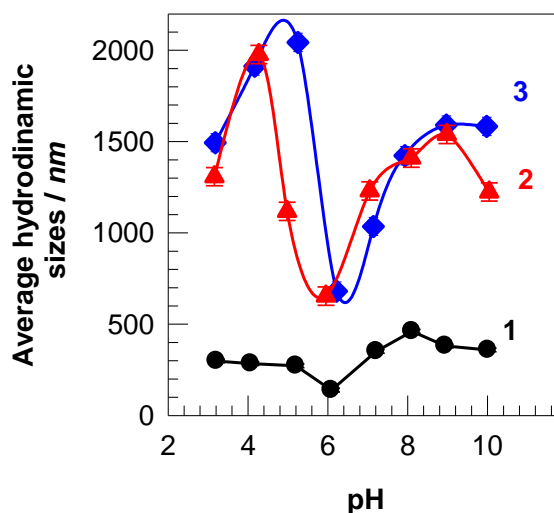
Figure 3.2.8 - pH-dependent average hydrodynamic size of AMPS-50 (1), AMPS-75 (2) and AMPS-25 (3) in aqueous solution

In the presence of KCl, the position of IEP shifts to higher values of pH up to 6.5-7.0. The specific binding of chloride ions with quaternary ammonium groups that diminishes the number of positive charges (leading to an apparent change of copolymer composition) and increases the value of IEP in comparison with the nonsalted solution [21].

The different behavior of unbalanced (AMPS-25 and AMPS-75) and balanced (AMPS-50) polyampholytes upon increasing the ionic strength is illustrated in figure 3.2.9. In aqueous solution AMPS-25 and AMPS-75 have an excess of positive ($Z = +50$) and negative ($Z = -40$) charges, while AMPS-50 is in electroneutral state ($Z = 0$).
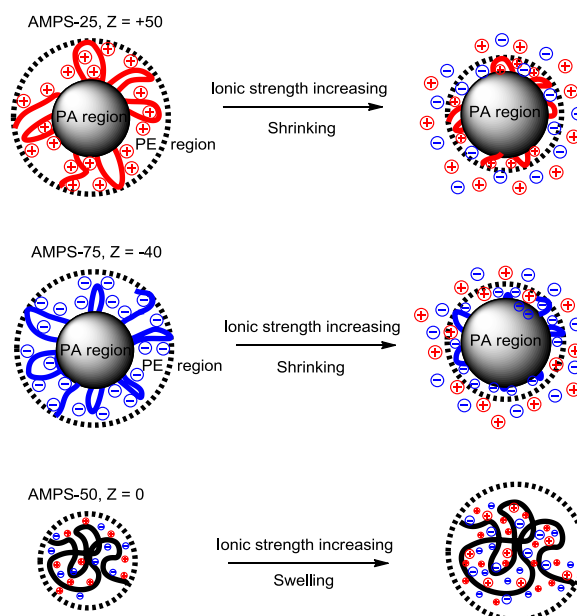
Figure 3.2.9 - Schematic representation of "core-shell" structure and behavior of AMPS-25, AMPS-50, and AMPS-75 in aqueous-salt solution

Increasing the ionic strength screens the electrostatic repulsion between uniformly charged groups, if polyelectrolyte effect dominates and shields the electrostatic attraction between oppositely charged monomers if polyampholyte effect prevails (table 3.2.1). In the former case, the macromolecular chain diminishes, whereas in the latter case, it expands.

Table 3.2.1 - Intrinsic viscosities of AMPS-APTAC copolymers depending on the ionic strength .

Code	Intrinsic viscosity(dL/·g) dependence on ionic strength, KCl (mol/L)					
	0	0.05 KCl mol/L	0.1 KCl mol/L	0.5 KCl mol/L	0.75 KCl mol/L	1.0 KCl mol/L
AMPS-25	46.4	-	2.68	-	2.32	1.12
AMPS-50	-	0.88	1.40	2.15	1.90	1.96
AMPS-75	53.8	-	2.93	-	2.42	1.47

The viscometric data reveal that in aqueous solutions of KCl, the intrinsic viscosities of AMPS-25 and AMPS-75 decrease while the intrinsic viscosity of AMPS-50 increases demonstrating antipolyelectrolyte behavior. In aqueous solution the conformation of AMPS-25 and AMPS-75 can be considered as core and shel structure where the core part exists in the polyampholyte regime, the shell part represents a polyelectrolyte regime. The addition of low-molecular-weight salts tends to shrink the shell part (polyelectrolyte region) and to swell the core part (polyampholyte region). Such antagonism between polyelectrolyte (shell) and polyampholyte (core) effects may cause a gradual decreasing of the intrinsic viscosity at relatively high ionic strengths.

3.2.3 Complexation of linear AMPS-APTAC polyampholytes with ionic dyes and surfactants, as well as the behavior of AMPS-APTAC polyampholytes in aqueous-organic solvents

3.2.3.1 Complexation of linear AMPS-APTAC polyampholytes with surfactants

Linear quenched AMPS-APTAC polyampholytes in solutions can form intramolecular and intermolecular associations upon interaction with low molecular weight surfactants. Complexes are formed as a result of interactions of positively and negatively charged links of the polymer chain with complementary charged surfactant groups (figures 3.2.10, 3.2.11).

Surfactants of the anionic (sodium dodecylbenzene sulfate) and cationic (cetyltrimethylammonium chloride) types were used to establish the complexation properties of polyampholytes. The presence of two potentially complexing groups determines the bifunctional nature of polyampholytes and contributes to a change in the hydrodynamic and conformational properties of the polymers [12].

The formation of intermolecular polyampholyte-surfactant associations, upon mixing sodium dodecylbenzene sulfate and cetyltrimethylammonium chloride with

AMPS-APTAC linear polyampholytes, was established using dynamic laser scattering and UV-spectroscopy (figures 3.2.10, 3.2.11). At a certain ratio of the reacting mixture, the formation of insoluble complexes is possible due to the hydrophobization of individual sections of the polymer chains, leading to the formation of compact phases, accompanied by the appearance of weak opalescence.

Linear AMPS-APTAC polyampholytes in solutions are capable of forming intra- and intermolecular associations when interacting with low-molecular-weight surfactants. As a result of interactions of positively and negatively charged links of the polymer chain with complementarily charged groups, surfactant complexation occurs. At a certain ratio of the reacting mixture, it is possible to form insoluble complexes due to the hydrophobization of individual sections of the polymer chains leading to the formation of compact phases accompanied by the appearance of weak opalescence.

Figure 3.2.10 - Concentration dependence of the average size, zeta potential, and turbidity of AMPS-25 in SDBS solution

The results presented in figures 3.2.10 and 3.2.11 demonstrate that the complexation of AMPS-APTAC polyampholyte with the corresponding surfactants is accompanied by a change in the total charge of the macromolecule. Gradual compensation of charges leads to a change in the zeta potential. The formation of a stable complex is achieved at a 2:3 molar ratio of AMPS-75 and CTMAC. Similarly, this occurs for AMPS-25 and SDBS at a ratio of 3:2. This stability is due to the fact that the formation of the intramolecular structure is achieved as a result of electrostatic binding of surfactant molecules to polyampholytes, and causes a more compressed conformation of the polymer coil. Subsequent sorption of surfactant molecules on polymeric sites of polyampholyte results in the recharging of macromolecules.
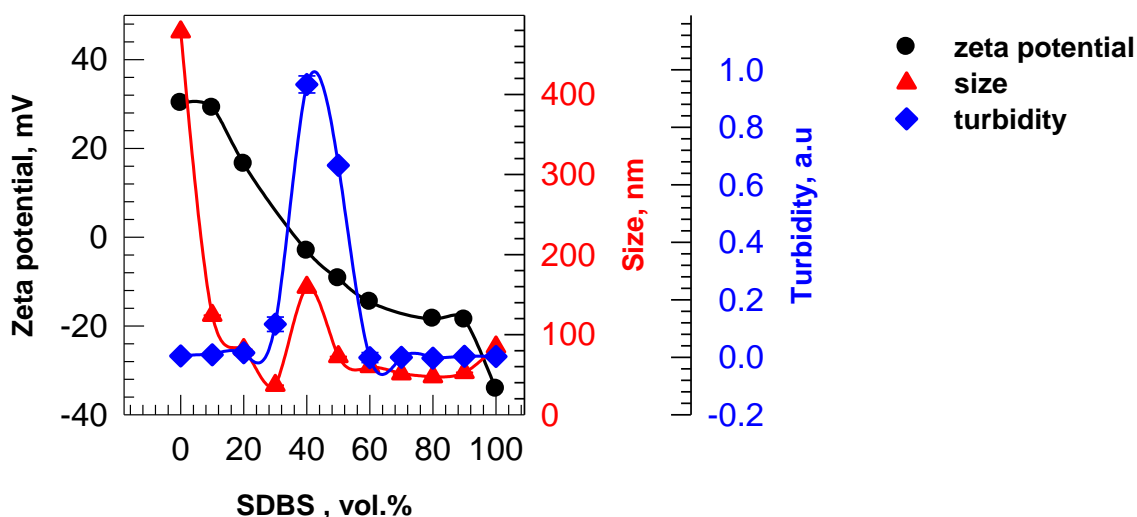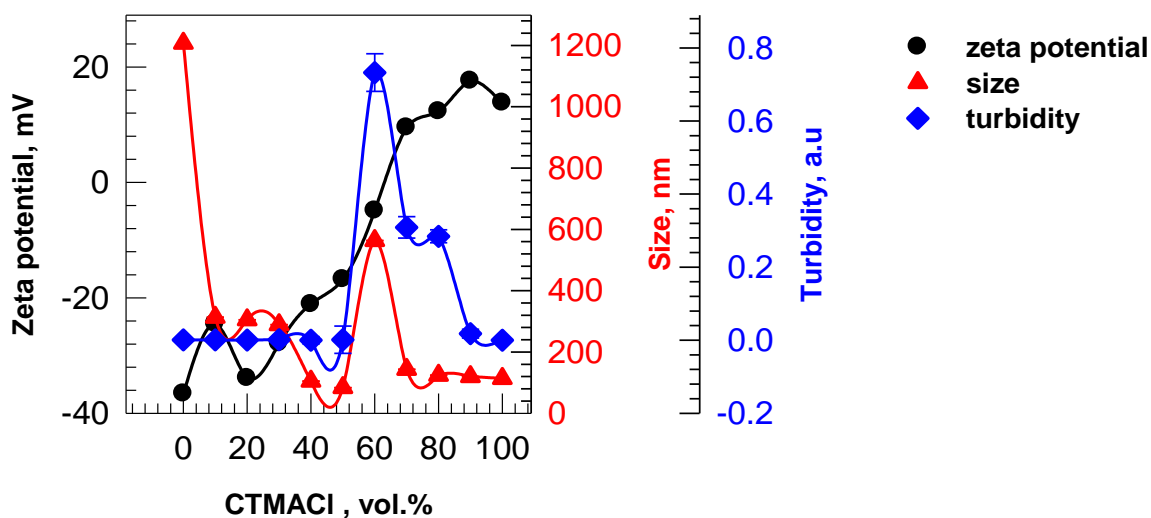
Figure 3.2.11 - Concentration dependence of the average size, zeta potential, and turbidity of AMPS-75 in CTMAC solution

The formation of a polyampholyte-surfactant complex is accompanied by the appearance of turbidity of the system. The dependence of the change in the optical density of the solution that is obtained by adding surfactants to the polyampholyte is shown in figures 3.2.10 and 3.2.11. The maximum cloud point of the solution AMPS-75 and CTMAC is set at a molar ratio of 2:3, and for the AMPS-25 and SDBS at 3:2 (figure 3.2.11). The turbidity of the solutions, due to the collapse of the macromolecule and the subsequent precipitation of the precipitate, causes the interaction of the surfactant with the polyampholyte (figure 3.2.10). This interaction is evidenced by the results of a change in the size of the polymer molecules during complexation with surfactants.

3.2.3.2 Complexation of linear AMPS-APTAC polyampholytes with dyes

In order to study the complexation behavior of linear polyampholytes with dyes, methylene blue (MB) and methyl orange (MO) were chosen.

The results show that the intensity of UV absorptions of the AMPS-APTAC solution:MB solution increase dramatically in higher concentrations of AMPS-APTAC solution. The combined solution does not fluoresce with a low polymer concentration dissolved in water (figures 3.2.12 and 3.2.13).

As seen in figure 3.2.12, the MB dye interacts easily with AMPS-75, but does not with the two other polymer compositions, AMPS-50 and AMPS-25. Oppositely, MO interacts only with AMPS-25 (figure 3.2.13).

This occurs because the polyampholyte with the highest concentration of the negative charged monomer AMPS interacts with the positively charged MB dye to form an associate stabilized by ionic bonds. In the case of MO, the interaction occurs with positively charged AMPS. However, as AMPS-50 has balanced charges, the dyes cannot interact with this polymer composition.
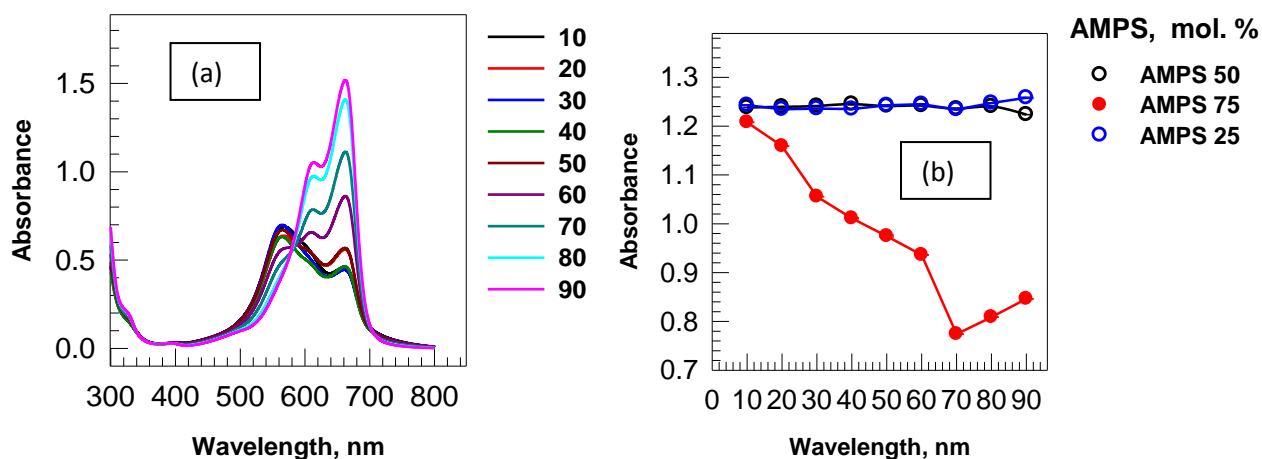
Figure 3.2.12 - Absorption of MB by AMPS-75 linear polyampholyte a), Sorption kinetics of MB by AMPS-APTAC linear polyampholytes b)
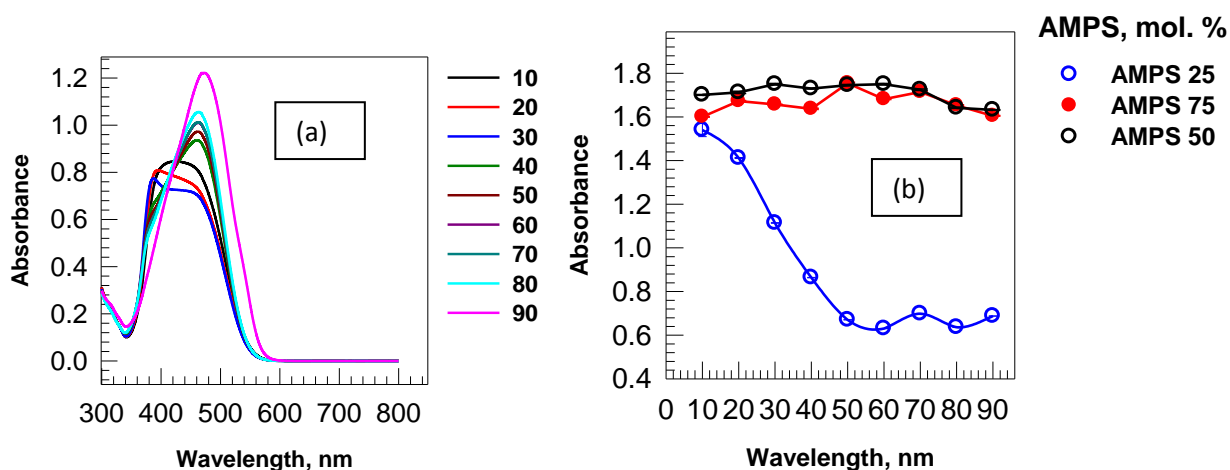
Figure 3.2.13 - Absorption of MO by AMPS-25 linear polyampholyte a), Sorption kinetics of MO by AMPS-APTAC linear polyampholytes b)

The binding of dyes with polyelectrolytes is accompanied by a characteristic spectral shift, which is a consequence of the effects of the electrostatic interaction. As a result, the interaction of dyes with the functional groups of a polymer leads to quenching of the absorption intensity, which is used in order to determine the polymer-dye associate.

As a result, the composition of the [AMPS-75 solution]:[MB] complex was determined to be approximately 1:3 (figure 3.2.12), whereas [AMPS -25 solution]:[MO] is 1:2 (figure 3.2.13).

3.2.3.3 Behavior of linear AMPS-APTAC polyampholytes in water-organic solvents

The dependence of the reduced viscosities of AMPS-APTAC polyampholytes on the composition of aqueous-organic solvents are shown in figures 3.2.14 and 3.2.15.

A significant decrease in the reduced viscosity of AMPS-25 and AMPS-75 is observed in an aqueous-organic mixture containing 40 vol.% ethanol and 60 vol.% acetone (figures 3.2.14 , 3.2.15). The decrease is due to a reduction in the dielectric constant of the solution, leading to the condensation of counterions with polyions, and to deterioration of the thermodynamic quality of the solvent with respect to the anionic and cationic groups of polyampholytes.

Figure 3.2.14 - Dependence of the reduced viscosity of AMPS-25 (1) and AMPS-75 (2) on the composition of the water-ethanol mixture

Figure 3.2.15 - Dependence of the reduced viscosity AMPS-25 (1) and AMPS-75 (2) on the composition of the water-acetone mixture

CONCLUSION TO CHAPTER 3.2

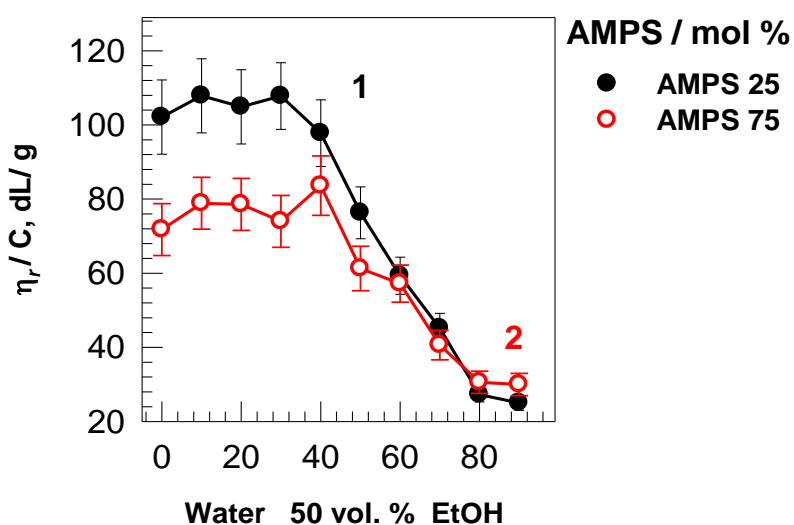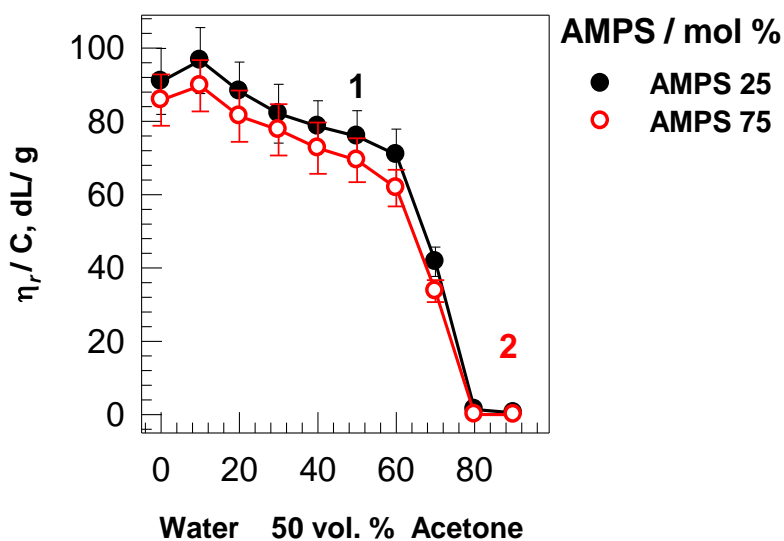Quenched (or high-charge-density) polyampholytes were prepared from anionic AMPS and cationic APTAC monomer pairs. Copolymers with large charge asymmetries (AMPS-25 and AMPS-75) exhibited good solubility in water. Equimolar polyampholyte (AMPS-50) was dispersed in water but soluble in aqueous solutions of KCl. Polyampholytes with an excess of anionic (AMPS-75) or cationic (AMPS-25) charges behave as neutral polymers, meaning that at a concentration range of 0.05-03 g/dL, the reduced viscosity linearly diminishes upon dilution. The viscometric data reveal that in aqueous solutions of KCl, the intrinsic viscosities of AMPS-25 and AMPS-75 decrease, whereas the intrinsic viscosity of AMPS-50 increases, demonstrating antipolyelectrolyte behavior. In aqueous solution, the conformation of AMPS-25 and AMPS-75 can be considered to have a core and shell structure, where the core part exists in the polyampholyte region and the shell part represents the polyelectrolyte region. The addition of low-molecular-weight salts tends to shrink the shell part and to swell the core part, and such antagonism between the shell and core may cause a minor decrease in the intrinsic viscosity at relatively high ionic strengths. In aqueous solution, the positions of the isoelectric points of strongly charged polyampholytes determined by DLS experiments showed a pH of around 6.3 ±0.2. In the presence of KCl, the position of the IEP shifts to pH 6.5-7.0, due to the specific binding of chloride ions by quaternary ammonium groups of APTAC. The results suggest that the alterable structure of the polyampholyte core of the IEP consists of a high density globule, low-density globule, dense coil and low-density coil.

The formation of a stable complex is found at a 2:3 molar ratio of [AMPS-75] and [CTMACl]. Similarly, [AMPS-25] and [SDBS] have a ratio of 3:2. The composition of the [AMPS-75]:[MB] complex was determined to be approximately 1:3, while that of [AMPS-25]:[MO] is 1:2.

A significant decrease in the reduced viscosity for AMPS-25 and AMPS-75 was observed in an aqueous-organic mixture containing 40 vol.% Ethanol and 60 vol.% Acetone, which caused a decrease in the dielectric constant of the solution, and led to condensation of counterions with polyions, as well as deterioration of the thermodynamic quality of the solvent containing the ionogenic groups of polyampholytes.

3.3 Mechanical and complexation properties of quenched polyampholyte hydrogels based on AMPS and APTAC

3.3.1 Swelling properties of AMPS-APTAC hydrogels

Figure 3.3.1 shows photographs of as-prepared and swollen (immersed in water) QPA hydrogels, as well as graphs of their relative weight m_{rel}, volume V_{rel}, and gel fraction W_g. All as-prepared (or initial) hydrogel samples have the same size. After immersion and equilibration in aqueous solution, the QPA hydrogels of AMPS-75H and AMPS-25H are transparent in the swollen state, while AMPS-50H is cloudy and in a shrunken state. The Donnan effect explains these results. In the case of AMPS-25H and AMPS-75H, due to an excess of positive and negative charges in the hydrogel network, the number of osmotically active ions in the hydrogel phase increases, leading to swelling of the hydrogels. Whereas, in the case of AMPS-50H, the equimolar amount of cationic and anionic charges compensate each other, and the excess free counterions that are not needed to satisfy the electroneutrality of the chain are effectively dialyzed from the hydrogel interior.

(a) **(b)**
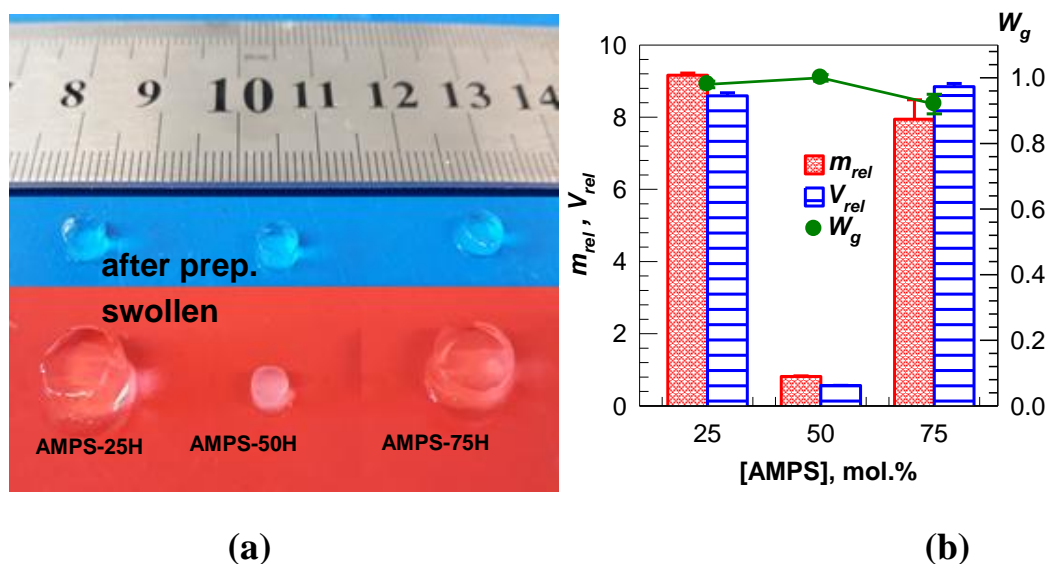
Figure 3.3.1 - Images of as-prepared (top) and swollen (bottom) QPA hydrogels in water (a). The relative weight m_{rel} (red bars), volume V_{rel} (blue bars), and gel fraction W_g (green symbol) of polyampholyte hydrogels as a function of [AMPS] in the feed (b)

3.3.2 Gelation of AMPS-APTAC hydrogels

The dynamics of gel formation were monitored by rheometric measurement using oscillatory deformation tests at an angular frequency ω of 6.3 rad·s^{-1} and strain amplitude γ_o of 0.01. Figure 3.3.2 a and b show the loss G'' and storage modulus G' of the reaction solutions plotted against the reaction time, together with the loss factor tan δ (G''/G') of the reaction system. As seen in figure 3.3.2 b, the gelation time decreases when the AMPS content of the reaction mixture is increased. According to previous research on determination of the monomer reactivity ratio and composition

[15-17], AMPS has a reactivity ratio of r_{AMPS} = 0.62-0.43, whereas that of APTAC is r_{APTAC} =0.360, which predicts that increased AMPS content in the initial monomer solution decreases the gelation time.
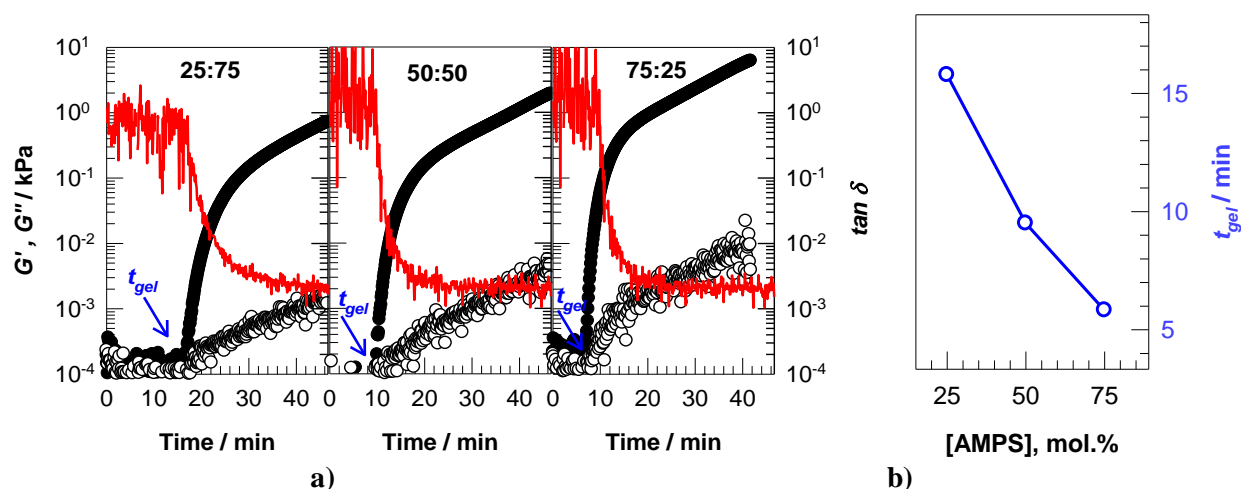
Figure 3.3.2 - Storage G' (filled symbols), loss modulus G'' (open symbols), and loss factor tan δ (red lines) of the reaction mixture as a function of reaction time. ω = 6.3 rad.s^{-1}. T = 60 °C. Blue arrows show the gelation point of the system. a) Gel points t_{gel} (tan δ = 1, open symbols) are plotted as a function of AMPS content in the reaction mixture. Error bars are smaller than the symbols where the bars are not shown b)

3.3.3 Mechanical and rheological properties of AMPS-APTAC hydrogels

The mechanical and rheological characteristics of polyampholyte hydrogels with different AMPS content are shown in table 3.3.1.

As seen in table 3.3.1, by increasing the AMPS content in the copolymer composition, the mechanical properties improve, as measured by Young's modulus (E_c), which increased by 3 times, and fracture stress (σ_f), which rose by 2 times. Such results demonstrate that higher ionic interaction in the system raises the mechanical properties of polyampholyte gels.

Figure 3.3.3 shows the results of rheological measurements, including storage G', loss modulus G'' and loss factor tanδ, of as-prepared QPA hydrogels. APMS-75H demonstrates stronger mechanical properties, but exhibits brittleness (lines on the third graph are approximated). These results are in good agreement with the loss factor tan δ (G''/G') of the reaction system.

Polyampholyte hydrogel AMPS-75 H in the as-prepared state has a higher viscous modulus than the others because of greater ionic bonding, resulting in increased bonding interactions in the hydrogel in the as-prepared state.

The corrected strain-stress curves of as-prepared and swollen QPA hydrogels at various AMPS concentrations are shown in figure 3.3.4 a and b. The Young's modulus E, fracture stress σ_f, and elongation characteristics of QPA hydrogels as a function of AMPS content are presented in figure 3.3.5 a and b. The highest values of

Young's modulus E and fracture stress σ_f are seen in the as-prepared sample of AMPS-75H.

Table 3.3.1 -. Compositions, swelling, and compressive mechanical properties of the hydrogels. Standard deviations less than 5% for H_2O and W_g values. Chemical cross-linker (MBAA) fixed to 20 mol.% with respect to monomers and initiator (APS) set as 10 mM

X_{AMPS}	m_{rel}	H_2O, %	W_g	As prepared state		Swollen state	
				E / kPa	σ_f / kPa	E / kPa	σ_f / kPa
AMPS-25H	9.2 ± 0.1	99.4	0.98	5.2 ± 0.4	24 ± 1	11.2 ± 0.7	6.0 ± 0.8
AMPS-50H	0.82 ± 0.02	99.5	1.00	12 ± 1	30 ± 2	23 ± 2	147 ± 12
AMPS-75H	7.9 ± 0.5	93.8	0.92	19 ± 4	55 ± 3	33 ± 1	27 ± 3
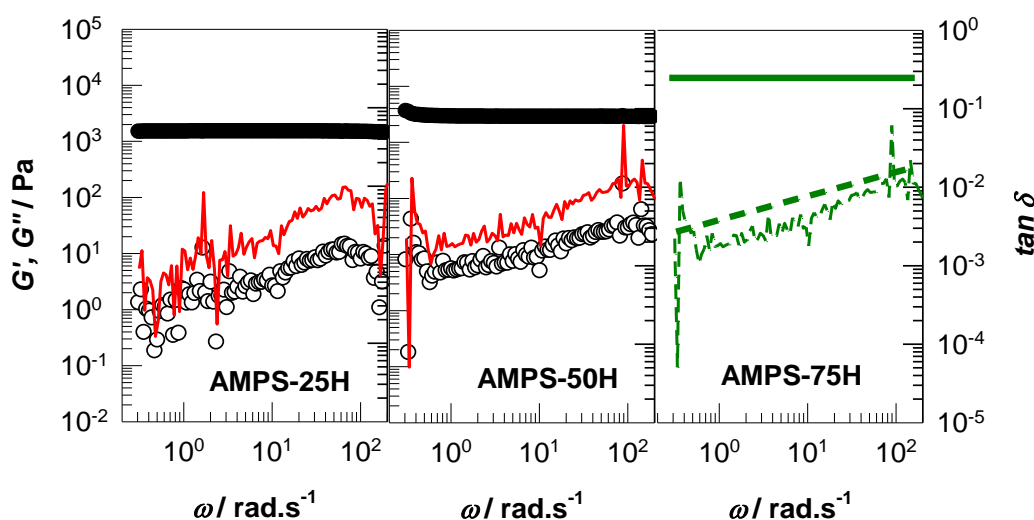
Figure 3.3.3 - Storage G' (filled symbols), loss modulus G''(open symbols), and loss factor tan δ (red lines) of QPA hydrogels prepared between rheometer plates at 60 °C for 1 h at 25 °C. $\gamma_0 = 0.01$. Hydrogel codes are indicated in the graphs. Note that the green lines are approximated data for AMPS-75H

However, in a swollen state, the AMPS-50H shows significantly improved mechanical characteristics. Of note is that the dialysis of as-prepared hydrogel samples in pure water plays a crucial role in enhancing ionic bond formation, at which point the polymer concentration governs the complexation between intra-chain and inter-chain ionic and hydrogen bonding, which forms a tough hydrogel [46, 48, 151, 181-183]. The results of the current study show that in dialyzed AMPS-50H hydrogels, the intra-ionic complexation between oppositely charged monomers leads to the formation of tough hydrogels (figures 3.3.4 b , 3.3.5 b).

Photographs of compression tests of swollen hydrogel samples are displayed in figure 3.3.6.
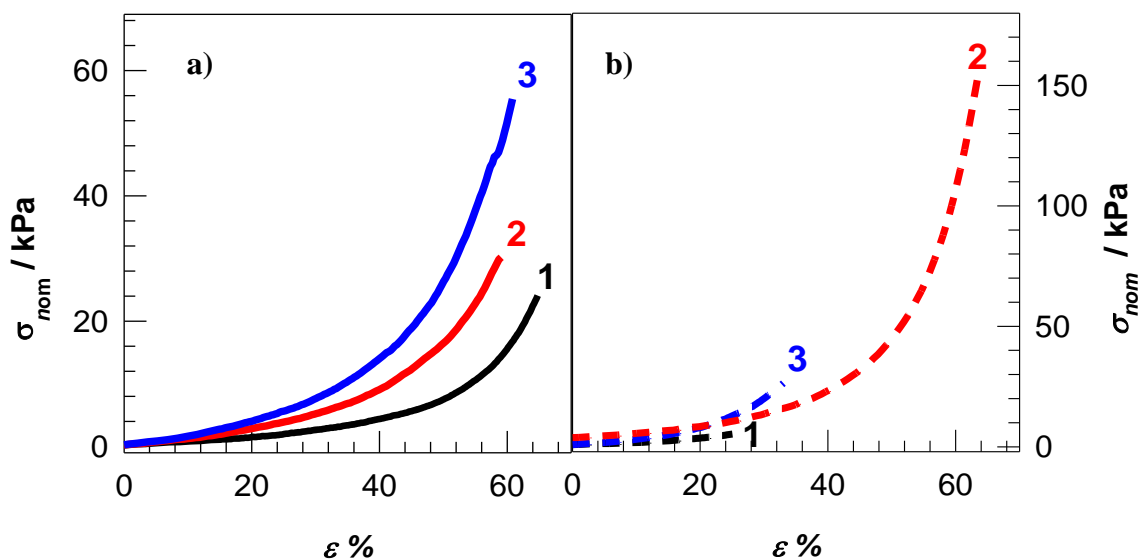
Figure 3.3.4 - Compressive stress-strain curves of as-prepared (a) and dialyzed (b) QPA hydrogels. MBAA = 20 mol.%. R= 3 mm/min. The black (1), red (2), and blue (3) curves correspond to AMPS-25H, AMPS-50H, and AMPS-75H, respectively
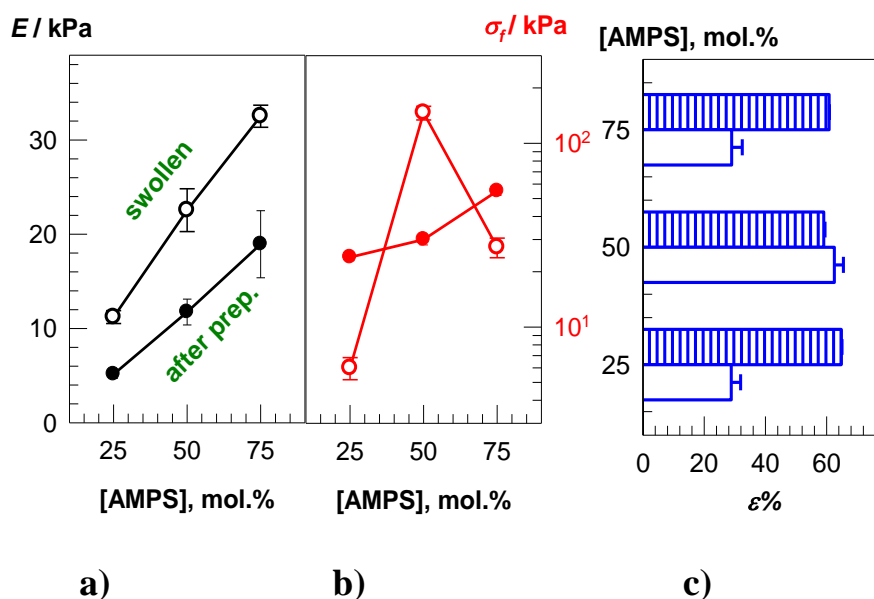
Figure 3.3.5 - The compressive modulus E_c (a), fracture stresses σ_f (b) and fracture strain $\varepsilon\%$ (c) of hydrogels in the as-prepared (filled symbols and bars) and swollen states (open symbols and bars) plotted against the AMPS mol ratio x_{AMPS} in the comonomer feed

Due to the fact that AMPS-25H is a polyelectrolyte gel and contains more water in comparison with collapsed AMPS-50H, which has a small amount of water and a lower degree of swelling, it ruptures under compression, whereas swollen AMPS-50H is stable under the same conditions. Therefore, AMPS-50H hydrogels have increased fracture stress (σ_f) in the swollen state at a level 6 times more than in

the as-prepared state. In the swollen state, those hydrogels with other compositions are more brittle and have reduced fracture stress (σ_f).
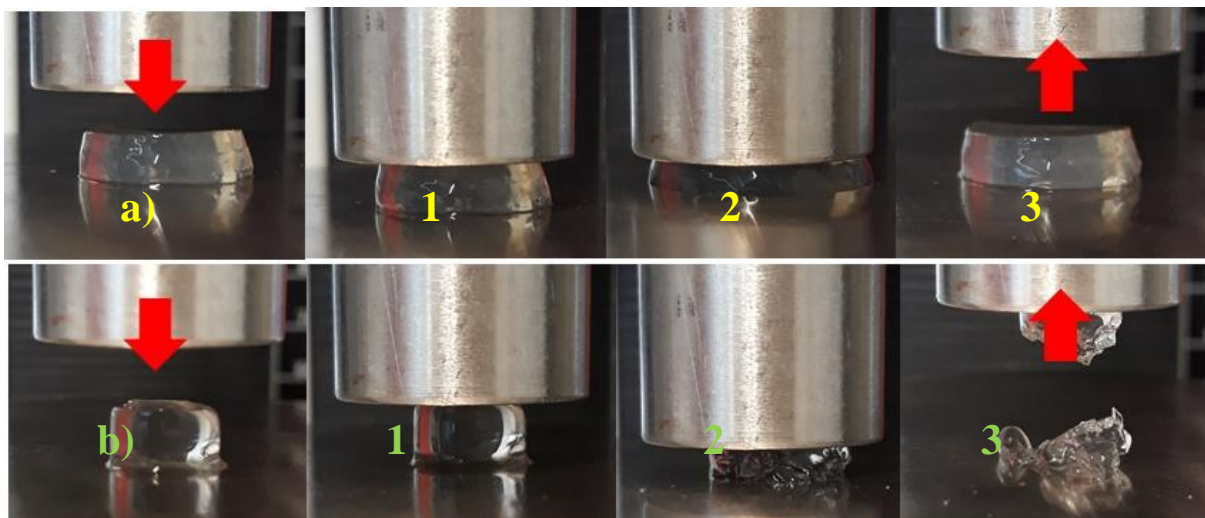
Figure 3.3.6 - Photographs of AMPS-75H (a) and AMPS-25H (b) hydrogel samples in the swollen state during compression tests. Images a1 – a3 show uniaxial compression up to a strain ε of 40%. Images b1–b3 show the rupture of the hydrogel specimen upon compression

3.3.4 Complexation of AMPS-APTAC hydrogels with dyes and surfactants, and the behavior of AMPS-APTAC hydrogels in organic solvents.

3.3.4.1 Sorption and desorption of dye molecules by AMPS-APTAC hydrogels
Figures 3.3.7 and 3.3.8 show the time-dependent absorption of MB and MO by AMPS-75H and AMPS-25H, respectively.
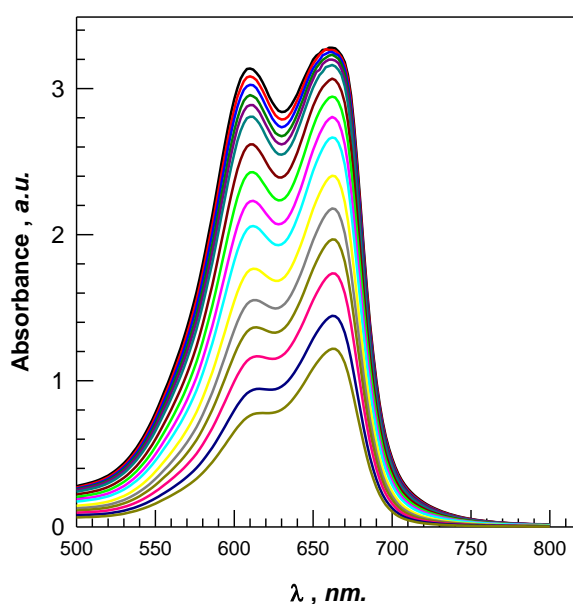
Figure 3.3.7 - Absorption of MB by AMPS-75H. [MBAA] = 20 mol.%
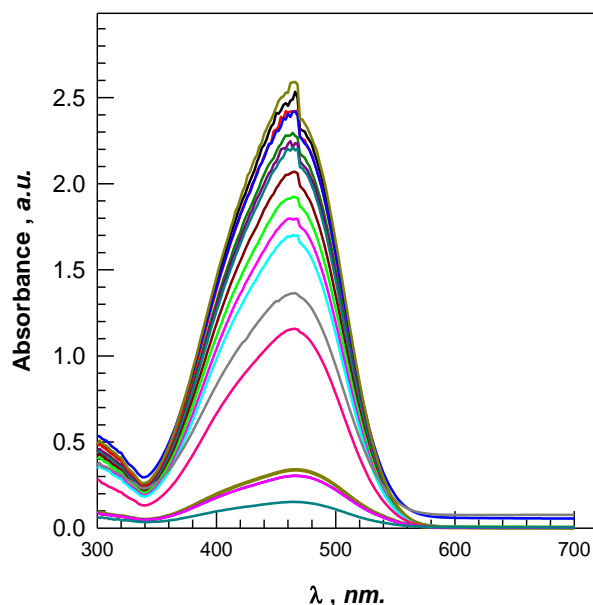
Figure 3.3.8 - Absorption of MO by AMPS-25H. [MBAA] = 20 mol.%

The gradually decreasing intensity of MB and MO in the presence of AMPS-75H and AMPS-25H confirms the absorption of dye molecules by the hydrogels. Sorption kinetics of positively charged dye, methylene blue (MB), and negatively charged dye, methyl orange (MO), by AMPS-APTAC hydrogels are shown in figures 3.3.9 and 3.3.10, respectively [4].

Hydrogels containing an excess of negative (AMPS-75H) and positive (AMPS-25H) charges effectively absorb MB and MO, respectively, due to electrostatic binding. No binding of MB is observed for AMPS-25H and AMPS-50H. The reason is that both AMPS-25H and MB are positively charged. In the case of AMPS-50H, the oppositely charged chains compensate each other, thus positively charged MB molecules are not able to penetrate the hydrogel matrix. The same phenomenon is observed for AMPS-75H and AMPS-50H, with respect to negatively charged MO molecules [4].

Nevertheless, AMPS-50H absorbs a small amount of MB, which is probably due to stronger electrostatic interaction between the quaternary ammonium groups of AMPS-50H and the sulfonate groups of MO. AMPS-75H and AMPS-25H absorb up to 80-90% of MB and MO molecules respectively (figure 3.3.11). As seen in figure 3.11, the initial hydrogel samples are transparent when in the swollen state, but following addition of the dye, are colored and in a shrunken state [4].

Penetration of dye molecules into the hydrogel matrix proceeds via the ion-hopping transport mechanism, resulting in gel contraction [33]. The driving force of this process is electrostatic binding of dye molecules with negative or positive charges in the hydrogels, thus continuous migration occurs as dye molecules penetrate deeply into the gel by exchanging one fragment of the network for another vacant place. Each transfer takes place at the gel-solution interface, and is directed towards the hydrogel phase, thus leading to the formation of a vacancy within the

network, which in turn is accessible to other dye molecules for transfer in the same direction (figure 3.3.12)[4].
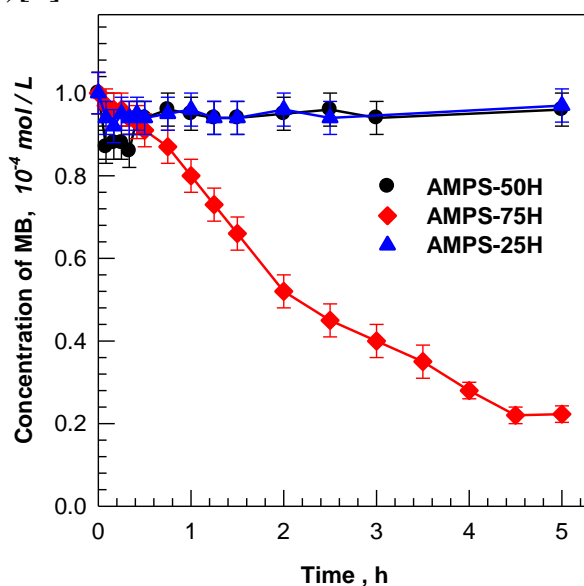
Figure 3.3.9- Sorption kinetics of MB by AMPS-APTAC hydrogels.
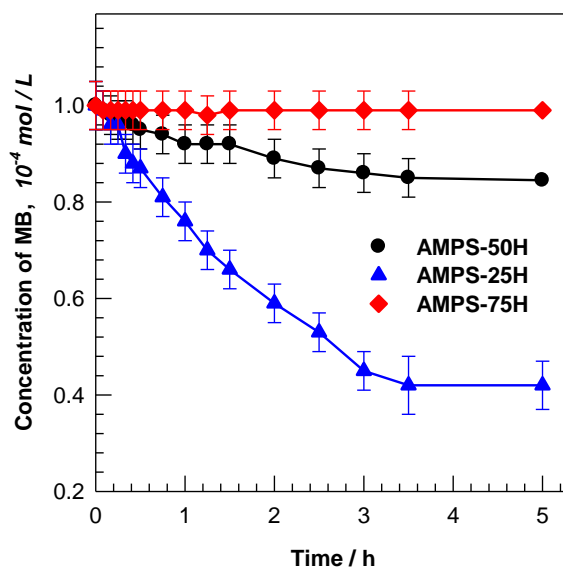
Figure 3.3.10-Sorption kinetics of MO by AMPS-APTAC hydrogels. [MBAA] = 20 mol.%
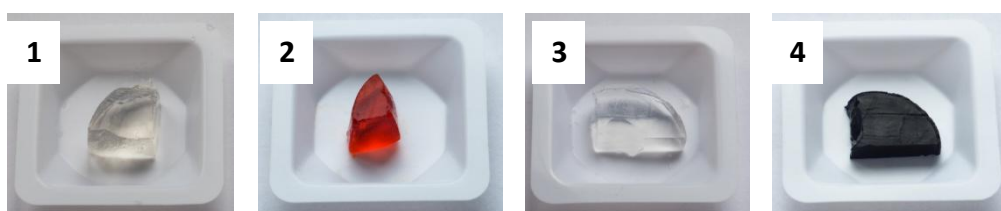
Figure 3.3.11 - Hydrogel samples of AMPS-25H (1,2) and AMPS-75H (1,3) before (1,3) and after (2,4) sorption of MO (2) and MB (4)
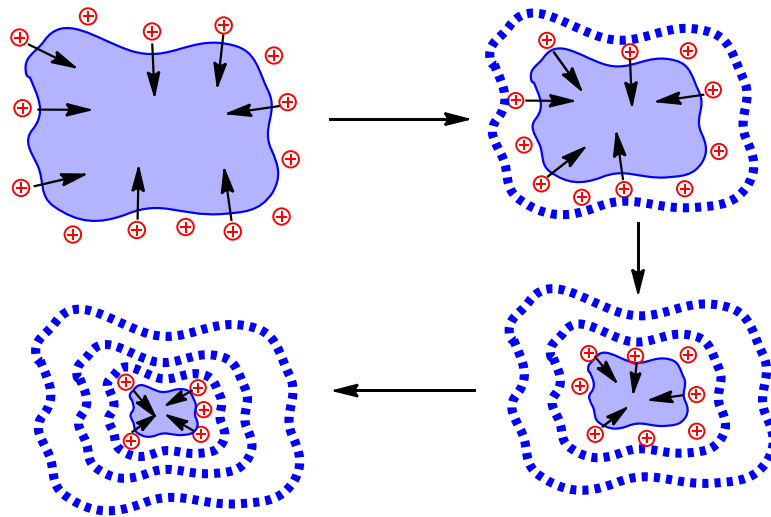
Figure 3.3.12 - Schematic illustration of penetration of dye molecules into the hydrogel matrix via the ion hopping transport mechanism and shrinking of hydrogel [4]

The release of dye molecules from the hydrogel matrix was performed in the medium of 0.5 M KCl (figure 3.3.13). The driving force of dye release from the hydrogel matrix is the replacement of electrostatically-bonded dye by low-molecular-weight salt ions. The quantity of dye molecules released over a period of 24 hours is 70-75%[4].
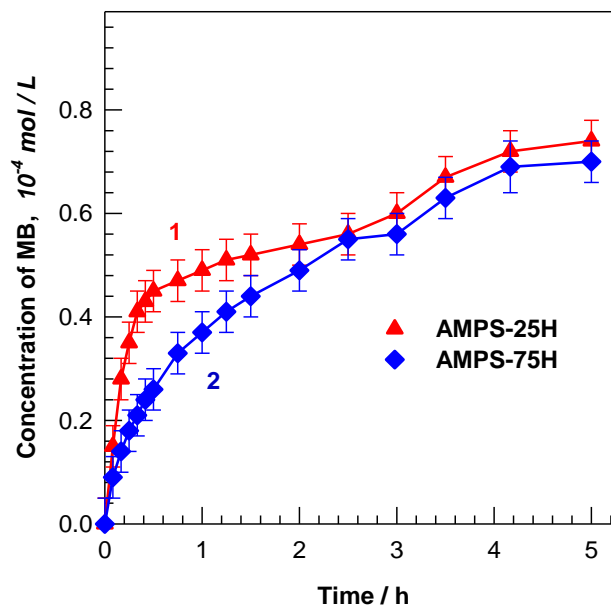
Figure 3.3.13 - Release kinetics of MO (1) and MB (2) from AMPS-25H and AMPS-75H hydrogel matrices, respectively

Isotherms of dye sorption are shown in figure 3.14.

a)

b)
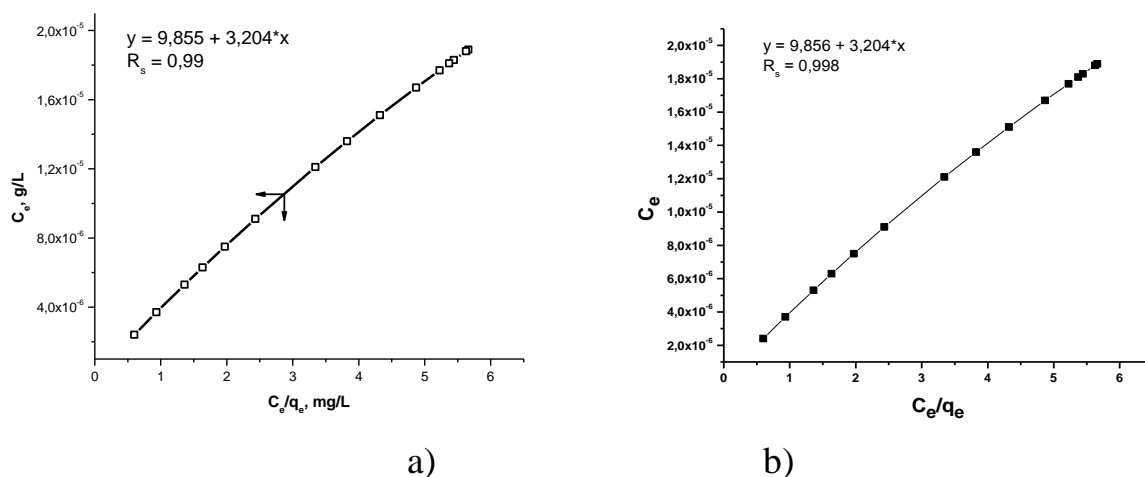
Figure 3.3.14 - Isotherm of dye sorption for a)AMPS-25H; b) AMPS-75H; hydrogels.

3.3.4.2 Sorption and desorption of surfactants by AMPS-APTAC hydrogel

The sorption kinetics of sodium dodecyl benzyl sulfonate (DDBSNa) and cetyltrimethylammonium chloride (CTMAC) by AMPS-APTAC hydrogels in aqueous solution is shown in figure 3.3.15.
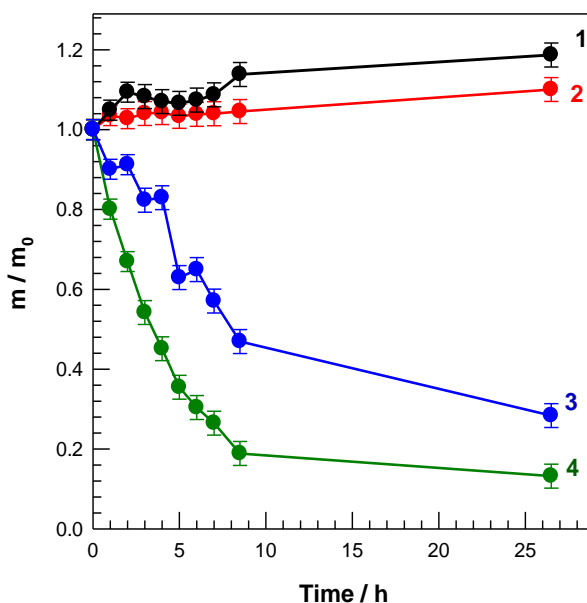
Figure 3.3.15 - Sorption kinetics of CTMAC (1, 3) and DDBSNa (2, 4) by AMPS-50H (1, 2) and AMPS-75H (3) and AMPS-25H (4). [DDBSNa] = $1*10^{-3}$ mol/L; [CTMACl] = $1*10^{-3}$ mol/L

It is seen that AMPS-25H and AMPS-75H shrink due to the complexation of AMPS-25H and AMPS-75H shrink due to the complexation of excessive anionic and cationic groups of hydrogels with cationic and anionic surfactants, accompanied by penetration of surfactant molecules into the hydrogel matrix. Consequently, the

formation of micellar structures within the hydrogel matrix and hydrophobization of the system leads to the overall shrinking of hydrogel volume (figure 3.3.16).
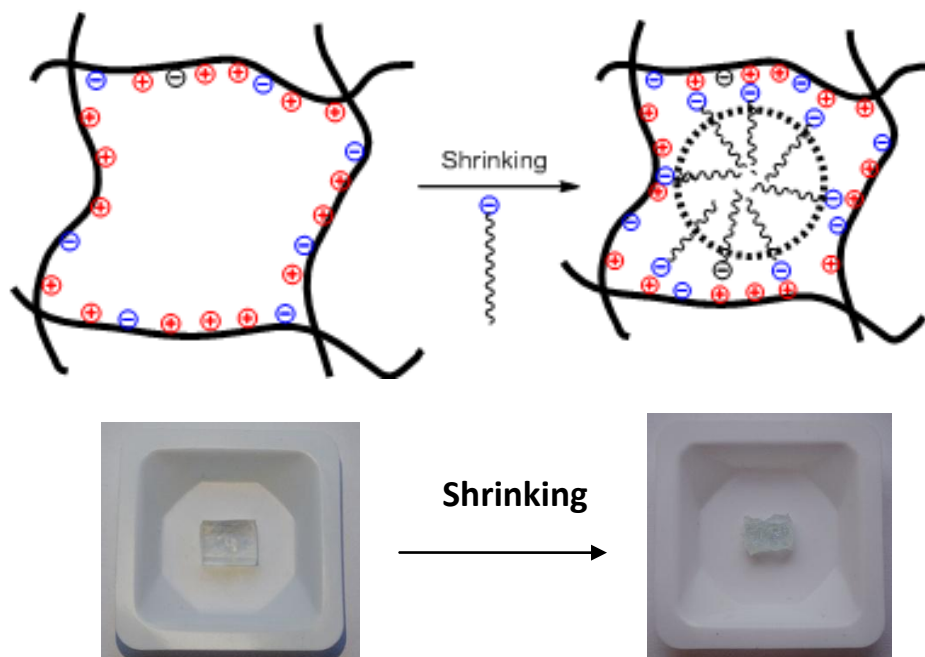
Figure 3.3.16 - Schematic representation of the penetration of SDBS into AMPS-25H hydrogel and formation polyampholyte-surfactant complexes with micellar structure

An analogous mechanism is expected to operate in the case of an anionic gel (AMPS-75H) and a cationic surfactant (CTMAC). The driving force of the formation of AMPS-25H/SDBS (or AMPS-75H/CTMAC) complex is the electrostatic binding of surfactants by excessive positive or negative charges of polyampholytes. Insignificant change and slight swelling of equimolar AMPS-50H in the presence of anionic and cationic surfactants are probably due to absorption of a small number of surfactant molecules into the hydrogel matrix.

3.3.4.3 Behavior of AMPS-APTAC copolymers in water-organic solvents
Dependence of the reduced viscosity and swelling degree of crosslinked AMPS-APTAC copolymers on water-acetone and water-ethanol mixture are shown in figures 3.3.17 and 3.3.18.
The effective shrinking of AMPS-50H, AMPS-75H, and AMPS-25H in water-ethanol mixture starts at volumes of 44, 63, and 63 vol.% of ethanol, respectively. The same tendency is also observed for AMPS-50H, AMPS-75H, and AMPS-25H at volumes of 20, 47, and 54 vol.% of acetone, respectively. Deswelling of AMPS-25 and AMPS-75 in water-organic mixtures is probably due to enhanced condensation of counter ions onto polyions and to the poor thermodynamic quality of the solvents, with respect to anionic and cationic groups.
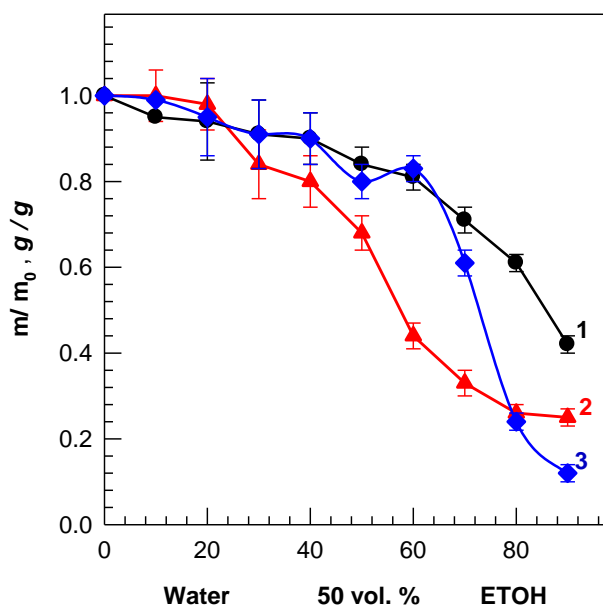
Figure 3.3.17 - Dependence of the swelling degree of AMPS-APTAC hydrogels on the water-ethanol mixture. 1 – AMPS-75H; 2 – AMPS-50H; 3 – AMPS-25H. [MBAA] = 20 mol.%
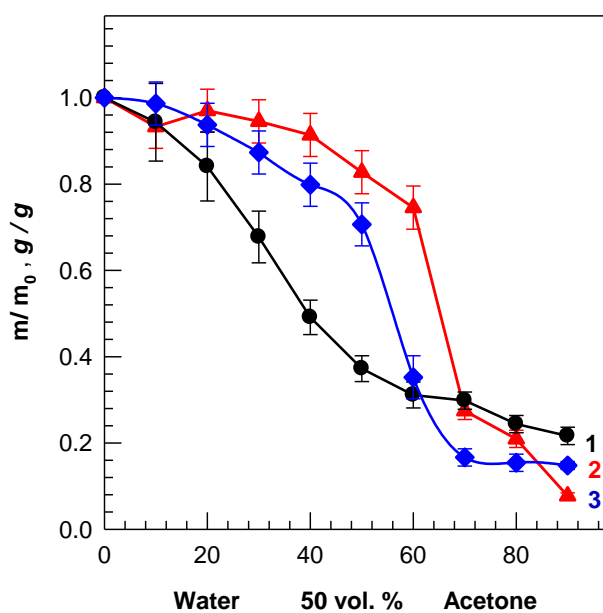
Figure 3.3.18 - Dependence of swelling degree of AMPS-APTAC hydrogels on water-acetone mixture. 1 – AMPS-50H; 2 – AMPS-75H; 3 – AMPS-25H. [MBAA] = 20 mol.%

3.3.5 Technological part

The technological scheme for the scaled up synthesis of equimolar AMPS-50 hydrogels is shown in figure 3.3.20.
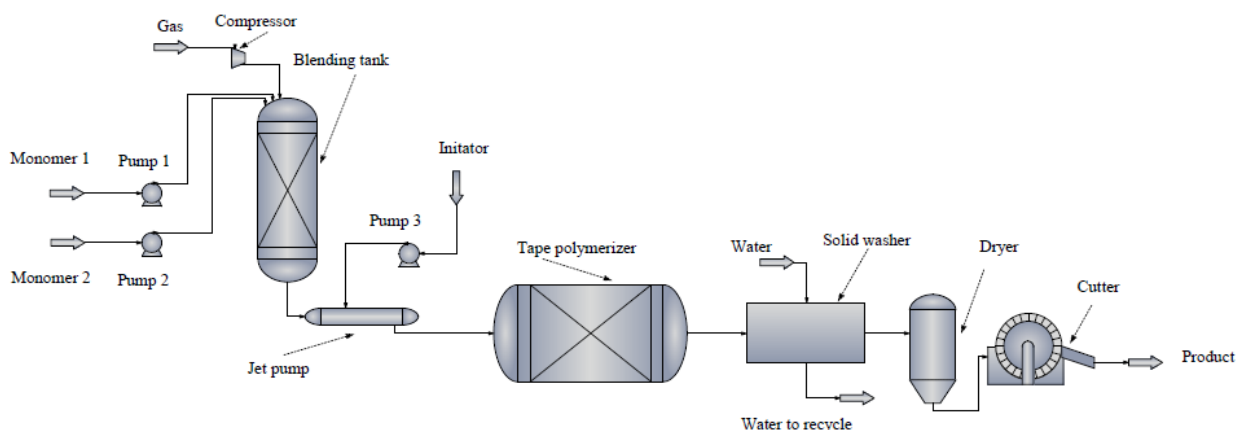
Figure 3.3.20 - The principle scheme for the synthesis of AMPS-50H hydrogels

As seen in figure 3.3.20, the monomers AMPS and APTAC, with the addition of a crosslinking agent and water as a solvent, are bubbled using nitrogen, which requires up to 1 h to purge the solution of all oxygen. Next, the initial monomer mixture passes through a jet pump, where it is injected with an APS initiator to begin the polymerization process. Further, in order to continue the polymerization process, the initial monomer mixture is passed into a tape polymerizer, with a constant temperature of 60 °C and where the solution is continuously maintained under atmospheric pressure.

The tape polymerizer is a metal sheet, stretched between two cylinders. The maximum permissible tape thickness is 2 mm, and the maximum tape size is 1.5 m. after polymerization, the as-prepared hydrogels are sliced with a cutter and pass through the washing and drying processes before finally entering the packaging process.

The material balance is provided in tables 3.3.2-3.3.3 where consumption indices of raw materials per 1 metric ton of prepared material are determined.

Table 3.3.2 - The feed composition of the AMPS-50H in percent ratio

Component code		Amount, mass %	Functional purpose
Technical	Chemical		
Monomer	AMPS	4.60	Initial components of the mixture
Monomer	APTAC	2.80	
Cross-linking agent	MBAA	0.60	
Initiator	APS	0.30	
Water	Water	91.70	Solvent

Table 3.3.3 - Material balance of free-radical polymerisation processes in 1 ton calculation

Component code	Credit , kg / day	Losses, kg / day	Debit, kg / day
AMPS	46.00	0.92	45.08
APTAC	28.00	0.56	27.44
MBAA	6.00	0.12	5.88
APS	3.00	0.06	2.94
Water	917.00	18.34	898.66
Total	1000.00	20.00	980.00

The formula used to calculate total heat flow rate Q_T:

$$Q_T = Q_C + Q_R + Q_A \qquad (3.3.1)$$

where Q_T – is the total heat loss; Q_C – heat loss through conduction; Q_R – heat loss to the reaction mixture; Q_A – heat loss through natural air exchange.

Heat loss through conduction:

$$Q_C = m_c \times c_C \times \Delta T \qquad (3.3.2)$$

where m_c is the mass flow rate of material, 1000 kg; c_C – is the specific heat of steel material "St3" brand is 0.47 kJ·(kg·K); ΔT – temperature differences.

The formula used to calculate heat loss to reaction mixture:

$$Q_R = m_R \times c_R \times \Delta T \qquad (3.3.3)$$

where Q_C – is the heat loss through a material; m_R – is the mass flow rate of material; ΔT – temperature differences.

c_R - is the specific heat of material which calculated by the formula:

$$c_R = (C_{H_2O} + C_{AMPS} + C_{APTAC} + C_{MBAA} + C_{APS})/4 \text{=2.05 J(kg *K)} \qquad (3.3.4)$$

Heat loss through natural air exchange:

$$Q_A = F \times \alpha \times \Delta T \times \tau \times 3600 \qquad (3.3.5)$$

where F – is the flow rate area, 0.75 m^2; τ-3.5 h; ΔT – Temperature differences;

A – heat transfer coefficient which calculated by the formula:

$$\alpha = 9.74 + 0.07\Delta T = 9.74 + 0.07 \times 33.15 = 14.38 \ W/(m^2 \times K)$$

Heat loss through conduction:

$$Q_C = 100 \times 0.47 \times (333.15 - 298) = 1652.05 \ kJ$$

Heat loss to reaction mixture:

$$Q_R = 1000 \ kg \times 2.05 \times 35.15 = 72.06 \ kJ$$

Heat loss through natural air exchange:

$$Q_A = 0.75 \times 14.38 \times 33.15 \times 3.5 \times 3600 = 4504.79 \ kJ$$

Total heat flow rate is equal:

$$Q_T = 4504.78 + 1652.05 + 72.06 = 13362.83 \ kJ$$

Heat balance is 13,363 kJ for synthesis of 1 metric ton of AMPS-50 hydrogels using a tape polymerizer.

CONCLUSION TO CHAPTER 3.3

Three samples of quenched, or high-charge-density, polyampholyte hydrogels were prepared from anionic AMPS and cationic APTAC monomers in the presence of MBAA as a cross-linking agent. They were characterized by swelling measurements, rheological experiments, and mechanical tests. The swelling and mechanical properties of initial and equilibrated QPA hydrogels are different due to excess or equal numbers of anionic and cationic monomers. Independent of composition, such hydrogels behave as either polyelectrolytes or polyampholytes. A dramatic increase in fracture stress accompanies the shrinking of the AMPS-50H gels σ_b and fracture strain $\varepsilon\%$. Dialysis of initial hydrogel samples in pure water plays a crucial role in the disparity between the repulsive polyelectrolyte effect of AMPS-25H and AMPS-75H, and the attractive polyampholyte effect of AMPS-50H, due to intra-ionic complexation between oppositely charged monomers. Both the fracture stress (σ_f) and fracture strain ($\varepsilon\%$) of swollen AMPS-50 are much higher than AMPS-25H and AMPS-75H. This is explained by the globular structure of AMPS-50H, stabilized by ionic bonds between oppositely charged monomers. Upon stretching, the globular parts unfold and extend, exhibiting improved mechanical properties. Supramolecular QPA, prepared by random copolymerization of oppositely charged ionic monomers at relatively high monomer concentration and equimolar monomer ratio, represents a new class of hydrogels, containing both strong and weak ionic bonds.

The swelling kinetics of AMPS-APTAC hydrogels in aqueous solution depends on copolymer composition. Shrinking of crosslinked QPAs in water-ethanol and water-acetone mixtures resulted. The sorption and desorption ability of QPAs was evaluated with respect to dyes and surfactants. Hydrogels containing an excess of negative (AMPS-75H) and positive (AMPS-25H) charges effectively absorb up to 80-90% of MB and MO respectively, due to electrostatic binding. Approximately 70-75% of dye molecules were released from the hydrogel matrix into the medium of 0.5M KCl over a period of 1 day. The driving force of dye release is the replacement of electrostatically bound dye molecules by low-molecular-weight salt.

The technical schematic for the synthesis of AMPS-50 hydrogels using a tape polymerizer is shown. Material balance and heat balance were calculated, where consumption indices of raw materials per 1 ton of prepared materials are provided.

3.4 Highly stretchable chemical cross-linked QPA hydrogels. DMA effect on mechanical properties of QPA hydrogels

3.4.1 Gelation. Swelling kinetics and rheological properties of chemically cross-linked QPA hydrogels

The previous chapter considered the mechanical properties of quenched polyampholyte (QPA) hydrogels synthesized by free-radical copolymerization in the presence of N,N-methylene bisacrylamide (MBAA) as a crosslinking agent, with the varying dependence on the molar amount of AMPS, abbreviated as AMPS-75H, AMPS-50H and AMPS-25H. The swelling, rheological, and mechanical properties of QPA hydrogels were evaluated for different compositions of copolymers at fixed initial monomer concentration $C_0 = 5$ wt.% and a constant amount of [MBAA] = 20 mol.%, showing that the attractive polyampholyte effect of AMPS-50H is due to intra-ionic complexation between oppositely charged monomers. Both the fracture stress (σ_f) and fracture strain (ε %) of swollen AMPS-50 are much higher than AMPS-25H and AMPS-75H. However, these samples were still brittle and not stretchable.

The present chapter examines the limit of initial monomer concentration for gelation depending on the crosslinking agent. Gong et al. [112, 143] claim that the limit of initial monomer concentration C_M is about 1.5 M, which is close to the result of the present study, 1.35 M (table 3.4.1).

Hydrogels are denoted as C30-x and C30-x/y, where x and y are the amounts of the chemical crosslinker, MBAA, and the hydrophilic monomer, DMA, respectively. Initial monomer concentration was fixed as 30 wt.% (1.35 M).

Table 3.4.1 - Synthesis parameters: $x_{AMPS} = 0.5$ and $C_M = 1.35$ M

Series	MBAA / mol%	DMA / mol%	APS / mM
a	5-0.1	-	10
b	0.5	5-20	10

For the purpose of studying the mechanical properties of polyampholyte hydrogels, an increased initial monomer concentration of 30 wt.% and proportionally decreased crosslinker concentration were chosen, in order to improve ionic interaction and make fewer chemical crosslinks. As a result, the present study achieved gelation by decreasing the cross-linking agent, MBAA, to 0.2 mol% with respect to total monomer concentration. Whereas, no gelation occurred at 0.1 mol%.

Table 3.4.2 shows the swelling properties of m_{rel}, gel ratio W_g, and the mechanical properties of polyampholyte hydrogels based on APTAC and AMPS. The highest mechanical properties and best gel ratio were found in the C30-5 sample. However, it is the most brittle, in comparison to the other samples, because of the large amount of cross-linker, 5 mol%, with respect to total monomer concentration.

As seen in figure 3.4.1 and 3.4.2, gelation time changes in accordance with increased concentrations of MBAA. As the amount of MBAA in the monomer mixture increases, gelation time decreases.
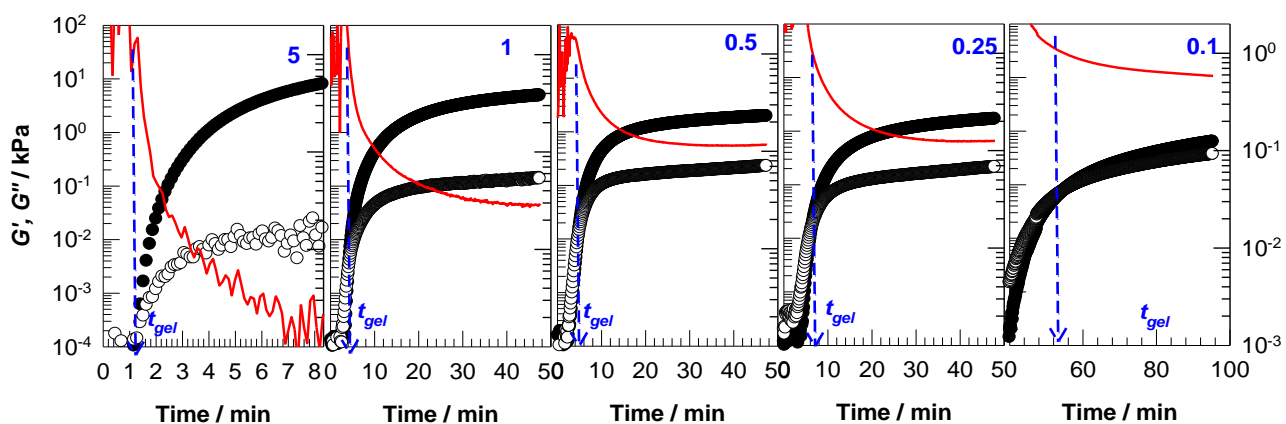
Figure 3.4.1 - Storage G' (filled symbols), loss modulus G'' (open symbols), and loss factor tan δ (red lines) of the reaction solutions plotted against the reaction time. $\omega = 6.3$ rad.s^{-1}. Temperature = 60 °C. Blue arrows show the gelation point of the system. MBAA contents (mol % with respect to monomers) are indicated on the graphs
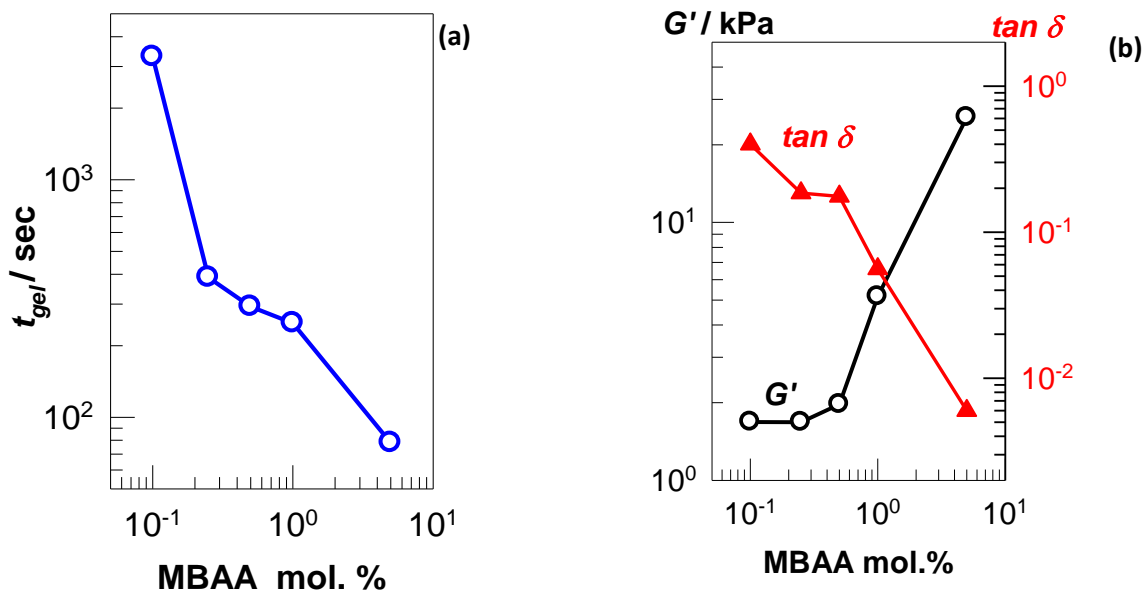
Figure 3.4.2 - Gel point t_{gel} (tan δ = 1, open symbols) plotted as a function of the mole ratio of the chemical crosslinker to total monomers. Error bars are smaller than the symbols where the bars are not shown (a), Storage modulus G' (circles) and loss factor tan δ (triangles) of the reaction solutions of the hydrogels prepared between rheometer plates at 60 °C for 1 h plotted against the MBAA content. $\omega = 6.3$ rad.s^{-1}. Temperature = 25 °C (b)

Figure 3.4.3 shows that with increased MBAA concentration in the monomer mixture, the mechanical properties also increase. The 0.1 mol.% of the MBAA does not have a straight line, which means the sample is nearly soluble, and can not be utilized as a real hydrogel, despite improved mechanical properties.

Table 3.4.2 - Compositions, swelling, and mechanical properties of hydrogels.

Code	m_{rel}	H_2O %	W_g	Compression		Tensile	
				E / kPa	σ_f / MPa	E / kPa	σ_f / kPa
C30-5	2.9 ± 0.1	90	1.00	199 ± 18	0.33 ± 0.01	Brittle	Brittle
C30-1	5.4 ± 0.4	96	0.98	18.3 ± 0.9	3.99 ± 0.03	10.8 ± 1.1	12.8 ± 1.1
C30-0.5	13.9 ± 1.0	98	0.86	11.7 ± 1.2	4.0 ± 0.2	1.8 ± 0.2	7.1 ± 0.5
C30-0.25	8.0 ± 0.9	96	0.69	5.8 ± 0.5	1.7 ± 0.2	1.8 ± 0.6	6.0 ± 0.4
*C30-0.1	-	-		-	-	-	-
*No data							
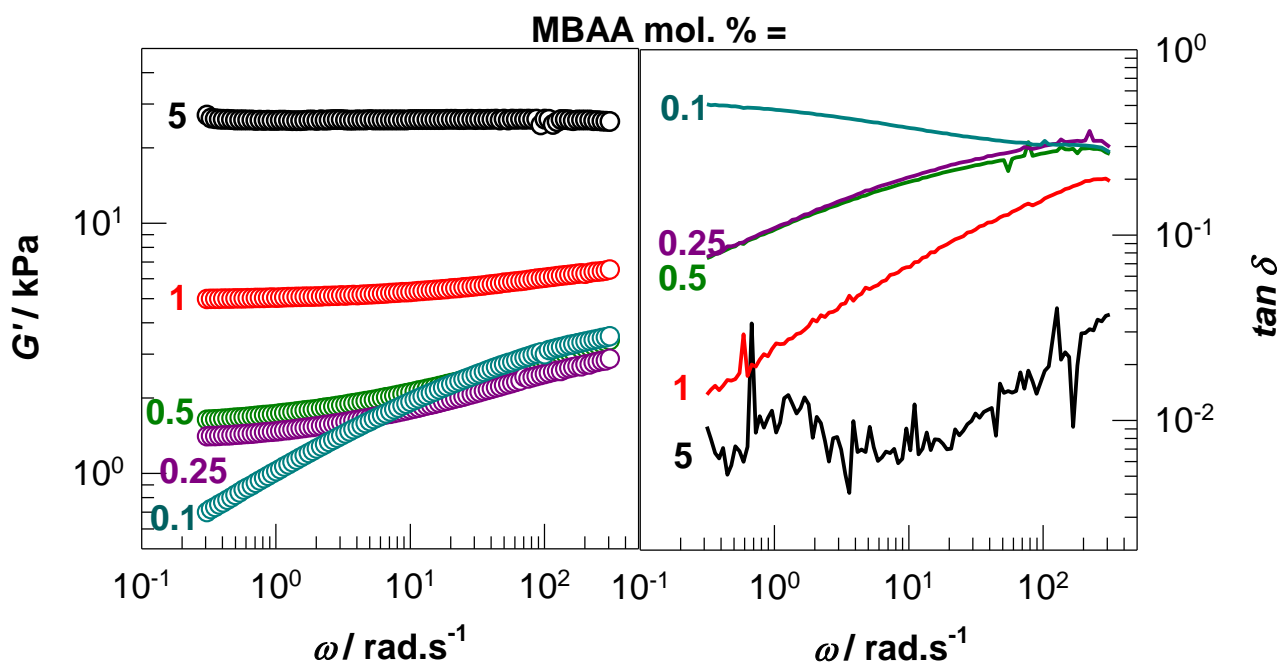
Figure 3.4.3 - Frequency ω dependences of the storage modulus G' (a, symbols), and loss factor tan δ (b, lines) of chemically crosslinked polyampholytes (after preparation) at 25 °C. $\gamma_o = 0.01$. MBAA contents of hydrogels shown in the figure

The swelling kinetics shown in figure 3.4.4 demonstrate that decreasing the MBAA concentration causes more swelling and eliminates the possibility of achieving an equilibrium state because of the loss of total monomer mass, where hydrogels C30-5 has about $W_g = 1$ while C30-0.2 is just 0.69.
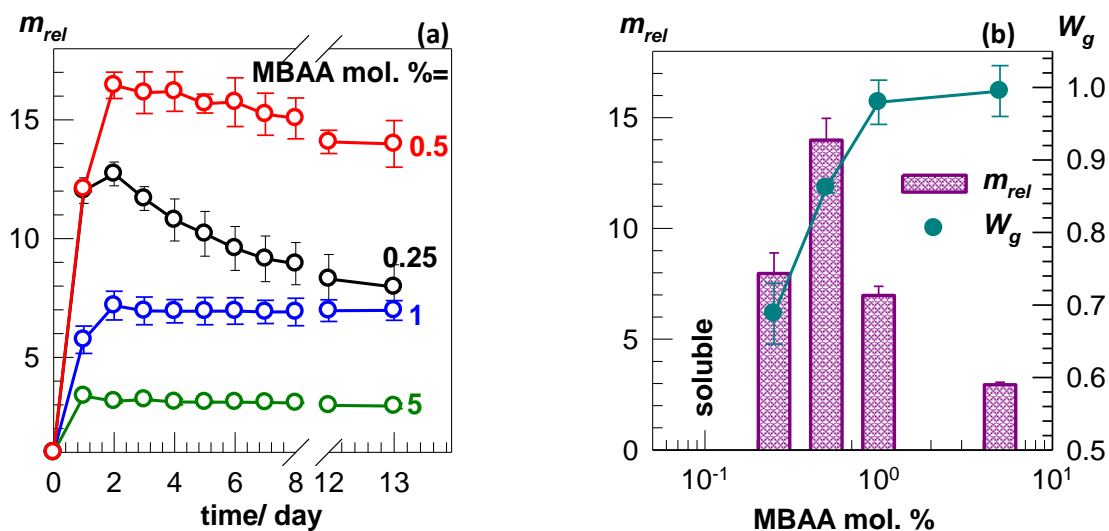
Figure 3.4.4 - Swelling kinetics of hydrogels according to swelling time. (a), Relative weight swelling m_{rel} (bars), and gel ratios W_g (symbols) of polyampholyte hydrogels as a function of MBAA mol% (b)

3.4.2 Mechanical properties of chemically cross-linked QPA hydrogels

The corrected strain-stress curves of the initial and swollen QPA hydrogels, at various MBAA concentrations, are shown in figure 3.4.5 a and b. The Young's modulus E and fracture stress σ_f of QPA hydrogels, as a function of MBAA content, are presented in figure 3.4.5 b. The highest values of Young's modulus E and fracture stress σ_f are exhibited in the initial C30-5 sample.
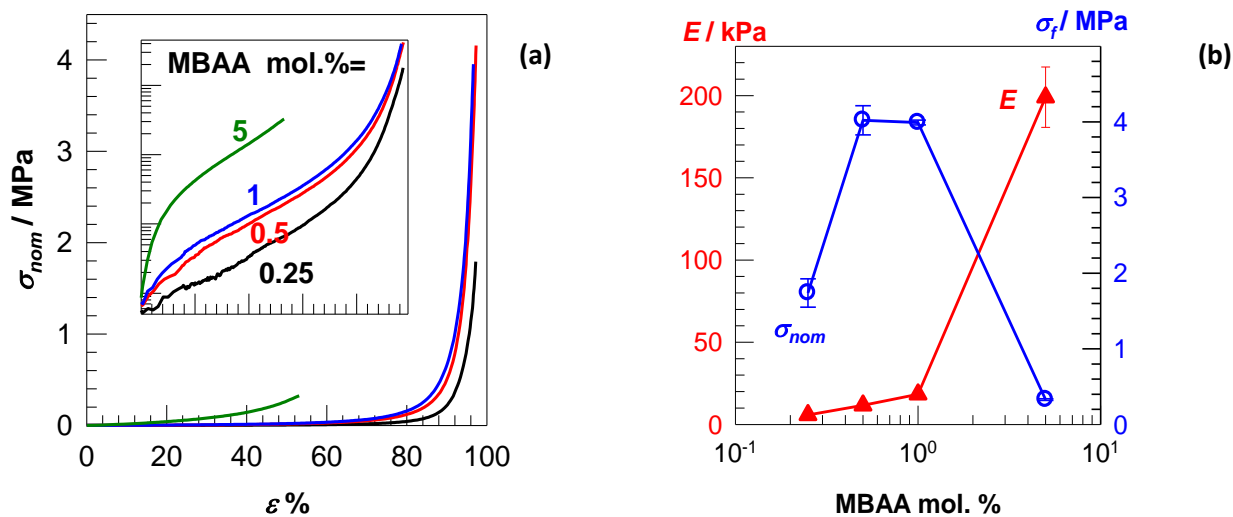
Figure 3.4.5 - Stress-strain curves of chemically crosslinked hydrogels (in the initial state) prepared in the presence of various ratios of MBAA. Total monomer concentration $C_M = 1.35$ M. The inset shows the curves on a semi-logarithmic scale (a), Young's modulus E and fracture stress σ_f of hydrogels as a function of MBAA mol% (b)

However, it was brittle, with fracture strain ε% of about 50%, which is half as much as C30-0.2. Average mechanical properties were found in the samples, MBAA 0.5 and 0.2 mol.%, with respect to total monomer concentration. Nevertheless, the stress-strain curves of the hydrogels in their initial state in the presence of various amounts of MBAA, ranging from 0.2 to 1 mol %, with respect to total monomer concentration, showed that C30-0.5 has the best tensile test with regards to Young's modulus E (1.8 kPa) and fracture stress σ_f (7.1 kPa), shown in figure 3.4.6 a and b. Therefore, C30-0.5 was chosen for its mechanical properties, as it is less brittle and more stretchable in the presence of DMA.
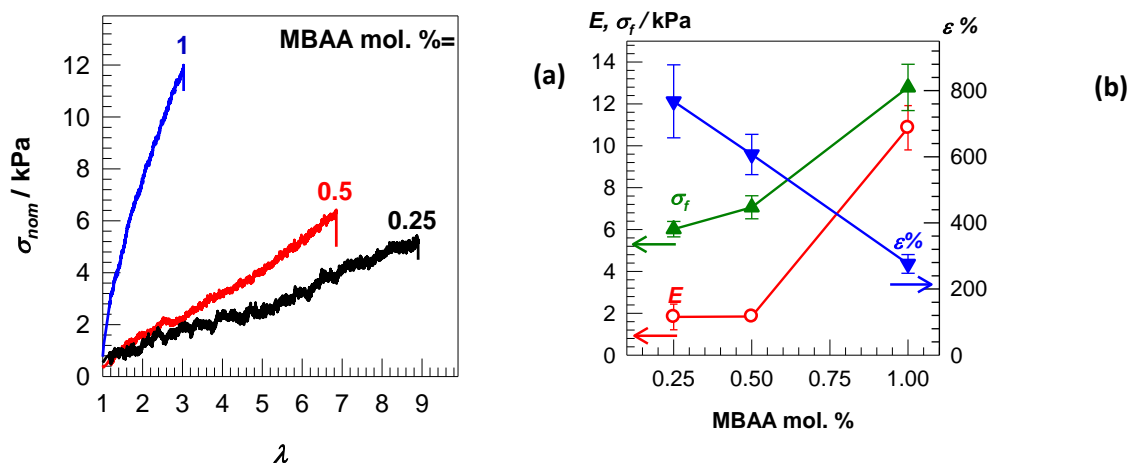
Figure 3.4.6 - Stress-strain curves of the hydrogels (in the initial state) prepared in the presence of various ratios of MBAA. Total ionic monomer concentration C_M = 1.35 M. MBAA contents of hydrogels shown on the graph (a), Young's modulus E (red circles) and fracture stress σ_f (green triangle up) and elongation at breaks $\varepsilon\%$ (blue triangle down) of hydrogels as a function of MBAA content (b)

3.4.3 Effect of DMA on the mechanical and rheological properties of cross-linked QPA hydrogels

Table 3.4.3 shows the mechanical and other characteristics of polyampholyte hydrogels with various amounts of DMA.

Table 3.4.3 Compositions, swelling, and mechanical properties of the hydrogels prepared in the presence of DMA. Standard deviation is less than 5% for H_2O and W_g values. The chemical cross-linker (MBAA) was fixed as 0.5 mol% with respect to monomers and the initiator (APS) set as 10 mM.

Code	m_{rel}	H_2O, %	W_g	Compression		Tensile	
				E / kPa	σ_f / MPa	E / kPa	σ_f / kPa
C30-0.5/0	2.9 ± 0.1	98	0.86	11.7 ± 1.2	4.0 ± 0.2	1.8 ± 0.2	7.1 ± 0.5
C30-0.5/5	5.4 ± 0.4	96	0.87	-	-	4.3 ± 0.5	10.2 ± 1.2
C30-0.5/10	13.9 ± 1.0	95	0.93	-	-	5.4 ± 0.1	14.0 ± 0.6
C30-0.5/20	8.0 ± 0.9	93	1.00	49.7 ± 3.9	4.7 ± 0.4	22.4 ± 1.6	36.8 ± 3.9

As shown in the table, as the DMA content was increased in the reaction solution, tensile strength rose, with E_c increased by 21 times and σ_f by 5 times, compared to QPaH without DMA, as a result of enhanced ionic interaction within the system, thus increasing the mechanical properties of the polyampholyte gels (figure 3.4.7).
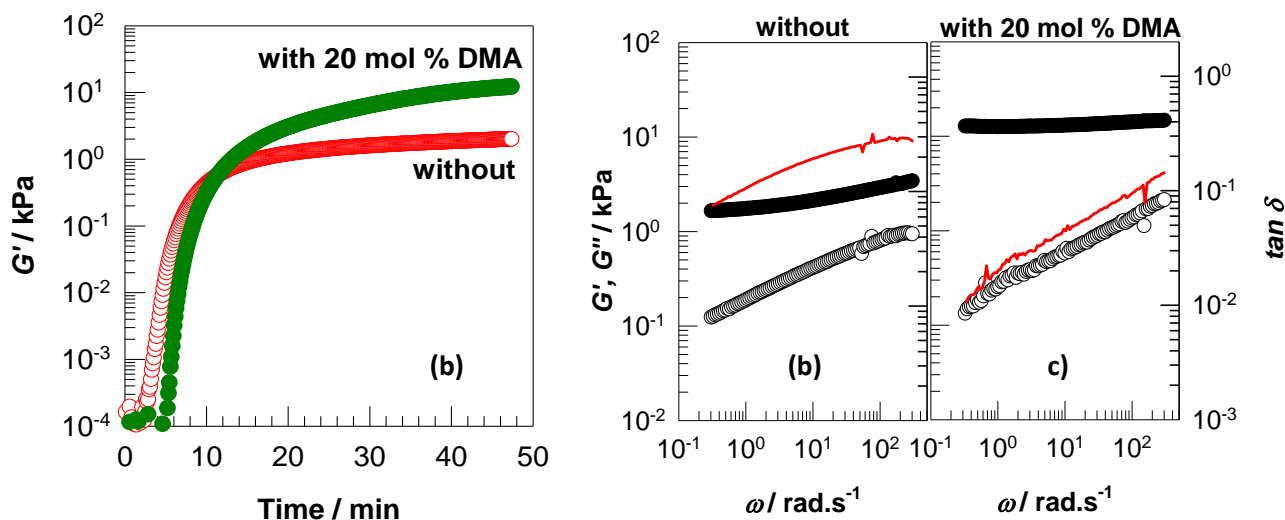
Figure 3.4.7 - Storage G' modulus of the reaction solutions plotted against the reaction time. $\omega = 6.3$ rad.s^{-1}. Temperature = 60 °C. Blue arrows show the gelation point of the system. MBAA contents fixed as 0.5 mol%. (a), Storage G' (filled symbols), loss modulus G'' (open symbols) and loss factor tan δ (red lines) of the hydrogels prepared in the absence (b) and presence (c) of 20 mol % DMA between rheometer plates at 60 °C for 1 h plotted against frequency at 25 °C. $\gamma_o = 0.01$ (b, c)

The effect of DMA significantly decreases the swelling properties of hydrogels by 3 times, compared to hydrogels without DMA (figure 3.4.8 a, b), with the mass ratio correspondingly increasing up to 1, which is a desirable result. The strain curves of the hydrogels prepared in the presence of various amounts of DMA demonstrate that adding it dramatically increases the tensile strength of hydrogels, up to 22.4 kPa. Elongation, $\varepsilon\%$, remains the same, regardless of the addition of DMA, which only alters the mechanical properties of hydrogels, as demonstrated by the change in Young's modulus E, making the addition of DMA a beneficial improvement (figure 3.4.9 a, b).

The polyampholyte hydrogels were studied using cyclic mechanical experiments to further examine the presence of a reduced number of bonds from the initial state. figure 3.4.10 shows the typical tensile cycles of five subsequent loading and unloading steps of the copolymer gel specimens C 30-x 0.5 and x 0.5 y 20. The tests were carried out by increasing maximum strain up to ε_{max} 300% over the five steps, as indicated by the arrows. In the first cycle, the polyampholyte hydrogels exhibited permanent deformation, whereas in the second through fifth cycles the copolymer gels fully and immediately recovered to their original sizes within 1 min

after unloading. This behavior is also illustrated in figures 3.4.11 a and b, and shown in the photograph of the *x0.5* hydrogel sample being manually stretched by around 300%, both without (c) and with the addition of 20 mol% DMA, *x 0.5 y 20* (d).

After stretching the specimens to 800%, they self-recover to their original sizes within 1 min upon releasing the load. Thus, DMA significantly contributes to the elasticity of polyampholyte hydrogels. The solid symbols in figure 3.4.11 show the hysteresis energies U_{hys} of the copolymer hydrogels, with and without the addition of DMA, as calculated from the area between the loading and unloading curves plotted against the maximum strain ε_{max}. Incorporation of DMA significantly increases the hysteresis energy, which reflects the number of bonds reversibly broken under strain.
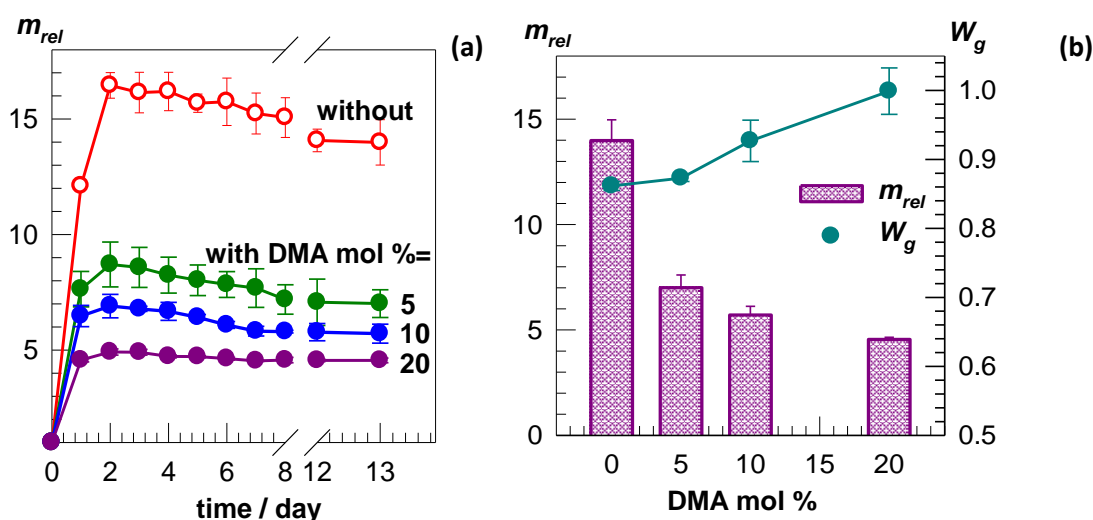
Figure 3.4.8 - Swelling kinetics of hydrogels based on swelling time. (a) Relative weight swelling m_{rel} (bars) and gel ratios W_g (symbols) of polyampholyte hydrogels as a function of DMA mol% in the comonomer feed (b)
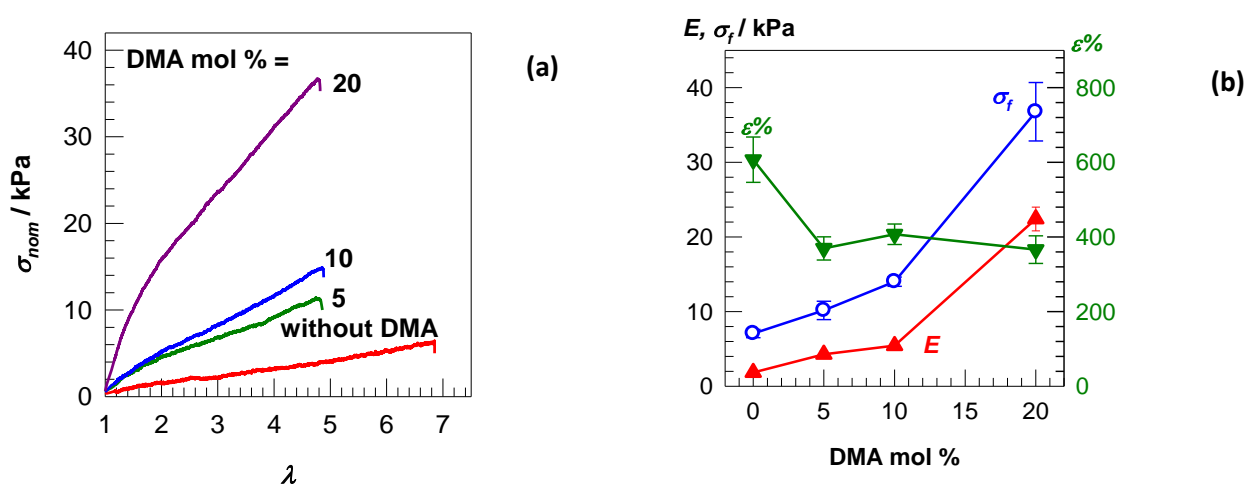
Figure 3.4.9 - Stress-strain curves of the hydrogels (in the initial state) in the presence of various amounts of DMA. Total ionic monomer concentration C_M= 1.35 M. MBAA contents of hydrogels fixed as 0.5 mol%. (a), Young's modulus E (red triangles up) and fracture stress σ_f (blue circles) and elongation at breaks $\varepsilon\%$ (green triangle down) of hydrogels as a function of DMA content (b)
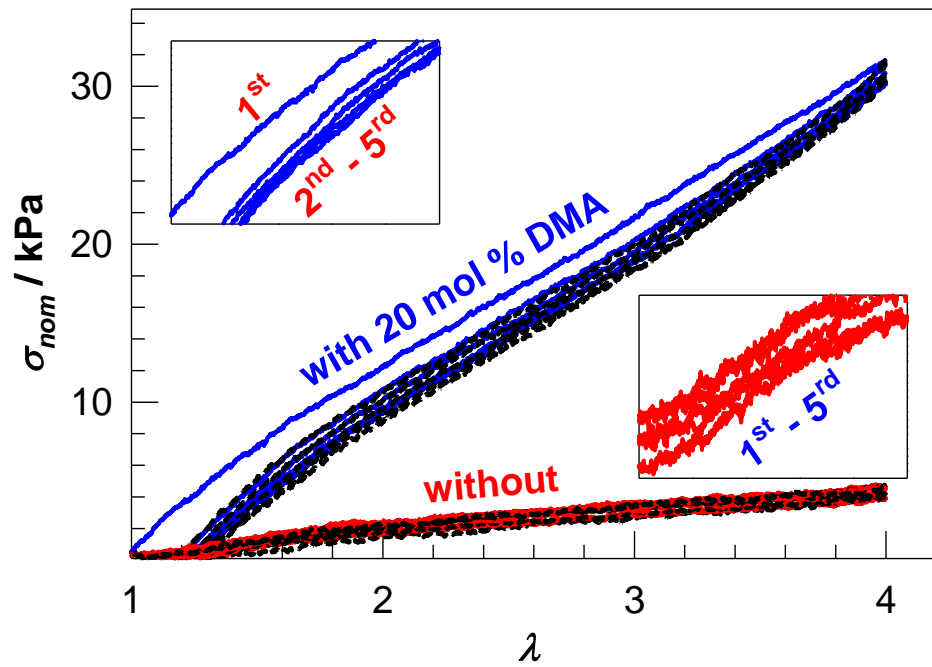
Figure 3.4.10 - Five successive tensile cyclic tests conducted without (red) and with 20 mol. % hydrogels (blue) up to a constant ε_{max} 300%. Strain rate = 1 min^{-1}. Loading and unloading curves are shown as solid lines and dots, respectively. The insets show loading curves
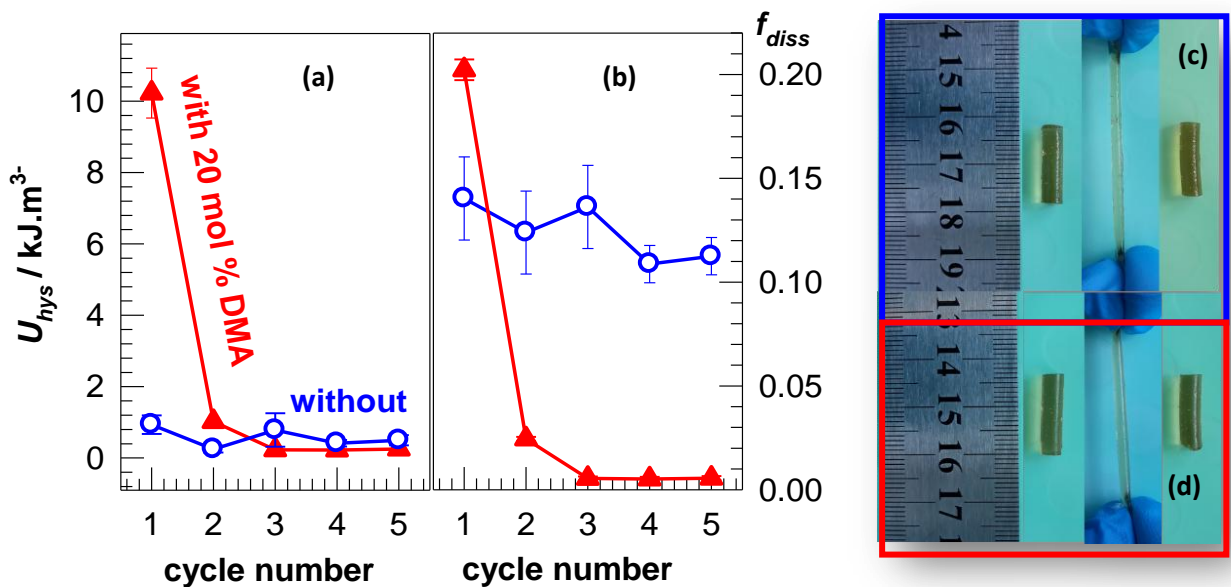
Figure 3.4.11 - U_{hys} (circle, a), energy dissipation fraction f_{diss} (triangle, b) of hydrogels without (open symbols) and with 20 mol.% DMA (filled symbols) after preparation plotted against the number of cycles. (a, b): Photograph of *w/o* hydrogel sample without (c) and with 20 mol.% DMA, *w* (d) during stretching and releasing manually to around 300% stretch ratio (c, d)

Table 3.4.4 and figure 3.4.12 show water contents and compressive mechanical properties of the hydrogels with *(w)* and without *(w/o)* 20 mol % DMA in the initial and swollen states. As seen in the table, adding DMA increased the compressive mechanical properties. Thus, the initial fracture stress, σ_f, was 4.7 MPa, which rose by 10 times to 55 MPa after the addition of DMA while the hydrogel was in a swollen state. However, without the addition of DMA, σ_f increased by just 3 times.

Table 3.4.4 - Water content and compressive mechanical properties of the hydrogels with (w) and without (w/o) 20 mol.% DMA in initial and swollen states. Standard deviations are less than 5% for H_2O and $\varepsilon\%$ values

Code	After prep.				Swollen			
	$H_2O\%$	E / kPa	σ_f / MPa	$\varepsilon\%$	$H_2O\%$	E / kPa	σ_f / kPa	$\varepsilon\%$
w/o	70	11.7 ± 1.2	4.0 ± 0.2	97	98	2.9 ± 0.1	12.4 ± 0.1	68
w	70	49.7 ± 3.9	4.7 ± 0.4	58	93	18.1 ± 0.4	54.8 ± 6.0	64
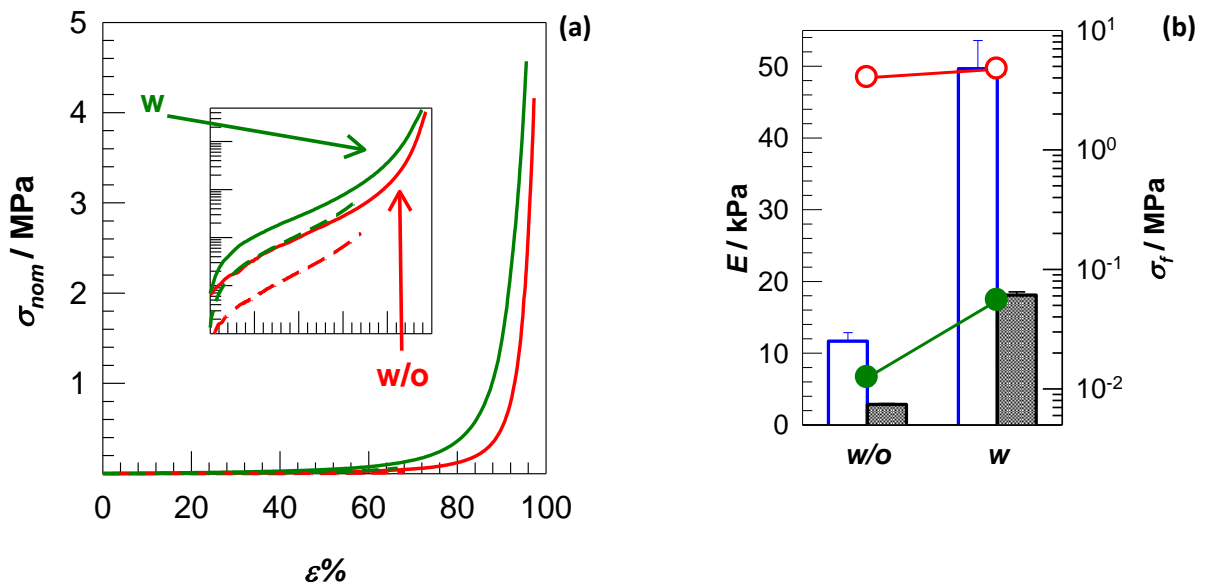
Figure 3.4.12 - (a): Compressive stress-strain curves of hydrogels in swollen (dashed lines) and initial states (solid lines). The inset shows the curves on a semi-logarithmic scale. (b): Young's modulus E (bars) and compressive stress σ_f (symbols) of the hydrogels in swollen (filled) and initial (open) states

CONCLUSION TO CHAPTER 3.4

Calculations were made in order to find the limit of initial monomer concentration to achieve highly stretchable hydrogels based on the crosslinking agent. Further, gelation was achieved by decreasing the cross-linking agent, MBAA, down to 0.2 mol%, with respect to total monomer concentration.

The highest mechanical properties and gel ratio were found in the C30-5 sample. However, it was the most brittle compared to other samples, because of the large amount of cross-linker, 5 mol.%, with respect to total monomer concentration.

The highest values of Young's modulus E and fracture stress σ_f were exhibited by the initial C30-5 sample, but it was brittle. With respect to average mechanical properties, C30-0.5 and C30-0.2 were the best.

DMA introduced into the reaction solution raised the tensile strength, with the result that Ec increased by 21 times and σ_f increased by 5 times above the initial state without DMA, which means increasing the ionic interaction and hydrogen bonding in the system raises the mechanical properties of polyampholyte gels. Additionally, DMA significant decreases the swelling properties of hydrogels by 3 times.

Strain curves of the hydrogels prepared in the presence of various amounts of DMA demonstrated that adding it into the monomer mixture dramatically increases the tensile strength of hydrogels up to 22.4 kPa according. However, elongation at breaks $\varepsilon\%$ were not altered by increasing the content of DMA, which, although raising the mechanical properties of hydrogels, does not improve self-healing ability.

3.5. Hydrophobically modified physical polyampholyte hydrogels based on AMPS-APTAC.

3.5.1 Chemically cross-linked AMPS-APTAC hydrogels fabricated by UV induced polymerization

Before highlighting the extraordinary properties of hydrophobically modified PA hydrogels, first have shown the behavior of the classical, chemically cross-linked PA hydrogels prepared at various mole fractions of AMPS in the comonomer feed. In the following subsections, have shown the properties of the physical PA hydrogels prepared at various hydrophobic monomer contents.

Chemically cross-linked PA hydrogels were prepared from oppositely charged AMPS and APTAC monomers at various mole fractions χ_{AMPS} of AMPS between 0 and 1 in the comonomer feed. They were synthesized at a monomer concentration C_M of 1.0 M in the presence of 1.25 mol% MBAA cross-linker. Figure 3.5.1 a shows the equilibrium weight swelling ratio $m_{rel, eq}$, and the gel fraction W_g of the hydrogels plotted against χ_{AMPS}. W_g equals to 0.66 and 0.9 in the absence and presence of AMPS, respectively, whereas it becomes unity at $\chi_{AMPS} = 1$. The increase in the gel fraction after incorporation of AMPS segments into the gel network could be attributed to the formation of hydrogen bonds between the polymer chains contributing to the cross-link density of the hydrogels [38]. As expected, visual observation showed that the hydrogels assume their most compacted state at $\chi_{AMPS} = 0.5$ (figure 3.5.1 b). At this state, the degree of swelling $m_{rel, eq}$ of the hydrogel is 14- and 11-fold smaller than that formed at $\chi_{AMPS} = 0$ and 1, respectively, due to the charge balance of the comonomer units.

All as-prepared hydrogels were too brittle in tension, and hence, they cannot be subjected to uniaxial tensile tests. Therefore, uniaxial compression tests were performed at a constant strain rate of 1 min^{-1} (figure 3.5.2). Figure 3.5.1 c shows Young's modulus E and compressive fracture stress δ_f of the hydrogels as a function of χ_{AMPS}. The modulus E attains a maximum value at $\chi_{AMPS} = 0.5$ (63 ± 3 kPa) while the fracture stress δ_f exhibits a minimum, i.e. below 2 MPa due to the ionic bonds between AMPS and APTAC segments in addition to the chemical MBAA cross-links, as well as low amount of water in the charge-balanced hydrogel. The results thus reveal poor mechanical properties of chemically cross-linked PA hydrogels due to the lack of an effective energy dissipation mechanism. In the following, was fixed the comonomer composition at $\chi_{AMPS} = 0.5$, whereas no cross-linker was used for the gel preparation.

Figure 3.5.1 - The equilibrium weight swelling ratio $m_{rel, eq}$, and the gel fraction W_g of the hydrogels plotted against χ_{AMPS}. (a), Young's modulus E and compressive fracture stress δ_f of the hydrogels shown as a function of χ_{AMPS}. (b), Images of polyampholyte hydrogels with various AMPS contents in their equilibrium swollen states in water (c)
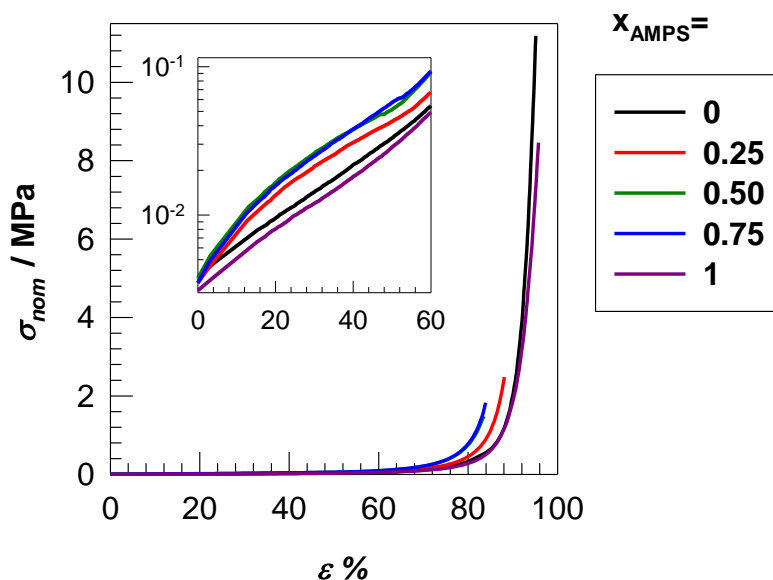
Figure 3.5.2 - Compressive stress-strain curves of chemically cross-linked PA hydrogels in their as-prepared states. The inset is a semi-logarithmic presentation of the data below 60% strain. The mole fraction x_{AMPS} in the AMPS-APTAC monomer mixture is indicated

3.5.2. Hydrophobically modified polyampholyte hydrogels: rheological, swelling, and mechanical characteristics

Instead of the chemical cross-linker, the hydrophobic monomer n-octadecyl acrylate (C18A) was incorporated into the backbone of PA chains to create hydrophobic associations between alkyl side chains of C18A units. It was observed that even adding a small amount of C18A creates gel. For example, images in figure 3.5.3 a, b display charged-balanced physical hydrogels formed with and without 2 mol at different monomer concentrations C_M. Comonomer feed ratio C18A, respectively. With C18A, a physical gel could be obtained at the lowest CM monomer concentration of 1.0 M, while without C18A, no below $C_M = 2.5$ M. Opacity presence in hydrophobically modified polyampholyte hydrogels shows nano-sized regions with hydrophobic interactions. The monomer concentration C_M was set at 1.0 M and the sum of C18A in the comonomer mixture ranged between 5 and 20 mol.%.
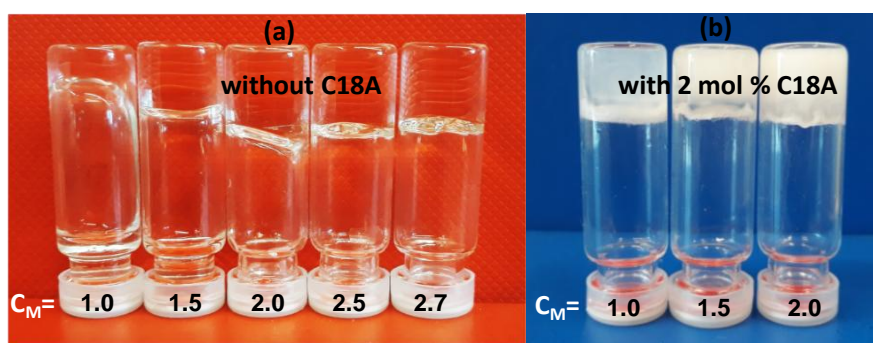
Figure 3.5.3 - Images of charge-balanced PA hydrogels at various monomer concentrations C_M without (a) and with 2 mol % C18A (b)

Figure 3.5.4 shows angular frequency (ω) dependences of the storage modulus G', loss modulus G'', and loss factor *tan δ* of charge-balanced hydrogels in their as-prepared states, formed at $C_M = 1.0$ M and at various C18A contents. The dynamic moduli and *tan δ* of the hydrogel without C18A are shown by the open symbols and dashed lines, respectively. Incorporation of C18A into the hydrogel leads to an increase of G' from the Pa to kPa level, and its frequency dependence decreases. For instance, G' at 10 rad s^{-1} is 0.4 kPa in the absence of C18A, while it around three-orders of magnitude increases at 25 mol.% C18A (31 kPa). Moreover, *tan δ* remains above 0.1 for all hydrophobically modified PA hydrogels revealing the existence of dynamic cross-links and hence their vicious character. The physical gels formed above 1 mol.% C18A were insoluble in water, similar to their chemically cross-linked analogs, as discussed in the previous section.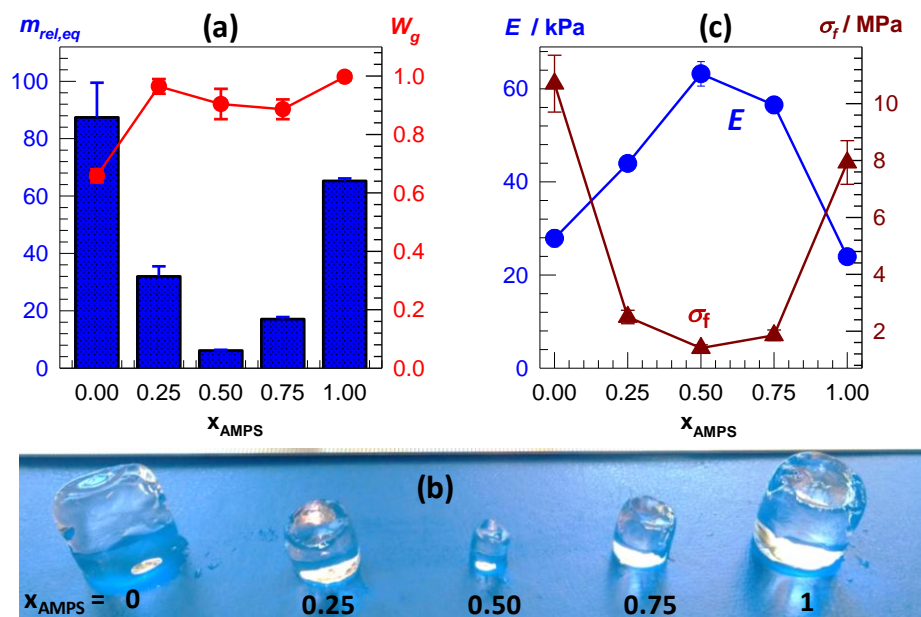 Figure 3.5.5 a shows the equilibrium swelling ratio $m_{rel, eq}$, and the gel fraction W_g of the hydrogels plotted against their hydrophobe contents. W_g is above 0.8 and it increases with increasing C18A content from 2 to 25 mol.%. Moreover, the swelling ratio of hydrophobically modified PA hydrogels is 2.5 ± 0.4 and almost independent on the amount of C18A, as compared to 6.1 ± 0.2 for chemically cross-linked PA hydrogel at the same AMPS

mole fraction (figure 3.5.1a). The lower swelling ratio after hydrophobic modification is attributed to the increased hydrophobicity of the resulting hydrogels.
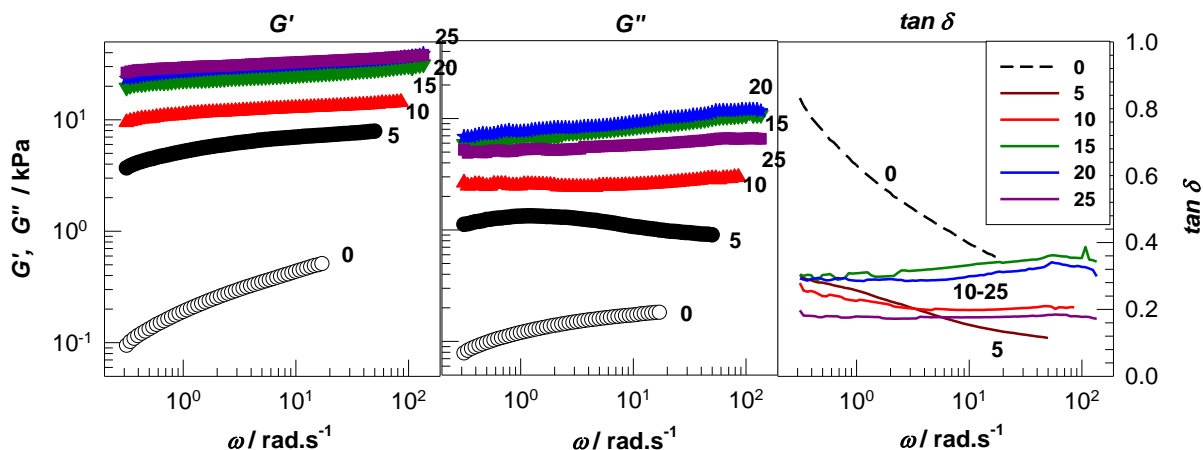
Figure 3.5.4 - Storage modulus G', loss modulus G'', and loss factor $tan\ \delta$ of charge-balanced hydrogels shown as a function of the angular frequency ω. $C_M = 1.0$ M. C18A contents are indicated

      Another characteristic feature of hydrophobically modified PA hydrogels was their unusual swelling kinetics in water, as shown in figure 3.5.5 b. The swelling ratio m_{rel} first increases up to a maximum value ($m_{rel,\ max}$) within one day while at longer swelling times, they start to deswell until attaining their swelling equilibrium after 10 days. Moreover, the lower the C18A content, the higher is $m_{rel,\ max}$ of the hydrogel. Similar swelling kinetics was reported before for non-ionic polyacrylamide hydrogels prepared via micellar polymerization in aqueous SDS solutions [32]. Because all hydrophobically modified PA hydrogels are charge-balanced, they behave as non-ionic hydrogels when immersed in water. However, the existence of Na$^+$ counterions of the surfactant SDS inside the gel network makes them ionic when immersed in water. Because of the osmotic pressure of SDS counterions, they significantly swell in water, as seen during the 1st day of the swelling time (figure 3.5.5 b). However, as SDS is extracted from the hydrogels, they gradually turn into non-ionic ones so that their swelling ratio decreases at longer times. As seen below, the cross-linking density of the hydrogels decreases with a decreasing amount of C18A. Thus, at a low cross-linking density, the diffusion of water inside the gel network is faster than the extraction of SDS from the hydrogel so that the hydrogels with lower C18A content exhibit higher maximum swelling ratios $m_{rel,\ max}$.
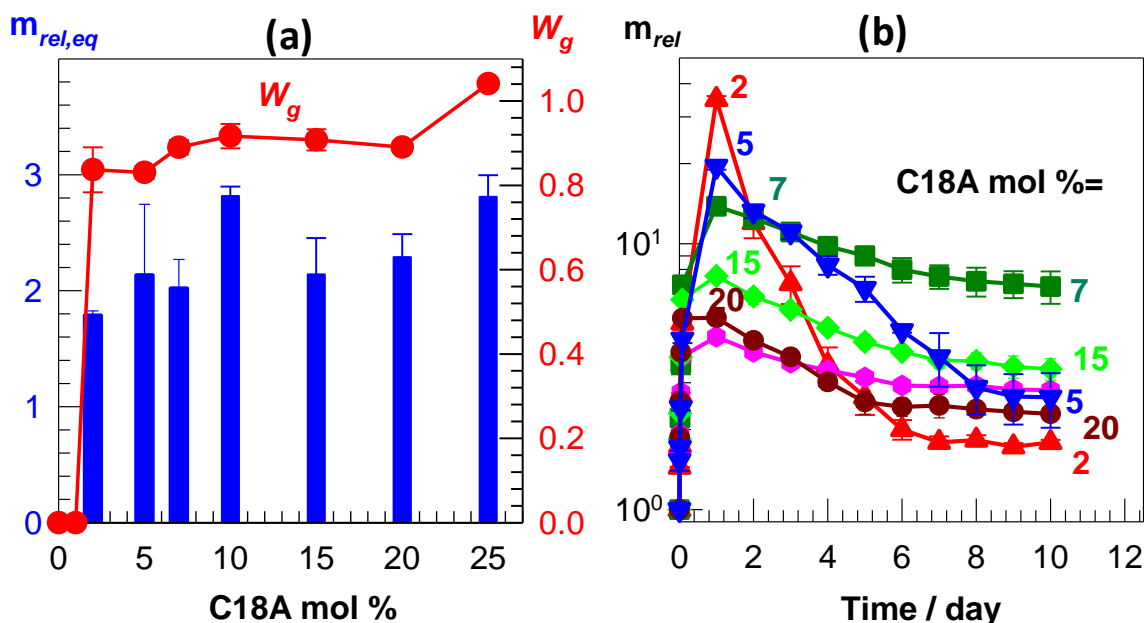
Figure 3.5.5 - The equilibrium weight swelling ratio $m_{rel,\,eq}$, and the gel fraction W_g of the physical hydrogels plotted against C18A mol%. (a) The weight swelling ratio m_{rel} plotted against the time of swelling of the hydrogels with various C18A contents (b)

In contrast to the chemically cross-linked PA's, all hydrophobically modified PA's were highly stretchable and the stretch ratio at break varied depending on the C18A content and on the gel state during the tensile tests. figures 3.5.6 a, b show tensile stress-strain curves of as prepared and water-swollen hydrogels, respectively. The results of the water-soluble hydrogels with < 2 mol. The dashed curves show % C18A. The Young's modulus E, tensile strength δ_f, and elongation ratio at break ε_f of the hydrogels are compiled in figure 3.5.6 c and table 3.5.1 as a function of C18A mol %. The modulus E and tensile strength δ_f increase with increasing hydrophobe content for both as-prepared and swollen hydrogels and they become 175 ± 25 and 202 ± 24 kPa, respectively, for swollen hydrogels with 25 mol.% C18A. The open circle in figure 3.5. 5 c representing the modulus E of the chemically cross-linked charge-balanced PA hydrogel in the as-prepared state reveals that, at above 10 mol.% C18A, hydrophobically modified physical PA hydrogels are much stiffer than the chemical hydrogel in both as-prepared and swollen states. The stretch at break is a decreasing function of C18A content and varies between $137 - 1400\%$.

An interesting point from figure 3.5.6 c and table 3.5.1 is that the swollen hydrogels at high C18A contents are stiffer than in their as-prepared states. This finding is unexpected as swelling of the hydrogels increases their water contents and hence, decreases the number of elastically effective cross-links in a unit gel volume. For instance, at 25 mol.% C18A, although the water content of the hydrogel increases from 60 to $87 \pm 1\%$ upon swelling in water (figure 3.5.7 a), its modulus E increases from 103 to 175 kPa.

Figure 3.5.6 - Tensile stress-strain curves of hydrophobically modified physical PA hydrogels in as-prepared (a) and swollen (b) states at various C18A contents, The modulus E, tensile strength δ_f, and elongation ratio at break ε_f of the hydrogels plotted against C18A mol% (c). The open circle represents the modulus of chemically cross-linked charge-balanced PA hydrogel

This behavior is attributed to the presence of surfactant is as-prepared hydrogels. Surfactant micelles are known to weaken hydrophobic interactions due to their solubilization effect and hence decreasing the lifetime of hydrophobic associations resulting in a decrease in the effective cross-link density of the hydrogels formed by micellar polymerization. To verify this hypothesis, the effective cross-linking density of the hydrogels was calculated using the theory of elasticity as,

$$E = 3\nu_e RT \left(\nu_2\right)^{1/3} \left(\nu_2^0\right)^{1/3} \tag{3.5.1}$$

where ν_2^0 and ν_2 are the volume fractions of the crosslinked polymer at the state of gel preparation, and during the mechanical tests, respectively, R is the gas constant, and T is the absolute temperature. Note that equation 3.5.1 assumes affine network behavior, which is reasonable for such hydrogels. Using the water contents (W) shown in figure 3.5.7 a ν_2^0 and ν_2 of the hydrogels were calculates as $d_p^{-1} (1 - W)$ where d_p is the polymer density, which was taken as the density of PAMPS (1.44 g/mL). Figure 3.5.7 b shows the calculated cross-link densities ν_e of PA hydrogels in their as-prepared and swollen states plotted against C18A mol%. ν_e of swollen

hydrogels containing more than 10 mol.% C18A is higher than that in their as-prepared states, reflecting the strengthening effect of surfactant removal on the stiffness of the hydrogels.

Table 3.5.1 - Water content (W %), Young's modulus E, tensile strength δ_f, and elongation at break ε_f of as-prepared and water-swollen hydrogels PA hydrogels with various C18A contents.

C18A mol%	W %		E / kPa		δ_f / kPa		ε_f %	
	as-prepared	swollen	as-prepared	swollen	as-prepared	swollen	as-prepared	Swollen
1	71 ± 3	soluble	14 ± 3	-	34 ± 1	-	1403 ±155	-
2	71 ±2	88 ± 2	22 ± 3	2 ± 1	40 ± 1	8 ± 1	1239±162	464 ± 48
5	70 ±3	90 ± 1	23 ± 11	9 ± 2	40± 1	68 ± 14	910 ± 47	523 ± 27
7	69 ±3	88 ± 1	31 ± 2	19± 2	59 ± 1	103 ± 9	921 ± 3	484 ± 36
10	64 ±2	90 ± 1	45 ± 6	65 ± 7	75 ± 5	112 ± 13	929 ± 146	490 ± 50
15	63 ±2	6± 1	64± 7	76 ± 2	99 ± 10	122 ± 20	779 ± 45	331 ± 34
20	61 ±1	87 ± 1	99 ± 8	97 ± 11	145 ± 15	213 ± 27	662 ± 16	257 ± 14
25	60 ± 1	87 ± 1	103 ± 7	174 ± 25	172± 9	202 ± 24	608 ± 11	137 ± 22
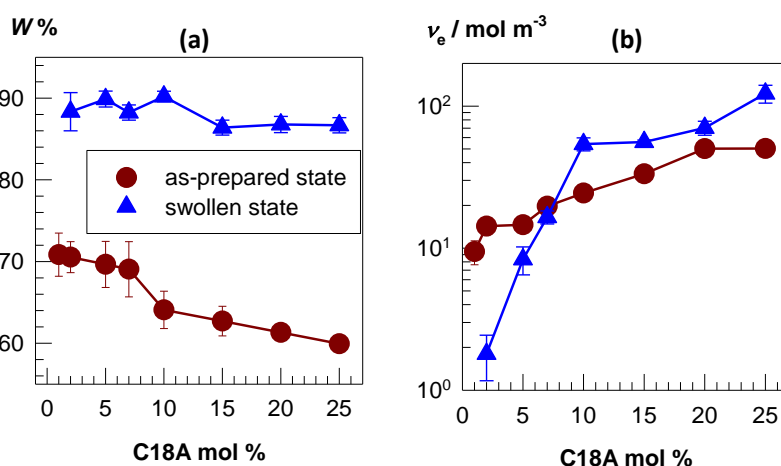
Figure 3.5.7 - The water contents W (a) and cross-link density ν_e (b) of hydrophobically modified physical PA hydrogels in as-prepared and swollen states plotted against C18A mol%.

In addition to the C18A amount, the mechanical properties of hydrophobically modified PA hydrogels can also be tuned by varying the monomer concentration C_M at the gel preparation at a fixed C18 mol%. For instance, with increasing C_M from 1.0 to 2.0 M at 2 mol.% C18A, both E, and δ_f increased from 2 to 16 ± 2 kPa and 8 to 89 ± 13 kPa, respectively, whereas the stretch at break slightly reduced from 1100 to 900% (figure 3.5.8). The 8-fold increase in the modulus by doubling the concentration C_M reveals the increasing extent of hydrophobic interactions between hydrophobically modified PA chains at high concentrations.
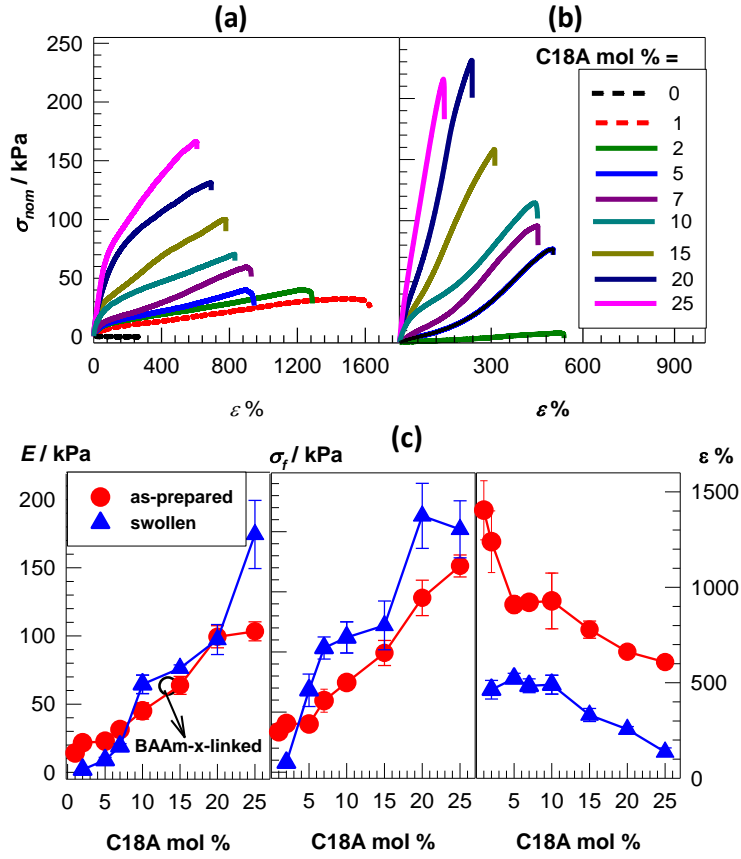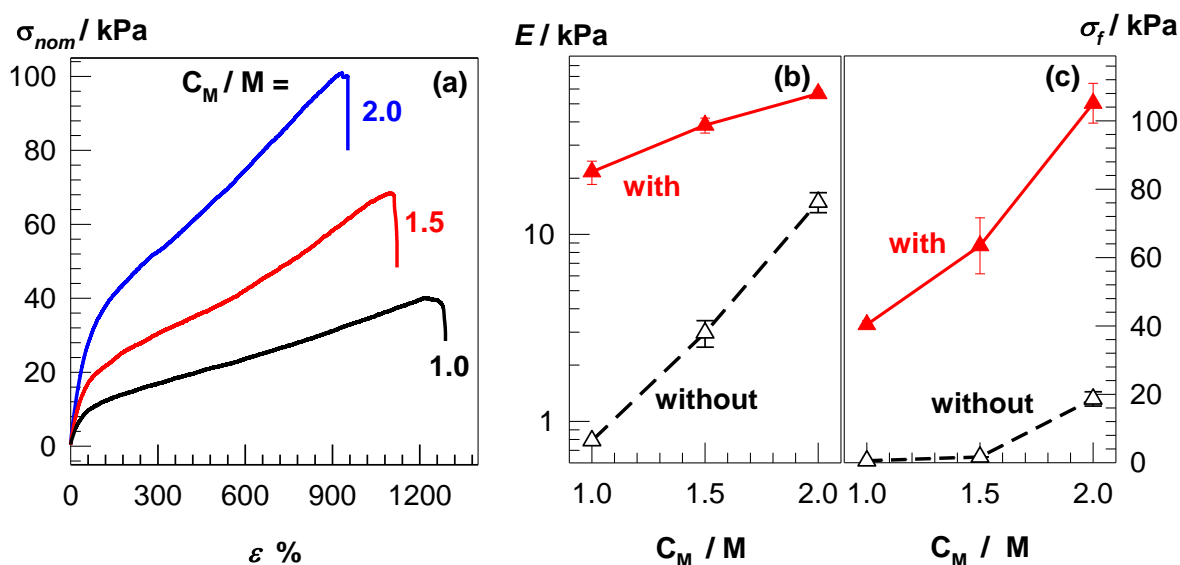
Figure 3.5.8. - (a): Tensile stress-strain curves of hydrophobically modified physical PA hydrogels in the as-prepared state formed at various monomer concentrations C_M. C18A = 2 mol%. (a), The modulus E (b), and tensile strength δ_f (c) of PA hydrogels without and with 2 mol% C18A plotted against C_M (b, c)

3.5.3. Self-healing behavior of hydrophobically modified polyampholyte hydrogels

Because hydrophobically modified PA hydrogels have poly(AMPS-co-APTAC) chains interconnected by non-covalent bonds, one may expect that they all can self-heal after damage. Cut-and heal tests indeed revealed the self-healing function of all hydrogels triggered at an elevated temperature, whereas those prepared via chemical cross-linker MBAA described in the first subsection cannot be healed. Cyclic mechanical tests are mean to understand the nature and reversibility of the intermolecular bonds in PA hydrogels. Figures 3.5.9 a, b show typical cyclic tensile stress-strain curves of a gel specimen with 20 mol.% C18A in its as-prepared and swollen states, respectively. During the tensile tests, the specimens were first stretched to 200% elongation at a fixed strain rate of 5 min^{-1} and then unloaded at the same rate to zero stress. These loading and unloading steps shown in the figures by solid and dotted curves, respectively, were repeated 4-times with waiting time between cycles of 1 min.

A negative deviation of all unloading curves from the loadings is seen in the figures reflecting the occurrence of damage in the intermolecular bonds during stretching. The hysteresis energies U_{hys} calculated from the difference between the areas under the loading and unloading curves are much larger in the as-prepared state as compared to the swollen state, and it decreases with the cycle number, as seen in figure 3.5.9 c. This reveals that a much larger number of bonds are broken in as-prepared hydrogels, which is, attributed to their weakness because of the surfactant micelles. Similar to surfactant micelles, ethanol is a good solvent for C18A segments able to solubilize their associations. Also was conducted successive cyclic tensile

tests on the hydrogel with 20 mol % C18A equilibrium swollen in ethanol (figure 3.5.10). It was found that U_{hys} significantly increases when measured from swollen ethanol hydrogels supporting this finding. The fraction of energy dissipated per loading energy f_{diss} is 40-57% and 6% for the as-prepared and swollen hydrogel, respectively, revealing that the hydrogels containing surfactant have a much effective energy dissipation mechanism as compared without surfactant. This also predicts a higher self-healing efficiency of as-prepared hydrogels as compared to their swollen states. Another feature of the hydrogels is their excellent self-recoverability in a short period after deformation. For instance, figure 3.5.9 d shows images of a gel specimen with 5 mol.% C18A during stretching to 500% deformation and just after unloading. The specimen recovers its initial length within seconds. This also highlights the good elastic behavior of the hydrogels due to the existence of dual intermolecular interactions, namely ionic interactions between AMPS and APTAC segments, and hydrophobic interactions between the polymer chains via C18A associations.

To highlight the self-healing behavior of the hydrogels, cut-and-heal tests were conducted at 50 ± 2 °C and at various healing times between $1 - 24$ h. Figure 3.5.11 a, b show stress-strain of virgin and healed hydrogels containing 5 and 20 mol.% C18A, respectively, after various healing times. The recovery of the original modulus after cut-and-heal tests was complete within 1 and 4 h for hydrogels with 5 and 20 mol.% C18A. The healing with respect to ultimate properties required longer healing times. For instance, after one day off, the healing efficiency with respect to the tensile strength is 100 and 56 ± 6% for hydrogels with 5 and 20 mol.% C18A. In figure 3.5.11 c, the modulus E and tensile strength δ_f of virgin and one-day healed hydrogels together with the healing efficiencies are shown as a function of C18A mol%. Independent on the hydrophobe content, i.e., the stiffness of the hydrogels, the healing efficiency with respect to the modulus E is complete, revealing recovery of the virgin network structure and the cross-link density. However, recovery of tensile strength δ_f continuously decreases with increasing C18A content and reduces to 40% at 25 mol.% C18A. Different healing behavior of initial and ultimate mechanical properties suggests that, although the virgin microstructure is recovered after healing, some weak points remain in the gel specimens leading to crack propagation at lower strains. It was found that these weak points locate at or in the vicinity of the cut regions of the healed hydrogels. For instance, Figures 3.5.12 a, b show images of one-day healed hydrogels with 5 and 20 mol.% C18A, respectively, during stretching up to their fracture points, were healed the blue arrows indicate cut regions. 5 mol.% C18A hydrogel sustaining up to around 1200% strain and exhibiting a complete healing efficiency fractured at any location in the middle of the gel specimens, as indicated by red circle. In contrast, the fracture of 20 mol.% C18A hydrogel occurred at the healed region, as indicated by the red arrow, revealing the existence of microcracks at the cut surfaces.
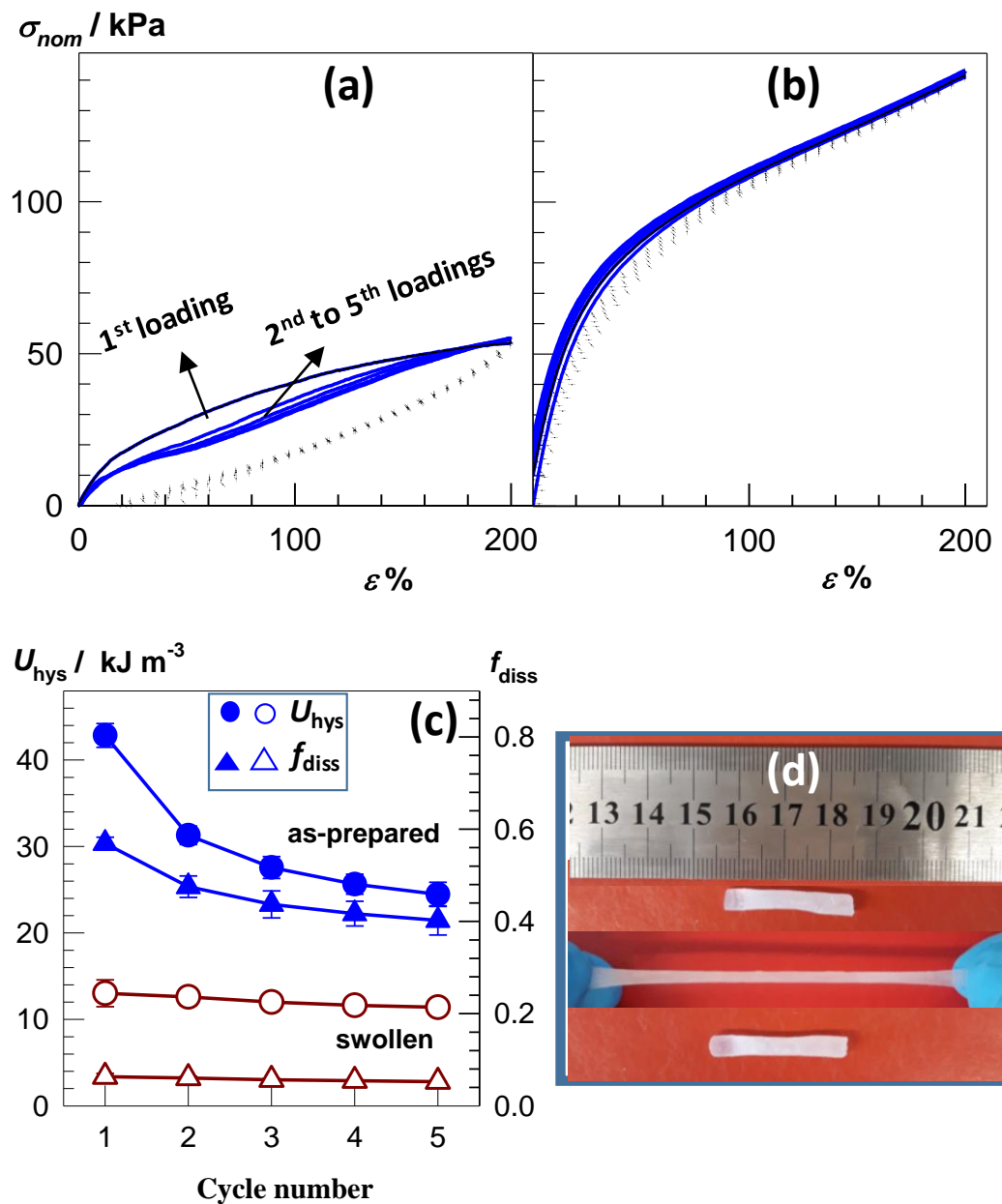
Figure 3.5.9 - Five successive cyclic tensile test results conducted on a gel specimen with 20 mol % C18A in its as-prepared (a) and swollen states (b). Solid and dotted curves, respectively, show loading and unloading steps. It is waiting time between cycles = 1 min. Hysteresis energies U_{hys} (circles), and fraction f_{diss} of dissipated energy (triangles) plotted against C18A mol%. (d): Images of a hydrogel specimen with 5 mol % C18A demonstrating its self-recoverability after stretching to 500% elongation (c)
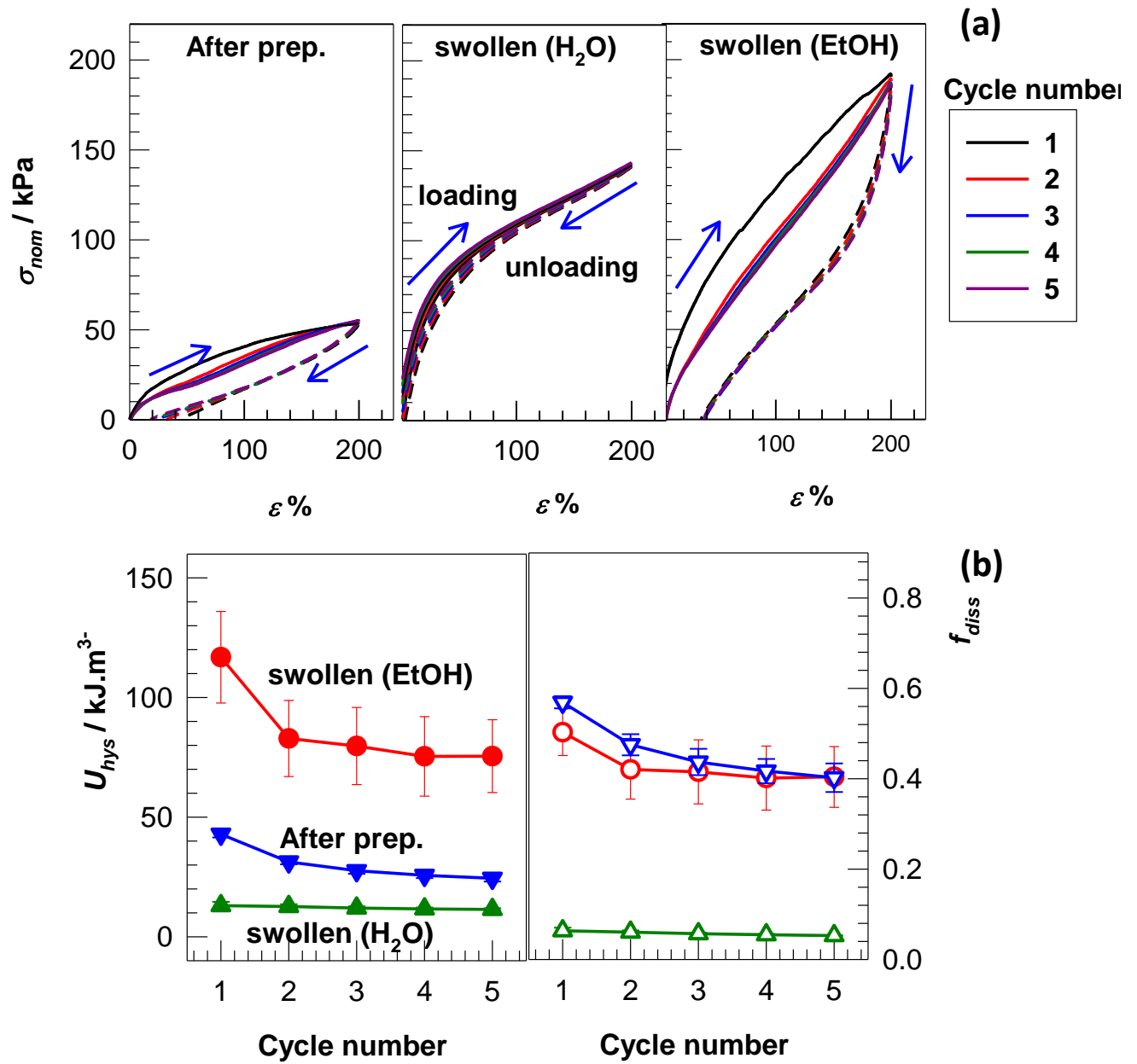
Figure 3.5.10 - (a): Five successive cyclic tensile test results conducted on a gel specimen with 20 mol.% C18A in its as-prepared, water-, and ethanol-swollen states. Solid and dotted curves, respectively, show loading and unloading steps. Waiting time between cycles = 1 min. (b): Hysteresis energies U_{hys} and fraction of dissipated energy f_{diss} plotted against the number of cycles
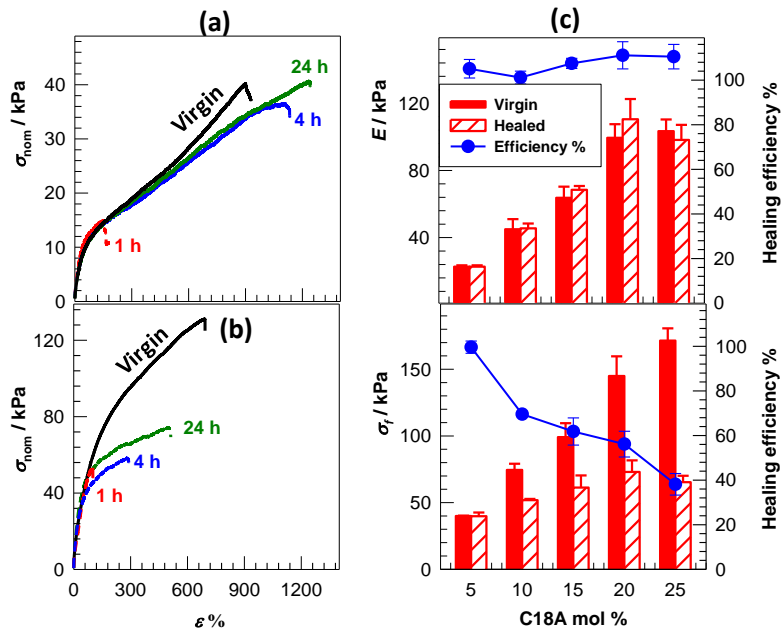
Figure 3.5.11 - Stress−strain curves of virgin and healed hydrogels with 5 (a) and 20 mol.% C18A (b) at various healing times at 50 ± 2 °C. (c): The modulus E (upper panel), and fracture stress σ_f (bottom panel) of virgin and healed hydrogels and the corresponding healing efficiencies (blue circles) plotted against C18A mol%. Healing time = 24 h
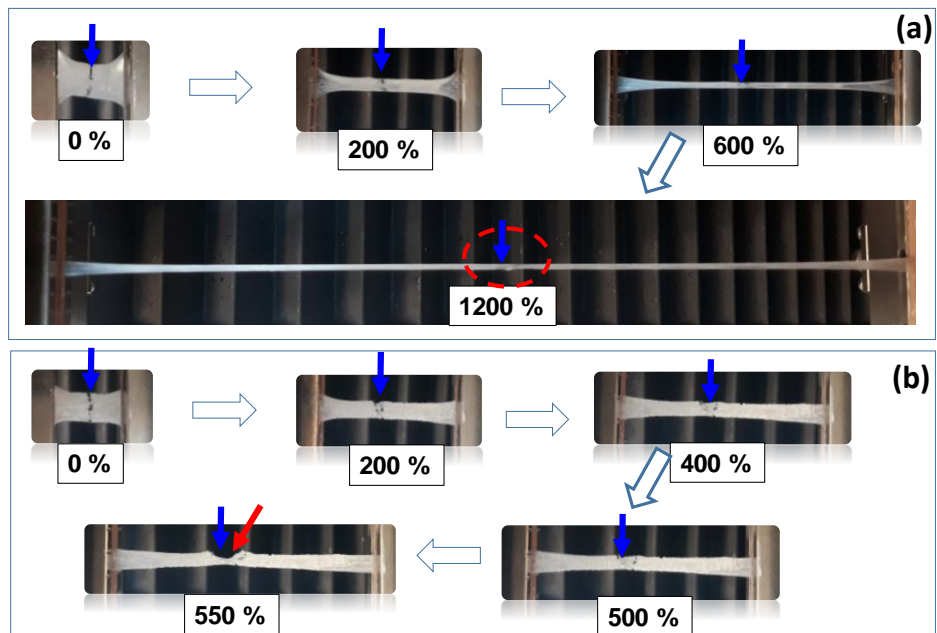
Figure 3.5.12 - Images of healed hydrogel specimens with 5 (a) and 20 mol.% C18A (b) during stretching. Healing time at 50 ± 2 °C 24 h. Healed areas, indicated by blue arrows, were colored with a dye for clarity. The locations of the fracture points are indicated by a red dashed circle, and a red arrow for (a) and (b), respectively

CONCLUSION TO CHAPTER 3.5

Polyampholytes attract interest for more than half a century due to their several interesting properties, such as their similarity to proteins, antipolyelectrolyte and isoelectric effects in aqueous solutions. Hydrophobically modified polyampholytes have found several application areas, including immobilization of metal catalysts, enhanced oil recovery, pour point depressant, wax inhibitor, cryopreservation of living cells, and drug/ gene/protein delivery. PA hydrogels also exhibit unique features such as their sensitivity against pH and salt concentration variations, low toxicity, good biocompatibility, and similarity to many biological systems, and hence, they have a variety of applications including antibacterial, anti-fouling, and saline-resistant materials. However, PA hydrogels generally exhibit poor mechanical properties such as a low modulus and tensile strength limiting their load-bearing applications. Here was presented self-healable hydrophobically modified physical PA hydrogels based on oppositely charged AMPS and APTAC monomers. PA hydrogels were prepared via micellar polymerization technique in the presence of n-octadecyl acrylate (C18A) as the hydrophobic monomer in aqueous solutions of SDS micelles. Charge-balanced PA hydrogels containing 60-90% water sustain a high tensile strength (up to 202 kPa) and exhibit a high stretchability (up to 1239%). Above 7 mol% C18A, swollen hydrogels containing around 90% water exhibit much better mechanical properties as compared to the corresponding as-prepared ones because of the stronger hydrophobic interactions in the absence of surfactant micelles. Cut-and-heal tests reveal that both as-prepared hydrogels exhibit a healing efficiency of 90 ± 10% with respect to their Young's modulus.

3.6 Hydrogenation of nitroaromatic compounds using gold nanoparticles immobilized within macroporous amphoteric cryogels

A survey of applicable literature reveals that the most studied superporous cryogels including metal nanoparticles have anionic or cationic characteristics. Superporous poly(acrylic acid), poly(4-vinylpyridine) and poly(2-acrylamido-2-methyl-1-propansulfonic acid) cryogels and their nanoparticle composites were used in hydrogen production using $NaBH_4$ hydrolysis and p-nitrophenol hydrogenation. Betaine type microgel based on poly(2-(methacryloyloxy) ethyl) dimethyl (3-sulfopropyl) ammonium hydroxide p(SBMA) was used as a template for in-situ synthesis of Ni nanoparticles and as a catalyst for hydrogenation of substrates-4-nitrophenol (4-NP),2-nitrophenol(2-NP) and 4-nitroaniline (4-NA) nitro-groups [172, 184].

The catalytic reduction of p-nitrobenzoic acid (p-NBA)[172, 184, 185] to p-aminobenzoic acid (p-ABA) has been widely described in the literature, and has been carried out in the presence of Pt / C and Pd / C, Pd and Ag nanocomposites, colloid Ag nanoparticles, cis-[Rh(CO)(2)(amine)(2)](PF6), and electrochemically. P-NBA and p-ABA derivatives are widely used as pharmaceuticals, dyes and pesticides, among others. P-ABA is the main source of anesthetics such as novocaine, butamben, procaine and risocaine, and is used as an ingredient in sunscreen formulations. Recently, magnetically recoverable gold nanorods and Fe_3O_4-C-supported palladium nanoparticles, hollow aluminosilicate microsphere and magnetic graphene oxide have been applied in the selective reduction of nitroarenes to corresponding aminoarenes.

In manufacturing, catalytic reduction of nitrogen compounds by hydrogen is usually performed at relatively high pressures (10-50 bar) and temperatures (100-150 °C), requiring the use of special and safe catalytic reactors. The literature suggested that the simple catalytic reduction of p-NP using gold nanoparticles (AuNPs) immobilized within poly(DMAEM-*co*-MAA)[173, 186] and other types of amphoteric cryogel matrixes [187-192] would also work with p-NBA.

Klivenko et al. [87, 184] demonstrated that the optimal catalytic properties of AuNPs immobilized within the macroporous polyampholyte cryogel, poly(DMAEM-*co*-MAA), which is of equimolar structure and crosslinked by 2.5 mol.% N, N-methylenebisacrylamide, was useful for flow-through catalytic studies.

In the present work, a specific composition for flow-through catalytic experiments of polyampholyte cryogels DMAEM-MAA was chosen with an equimolar structure and 2.5 mol.% N,N-methylenebisacrylamide with respect to total monomer concentration. For study of the flow-through catalytic properties, cryogels based on APTAC-AMPS were synthesized at different molar ratios, where the content of AMPS was varied between 25 and 75 mol.% in the presence of MBAA as a cross-linker and TEMED (0.25 v/v%) as a catalyst. Initial monomer concentration was fixed at 5 wt% and the cross-linking agent set at 10 mol.% with respect to monomers. Then, the mechanical properties and catalytic properties of the chosen cryogels were studied.

The main advantage of this approach is that aqueous solutions of nitroaromatic compounds passing through the macroporous heterogenic polymer matrix are

converted to final products – amino aromatic compounds, excluding the separation of key products from the catalysts.

3.6.1 Swelling and mechanical characteristics of polyampholyte cryogels

Swelling properties were calculated according to the formulas 3.6.1,3.6.2.

Firstly, equilibrium weight (q_w) and volume (q_v) swelling ratios were determined with the following equations:

$$q_w = \frac{m_{swl}}{m_{dry}} \tag{3.6.1}$$

$$q_v = (\frac{D_{swl}}{D_{dry}})^3 \tag{3.6.2}$$

where D_{dry} and D_{swl} are the diameters of the specimens in the dry and swollen states while m_{dry} and m_{swl} are the weights of the specimens in the dry and swollen states, respectively.

Figure 3.6.1 shows equilibrium weight (q_w) and volume (q_v) swelling ratios of the polyampholyte cryogels prepared at fixed initial monomer concentrations with respect to swelling time in water. As seen in figure 3.6.1, C-AMPS 50 swell less due to their composition, because of charge-balanced monomers. C-AMPS 25 and C-AMPS75 cryogels have approximately the same results.

The compression tests were performed at room temperature on a Zwick Roell machine using a 500 N load cell. Initial compressive contact to 0.05 N was applied to ensure complete contact between the sample and the surface. Load and displacement data were collected during the experiments at a constant crosshead speed of 3 mm/min. Compressive stress was presented in its nominal σ_{nom} and true values σ_{true}, which are the force per cross-sectional area of the undeformed and deformed specimens, respectively. Assuming the sample volume remains constant during deformation, the true stress σ_{true} was calculated as $\sigma_{true} = \lambda \, \sigma_{nom,}$ where λ is the deformation ratio (deformed length/original length). The compressive strain is given by the compression ratio ε which is the change in the sample length relative to its initial length, i.e., $\varepsilon = 1 - \lambda$. Figure 3.6.2 shows typical stress-strain curves of C-AMPS50 cryogels, where the σ_{nom} and σ_{true} are plotted against the strain ε.

The samples were compressed in a dry state. The green dashed lines indicate calculations of the compressive ε_c and fracture strain ε_f, while black dashed lines show fracture σ_f and compressive σ_c strain from the maximum and beginning of plateau in σ_{true} - λ plot, respectively

Figure 3.6.3 a and b show corrected strain-stress curves of polyampholyte cryogels, prepared with various amounts of AMPS, in the initial and swollen states. As seen in these graphs, the highest values of Young's modulus E and fracture stress σ_f are seen in the C-AMPS-50 sample. C-AMPS-75 and C-AMPS-25 showed lower mechanical characteristics. Charge-balanced cryogels have both good electrostatic interaction and hydrogen bonding, which improve all mechanical properties. The

compressive modulus E, compressive σ_{comp} and fracture stress σ_f of dry cryogels are shown in table 3.6.1.
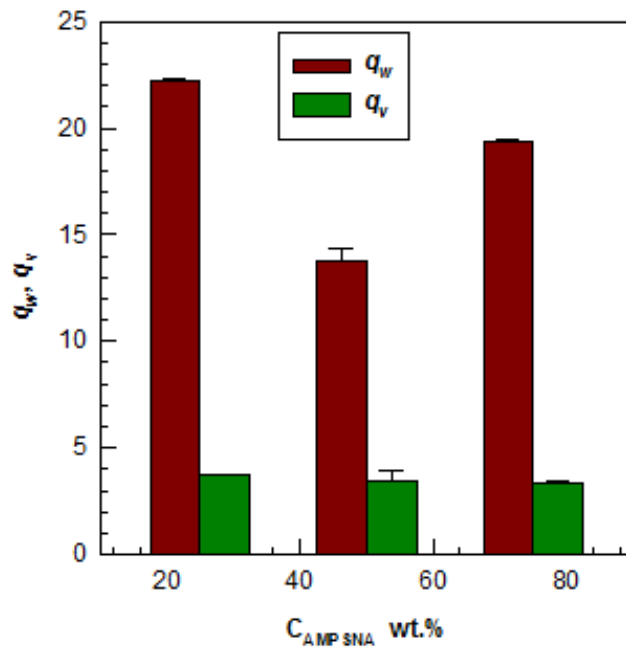
Figure 3.6.1 - The weight q_w and volume swelling ratios $q_{\bar{v}}$ of cryogels plotted against AMPS composition
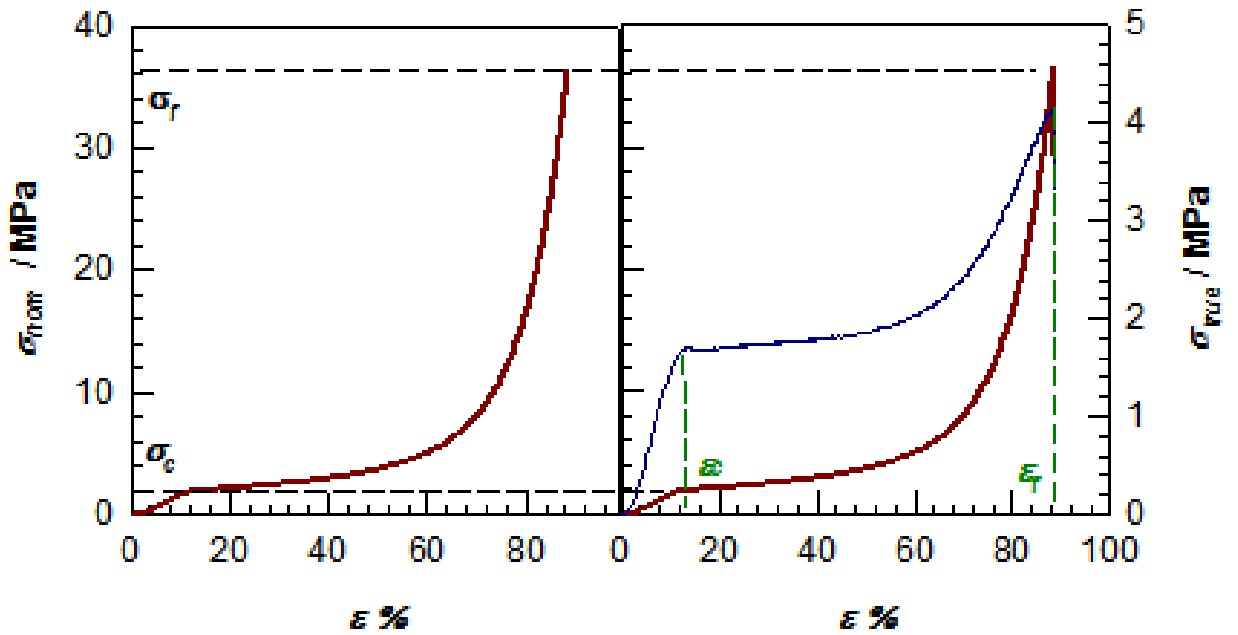
Figure 3.6.2 - Typical stress-strain curves of cryogel samples, where the nominal stress σ_{nom} and true stress σ_{true} are plotted against the compressive strain ε. $R = 3$ mm/min.
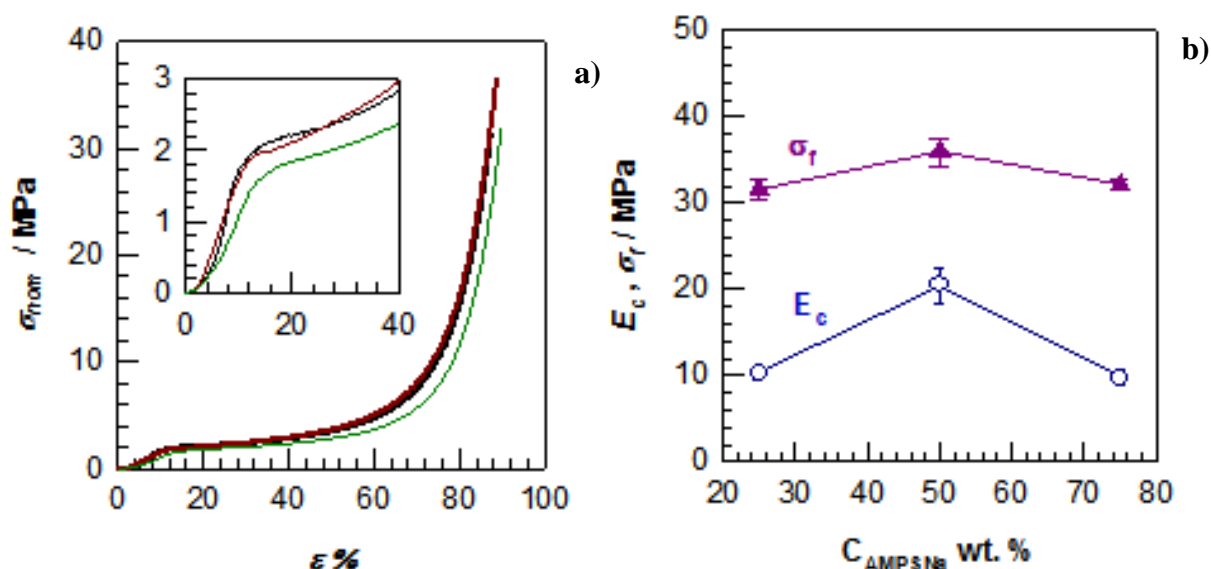
Figure 3.6.3 - a) Stress-strain curves of cryogel samples (C-AMPS25: black, C-AMPS50: red, C-AMPS 75:green lines) where the nominal stress δ_{nom} is plotted against the compressive strain ε. R= 3 mm/min. b) The compressive modulus E and fracture stress σ_f of dry cryogels are plotted against the amount of AMPS.

Table 3.6.1. Compressive modulus E, compressive $\sigma_{comp,}$ and fracture stress σ_f of dry cryogels.

Code	E / MPa	σ_f / MPa	$\lambda*$	σ_{comp*}	λ_{comp*}
C-AMPS25	10.33 ±0.50	31.55 ± 1.14	0.12	1.80	0.89
C-AMPS50	20.44± 2.13	35.92 ± 1.56	0.11	1.83	0.88
C-AMPS75	9.75± 0.86	32.13 ± 0.58	0.10	1.61	0.86
*Standart deviations are less than 10%.					

As a result, C-AMPS 50 was chosen as the best composition for the flow-through catalytic experiments using polyampholyte cryogels based on APTAC-AMPS.

3.6.2 Morphology of DMAEM-MAA, AMPS-APTAC cryogels, and AuNPs immobilized macroporous cryogels

According to SEM images, the average pore size of DMAEM-MAA and AMPS-APTAC samples is varied from 40 to 80 μm. The structure of AuNPs immobilized within macroporous amphoteric cryogel represents the myriads of gold nanoparticles distributed in both surface and inner parts of macropores. Most of them are triangular, although the hexagonal, spherical and rod-like species are observed (figures 3.6.5 and 3.6.6). The bigger sizes of AuNPs triangles immobilized within DMAEM-MAA cryogels are varied from 3 to 10 μm. For APTAC-AMPS cryogels are varied from 1to 5 μm. The photo of cryogels before and after immobilizing of gold nanoparticles (AuNPs) into the matrix of cryogels have shown in figure 3.6.4.
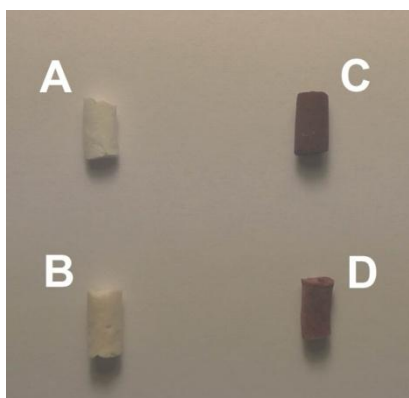
Figure 3.6.4 - Images of cryogels :A-poly(MAA-DMAEM) cryogel, B-poly(APTAC-AMPS) cryogel, C-AuNPs/poly(MAA-DMAEM) catalyst, D-AuNPs/poly(APTAC-AMPS) catalyst [172]
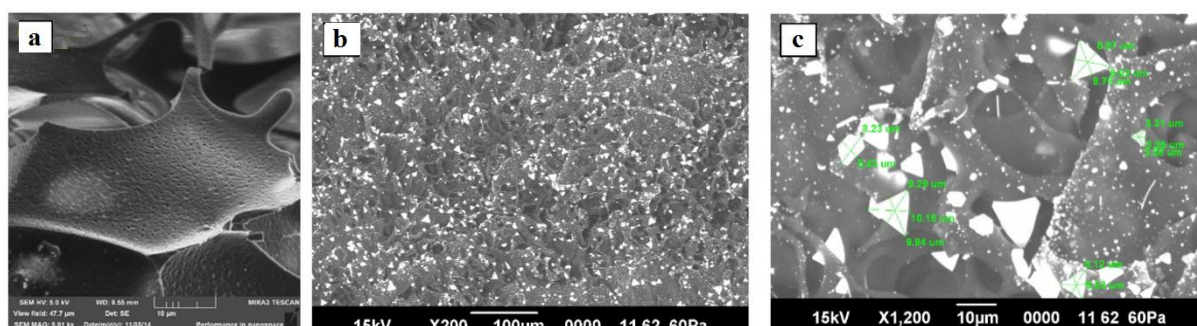
Figure 3.6.5 - Morphology of pristine (a) and AuNPs immobilized macroporous amphoteric DMAEM-MAA cryogel (b,c) [172]
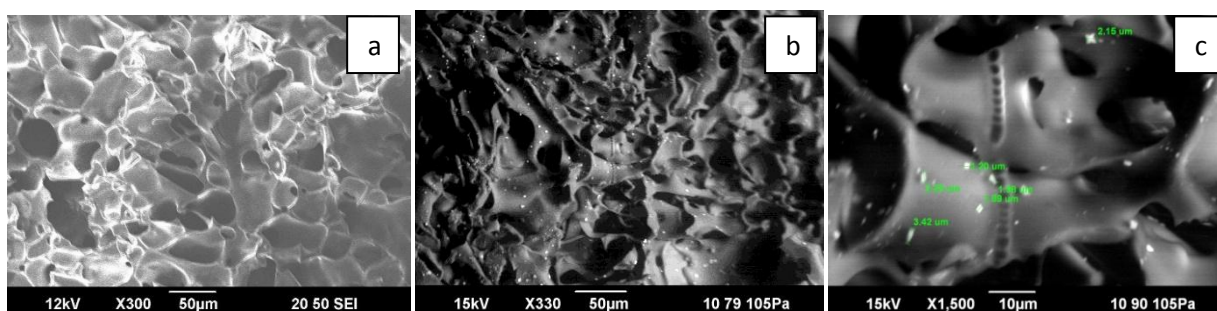
Figure 3.6.6 - Morphology of pristine (a) and AuNPs immobilized macroporous polyampholyte APTAC-AMPS cryogel (b,c)

3.6.3 Catalytic activity of AuNPs immobilized into cryogel pores in the hydrogenation of *p*-NBA

The advantage of the reduction of *p*-NBA to *p*-ABA by $NaBH_4$ catalyst over its analogs is its durability. The catalyst does not lose activity for even 50 catalytic cycles, while the conversion of 4-NBA on other catalysts begins to decrease after 5 cycles.

The reduction of *p*-NP to *p*-AP by [3, 49, 184, 185, 193-197] $NaBH_4$ as a

model reaction is easily monitored by measurement of the absorption spectra of substrate and reaction product at 400 and 300 nm, respectively [172]. The reaction of The reduction of *p*-NBA to *p*-ABA by NaBH$_4$ and progress analysis by UV-spectrometry have shown in figures 3.6.7 and 3.6.8, respectively.
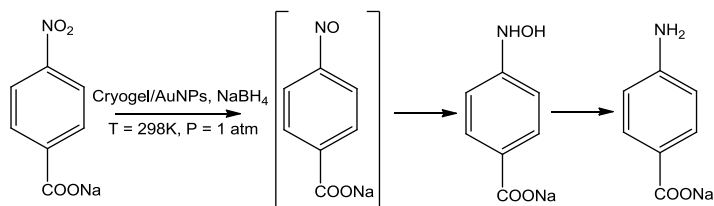
Figure 3. 6.7 - The model reaction of the reduction of *p*-NBA to *p*-ABA by NaBH$_4$ [172]
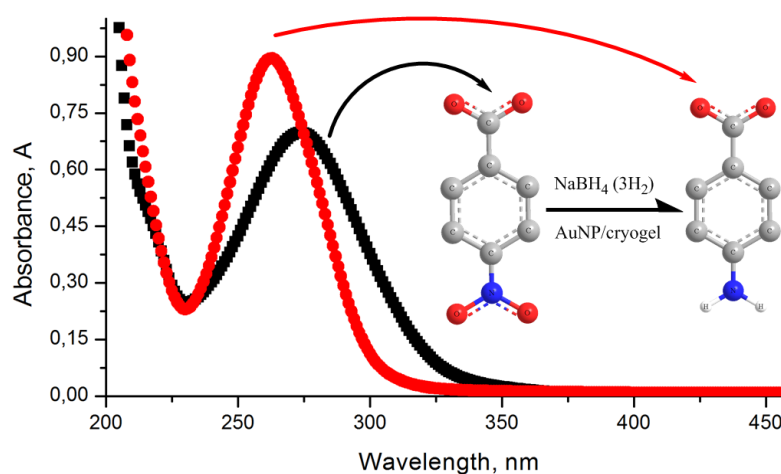
Figure 3.6.8 - Reaction progress analysis by UV-spectroscopy

The equation expresses the kinetics of p-NBA reduction:

$$\ln \frac{A_t}{A_0} = \ln \frac{C_t}{C_0} = -kt \qquad (3.6.3)$$

where A$_t$ and A$_0$ are absorbance of nitrophenolate-anions corresponding to concentrations of nitrophenolate-anions C$_t$ and C$_0$ at definite time t and t = 0.

The conversion of *p*- *p*-NBA to *p*-ABA was calculated by equation :

$$Conversion \ (\%) = \frac{C_0 - C_t}{C_0} \times 100 \qquad (3.6.4)$$

where C_0 is the initial concentration of *p*-NP, C_t is the concentration of *p*-NP at definite time *t*.

The lifetime of the catalyst is usually expressed through the turnover number (TON) that is the number of moles of the substrate that a mole of the catalyst can convert before inactivation [33]. The stability of AuNPs/poly(DMAEM-*co*-MAA) catalyst, the so-called TON that is defined as

$$TON = \frac{[p-NP]}{[AuNPs]} * OCT \qquad (3.6.5)$$

where [*p*-NP] and [AuNPs] are the molar concentrations of substrate and catalyst, OCT is the overall catalytic time) and the turnover frequency (TOF) calculated (for the first cycle) according to the equation

$$TOF = \frac{[p-NP] \times [conversation]}{[AuNPs] \times t} \qquad (3.6.6)$$

The activation energy and thermodynamic parameters of *p*-NP reduction by NaBH$_4$ were calculated according to the Arrhenius and Eyring equations from the

$$LnK \; vs. \; 1/T \qquad (3.6.7)$$

$$and \; Ln \, (K/T) \; vs. \; 1/T \qquad (3.6.8)$$

where K – the constant reaction rate, T – the temperature of the reaction.

3.6.3.1 Catalytic activity of AuNPs immobilized into poly(DMAEM-*co*-MAA cryogel pores in the hydrogenation of *p*-NBA

Absorption spectra of *p*-NBA and *p*-ABA mixtures at various volume ratios have shown in figure 3.6.9.

In the course of *p*-NBA hydrogenation, the adsorption peak at 274 nm that belongs to *p*-NBA gradually increases and shifts to 264 nm that is characteristic for adsorption of *p*-ABA. The time-dependent conversion of *p*-NBA to *p*-ABA was calculated from the 1st to 5th cycles. The average reduction degree of *p*-NBA during 18-21 min is 58% (figure 3.6.9) [3].

It should be noted that starting from the 6th cycle of *p*-NBA hydrogenation, an additional two absorption peaks at 285 nm and 311 nm are observed (figure 3.6.9 b). The intensity of these peaks does not change up to the 12th cycle. The appearance of two peaks is connected with formation of *p,p'*-azodibenzoate due to catalytic coupling condensation of nitroso compound with hydroxylamine with participation of hydrogen atoms that are generated from sodium borohydride through formation of azoxy compound which is reduced in a series of consecutive steps to the azocompound (figure 3.6.10) [3].
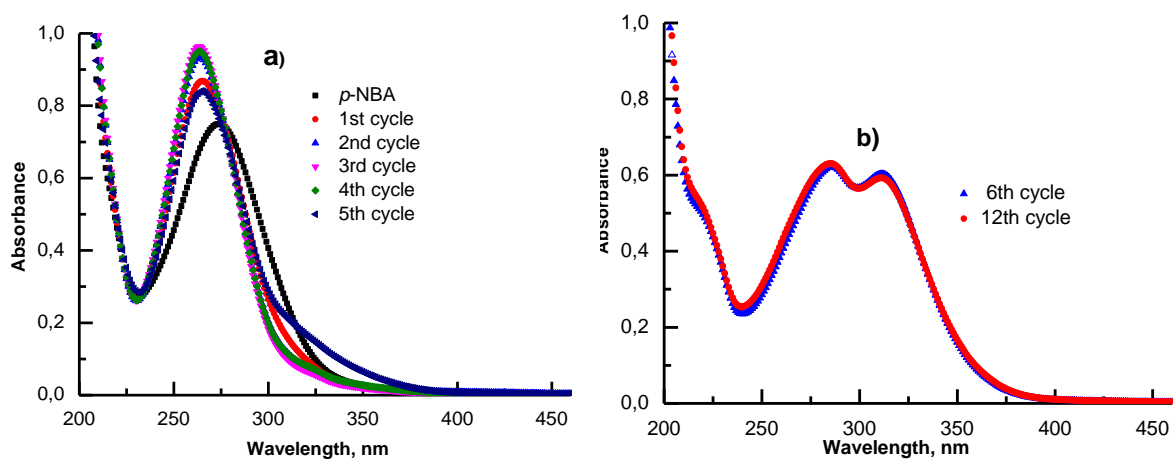
Figure 3.6.9 - Absorption spectra of *p*-NBA hydrogenated from the 1st to 5th cycles. (b) Absorption spectra of *p*-NBA hydrogenated from the 6th to 12th cycles. Molar ratio of [*p*-NBA]:[NaBH$_4$] = 1:200. [*p*-NBA] = 5·10^{-5} mol/L. [NaBH$_4$] = 1·10^{-2} mol/L. T = 298K [3]
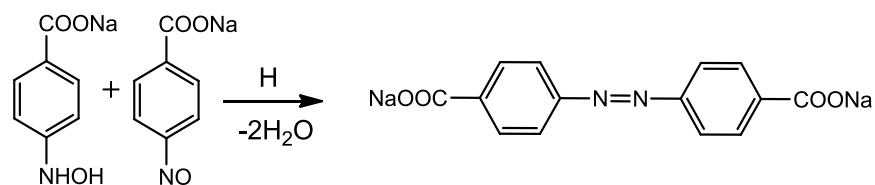
Figure 3.6.10 - Possible mechanism of formation of *p,p'*-azodibenzoate [3]

The formation of *p,p'*-azodibenzoate is confirmed by Raman spectroscopy. Spectra were registered on NTEGRA Spectra spectrometer (NT-MDT), using 473 nm excitation.(figure 3.6.11, table 3.6.2).
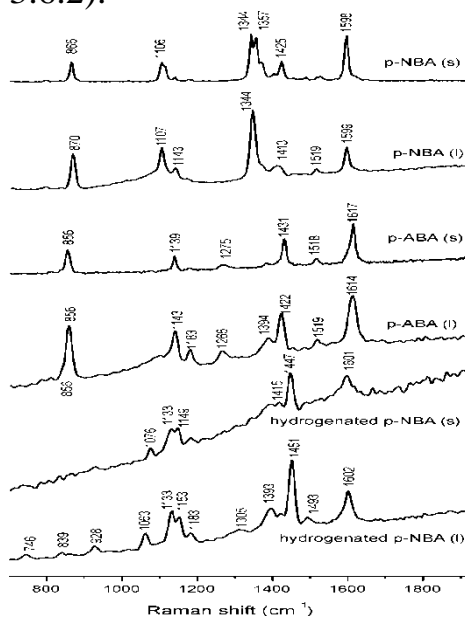
Figure 3.6.11 - Comparison of Raman spectra of *p*-NBA, *p*-ABA and hydrogenated product of *p*-NBA in solid-state and aqueous solution (where s is solid, l is liquid) [3]

111

Table 3.6.2 - Raman spectra of *p*-NBA, *p*-ABA, and hydrogenated products of *p*-NBA

p-NBA, cm^{-1}		*p*-ABA, cm^{-1}		Hydrogenated product of *p*-NBA, cm^{-1}		Band assignments* and Refs
Solid	Aqueous solution	Solid	Aqueous solution	Solid	Aqueous solution	
866 s	870 s					NO_2 bending
		856 s	860 s		839 vw	COO$^-$ bending
				1076 w	1063 m	Peaks can be assigned to *p*-ABA adsorbed on the surface of AuNPs
1106 s	1107 s					C-NO_2 stretches coupled with C-H in-plane bending
				1133 m	1133 s	Peaks can be assigned to *p,p'*-azodibenzoate
1143 vw	1143 w	1139 m	1143 s			C-CO_2 stretches coupled with C-H in-plane bending
				1149 m	1153 m	Peaks can be assigned to *p,p'*-azodibenzoate
			1183 w		1183 w	C–N stretching coupled with C–H in-plane bending
		1275 w	1266 w		1276 w	C-N stretching
1344 vs	1344 vs					NO_2 symmetric stretching
1357 vs						Symmetric stretches of the carboxylate groups
			1394 w			COO$^-$ symmetric stretching
				1394 vw	1393 w	N=N stretching coupled with C–C stretching
1425 s	1413 w	1431 s	1422 s			Can be ascribed to photo-induced reduction products of PNBA
				1447 vs	1451 vs	N=N stretching coupled with C–C stretching
		1518 w	1519 w			in-plane benzene ring stretching vibrations
1598 vs	1599 s					C-C stretching of benzene
				1601 s	1602 s	or C–C stretching in two benzene rings
		1617 vs	1614 s			NH_2 bending
* Identification of Raman spectra is based on literature data [3, 193, 195, 198-207]. Notes: s-strong; m-medium; w-weak; vs-very strong; vw-very weak.						

Surface-enhanced Raman scattering (SERS) is an effective tool to detect, at trace level, the reactants, products, or by-products in reactions that take place on the surface of the metal nanoparticles. The formation of azodibenzoate from *p*-NBA adsorbed on Ag nanoparticles or films were observed by SERS and evidenced by the appearance of a strong band near 1460 cm^{-1} and a strong doublet near 1150 cm^{-1}.

Later on this statement was confirmed by authors Liang et al. [3, 134, 147, 208-210] using the SERS experiments. Raman spectra of hydrogenated p-NBA contain mostly the characteristic bands of p-ABA. However, additional bands at 1133, 1149, 1447 cm^{-1} in powder, and at 1133, 1153, 1451 cm^{-1} in aqueous solution have appeared in the hydrogenated product of p-NBA. They may belong to –N=N– groups of p,p'-azodibenzoate. A. Gainar and co. [211, 212] compared the catalytic activity of mono- and bimetallic nanoparticles composed of pure Ag and Ag/Pd (96:4 mol/mol) colloids and the SERS spectra of p-NBA. In pure Ag colloid, only bands attributable to the carboxylate anion of p-NBA are seen, while in Ag/Pd colloid after 1 day, the SERS bands that belong to the p,p'-azodibenzoate anion are detected (figure 3.6.12) [3, 6, 10, 128, 198, 213, 214].
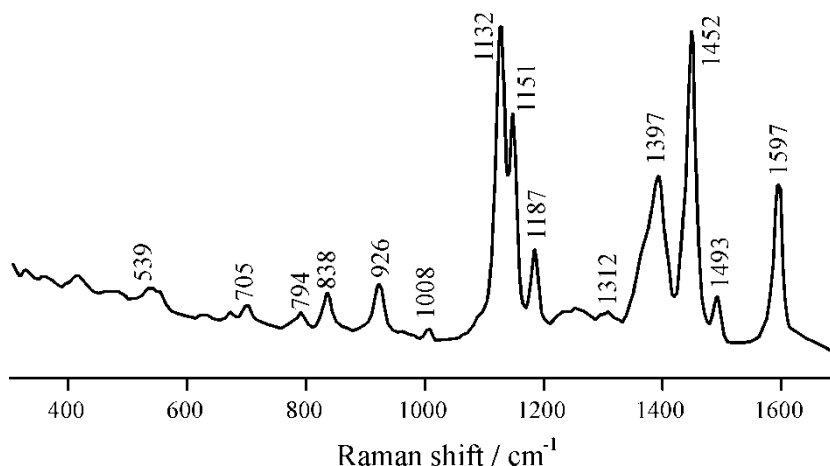
Figure 3.6.12 - SERS spectrum of p-NBA in the presence of Ag/Pd colloid obtained after 1 day. The excitation wavelength is 514.5 nm[3, 6, 10, 128, 198, 213, 214].

Comparison of Raman spectrum of the hydrogenated product of p-NBA over DMAEM-co-MAA/AuNPs catalyst (as powder and aqueous solution) and SERS spectrum of p-NBA over Ag/Pd colloids (figure 3.6.12) shows that the characteristic bands of functional groups in both cases are the same, and they belong to p,p'-azodibenzoate. Only one difference is the appearance of additional bands at 1063 and 1076 cm^{-1} in Raman spectra of the hydrogenated product of p-NBA over DMAEM-co-MAA/AuNPs catalyst. These bands can be can be assigned to p-ABA adsorbed on the surface of AuNPs. Thus, intensive Raman bands at 1133, 1149, 1153, 1447 and 1451 cm^{-1} that exist in the hydrogenated products of p-NBA can be used for the identification of reaction products and prediction of reaction mechanisms [3].

The ^{1}H NMR spectra of p-NBA, p-ABA, and hydrogenated products of p-NBA are compared in figure 3.6.13. The ^{1}H NMR spectra of p-ABA contain the doublets at $\delta = 6.65$ and 7.55 ppm that belong to H^{2,6} and H^{3,5} protons of the aromatic ring. However, NH$_2$ groups in p-ABA are not seen in ^{1}H NMR spectra due to the easy replacement of amine protons to deuterium. The ^{1}H NMR spectra of p-NBA consist of doublets at $\delta = 7.75$ and 7.87 ppm that belong to H^{2,6} and H^{3,5} protons of the aromatic ring. In the hydrogenated product of p-NBA together with doublets at $\delta =$

6.65 and 7.55 ppm, a new intensive signal at δ = 8.28 ppm appears. It can be related to NH groups of amide bonds due to the condensation of terminal NH_2 and COONa groups of p-ABA (figure 3.6.14). According to Lili , a peak around δ = 8.31 ppm is attributed to NH groups[3].
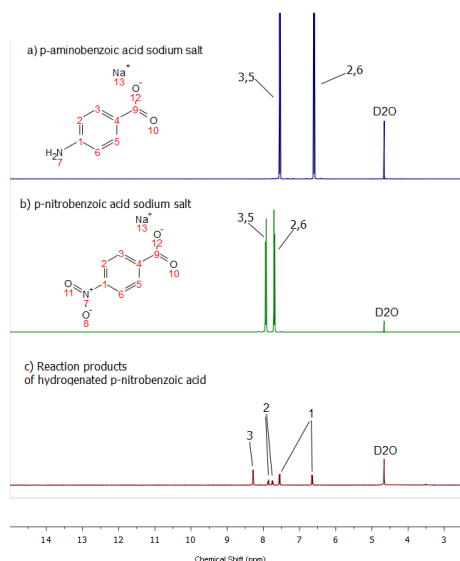
Figure 3.6.13 - Comparison of ^{1}H NMR spectra of p-ABA (a), p-NBA (b), and hydrogenated product of p-NBA (c) in D_2O. The signals of reaction products are related to benzene rings of p-ABA (1) and p-NBA (2), respectively. The signal at δ = 8.28 ppm can be referred to NH groups of sodium 4-(4-aminobenzamido)benzoate (3) [3]
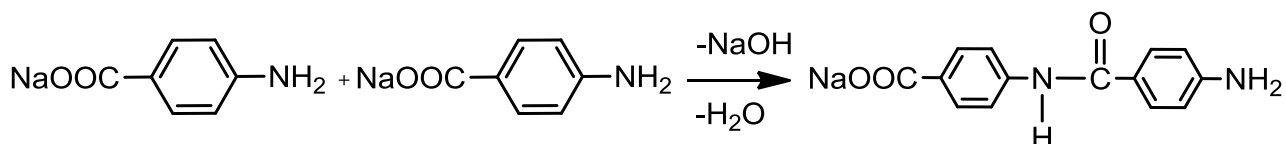
Figure 3.6.14 - Proposed mechanism of formation of sodium 4-(4-aminobenzamido)benzoate

Verneker and co-workers performed a direct condensation polymerization of N-alkylated p-ABA, containing methyl, propyl, butyl, pentyl, heptyl, octyl, and heptadecyl substituents, to obtain N-alkylated poly(p-benzamide) using hexachloroethane, triphenylphosphine, and pyridine as condensation reagents (figure 3.6.15) [3].
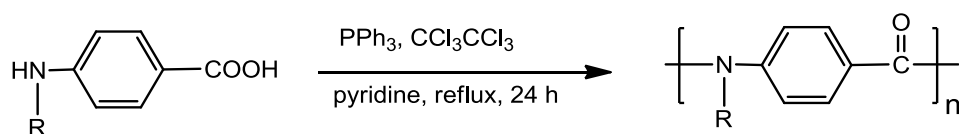
Figure 3.6.15 - Condensation polymerization of N-alkylated *p*-aminobenzoic acid. R is H or alkyl groups.

Analysis of integral peaks of ^{1}H NMR spectra of *p*-NBA and *p*-ABA reveals that approximately 62.6% of *p*-NBA is converted to *p*-ABA (figure 3.6.16).
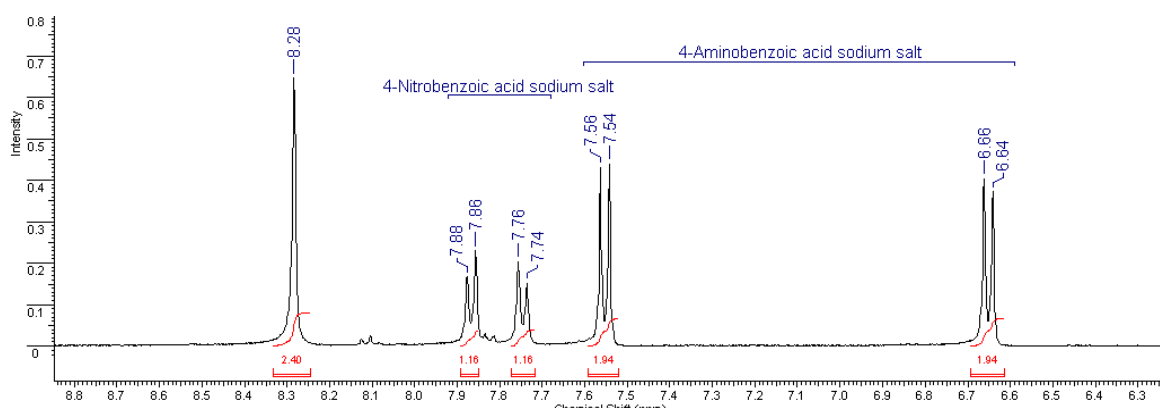
Figure 3.6.16 - Scaled ^{1}H NMR spectra of hydrogenated *p*-NBA over DMAEM-*co*-MAA/AuNPs catalyst [3]

To confirm the condensation of *p*-ABA and formation of sodium 4-(4-aminobenzamido)benzoate, we have run 10 times an aqueous solution of pure *p*-ABA through DMAEM-*co*-MAA/AuNPs. As seen from ^{1}H NMR spectra, in addition to $H^{2.6}$ and $H^{3.5}$ protons of an aromatic ring the intensive signal at $\delta = 8.28$ ppm appears that is specific for NH groups (figure 3.6.17) [3].
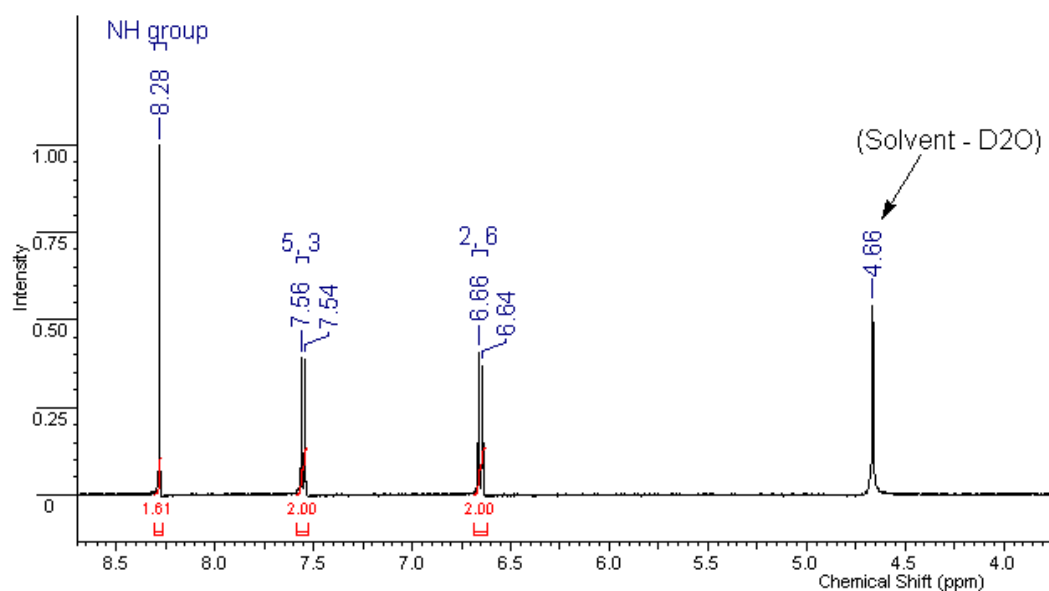
Figure 3.6.17 - ^{1}H NMR spectra of pure *p*-ABA passed 5-10 times through DMAEM-*co*-MAA/AuNPs [3]

From the results of figure 3.6.13, the content of NH groups was calculated. It was found that the amount of NH groups is 44.6%, meaning that such amount of p-ABA is converted to sodium 4-(4-aminobenzamido)benzoate.

The reduction rate kinetics was treated as a pseudo-first-order in p-NBA concentration. The absorbance A_t at time t divided by the absorbance A_0 measured at $t = 0$ gives the corresponding concentration ratios C/C_0 of p-NBA. Thus we get the following equation:

$$\frac{dC_t}{dt} = -k_{\mathrm{app}}t \text{ or } \ln\frac{C_0}{C_t} = \ln\frac{A_0}{A_t} = -k_{\mathrm{app}}t, \qquad (3.6.9)$$

where C_t is the concentration of p-NBA at time t, and k_{app} is the apparent rate constant.

Based on the linear plots of $\ln(C/C_0)$ versus t, the values of the apparent rate constant k_{app} at different temperatures were calculated. The apparent constants of p-NBA reduction at temperature intervals from 25 to 55 °C are in the range of 0.030 min^{-1} and 0.051 min^{-1}. The activation energy calculated from the Arrhenius equation is equal to 13.80 kJ/mol.Proposed mechanism of p-NBA hydrogenation over DMAEM-co-MAA/AuNPs [3].

The proposed mechanism of p-NBA reduction is based on literature data [3, 195, 199-202]. According to the literature survey, the reduction of p-NBA as the heterogeneous catalytic reaction takes place on the surface of AuNPs adsorbed on the cryogel surface. At first, the p-NBA is fixed on the surface of amphoteric cryogel via electrostatic attraction between tertiary amine groups of cryogel matrix and nitrocarboxyalate ions of p-NBA. Three different routes of p-NBA conversion are proposed. In all cases, the immobilized AuNPs in cryogel pores generates hydrogen atoms from the NaBH$_4$ that, in turn, hydrogenate the nitro groups and participate in the formation of intermediate nitroso and hydroxylamine compounds.

According to the first route, the AuNPs react with NaBH$_4$ and form the metal hydride on the surface of AuNPs (step 1). In step 2, the formation of a nitroso compound is accompanied by the elimination of water molecules. In step 3, the nitroso compound is converted to hydroxylamine. In steps 4-6, the hydroxylamine is reduced to the amine (figure 3.6.18 a).

The proposed mechanism of formation of p,p'-azodibenzoate on DMAEM-co-MAA/AuNPs is in good agreement with the reaction route for photoreduction of p-NBA on nanostructured silver through photoinduced surface catalytic coupling reactions suggested by authors [3].

Finally, in the frame of the third route, the aminocarboxylate ions fixed on the surface of cryogel matrix undergoes the further conversion to form sodium 4-(4-aminobenzamido)benzoate according to figure 3.6.18 c.

Thus the preparation protocol of amphoteric cryogel based catalyst is very simple, and the catalytic reduction of nitroaromatic compounds with the help of a flow-through catalytic reactor is green and cost-effective exhibiting a great potential for practical application.
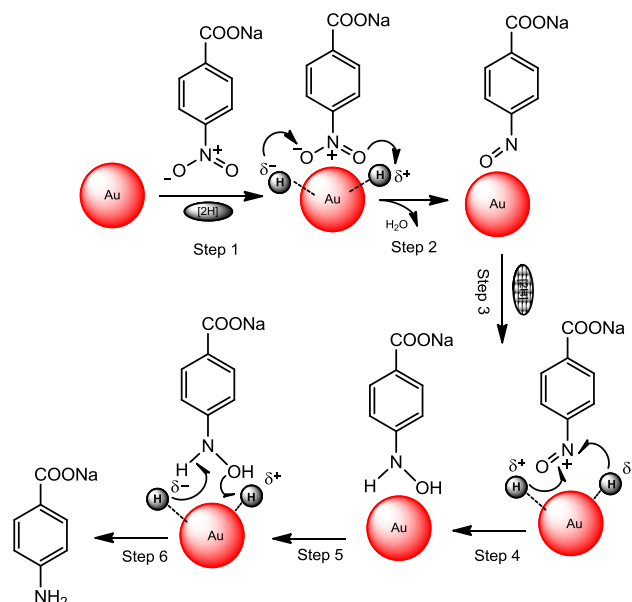
Figure 3.6.18 - a- The proposed mechanism of hydrogenation of *p*-NBA to *p*-ABA [3]

According to the second route, the condensation of the nitroso compound with hydroxylamine produces the azoxy compound (Step i). It is reduced in a series of consecutive steps (Steps ii and iii) to the azo groups (figure 3.6.18 b).
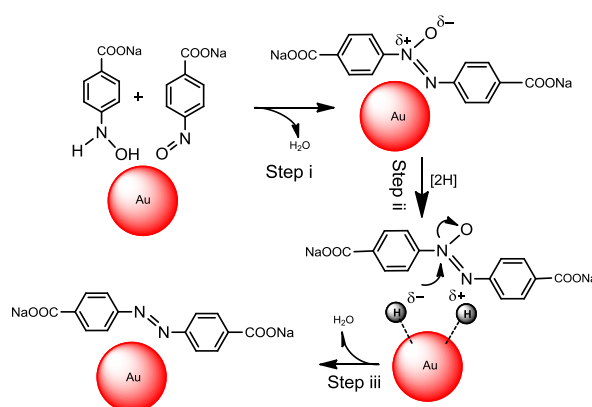
Figure 3.6.18 - b - The proposed mechanism of formation of *p,p'*-azodibenzoate [3]
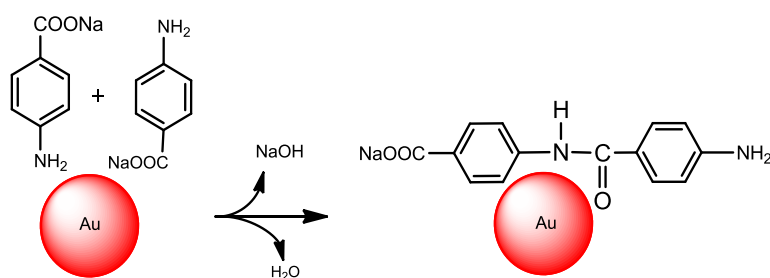
Figure 3.6.18 - c- The proposed mechanism of formation of sodium 4-(4-aminobenzamido) benzoate [3].

Figures 3.6.19 showed absorption spectra for poly(APTAC-co-AMPS) of p-NBA and p-ABA mixtures at various volume ratios. From the 3rd cycle of p-NBA hydrogenation, two additional peaks of 285 nm and 311 nm are observed (Figure 3.6.19 b). The presence of two peaks is related to the formation of p, p'-azodibenzoate due to catalytic coupling condensation of nitroso compound with hydroxylamine with the involvement of hydrogen atoms produced from sodium borohydride by the formation of azoxy compound which is reduced to azocompound in a series of consecutive steps.
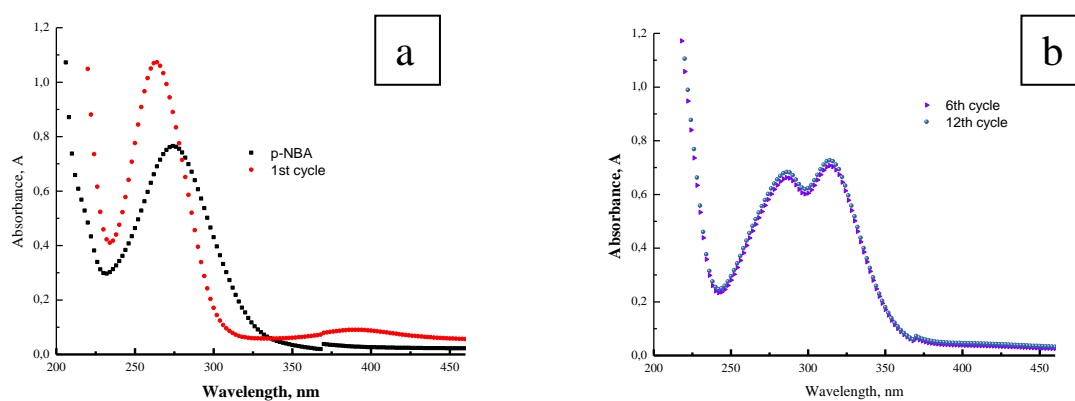
Figure 3.6.19 - Absorption spectra of *p*-NBA and *p*-ABA mixtures at various volume ratios. Curve A is an adsorption peak of pure *p*-ABA, curve K is the adsorption peak of pure *p*-NBA. [P-NBA:NaBH$_4$] [5×10^{-4} M:0.05M] in 25 °C

In the course of *p*-NBA hydrogenation, the adsorption peak at 274 nm that belongs to *p*-NBA gradually increases and shifts to 264 nm that is characteristic for adsorption of *p*-ABA. The time-dependent conversion of *p*-NBA to *p*-ABA was calculated from the 1st to 2nd cycles. The average reduction degree of *p*-NBA during 18-21 min is 89.01% Rate constants (K) lie (or fall) is 0.058 min^{-1} at 25 °C.

As have seen from table 3.6.3 according to dependence cryogel type on rate constants the better catalytic properties poly(APTAC-*co*-AMPS) with conversation 89.01% than poly(MAA-*co*-DMAEM) with conversation 76.31%.

Table 3.6.3 - Comparison of the effectiveness of cryogel carriers

Cryogel support	poly(APTAC-co-AMPS)	poly(MAA-co-DMAEM)
K$_{app}$, min^{-1}	0.058	0.128
Conversion, %	89.01	58

CONCLUSION TO CHAPTER 3.6

The AuNPs were immobilized within the cryogel matrix of poly(DMAEM-*co*-MAA) and poly (APTAC-*co*-AMPS) by boiling $HAuCl_4$ solution in the presence of cryogel samples. Both the outer surface and matrix of the cryogels are mostly covered by triangular, hexagonal and spherical AuNPs of different sizes. $NaBH_4$, run through amphoteric cryogel containing AuNPs, leads to an additional reduction of Au^{3+} to Au^0 and a reduction of *p*-NBA to *p*-ABA. The average size of AuNPs accumulated on both the surface and in the longitudinal parts of the cryogel was less than 100 nm.

According to UV-Vis and ^{1}H NMR data, approximately 58-62.6% of *p*-NBA is converted to *p*-ABA at a level of activation energy for poly(DMAEM-*co*-MAA) is equal to 13.80 kJ/mol for poly(APTAC-*co*-AMPS) 35.48 kJ/mol. The cryogel catalyst AuNPs/poly(DMAEM-*co*-MAA) and poly (APTAC-*co*-AMPS) shows highly catalytic activity in the hydrogenation of *p*-NBA, and sustains 12 cyclic conversions of the substrate in the range of 75-90% at 25°C.

Moreover, partial leaching of AuNPs was observed in the course of the reduction of sequential portions of the substrate. In the reduction of *4*-NBA, the values of TON and TOF of cryogel catalysts were equal to 38.17 and 21.56 h^{-1}, respectively.

In the case of DMAEM-co-MAA/AuNPs, starting from the 6th cycle of *p*-NBA hydrogenation, an additional two absorption peaks at 285 nm and 315 nm are observed. The appearance the additional two absorption peaks seems to be connected with the formation of *p,p'*-azodibenzoate. Another by-product of *p*-NBA hydrogenation is sodium 4-(4-aminobenzamido)benzoate, due to the condensation of amine and carboxylic groups of *p*-ABA molecules. The proposed mechanism of formation of *p,p'*-azodibenzoate, and 4-(4-aminobenzamido)benzoate is confirmed by Raman spectroscopy and ^{1}H NMR. Amphoteric cryogel samples with immobilized AuNPs are shown to be effective flow-through units for continuous hydrogenation of *p*-NBA. The results obtained may provide a new strategy for the syntheses of amino compounds, azo dyes, or benzamides from aromatic nitro compounds on gold nanoparticles immobilized within a cryogel matrix.

REFERENCES

1. Kudaibergenov S. E. Polyampholytes Synthesis, Characterization and Application. – New York: Kluwer Academic/Plenum Publishers, 2002. – 212 p.

2. Dobrynin A. V., Colby R. H., Rubinstein M. Polyampholytes // Journal of Polymer Science Part B-Polymer Physics. – 2004. – Т. 42, № 19. – C. 3513-3538.

3. Kudaibergenov S., Dauletbekova M., Toleutay G., Kabdrakhmanova S., Seilkhanov T., Abdullin K. Hydrogenation of p-Nitrobenzoic Acid by Gold and Palladium Nanoparticles Immobilized Within Macroporous Amphoteric Cryogels in Aqueous Solution // Journal of Inorganic and Organometallic Polymers and Materials. – 2018. – Т. 28, № 6. – P. 2427-2438.

4. Toleutay G., Dauletbekova M., Shakhvorostov A., Kudaibergenov S. Quenched Polyampholyte Hydrogels Based on (3-Acrylamidopropyl)trimethyl Ammonium Chloride and Sodium Salt of 2-Acrylamido-2-methyl-1-Propanesulfonic Acid // Macromolecular Symposia. – 2019. – Т. 385, № 1.

5. Namiki N., Takagi T., Kagi N., Morita T., Kobayashi S. Abatement of VOCs by Atomizing Acrylamide Polyampholyte (APA) Solution using Spray Nozzles // Kagaku Kogaku Ronbunshu. – 2014. – Т. 40, № 4. – P. 306-312.

6. Nesteronok P. V., Soldatov V. S. Acid-base properties of ion exchangers. Iv. Synthesis and potentiometric analysis of polyampholytes on the base of polyacrylonitrile fibers // Solvent Extraction and Ion Exchange. – 2012. – Т. 30, № 4. – P. 414-421.

7. Soll S., Zhao Q., Weber J., Yuan J. Y. Activated CO2 Sorption in Mesoporous Imidazolium-Type Poly(ionic liquid)-Based Polyampholytes // Chemistry of Materials. – 2013. – Т. 25, № 15. – P. 3003-3010.

8. Zhulina E. B., Dobrynin A. V., Rubinstein M. Adsorption isotherms of polyampholytes at charged spherical particles // Journal of Physical Chemistry B. – 2001. – Т. 105, № 37. – P. 8917-8930.

9. Dobrynin A. V., Rubinstein M., Joanny J. F. Adsorption of a polyampholyte chain on a charged surface // Macromolecules. – 1997. – Т. 30, № 15. – P. 4332-4341.

10. Mahltig B., Walter H., Harrats C., Muller-Buschbaum P., Jerome R., Stamm M. Adsorption of polyampholyte copolymers at the solid/liquid interface: the influence of pH and salt on the adsorption behaviour // Physical Chemistry Chemical Physics. – 1999. – Т. 1, № 17. – P. 3853-3856.

11. Lowe A. B., McCormick C. L. Synthesis and solution properties of zwitterionic polymers // Chemical Reviews. – 2002. – Т. 102, № 11. – P. 4177-4189.

12. Williams J. G. Polymeric materials encyclopedia // Journal of the American Chemical Society. – 1998. – Т. 120, № 27. – P. 6848-6849.

13. Maire M. L., Tanford C. Molecular characterization of enzymatically active, detergent-solubilized ca++ atpase from sarcoplasmic-reticulum // Biophysical Journal. – 1976. – Т. 16, № 2. – P. A82-A82.

14. Laschewsky A. Structures and Synthesis of Zwitterionic Polymers // Polymers. – 2014. – Т. 6, № 5. – P. 1544.

15. Constantinou A. P., Elladiou M., Patrickios C. S. Regular and Inverse Polyampholyte Hydrogels: A Detailed Comparison // Macromolecules. – 2016. – T. 49, № 10. – P. 3869-3880.

16. Petzold A. The relevance of buffer system ionic strength in immunoassay development // Journal of Immunological Methods. – 2019. – T. 465. – P. 27-30.

17. Hammid A. T., Bin Sulaiman M. H., Awad O. I. A robust firefly algorithm with backpropagation neural networks for solving hydrogeneration prediction // Electrical Engineering. – 2018. – T. 100, № 4. – P. 2617-2633.

18. Long T. J., Li Y. X., Fang X., Sun J. Q. Salt-Mediated Polyampholyte Hydrogels with High Mechanical Strength, Excellent Self-Healing Property, and Satisfactory Electrical Conductivity // Advanced Functional Materials. – 2018. – T. 28, № 44. – P. 9.

19. Rumyantsev A. M., Zhulina E. B., Borisov O. V. Scaling Theory of Complex Coacervate Core Micelles // Acs Macro Letters. – 2018. – T. 7, № 7. – P. 811-816.

20. Yaagoob I. Y., Ali S. A., Al-Muallem H. A., Mazumder M. A. J. Scope of sulfur dioxide incorporation into alkyldiallylamine-maleic acid-SO2 tercyclopolymer // Rsc Advances. – 2018. – T. 8, № 68. – P. 38891-38902.

21. Roy C. K., Guo H. L., Sun T. L., Bin Ihsan A., Kurokawa T., Takahata M., Nonoyama T., Nakajima T., Gong J. P. Self-Adjustable Adhesion of Polyampholyte Hydrogels // Advanced Materials. – 2015. – T. 27, № 45. – P. 7344-.

22. Teoh S. K., Ravi P., Dai S., Tam K. C. Self-assembly of stimuli-responsive water-soluble 60 fullerene end-capped ampholytic block copolymer // Journal of Physical Chemistry B. – 2005. – T. 109, № 10. – P. 4431-4438.

23. Bin Ihsan A., Sun T. L., Kurokawa T., Karobi S. N., Nakajima T., Nonoyama T., Roy C. K., Luo F., Gong J. P. Self-Healing Behaviors of Tough Polyampholyte Hydrogels // Macromolecules. – 2016. – T. 49, № 11. – P. 4245-4252.

24. Argun A., Gulyuz U., Okay O. Semi-Crystalline, Three-Segmented Hybrid Gels with Multiple Shape-Memory Effect // Macromolecular Symposia. – 2019. – T. 385, № 1.

25. Nakahata R., Yusa S.-I. Solution Properties of Amphoteric Random Copolymers Bearing Pendant Sulfonate and Quaternary Ammonium Groups with Controlled Structures // Langmuir : the ACS journal of surfaces and colloids. – 2018.

26. Suner S. S., Demirci S., Yetiskin B., Fakhrullin R., Naumenko E., Okay O., Ayyala R. S., Sahiner N. Cryogel composites based on hyaluronic acid and halloysite nanotubes as scaffold for tissue engineering // International Journal of Biological Macromolecules. – 2019. – T. 130. – P. 627-635.

27. Su E., Okay O. Cryogenic formation-structure-property relationships of poly(2-acrylamido-2-methyl-1-propanesulfonic acid) cryogels // Polymer. – 2019. – T. 178.

28. Zvukova N. D., Klimova T. P., Ivanov R. V., Ryabev A. N., Tsiskarashvili A. V., Lozinsky V. I. Cryostructuring of Polymeric Systems. 52. Properties, Microstructure and an Example of a Potential Biomedical Use of the Wide-Pore Alginate Cryostructurates // Gels. – 2019. – T. 5, № 2.

29. Daglioglu E., Okay O., Dalgic A., Albayrak A. L., Ergungor F. Cystic olfactory schwannoma of the anterior cranial base // British Journal of Neurosurgery. – 2008. – Т. 22, № 5. – P. 697-699.

30. Li D., Xu Z., Ji X. X., Liu L. B., Gai G. J., Yang J. B., Wang J. J. Deep insight into ionic transport in polyampholyte gel electrolytes towards high performance solid supercapacitors // Journal of Materials Chemistry A. – 2019. – Т. 7, № 27. – P. 16414-16424.

31. Ergungor F., Daglioglu E., Akdemir G., Okay O., Dalgic A., Hatipoglu G. Delayed chiasmal herniation after transsphenoidal removal of a pituitary adenoma - case report // Neurologia I Neurochirurgia Polska. – 2008. – Т. 42, № 1. – P. 60-63.

32. Li Q. W., Liu C. L., Wen J. R., Wu Y. Z., Shan Y., Liao J. F. The design, mechanism and biomedical application of self-healing hydrogels // Chinese Chemical Letters. – 2017. – Т. 28, № 9. – P. 1857-1874.

33. Kruse J. H., Biehl P., Schacher F. H. Different Routes to Ampholytic Polydehydroalanine: Orthogonal versus Simultaneous Deprotection // Macromolecular Rapid Communications. – 2019. – Т. 40, № 10.

34. Shew C. Y., Yoshikawa K., Ito T., Yoshihara C., Koyama Y. Dissociation of DNA-polycation complexes by polyanions and polyampholytes // Chemical Physics Letters. – 2007. – Т. 446, № 1-3. – P. 59-64.

35. Xu W. J., Rudov A. A., Schroeder R., Portnov I. V., Richtering W., Potemkin, II, Pich A. Distribution of Ionizable Groups in Polyampholyte Microgels Controls Interactions with Captured Proteins: From Blockade and "Levitation" to Accelerated Release // Biomacromolecules. – 2019. – Т. 20, № 4. – P. 1578-1591.

36. Daligic A., Secer M., Ergungor F., Okay O., Akdag R., Ciliz D. Dural sinus thrombosis following head injury: Report of two cases and review of the literature // Turkish Neurosurgery. – 2008. – Т. 18, № 1. – P. 70-77.

37. Tuncaboylu D. C., Sahin M., Argun A., Oppermann W., Okay O. Dynamics and Large Strain Behavior of Self-Healing Hydrogels with and without Surfactants // Macromolecules. – 2012. – Т. 45, № 4. – P. 1991-2000.

38. Sayil C., Okay O. The effect of preparation temperature on the swelling behavior of poly(N-isopropylacrylamide) gels // Polymer Bulletin. – 2000. – Т. 45, № 2. – P. 175-182.

39. Gezici A. R., Ergun R., Gurel K., Yilmaz F., Okay O., Bozdogan O. The Effect of Risedronate on Posterior Lateral Spinal Fusion in a Rat Model // Journal of Korean Neurosurgical Society. – 2009. – Т. 46, № 1. – P. 45-51.

40. Marchand A., Gendreau M., Blais M., Emiel G. Efficient Tabu Search Procedure for Short-Term Planning of Large-Scale Hydropower Systems // Journal of Water Resources Planning and Management. – 2019. – Т. 145, № 7.

41. Shi R., Sun T. L., Luo F., Nakajima T., Kurokawa T., Bin Y. Z., Rubinstein M., Gong J. P. Elastic-Plastic Transformation of Polyelectrolyte Complex Hydrogels from Chitosan and Sodium Hyaluronate // Macromolecules. – 2018. – Т. 51, № 21. – P. 8887-8898.

42. Marudova-Zsivanovits M. G., Yancheva E. L., Zsivanovits G. I., Rashkov I. B. Electrostatic interactions and complex formation of N-carboxyethylchitosan

with pectin // Six International Conference of the Balkan Physical Union / Cetin S. A., Hikmet I., 2007. – P. 817-817.

43. Huang Y. W., King D. R., Sun T. L., Nonoyama T., Kurokawa T., Nakajima T., Gong J. P. Energy-Dissipative Matrices Enable Synergistic Toughening in Fiber Reinforced Soft Composites // Advanced Functional Materials. – 2017. – T. 27, № 9.

44. Zheng Y. N., Chen F., He W. Epoxy-Amine microgels-mediated green preparation of gold nanoparticles // Colloids and Surfaces a-Physicochemical and Engineering Aspects. – 2019. – T. 575. – P. 94-101.

45. Rosas-Jaimes O. A., Munoz-Hernandez G. A., Mino-Aguilar G., Castaneda-Camacho J., Gracios-Marin C. A. Evaluating Fractional PID Control in a Nonlinear MIMO Model of a Hydroelectric Power Station // Complexity. – 2019.

46. King D. R., Sun T. L., Huang Y. W., Kurokawa T., Nonoyama T., Crosby A. J., Gong J. P. Extremely tough composites from fabric reinforced polyampholyte hydrogels // Materials Horizons. – 2015. – T. 2, № 6. – P. 584-591.

47. Takeoka Y., Berker A. N., Du R., Enoki T., Grosberg A., Kardar M., Oya T., Tanaka K., Wang G. Q., Yu X. H., Tanaka T. First order phase transition and evidence for frustrations in polyampholytic gels // Physical Review Letters. – 1999. – T. 82, № 24. – P. 4863-4865.

48. Li X. D., Liu L., Wang X. Z., Ok Y. S., Elliott J. A. W., Chang S. X., Chung H. J. Flexible and Self-Healing Aqueous Supercapacitors for Low Temperature Applications: Polyampholyte Gel Electrolytes with Biochar Electrodes // Scientific Reports. – 2017. – T. 7.

49. Valueva S. V., Kopeikin V. V., Kipper A. I., Filippov A. P., Shishkina G. V., Khlebosolova E. N., Rumyantseva N. V., Nazarkina Y. I., Borovikova L. N. Formation of zero-valence selenium nanoparticles in polyampholyte aqueous solutions in the presence of redox systems // Polymer Science Series B. – 2005. – T. 47, № 5-6. – P. 143-145.

50. Dinu M. V., Ozmen M. M., Dragan E. S., Okay O. Freezing as a path to build macroporous structures: Superfast responsive polyacrylamide hydrogels // Polymer. – 2007. – T. 48, № 1. – P. 195-204.

51. Bajomo M., Robb I., Steinke J. H. G., Bismarck A. Fully Reversible pH-Triggered Network Formation of Amphoteric Polyelectrolyte Hydrogels // Advanced Functional Materials. – 2011. – T. 21, № 1. – P. 172-176.

52. Elsharma E. M., Saleh A. S., Abou-Elmagd W. S. I., Metwally E., Siyam T. Gamma radiation induced preparation of polyampholyte nanocomposite polymers for removal of Co(II) // International Journal of Biological Macromolecules. – 2019. – T. 136. – P. 1273-1281.

53. Nakajima T. Generalization of the sacrificial bond principle for gel and elastomer toughening // Polymer Journal. – 2017. – T. 49, № 6. – P. 477-485.

54. Baumketner A., Shimizu H., Isobe M., Hiwatari Y. Helix transition in di-block polyampholyte // Journal of Physics-Condensed Matter. – 2001. – T. 13, № 46. – P. 10279-10291.

55. Ingverud T., Malkoch M. Helux: A Heterofunctional Hyperbranched Poly(amido amine) Carboxylate // Acs Applied Polymer Materials. – 2019. – T. 1, № 7. – P. 1845-1853.

56. Tuncaboylu D. C., Okay O. Hierarchically Macroporous Cryogels of Polyisobutylene and Silica Nanoparticles // Langmuir. – 2010. – T. 26, № 10. – P. 7574-7581.

57. Muslumova S., Yetiskin B., Okay O. Highly Stretchable and Rapid Self-Recoverable Cryogels Based on Butyl Rubber as Reusable Sorbent // Gels. – 2019. – T. 5, № 1.

58. Uzumcu A. T., Guney O., Okay O. Highly Stretchable DNA/Clay Hydrogels with Self-Healing Ability // Acs Applied Materials & Interfaces. – 2018. – T. 10, № 9. – P. 8296-8306.

59. Yetiskin B., Okay O. High-strength and self-recoverable silk fibroin cryogels with anisotropic swelling and mechanical properties // International Journal of Biological Macromolecules. – 2019. – T. 122. – P. 1279-1289.

60. Ilseven E., Gol M. Hydro-Optimization-Based Medium-Term Price Forecasting Considering Demand and Supply Uncertainty // Ieee Transactions on Power Systems. – 2018. – T. 33, № 4. – P. 4074-4083.

61. Wang T., Zhang Y.-l., Pan J.-h., Li B.-r., Wu L.-g., Jiang B.-q. Hydrothermal reduction of commercial P25 photocatalysts to expand their visible-light response and enhance their performance for photodegrading phenol in high-salinity wastewater // Applied Surface Science. – 2019. – T. 480. – P. 896-904.

62. Chen W., Yan R.-Q., Chen G.-H., Chen M. Y., Huang G.-B., Liu X.-H. Hydrothermal route to synthesize helical core-shell heterostructures with enhanced photocatalytic hydrogeneration activity // Ceramics International. – 2019. – T. 45, № 2. – P. 1803-1811.

63. Mariner E., Haag S. L., Bernards M. T. Impacts of cross-linker chain length on the physical properties of polyampholyte hydrogels // Biointerphases. – 2019. – T. 14, № 3.

64. Pang Y., Yu Y., Chen H., Xu G., Miao L., Liu X., Pan Z., Kou Z., Wu Y., Wang J. In situ electrochemical oxidation of electrodeposited Ni-based nanostructure promotes alkaline hydrogen production // Nanotechnology. – 2019. – T. 30, № 47.

65. Rocha S., Thuneman A. F., Pereira M. D., Coelho M., Mohwald H., Brezesinski G. Influence of fluorinated and hydrogenated nanoparticles on the structure and fibrillogenesis of amyloid beta-peptide // Biophysical Chemistry. – 2008. – T. 137, № 1. – P. 35-42.

66. Dalgic A., Yildirim A. E., Okay O., Uckun O., Alagoz F., Polat O., Akdag R., Nacar O., Daglioglu E., Belen D. Initial Discectomy Associated with Aging Leading to Adjacent Disc Disease and Recurrence // Turkish Neurosurgery. – 2016. – T. 26, № 4. – P. 595-600.

67. Stevens M. J., Hoh J. H. Interactions between Planar Grafted Neurofilament Side-Arms // Journal of Physical Chemistry B. – 2011. – T. 115, № 23. – P. 7541-7549.

68. Matsumura K., Ahmed S. Intracellular delivery of biomolecules via freeze concentration using polyampholyte nanocarriers // Abstracts of Papers of the American Chemical Society. – 2019. – T. 257.

69. Blackman L. D., Gunatillake P. A., Cass P., Locock K. E. S. An introduction to zwitterionic polymer behavior and applications in solution and at surfaces // Chemical Society Reviews. – 2019. – T. 48, № 3. – P. 757-770.

70. Riggleman R. A., Kumar R., Fredrickson G. H. Investigation of the interfacial tension of complex coacervates using field-theoretic simulations // Journal of Chemical Physics. – 2012. – T. 136, № 2.

71. Bakhshandeh A., dos Santos A. P., Diehl A., Levin Y. Isothermal adsorption of polyampholytes on charged nanopatterned surfaces // Journal of Chemical Physics. – 2019. – T. 151, № 8.

72. Lowe A. B., McCormick C. L. Synthesis, aqueous solution properties, and biomedical application of polymeric betaines // Polyelectrolytes and Polyzwitterions: Synthesis, Properties, and Applications / Lowe A. B., McCormick C. L., 2006. – P. 65-78.

73. Drozdov A. D., Christiansen J. D. The effects of pH and ionic strength on equilibrium swelling of polyampholyte gels // International Journal of Solids and Structures. – 2017. – T. 110. – P. 192-208.

74. Hamad F. G., Chen Q., Colby R. H. Linear Viscoelasticity and Swelling of Polyelectrolyte Complex Coacervates // Macromolecules. – 2018. – T. 51, № 15. – P. 5547-5555.

75. Gao M., Gawel K., Stokke B. T. Polyelectrolyte and antipolyelectrolyte effects in swelling of polyampholyte and polyzwitterionic charge balanced and charge offset hydrogels // European Polymer Journal. – 2014. – T. 53. – P. 65-74.

76. Morishima Y., Lim H. S., Nozakura S., Sturtevant J. L. Effect of monomer sequence distribution in 2-vinylnaphthalene maleic-acid copolymers on energy migration and excimer formation in aqueous-solution // Macromolecules. – 1989. – T. 22, № 3. – P. 1148-1154.

77. Creutz S., Teyssie P., Jerome R. Living anionic homopolymerization and block copolymerization of 4-vinylpyridine at "elevated" temperature and its characterization by size exclusion chromatography // Macromolecules. – 1997. – T. 30, № 1. – P. 1-5.

78. Patrickios C. S., Hertler W. R., Abbott N. L., Hatton T. A. Diblock, abc triblock, and random methacrylic polyampholytes - synthesis by group-transfer polymerization and solution behavior (vol 27, PG 930, 1994) // Macromolecules. – 1994. – T. 27, № 8. – P. 2364-2364.

79. Webster O. W. Group-transfer polymerization and its relationship to other living systems // Macromolecular Engineering: Recent Advances. – 1995. – P. 1-9.

80. Lowe A. B., Billingham N. C., Armes S. P. Synthesis and characterization of zwitterionic block copolymers // Macromolecules. – 1998. – T. 31, № 18. – P. 5991-5998.

81. Georges M. K., Veregin R. P. N., Kazmaier P. M., Hamer G. K. Narrow molecular-weight resins by a free-radical polymerization process // Macromolecules. – 1993. – T. 26, № 11. – P. 2987-2988.

82. Wang J. S., Matyjaszewski K. Controlled living radical polymerization - atom-transfer radical polymerization in the presence of transition-metal complexes // Journal of the American Chemical Society. – 1995. – T. 117, № 20. – P. 5614-5615.

83. Chiefari J., Chong Y. K., Ercole F., Krstina J., Jeffery J., Le T. P. T., Mayadunne R. T. A., Meijs G. F., Moad C. L., Moad G., Rizzardo E., Thang S. H. Living free-radical polymerization by reversible addition-fragmentation chain transfer: The RAFT process // Macromolecules. – 1998. – T. 31, № 16. – P. 5559-5562.

84. Kudaibergenov S., Adilov Z., Berillo D., Tatykhanova G., Sadakbaeva Z., Abdullin K., Galaev I. Novel macroporous amphoteric gels: Preparation and characterization // Express Polymer Letters. – 2012. – T. 6, № 5. – P. 346-353.

85. Ibraeva Z. E., Hahn M., Jaeger W., Bimendina L. A., Kudaibergenov S. E. Solution properties and complexation of polyampholytes based on N,N-dimethyldiallyl ammonium chloride and maleic acid or alkyl (aryl) derivatives of maleamic acids // Macromolecular Chemistry and Physics. – 2004. – T. 205, № 18. – P. 2464-2472.

86. Ibraeva Z. E., Hahn M., Jaeger W., Laschewsky A., Bimendina L. A., Kudaibergenov S. E. Swelling behavior and complex formation ability of ternary amphoteric gels based on allylamine derivatives and maleic acid // Macromolecular Materials and Engineering. – 2005. – T. 290, № 8. – P. 769-777.

87. Kudaibergenov S. E., Tatykhanova G. S., Klivenko A. N. Complexation of macroporous amphoteric cryogels based on N,N-dimethylaminoethyl methacrylate and methacrylic acid with dyes, surfactant, and protein // Journal of Applied Polymer Science. – 2016. – T. 133, № 32. – P. 9.

88. Dyakonova M. A., Berezkin A. V., Kyriakos K., Gkermpoura S., Popescu M. T., Filippov S. K., Stepanek P., Di Z. Y., Tsitsilianis C., Papadakis C. M. Salt-Induced Changes in Triblock Polyampholyte Hydrogels: Computer Simulations and Rheological, Structural, and Dynamic Characterization // Macromolecules. – 2015. – T. 48, № 22. – P. 8177-8189.

89. Alfrey T. Structure property relationships in polymers // Acs Symposium Series. – 1985. – T. 285. – P. 241-252.

90. Nair A. K. N., Jimenez A. M., Sun S. Y. Complexation Behavior of Polyelectrolytes and Polyampholytes // Journal of Physical Chemistry B. – 2017. – T. 121, № 33. – P. 7987-7998.

91. Batyrbekov A. A., Evdakov V. P., Kabanov V. A., Kozhinova E. V., Petrov R. V., Savinova I. V., Fedoseyeva N. A., Khaitov R. M., Khaustova L. I. Study of mechanism of polyelectrolyte and polyampholyte action on immune-response // Tsitologiya. – 1976. – T. 18, № 10. – P. 1259-1263.

92. Bekturov E. A., Kudaibergenov S. E., Zhaimina G. M. Reaction of synthetic styrene polyampholyte-copolymer and n,n-dimethylaminopropylmonoamide of maleic-acid, with cu2+ and fe3+ ions in aqueous-solution // Koordinatsionnaya Khimiya. – 1984. – T. 10, № 7. – P. 942-946.

93. Dobrynin A. V., Rubinstein M., Joanny J. F. Polyampholyte solutions between charged surfaces: Debye-Huckel theory // Journal of Chemical Physics. – 1998. – T. 109, № 20. – P. 9172-9176.

94. Kudaibergenov S., Jaeger W., Laschewsky A. Polymeric betaines: Synthesis, characterization, and application // Supramolecular Polymers Polymeric Betains Oligomers / Donnio B. и др. – Berlin: Springer-Verlag Berlin, 2006. – P. 157-224.

95. Baker J. P., Blanch H. W., Prausnitz J. M. Swelling properties of acrylamide-based ampholytic hydrogels - comparison of experiment with theory // Polymer. – 1995. – T. 36, № 5. – P. 1061-1069.

96. Ali S. A., Rasheed A. Synthesis and solution properties of a betaine-sulfur dioxide polyampholyte // Polymer. – 1999. – T. 40, № 24. – P. 6849-6857.

97. McCormick C. L., Salazar L. C. Water-soluble copolymers .46. Hydrophilic sulfobetaine copolymers of acrylamide and 3-(2-acrylamido-2-methylpropanedimethyl-ammonio)-1-propanesulphonate // Polymer. – 1992. – T. 33, № 21. – P. 4617-4624.

98. Jaeger W., Wendler U., Lieske A., Bohrisch J. Novel modified polymers with permanent cationic groups // Langmuir. – 1999. – T. 15, № 12. – P. 4026-4032.

99. Wendler U., Bohrisch J., Jaeger W., Rother G., Dautzenberg H. Amphiphilic cationic block copolymers via controlled free radical polymerization // Macromolecular Rapid Communications. – 1998. – T. 19, № 4. – P. 185-190.

100. Kaladas J. J., Kastrup R., Schulz D. N. Poly(cyclosulfobetaines): Synthesis, characterization and solution properties // Abstracts of Papers of the American Chemical Society. – 1998. – T. 215. – P. 399-399.

101. Favresse P., Laschewsky A. New poly(carbobetaine)s made from zwitterionic diallylammonium monomers // Macromolecular Chemistry and Physics. – 1999. – T. 200, № 4. – P. 887-895.

102. Ali M. M., Perzanowski H. P., Ali S. A. Polymerization of functionalized diallyl quaternary ammonium salt to poly(ampholyte-electrolyte) // Polymer. – 2000. – T. 41, № 15. – P. 5591-5600.

103. Candau F., Ohlemacher A., Munch J. P., Candau S. J. Effect of the net charge distribution on the aqueous solution properties of polyampholytes // Revue De L Institut Francais Du Petrole. – 1997. – T. 52, № 2. – P. 133-137.

104. Corpart J. M., Candau F. Formulation and polymerization of microemulsions containing a mixture of cationic and anionic monomers // Colloid and Polymer Science. – 1993. – T. 271, № 11. – P. 1055-1067.

105. McCormick C. L., Salazar L. C. Water-soluble copolymers .43. Ampholytic copolymers of sodium 2-(acrylamido)-2-methylpropanesulfonate with 2-(acrylamido)-2-methylpropyl trimethylammonium chloride // Macromolecules. – 1992. – T. 25, № 7. – P. 1896-1900.

106. Kudaibergenov S. E., Nuraje N. Intra- and Interpolyelectrolyte Complexes of Polyampholytes // Polymers. – 2018. – T. 10, № 10. – P. 34.

107. Ezell R. G., Gorman I., Lokitz B., Ayres N., McCormick C. L. Stimuli-responsive ampholytic terpolymers of N-acryloyl-valine, acrylamide, and (3-acrylamidopropyl)trimethylammonium chloride: Synthesis, characterization, and solution properties // Journal of Polymer Science Part a-Polymer Chemistry. – 2006. – T. 44, № 9. – P. 3125-3139.

108. Cherstvy A. G. Collapse of Highly Charged Polyelectrolytes Triggered by Attractive Dipole-Dipole and Correlation-Induced Electrostatic Interactions // Journal of Physical Chemistry B. – 2010. – T. 114, № 16. – P. 5241-5249.

109. Higgs P. G., Joanny J. F. Theory of polyampholyte solutions // Journal of Chemical Physics. – 1991. – T. 94, № 2. – P. 1543-1554.

110. Jeon J., Dobrynin A. V. Monte Carlo simulations of polyampholyte-polyelectrolyte complexes: Effect of charge sequence and strength of electrostatic interactions // Physical Review E. – 2003. – T. 67, № 6.

111. Su E., Okay O. Polyampholyte hydrogels formed via electrostatic and hydrophobic interactions // European Polymer Journal. – 2017. – T. 88. – P. 191-204.

112. Dobrynin A. V., Rubinstein M. Flory theory of a polyampholyte chain // Journal De Physique Ii. – 1995. – T. 5, № 5. – P. 677-695.

113. An H., Lu C., Wang P., Li W., Tan Y., Xu K., Liu C. A novel hydrophobically associating polyampholytes of poly(AM/AA/AMQC12): preparation, characterization, and solution properties // Polymer Bulletin. – 2011. – T. 67, № 1. – P. 141-158.

114. Han X., Feng J., Dong F., Zhang X. X., Liu H. L., Hu Y. Thermo-/pH-responsive behaviours of base-rich diblock polyampholytes in aqueous solution: experiment and simulation // Molecular Physics. – 2014. – T. 112, № 15. – P. 2046-2057.

115. Ezell R. G., McCormick C. L. Electrolyte- and pH-responsive polyampholytes with potential as viscosity-control agents in enhanced petroleum recovery // Journal of Applied Polymer Science. – 2007. – T. 104, № 5. – P. 2812-2821.

116. McCormick C. L., Salazar L. C. Water-soluble copolymers .44. Ampholytic terpolymers of acrylamide with sodium 2-acrylamido-2-methylpropanesulfonate and 2-acrylamido-2-methylpropanetrimethylammonium chloride // Polymer. – 1992. – T. 33, № 20. – P. 4384-4387.

117. McCormick C. L., Kirkland S. E., York A. W. Synthetic Routes to Stimuli-Responsive Micelles, Vesicles, and Surfaces via Controlled/Living Radical Polymerization // Journal of Macromolecular Science, Part C. – 2006. – T. 46, № 4. – P. 421-443.

118. Skouri M., Munch J. P., Candau S. J., Neyret S., Candau F. Conformation of neutral polyampholyte chains in salt-solutions - a light-scattering study // Macromolecules. – 1994. – T. 27, № 1. – P. 69-76.

119. Corpart J. M., Candau F. Aqueous-solution properties of ampholytic copolymers prepared in microemulsions // Macromolecules. – 1993. – T. 26, № 6. – P. 1333-1343.

120. Katchalsky A., Kedemo. Thermodynamics of flow processes in biological systems // Biophysical journal. – 1962. – T. 2, № 2 Pt 2. – P. 53-78.

121. Katchalsky A. Polyelectrolytes and their biological interactions // Biophysical journal. – 1964. – T. 4. – P. 9-41.

122. Katchalsky A., Danon D., Nevo A. Interactions of basic polyelectrolytes with the red blood cell. II. Agglutination of red blood cells by polymeric bases // Biochimica et biophysica acta. – 1959. – T. 33, № 1. – P. 120-38.

123. Kantor Y., Kardar M., Li H. Statistical-mechanics of polyampholytes // Physical Review E. – 1994. – Т. 49, № 2. – Р. 1383-1392.

124. Dobrynin A. V. Polyampholyte adsorption on a charged sphere // Physical Review E. – 2001. – Т. 63, № 5.

125. Kudaibergenov S. E., Nurgalieva D. E., Bekturov E. A., Shaikhutdinov E. M., Nurkeeva Z. S., Sigitov V. B. Study of polyampholyte hydrogels and interpenetrating polyelectrolyte networks based on 4-(but-3-en-1-ynyl)-1-methylpiperidin-4-ol // Macromolecular Chemistry and Physics. – 1994. – Т. 195, № 9. – Р. 3033-3038.

126. Ghosh R., Das S., Chatterjee D. P., Nandi A. K. Surfactant-Triggered Fluorescence Turn "on/off" Behavior of a Polythiophene-graft-Polyampholyte // Langmuir. – 2016. – Т. 32, № 33. – Р. 8413-8423.

127. Luo F., Sun T. L., Nakajima T., King D. R., Kurokawa T., Zhao Y., Bin Ihsan A., Li X. F., Guo H. L., Gong J. P. Strong and Tough Polyion-Complex Hydrogels from Oppositely Charged Polyelectrolytes: A Comparative Study with Polyampholyte Hydrogels // Macromolecules. – 2016. – Т. 49, № 7. – Р. 2750-2760.

128. Walter H., Harrats C., Muller-Buschbaum P., Jerome R., Stamm M. Adsorption of ampholytic diblock copolymers from dilute aqueous solution at the solid/liquid interface // Langmuir. – 1999. – Т. 15, № 4. – Р. 1260-1267.

129. Dobbins S. C., McGrath D. E., Bernards M. T. Nonfouling Hydrogels Formed from Charged Monomer Subunits // Journal of Physical Chemistry B. – 2012. – Т. 116, № 49. – Р. 14346-14352.

130. Lei H. Y., Wang M. M., Tang Z. C., Luan Y. F., Liu W., Song B., Chen H. Control of Lysozyme Adsorption by pH on Surfaces Modified with Polyampholyte Brushes // Langmuir. – 2014. – Т. 30, № 2. – Р. 501-508.

131. Kudaibergenov S. E. Synthesis and characterization of polyampholyte hydrogels // Berichte Der Bunsen-Gesellschaft-Physical Chemistry Chemical Physics. – 1996. – Т. 100, № 6. – Р. 1079-1082.

132. Kudaibergenov S. E., Sigitov V. B. Swelling, shrinking, deformation, and oscillation of polyampholyte gels based on vinyl 2-aminoethyl ether and sodium acrylate // Langmuir. – 1999. – Т. 15, № 12. – Р. 4230-4235.

133. Baker J. P., Stephens D. R., Blanch H. W., Prausnitz J. M. Swelling equilibria for acrylamide-based polyampholyte hydrogels // Macromolecules. – 1992. – Т. 25, № 7. – Р. 1955-1958.

134. Cui K. P., Sun T. L., Kurokawa T., Nakajima T., Nonoyama T., Chen L., Gong J. P. Stretching-induced ion complexation in physical polyampholyte hydrogels // Soft Matter. – 2016. – Т. 12, № 43. – Р. 8833-8840.

135. Tavsanli B., Can V., Okay O. Mechanically strong triple network hydrogels based on hyaluronan and poly(N,N-dimethylacrylamide) // Soft Matter. – 2015. – Т. 11, № 43. – Р. 8517-8524.

136. Okay O. DNA Hydrogels: New Functional Soft Materials // Journal of Polymer Science Part B-Polymer Physics. – 2011. – Т. 49, № 8. – Р. 551-556.

137. Argun A., Gulyuz U., Okay O. Interfacing Soft and Hard Materials with Triple-Shape-Memory and Self-Healing Functions // Macromolecules. – 2018. – Т. 51, № 7. – Р. 2437-2446.

138. Nisato G., Munch J. P., Candau S. J. Swelling, structure, and elasticity of polyampholyte hydrogels // Langmuir. – 1999. – T. 15, № 12. – P. 4236-4244.

139. Zhou M. Y., Liu H. W., Venkiteshwaran A., Kilduff J., Anderson D. G., Langer R., Belfort G. High throughput discovery of new fouling-resistant surfaces // Journal of Materials Chemistry. – 2011. – T. 21, № 3. – P. 693-704.

140. Haag S. L., Bernards M. T. Polyampholyte Hydrogels in Biomedical Applications // Gels. – 2017. – T. 3, № 4.

141. Zurick K. M., Bernards M. Recent Biomedical Advances with Polyampholyte Polymers // Journal of Applied Polymer Science. – 2014. – T. 131, № 6.

142. Shen H. Y., Akagi T., Akashi M. Nano polyampholyte gels prepared by amphoteric poly (amino acid) for protein nanocarrier // Abstracts of Papers of the American Chemical Society. – 2011. – T. 242.

143. Shen H. Y., Akagi T., Akashi M. Polyampholyte Nanoparticles Prepared by Self-Complexation of Cationized Poly(gamma-glutamic acid) for Protein Carriers // Macromolecular Bioscience. – 2012. – T. 12, № 8. – P. 1100-1105.

144. Shen X., Yin X., Zhao Y., Chen L. Antifouling enhancement of PVDF membrane tethered with polyampholyte hydrogel layers // Polymer Engineering and Science. – 2015. – T. 55, № 6. – P. 1367-1373.

145. Shen X., Yin X. B., Zhao Y. P., Chen L. Improved protein fouling resistance of PVDF membrane grafted with the polyampholyte layers // Colloid and Polymer Science. – 2015. – T. 293, № 4. – P. 1205-1213.

146. Sun T. L., Kurokawa T., Kuroda S., Bin Ihsan A., Akasaki T., Sato K., Haque M. A., Nakajima T., Gong J. P. Physical hydrogels composed of polyampholytes demonstrate high toughness and viscoelasticity // Nature Materials. – 2013. – T. 12, № 10. – P. 932-937.

147. Wang H. W., Li P. C., Xu K., Tan Y., Lu C. G., Li Y. L., Liang X. C., Wang P. X. Synthesis and characterization of multi-sensitive microgel-based polyampholyte hydrogels with high mechanical strength // Colloid and Polymer Science. – 2016. – T. 294, № 2. – P. 367-380.

148. Sun T. L., Luo F., Kurokawa T., Karobi S. N., Nakajima T., Gong J. P. Molecular structure of self-healing polyampholyte hydrogels analyzed from tensile behaviors // Soft Matter. – 2015. – T. 11, № 48. – P. 9355-9366.

149. Dyakonova M. A., Stavrouli N., Popescu M. T., Kyriakos K., Grillo I., Philipp M., Jaksch S., Tsitsilianis C., Papadakis C. M. Physical Hydrogels via Charge Driven Self-Organization of a Triblock Polyampholyte - Rheological and Structural Investigations // Macromolecules. – 2014. – T. 47, № 21. – P. 7561-7572.

150. Chen Y. Y., Shull K. R. High-Toughness Polycation Cross-Linked Triblock Copolymer Hydrogels // Macromolecules. – 2017. – T. 50, № 9. – P. 3637-3646.

151. Karobi S. N., Sun T. L., Kurokawa T., Luo F., Nakajima T., Nonoyama T., Gong J. P. Creep Behavior and Delayed Fracture of Tough Polyampholyte Hydrogels by Tensile Test // Macromolecules. – 2016. – T. 49, № 15. – P. 5630-5636.

152. Huang W., Duan H. D., Zhu L. P., Li G. Q., Ban Q., Lucia L. A. A semi-interpenetrating network polyampholyte hydrogel simultaneously demonstrating remarkable toughness and antibacterial properties // New Journal of Chemistry. – 2016. – Т. 40, № 12. – P. 10520-10525.

153. Jain M., Matsumura K. Polyampholyte- and nanosilicate-based soft bionanocomposites with tailorable mechanical and cell adhesion properties // Journal of Biomedical Materials Research Part A. – 2016. – Т. 104, № 6. – P. 1379-1386.

154. Matsumura K., Hayashi F., Nagashima T., Hyon S. H. Long-term cryopreservation of human mesenchymal stem cells using carboxylated poly-l-lysine without the addition of proteins or dimethyl sulfoxide // Journal of Biomaterials Science-Polymer Edition. – 2013. – Т. 24, № 12. – P. 1484-1497.

155. Rajan R., Jain M., Matsumura K. Cryoprotective properties of completely synthetic polyampholytes via reversible addition-fragmentation chain transfer (RAFT) polymerization and the effects of hydrophobicity // Journal of Biomaterials Science-Polymer Edition. – 2013. – Т. 24, № 15. – P. 1767-1780.

156. Rajan R., Hayashi F., Nagashima T., Matsumura K. Toward a Molecular Understanding of the Mechanism of Cryopreservation by Polyampholytes: Cell Membrane Interactions and Hydrophobicity // Biomacromolecules. – 2016. – Т. 17, № 5. – P. 1882-1893.

157. Bekturov E. A., Kudaibergenov S. E., Sigitov V. B. Complexation of amphoteric copolymer of 2-methyl-5-vinylpyridine acrylic-acid with copper(ii) ions and catalase-like activity of polyampholyte metal-complexes // Polymer. – 1986. – Т. 27, № 8. – P. 1269-1272.

158. Rudov A. A., Gelissen A. P. H., Lotze G., Schmid A., Eckert T., Pich A., Richtering W., Potemkin, II. Intramicrogel Complexation of Oppositely Charged Compartments As a Route to Quasi-Hollow Structures // Macromolecules. – 2017. – Т. 50, № 11. – P. 4435-4445.

159. Mishra R. K., Ramasamy K., Ban N. N., Majeed A. B. A. Synthesis of poly 3-(methacryloylamino) propyl trimethylammonium chloride-co-methacrylic acid copolymer hydrogels for controlled indomethacin delivery // Journal of Applied Polymer Science. – 2013. – Т. 128, № 5. – P. 3365-3374.

160. Cao Z. F., Jin Y., Miao Q., Ma C. Y., Zhang B. Preparation and properties of a dually responsive hydrogels based on polyampholyte for oral delivery of drugs // Polymer Bulletin. – 2013. – Т. 70, № 10. – P. 2675-2689.

161. Sankar R. M., Meera K. M. S., Samanta D., Jithendra P., Mandal A. B., Jaisankar S. N. The pH-sensitive polyampholyte nanogels: Inclusion of carbon nanotubes for improved drug loading // Colloids and Surfaces B-Biointerfaces. – 2013. – Т. 112. – P. 120-127.

162. Wang H. C., Grolman J. M., Rizvi A., Hisao G. S., Rienstra C. M., Zimmerman S. C. pH-Triggered Release from Polyamide Microcapsules Prepared by Interfacial Polymerization of a Simple Diester Monomer // Acs Macro Letters. – 2017. – Т. 6, № 3. – P. 321-325.

163. Schulze N., Tiersch B., Zenke I., Koetz J. Polyampholyte-tuned lyotrop lamellar liquid crystalline systems // Colloid and Polymer Science. – 2013. – Т. 291, № 11. – P. 2551-2559.

164. Schulze N., Appelhans D., Tiersch B., Koetz J. Morphological transformation of vesicles into tubular structures by adding polyampholytes or dendritic glycopolymers // Colloids and Surfaces a-Physicochemical and Engineering Aspects. – 2014. – T. 457. – P. 326-332.

165. Schulze N., Prietzel C., Koetz J. Polyampholyte-mediated synthesis of anisotropic gold nanoplatelets // Colloid and Polymer Science. – 2016. – T. 294, № 8. – P. 1297-1304.

166. Schulze N., Koetz J. Kinetically controlled growth of gold nanotriangles in a vesicular template phase by adding a strongly alternating polyampholyte // Journal of Dispersion Science and Technology. – 2017. – T. 38, № 8. – P. 1073-1078.

167. Ekici S., Tetik A. Development of polyampholyte hydrogels based on laponite for electrically stimulated drug release // Polymer International. – 2015. – T. 64, № 3. – P. 335-343.

168. Ali S. A., Al-Muallem H. A., Al-Hamouz O., Estaitie M. K. Synthesis of a novel zwitterionic bisphosphonate cyclopolymer containing residues of alendronic acid // Reactive & Functional Polymers. – 2015. – T. 86. – P. 80-86.

169. Asayama S., Seno K., Kawakami H. Synthesis of Carboxymethyl Poly(1-vinylimidazole) as a Polyampholyte for Biocompatibility // Chemistry Letters. – 2013. – T. 42, № 4. – P. 358-360.

170. Ladika M., Kalantar T. H., Shao H., Dean S. L., Harris J. K., Sheskey P. J., Coppens K., Balwinski K. M., Holbrook D. L. Polyampholyte Acrylic Latexes for Tablet Coating Applications // Journal of Applied Polymer Science. – 2014. – T. 131, № 7.

171. Kudaibergenov S. E. Physicochemical, Complexation and Catalytic Properties of Polyampholyte Cryogels // Gels. – 2019. – T. 5, № 1.

172. Aldabergenov M., Dauletbekova M., Toleutay G., Kudaibergenov S., Klivenko A. Reduction of 4-Nitrobenzoic Acid by AuNPs/Cryogel and PdNPs/Cryogel Nanocomposites // 7th IEEE International Conference Nanomaterials - Application and Properties (NAP); Ieee M. E. S. U. и др.: Proceedings of the international conference Nanomaterials-Applications and properties – Odessa, UKRAINE: Ieee, 2017.

173. Kudaibergenov S. E., Tatykhanova G. S., Selenova B. S. Polymer Protected and Gel Immobilized Gold and Silver Nanoparticles in Catalysis // Journal of Inorganic and Organometallic Polymers and Materials. – 2016. – T. 26, № 6. – P. 1198-1211.

174. G.Toleutay, S.Kudaibergenov S.Kabdrakhmanova, A. Shakhvorostov Solution behavior of quenched or strongly charged polyampholytes in aqueous-salt solutions // Bulletin of the Karaganda University, Chemistry Series. –// B9. – T. 94, № 2. – P. 36-43.

175. G.Toleutay, E.Su, S.Kudaibergenov Swelling and mechanical properties of quenched polyampholyte hydrogels based on 2-acrylamido-2-methyl-1-propanesulfonic acid sodium salt (AMPS) and (3-acrylamidopropyl) trimethylammonium chloride (APTAC) // Bulletin of the Karaganda University, Chemistry Series. – 2019. – T. 94, № 4. – P. 35-44.

176. . Shakhvorostov, G. Toleutay, S. Kudaibergenov. Synthesis, physico-chemical and complexation properties of "quenched" polyampholytes based on fully charged monomers // Materials of the International Conference "Polyelectrolytes in Chemistry, Biology and Technology"- Singapore, 2018.- P03.

177. Kudaibergenov, A. Shakhvorostov, M. Dauletbekova, G. Toleutay, Zh. Nurakhmetova, G. Kudaibergenova. Solution and volume-phase properties of linear and crosslinked "quenched" polyampholytes // Materials of the 12-th International Symposium on Polyelectrolytes ISP - Wageningen, The Netherlands, 2018.- P. 102

178. . Кудайбергенов, Г. Толеутай, А. Шахворостов. Физико-химические, комплексообразующие и каталитические свойства сильнозаряженных полиамфолитов линейного и сшитого строения // Сборник тезисов докладов «Современные проблемы науки о полимерах», Ташкент, 2017.- P. 18-20.

179. M.Dauletbekova, G. Toleutay, S.Kabdrakhmanova, S.Kudaibergenov Hydrogenation of P-Nitrobenzoic acid by gold and palladium Nanoparticiles Immobilized with in macroporous amphoteric cryogels in aqueus solution // Materials of the 82nd Prague meeting on Macromolecules 24th Polymer networks group meeting- Pragua, 2018.- P-06.

180. . M.Dauletbekova, G. Toleutay, S.Kabdrakhmanova, S.Kudaibergenov Hydrogenation of P-Nitrobenzoic acid by gold and palladium Nanoparticiles Immobilized with in macroporous amphoteric cryogels in aqueus solution // Materials of the 82nd Prague meeting on Macromolecules 24th Polymer networks group meeting- Pragua, 2018.- P-06.

181. Sun T. L., Luo F., Hong W., Cui K. P., Huang Y. W., Zhang H. J., King D. R., Kurokawa T., Nakajima T., Gong J. P. Bulk Energy Dissipation Mechanism for the Fracture of Tough and Self-Healing Hydrogels // Macromolecules. – 2017. – Т. 50, № 7. – P. 2923-2931.

182. Luo F., Sun T. L., Nakajima T., Kurokawa T., Zhao Y., Bin Ihsan A., Guo H. L., Li X. F., Gong J. P. Crack Blunting and Advancing Behaviors of Tough and Self-healing Polyampholyte Hydrogel // Macromolecules. – 2014. – Т. 47, № 17. – P. 6037-6046.

183. Li X. D., Liu L., Wang X. Z., Ok Y. S., Elliott J. A. W., Chang S. X., Chung H. J. Flexible and Self-Healing Aqueous Supercapacitors for Low Temperature Applications: Polyampholyte Gel Electrolytes with Biochar Electrodes // Scientific Reports. – 2017. – Т. 7. – P. 11.

184. Klivenko A. N., Tatykhanova G. S., Nuraje N., Kudaibergenov S. E. Hydrogenation of p-nitrophenol by gold nanoparticles immobilized within macroporous amphoteric cryogel based on N, N-dimethylaminoethylmethacrylate and methacrylic acid // Bulletin of the University of Karaganda-Chemistry. – 2015. № 80. – P. 10-15.

185. Sahiner N., Seven F. Energy and environmental usage of super porous poly(2-acrylamido-2-methyl-1-propan sulfonic acid) cryogel support // Rsc Advances. – 2014. – Т. 4, № 45. – P. 23886-23897.

186. Dolya N., Rojas O., Kosmella S., Tiersch B., Koetz J., Kudaibergenov S. "One-Pot" In Situ Formation of Gold Nanoparticles within Poly(acrylamide)

Hydrogels // Macromolecular Chemistry and Physics. – 2013. – Т. 214, № 10. – P. 1114-1121.

187. Arvidsson P., Plieva F. M., Savina I. N., Lozinsky V. I., Fexby S., Bulow L., Galaev I. Y., Mattiasson B. Chromatography of microbial cells using continuous supermacroporous affinity and ion-exchange columns // Journal of Chromatography A. – 2002. – Т. 977, № 1. – P. 27-38.

188. Andryushina V. A., Karpova N. V., Druzhinina A. V., Stytsenko T. S., Podorozhko E. A., Ryabev A. N., Lozinsky V. I. Novel Immobilized Biocatalyst for Microbiological Synthesis of Pharmaceutical Steroids // Applied Biochemistry and Microbiology. – 2015. – Т. 51, № 5. – P. 530-538.

189. Lozinsky V. I., Zubov A. L., Titova E. F. Poly(vinyl alcohol) cryogels employed as matrices for cell immobilization .2. Entrapped cells resemble porous fillers in their effects on the properties of PVA-cryogel carrier // Enzyme and Microbial Technology. – 1997. – Т. 20, № 3. – P. 182-190.

190. Lozinsky V. I., Plieva F. M. Poly(vinyl alcohol) cryogels employed as matrices for cell immobilization. 3. Overview of recent research and developments // Enzyme and Microbial Technology. – 1998. – Т. 23, № 3-4. – P. 227-242.

191. Kuyukina M. S., Rubtsova E. V., Ivshina I. B., Lvanov R. V., Lozinsky V. I. Selective adsorption of hydrocarbon-oxidizing Rhodococcus cells in a column with hydrophobized poly(acrylamide) cryogel // Journal of Microbiological Methods. – 2009. – Т. 79, № 1. – P. 76-81.

192. Podorozhko E. A., Lunev I. A., Ryabev A. N., Kil'deeva N. R., Lozinsky V. I. A study of cryostructuring of a polymer system. 39. Poly(vinyl alcohol) composite cryogels filled with chitosan microparticles // Colloid Journal. – 2015. – Т. 77, № 2. – P. 186-195.

193. Li Y. S., Wang Y. Chemically prepared silver alumina substrate for surface-enhanced raman-scattering // applied spectroscopy. – 1992. – t. 46, № 1. – p. 142-146.

194. Zhao P., Zhang W., Kaneti Y. V., Azhar A., Alshehri A. A., Yamauchi Y., Hu M. Confined Synthesis of Coordination Frameworks inside Double-Network Hydrogel for Fabricating Hydrogel-Based Water Pipes with High Adsorption Capacity for Cesium Ions // Bulletin of the Chemical Society of Japan. – 2018. – Т. 91, № 9. – P. 1357-1363.

195. Muniz-Miranda M., Caporali S., Marsili P., Giorgetti E. Fabrication and characterization of Ag/Pd colloidal nanoparticles as stable platforms for SERS and catalytic applications // Materials Chemistry and Physics. – 2015. – Т. 167. – P. 188-193.

196. Rainina E. I., Pusheva M. A., Ryabokon A. M., Bolotina N. P., Lozinsky V. I., Varfolomeyev S. D. Microbial-cells immobilized in poly(vinyl alcohol) cryogels .1. Microbial-cells immobilized in poly(vinyl alcohol) cryogels - biocatalytic reduction of co2 by the thermophilic homoacetogenic bacterium acetogenium-kivui // Biotechnology and Applied Biochemistry. – 1994. – Т. 19. – P. 321-329.

197. Miao C. W., Ran Q. P., Liu J. P., Mao Y. L., Shang Y., Sha J. F. New Generation Amphoteric Comb-like Copolymer Superplasticizer and Its Properties // Polymers & Polymer Composites. – 2011. – Т. 19, № 1. – P. 1-8.

198. Leverette C. L., Jacobs S. A., Shanmukh S., Chaney S. B., Dluhy R. A., Zhao Y. P. Aligned silver nanorod arrays as substrates for surface-enhanced infrared absorption spectroscopy // Applied Spectroscopy. – 2006. – Т. 60, № 8. – P. 906-913.

199. Cheng H., Zhou Z. Y., Qin D. F., Huang W. Y., Feng J., Tang T. F., Hu G. Z., Li L. J. Electrochemical Sensor Based on Electrospun Three-Dimensional Carbon Nanofibers to Determine Trace Levels of Cu(II) // Science of Advanced Materials. – 2020. – Т. 12, № 5. – P. 693-700.

200. Muthamizh S., Sengottaiyan C., Jayavel R., Narayanan V. Facile Synthesis of Phase Tunable MoO3 Nanostructures and Their Electrochemical Sensing Properties // Journal of Nanoscience and Nanotechnology. – 2020. – Т. 20, № 5. – P. 2823-2831.

201. Zhang W., Cheng W., Ziemann E., Be'er A., Lu X. L., Elimelech M., Bernstein R. Functionalization of ultrafiltration membrane with polyampholyte hydrogel and graphene oxide to achieve dual antifouling and antibacterial properties // Journal of Membrane Science. – 2018. – Т. 565. – P. 293-302.

202. Zoppi A., Trigari S., Margheri G., Muniz-Miranda M., Giorgetti E. Gold nanostars as SERS-active substrates for FT-Raman spectroscopy // Rsc Advances. – 2015. – Т. 5, № 11. – P. 8523-8532.

203. Kitano H., Imai M., Sudo K., Ide M. Hydrogen-bonded network structure of water in aqueous solution of sulfobetaine polymers // Journal of Physical Chemistry B. – 2002. – Т. 106, № 43. – P. 11391-11396.

204. Villanueva M. E., Diez A. M. D., Gonzalez J. A., Lazaro-Martinez J. M., Dall'Orto V. C., Copello G. J. Phosphorus adsorption by a modified polyampholyte-diatomaceous earth material containing imidazole and carboxylic acid moieties: batch and dynamic studies // New Journal of Chemistry. – 2017. – Т. 41, № 15. – P. 7667-7673.

205. Kondo T., Gemmei-Ide M., Kitano H., Ohno K., Noguchi H., Uosaki K. Sum frequency generation study on the structure of water in the vicinity of an amphoteric polymer brush // Colloids and Surfaces B-Biointerfaces. – 2012. – Т. 91. – P. 215-218.

206. Li Y. S., Cheng J., Chung K. T. Surface-enhanced Raman spectroscopy using silver nanoparticles on a precoated microscope slide // Spectrochimica Acta Part a-Molecular and Biomolecular Spectroscopy. – 2008. – Т. 69, № 2. – P. 524-527.

207. Saravanakumar B., Haritha A., Ravi G., Yuvakkumar R. Synthesis of X-3(PO4)(2) X = Ni, Cu, Mn Nanomaterials as an Efficient Electrode for Energy Storage Applications // Journal of Nanoscience and Nanotechnology. – 2020. – Т. 20, № 5. – P. 2813-2822.

208. Cui K. P., Sun T. L., Liang X. B., Nakajima K., Ye Y. N., Chen L., Kurokawa T., Gong J. P. Multiscale Energy Dissipation Mechanism in Tough and Self-Healing Hydrogels // Physical Review Letters. – 2018. – Т. 121, № 18.

209. Wang H. W., Liang X. C., Xu K., Tan Y., Lu C. G., Wang P. X. Synthesis and Characterization of Polyampholyte Hydrogels Based on Hyperbranched Polymer // Chemical Journal of Chinese Universities-Chinese. – 2016. – Т. 37, № 4. – P. 752-760.

210. Sui K. Y., Zhao X., Wu Z. M., Xia Y. Z., Liang H. C., Li Y. J. Synthesis, Rapid Responsive Thickening, and Self-Assembly of Brush Copolymer Poly(ethylene oxide)-graft-Poly(N,N-dimethylaminoethyl methacrylate) in Aqueous Solutions // Langmuir. – 2012. – Т. 28, № 1. – P. 153-160.

211. Gainar A., Stevens J. S., Jaye C., Fischer D. A., Schroeder S. L. M. NEXAFS Sensitivity to Bond Lengths in Complex Molecular Materials: A Study of Crystalline Saccharides // Journal of Physical Chemistry B. – 2015. – Т. 119, № 45. – P. 14373-14381.

212. Gainar A., Stevens J. S., Suljoti E., Xiao J., Golnak R., Aziz E. F., Schroeder S. L. M., Iop. The Structure of p-Aminobenzoic Acid in Water: Studies Combining UV-Vis, NEXAFS and RIXS Spectroscopies // 16th International Conference on X-ray Absorption Fine Structure (XAFS); Karlsruhe Inst T. – Т. 712: Journal of Physics Conference Series – Karlsruhe Inst Technol, Karlsruhe, GERMANY, 2015.

213. Wahlund P. O., Galaev I. Y., Kazakov S. A., Lozinsky V. I., Mattiasson B. "Protein-like" copolymers: Effect of polymer architecture on the performance in bioseparation process // Macromolecular Bioscience. – 2002. – Т. 2, № 1. – P. 33-42.

214. Tran Y., Perrin P., Deroo S., Lafuma F. Adsorption of randomly annealed polyampholytes at the silica-water interface // Langmuir. – 2006. – Т. 22, № 18. – P. 7543-7551.

ҚАЗАҚСТАН РЕСПУБЛИКАСЫ

РЕСПУБЛИКА КАЗАХСТАН

REPUBLIC OF KAZAKHSTAN

ПАТЕНТ
PATENT

№ 33596

ӨНЕРТАБЫСҚА / НА ИЗОБРЕТЕНИЕ / FOR INVENTION

(21) 2017/0573.1

(22) 05.07.2017

Қазақстан Республикасы өнертабыстары мемлекеттік тізілімінде тіркеу күні /
Дата регистрации в Государственном реестре изобретений Республики
Казахстан / Date of the registration in the State Register of Inventions of the
Republic of Kazakhstan: 26.04.2019

(54) П-аминобензой қышқылын алу тәсілі
Способ получения п-аминобензойной кислоты
Method for obtaining p-aminobenzoic acid

(73) "Қ.И. Сәтбаев атындағы Қазақ ұлттық техникалық зерттеу университеті" коммерциялық емес акционерлік
қоғамы (KZ)
Некоммерческое акционерное общество "Казахский национальный исследовательский технический
университет имени К.И. Сатпаева" (KZ)
"K.I. Satbayev Kazakh National Research Technical University» Non-commercial joint-stock company (KZ)

(72) Құдайбергенов Саркыт (KZ)
Алдабергенов Мади Жанарович (KZ)
Толеутай Гаухар (KZ)
Селенова Бағадат Самитовна (KZ)
Кабдрахманова Сана Канатбековна (KZ)

Kudaibergenov Sarkyt (KZ)
Aldabergenov Madi Zhanarovich (KZ)
Toleutay Gaukhar (KZ)
Selenova Bagadat Samatovna (KZ)
Kabdrakhmanova Sana Kanatbekovna (KZ)

«Ұлттық зияткерлік меншік» институты» РМК директорынын м.а.
И.о. директора РГП «Национальный институт интеллектуальной собственности»
Executive director of RSE «National institute of intellectual property»

APPENDIX B

İSTANBUL TEKNİK ÜNİVERSİTESİ
FEN EDEBİYAT FAKÜLTESİ, KİMYA BÖLÜMÜ
Prof. Dr. Oğuz OKAY
Maslak 34469, İstanbul
Tel: (+90-212) 285 3156
Fax: (+90-212) 285 6386
e-mail: okayo@.itu.edu.tr
http://www.kimya.itu.edu.tr/ookay

Istanbul, 6.1.2020

Laboratory test report

Synthesis and characterization of a series of hydrophobically modified physical polyampholyte (PA) hydrogels under various reaction conditions were carried out at the Polymeric Gels Research Laboratories of the Chemistry Department of Istanbul Technical University, Istanbul, Turkey. The reactions were conducted via micellar polymerization in aqueous solutions of worm-like sodium dodecyl sulfonate micelles. 2-acrylamido-2-methylpropane-1-sulfonic acid sodium salt (AMPS) and (3-acrylamidopropyl) trimethylammonium chloride (APTAC) were used as anionic and cationic monomers, respectively. The results obtained were reproducible and showed that:

a) Micellar copolymerization of charge-balanced AMPS and APTAC in the presence of the hydrophobic monomer n-octadecyl acrylate (C18A) without a chemical cross-linker leads to physical PA hydrogels that are stable in water.

b) The hydrophobically modified PA hydrogels contain 60-90% water.

c) They sustain a high tensile strength (up to 202 kPa) and exhibit a high stretchability (up to 1239%).

d) Above 7 mol % C18A, swollen PA hydrogels containing around 90% water exhibit much better mechanical properties as compared to the corresponding as-prepared ones.

e) The hydrogels exhibit self-healing ability. Cut-and-heal tests conducted at 50 °C reveal a complete healing efficiency with respect to Young's modulus for all as-prepared PA hydrogels.

The results thus indicate that these novel PA hydrogels with self-healing ability will have a wide range of application areas including enhanced oil recovery, immobilization of metal catalysts, wax inhibitor, pour point depressant, drug/gene/protein delivery, and cryopreservation of living cells.

Prof. Dr. Oğuz OKAY
Project Leader, Department of Chemistry,
Istanbul Technical University

Prof. Dr. Oğuz OKAY
İ.T.Ü. Fen- Edebiyat Fakültesi
Kimya Bölümü
34469 Maslak / İstanbul